

Constraining stellar and orbital co-evolution through ensemble seismology of solar-like oscillators in binary systems[★]

A census of oscillating red giants and dwarf stars in *Gaia* DR3 binaries

P. G. Beck^{1,2,3}, D. H. Grossmann³, L. Steinwender^{3,4}, L. S. Schimak³, N. Muntean³, M. Vrad^{5,6}, R. A. Patton^{5,6}, J. Merc⁷, S. Mathur^{1,2}, R. A. Garcia⁸, M. H. Pinsonneault^{5,6}, D. M. Rowan^{5,6}, P. Gaulme⁹, C. Allende Prieto^{1,2}, K. Z. Arellano-Córdova^{10,11}, L. Cao^{5,6}, E. Corsaro¹², O. Creevey¹³, K. M. Hambleton⁴, A. Hanslmeier³, B. Holl¹⁴, J. Johnson^{5,6}, S. Mathis⁸, D. Godoy-Rivera^{1,2}, S. Símón-Díaz^{1,2}, and J. C. Zinn¹⁵

(Affiliations can be found after the references)

submitted: May 4, 2023; accepted: October 25, 2023

ABSTRACT

Context. Binary systems constitute a valuable astrophysics tool for testing our understanding of stellar structure and evolution. Systems containing at least one oscillating component are interesting in this regard because asteroseismology offers independent parameters for the oscillating component that aid in the analysis. Systems of particular interest include those with known inclinations. With ~0.8 million binary candidates, the two-body orbit catalog (TBO) of *Gaia* Data Release 3 (DR3) substantially increases the number of known binaries and the quality of the astrometric data available for them.

Aims. To enlarge the sample of these astrophysically valuable benchmark objects, we searched for new binary system candidates identified in the *Gaia* DR3 TBO, for which one component has a detection of solar-like oscillations reported in the literature.

Methods. We cross-matched the TBO, the full non-single star (NSS) and eclipsing binary catalogs from *Gaia* DR3 with catalogs of confirmed solar-like oscillators in the main-sequence and red-giant phase from the NASA *Kepler* mission and stars in the Southern Continuous Viewing Zone of NASA TESS. The wealth of seismic information is used to characterize the oscillating primary. To test the completeness and robustness of the values reported in the TBO catalog, we performed a similar analysis on stars of the Ninth Catalog of Spectroscopic Binary Orbits (SB9).

Results. The analysis of the SB9 reveals an overall completeness factor for the *Gaia* TBO catalog of up to ~30% providing reliable orbital parameters for $\geq 90\%$ of the systems below $P_{\text{orb,SB9}} \leq 250$ d. We obtained new 954 unique binary system candidates from *Gaia* DR3, which host solar-like oscillators, of which we found 45 stars in binary candidates to be on the main sequence and 909 in the red giant phase. Additionally, we report 918 oscillators in potentially long-periodic systems. We present the seismic properties of the full sample and test whether the reported orbital periods are physically possible. For 146 giants, the evolutionary state has been determined from their mixed-mode period spacing, showing a clear trend to long periodic and less eccentric systems in the advanced phases of stellar evolution. Two new eclipsing binary systems, hosting a red-giant primary were found. For another 146 systems hosting oscillating stars, the values for the orbital inclination were found in the TBO. Of 181 TBO candidate systems observed multiple times with APOGEE, 149 (82%) are confirmed as binaries from radial-velocity (RV) measurement.

Conclusions. We conclude that the grand majority of the orbital elements reported in the TBO catalog are physically reasonable and realistic. This finding increases the number included in the sample of known solar-like oscillators in binary systems by an order of magnitude. The large fraction of confirmed binaries from APOGEE RV measurements indicates that the TBO catalog is robust. We suggest that due to instrumental noise, the seismically inferred masses and radii of stars observed with the TESS satellite and with an excess of oscillation power of $\nu_{\text{max}} \lesssim 30 \mu\text{Hz}$ could be significantly overestimated. The differences in the distributions of the orbital period and eccentricity are due to the accumulative effect of the equilibrium tide acting in these evolved binary systems.

Key words. Asteroseismology – (Stars:) binaries: spectroscopic – Stars: late-type – Stars: oscillations (including pulsations).

1. Introduction

Among the 5000 stars visible to the naked eye, about 2000 are known to be multiple-star systems. Naked-eye stars are a small fraction of all stars in the Milky Way, but they are reasonably representative of the incidence of binarity, which is estimated to be between 50 and almost 100% (e.g., Eggleton 2006). Some systems are close enough to be in contact and most are far apart enough to evolve almost independently. Binary systems are known with orbital periods as short as 0.2 days or as long as thousands of years. Stars in multiple systems are also precious test benches for testing our understanding of stellar struc-

ture and evolution (Moe & Di Stefano 2017; Offner et al. 2022). While their components may vary significantly in temperature, luminosity, radius, and lithium abundance, both components are identical in their initial conditions, age, and distance (e.g., Prša 2018).

The advent of space telescopes, such as Convection, Rotation et Transits planétaires (CoRoT Baglin et al. 2006), *Kepler* (Borucki et al. 2010) and its refurbished K2 mission (Howell et al. 2014), and Transiting Exoplanet Survey Satellite (TESS Ricker et al. 2014) have allowed for the detection of solar-like oscillations in late-type stars. These convection-driven oscillations provide a frequency pattern that allows for direct identification of the spherical degree of the oscillation mode (see monograph by Aerts, Christensen-Dalsgaard, & Kurtz 2010, and references therein), providing optimal input information for stellar

[★] Tables B.1, B.2, and B.3 are only available in electronic form at the CDS via anonymous ftp to cdsarc.cds.unistra.fr (130.79.128.5) or via <https://cdsarc.cds.unistra.fr/cgi-bin/qcat?J/A+A/>

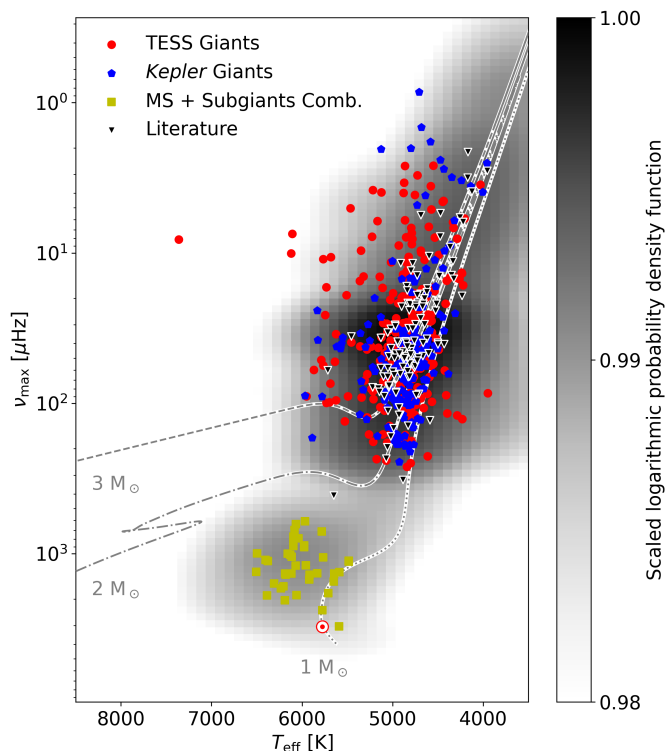


Fig. 1. Distribution of the sample in the seismic HRD with the frequency of the oscillation-power excess on the left vertical axis. The colored symbols show binary candidates reported in *Gaia* DR3 hosting giant or main-sequence solar-like oscillators. Red marks red giants with asteroseismic solutions obtained from TESS data. Blue denotes red giants with asteroseismic solutions from the *Kepler* mission. Yellow shows oscillating solar-like main sequence stars and subgiants, observed with *Kepler*. In black triangles, the literature sample is depicted. Only systems with APOGEE temperatures are shown. For the literature sample, all targets with asteroseismic solutions are shown, independently of whether a solution in the *Gaia* DR3 TBO catalog exists. With grey lines, the evolutionary paths for stars of $1 M_{\odot}$, $2 M_{\odot}$, and $3 M_{\odot}$ and with solar metallicity are shown. The grey probability distribution, underlying the scatter and curves, is the distribution of all targets with asteroseismic solutions of the above-mentioned catalogs.

modeling. For stars where an individual mode fitting is not feasible, the information content from the power spectrum can be summarized by two characteristic frequencies. These frequencies can then be combined through scaling relations to yield stellar mass and radius (Brown et al. 1991; Kjeldsen & Bedding 1995). The detection and exploitation of non-radial modes in giant stars by De Ridder et al. (2009), followed by those of dipole-mixed modes (Beck et al. 2011, 2012; Bedding et al. 2011; Mosser et al. 2011a), have unlocked the full potential of the asteroseismic analysis of red-giant stars. The constraint set by stellar binarity, amended with the independent information on stellar structure and its properties, offers a unique opportunity for testing the complex microscopic and macroscopic physics involved in building stellar models (e.g., Beck et al. 2018a; Li et al. 2018; Johnston et al. 2021).

The number of known binaries with solar-like oscillating components is still limited. From photometry, binaries are only detectable if their orbital geometry leads to eclipses or if the hydrostatic readjustment due to the tidal interaction of the stars at periastron gives rise to significant flux modulations (Kumar et al. 1995). The latter systems are colloquially referred to as “heart-beat stars.” In a recent effort, Beck et al. (2022) made an inven-

tory of the red-giant oscillators that belong to binary systems (eclipsing and otherwise) in the literature, while also searching for more in the Ninth Catalog of Spectroscopic Binary Orbits (SB9, Pourbaix et al. 2004), leading to a total of 182 oscillating red giants in binary systems with resolved orbital parameters (see Fig. 1). Following a different approach, Hon et al. (2022) provided a catalog of seismic parameters of members of 99 binary systems, whereby the red giant primary is spatially resolved from the secondary. Because of their very long orbits, the orbital periods are hardly known for these systems.

An area of particular interest are the double-lined spectroscopic binaries (SB2), where spectral lines from both components are detectable, with a known inclination angle of 90 degrees, for which stellar masses and radii can be accurately determined. Gaulme et al. (2016) used ten of these systems to test the accuracy and precision of the asteroseismic scaling relations, suggesting an offset of up to 15% in mass and 5% in radius. Themeßl et al. (2018) and Benbakoura et al. (2021) added another four eclipsing systems, increasing the count of these high-value targets to 14 (see Beck et al. 2022, for a complete list). For a robust analysis of the comparison of dynamical and seismic masses, a substantially larger number of systems with known inclination angles is necessary.

The third data release (DR3) of the ESA *Gaia* mission (Gaia Collaboration et al. 2016, 2023b) is the first *Gaia* DR to include a specific analysis for non-single stars (see Gaia Collaboration et al. 2023a; Holl et al. 2023; Halbwegs et al. 2023; Mowlavi et al. 2023, Siopis et al. subm., Damerджи et al. subm., and Gosset et al. subm., for catalogs and details of the analysis). In the *Gaia* data, a multiple-star system can be identified with one or several of the following: (i) astrometric measurements, (ii) detections of periodic photometric dimming caused by eclipses or phase effects, (iii) radial velocity measurements obtained by the high-resolution spectrometric channel, and (iv) by the low-resolution spectro-photometry from SED fitting. From 34 months or 1034 days of observations of the whole sky, Gaia Collaboration et al. (2023a) reports about 814 000 binaries in *Gaia* DR3, resulting from *Gaia* astrometric (Halbwegs et al. 2023; Holl et al. 2023), and radial velocity orbital fitting (Gosset, et al., 2023; Damerджи, et al. 2023). This catalog contains only a small subset of the 2.2 million eclipsing binaries¹ detected by photometry Mowlavi et al. (2023), for which an orbital solution has been computed (Siopis et al. subm.). In the optimal case, astrometric solutions offer the possibility to obtain the inclination of the orbital plane in the sky, which allows us to measure the masses of their components and utilize non-eclipsing systems for calibrating asteroseismology. This new catalog of non-single stars released by *Gaia* constitutes a major change in the known inventory of such types of systems.

It will take a long time to go through the data from the past CoRoT, *Kepler*, and K2 missions, the current TESS, and the forthcoming Chinese *Earth 2.0* (Ge et al. 2022), ESA PLATO (Rauer et al. 2014), and the NASA *Roman* (Johnson et al. 2020; Huber et al. 2023) missions, which are expected to be operational by the end of the decade. Before exploring the archived photometric data, a natural first step consists of checking which of the known stellar pulsators are listed as non-single stars in the *Gaia* DR3 catalog. This work presents the successful search for solar-like oscillating stars in binary systems, revealed through photometric, spectroscopic, and astrometric solutions in the *Gaia* DR3.

¹ see the more complete `gaiadr3.vari_eclipsing_binary` catalog

The paper is structured as follows. In Sect. 2, we describe the selection of the sample red-giant stars and our search for orbital solutions reported in the *Gaia* DR3. The general asteroseismic properties of the found sample of binary candidates with oscillating red-giant primaries are described in Sect. 3. The history of tidal interaction and stellar activity and rotation is analyzed in Sect. 4. In Sect. 5, we present an eclipsing binary system, listed in the *Gaia* DR3 eclipsing binary catalog and report oscillations and updated orbital period from TESS photometry. Furthermore, we present 146 solar-like oscillators in systems with *Gaia* inclinations. In this chapter, we discuss why eclipsing binaries are difficult to find, resulting in their small number compared to the known binary population. Independent confirmation for 181 reported binary candidates through RV variations, mainly from *Apache Point Observatory Galactic Evolution Experiment* (APOGEE, Majewski et al. 2017) is provided in Sect. 6. Section 7 discusses symbiotic binaries and giants with anomalous peaks in the power-spectral density (PSD), two related science cases (including red-giant binaries) onto which the data from *Gaia* DR3 shed new light.

2. Sample selection and binary statistics

Using the *Simbad* module in the *AstroPy* package (Astropy Collaboration et al. 2018, and references therein), we created a table of cross-identifiers. This list was then used to query the inventory of the two-body orbit (TBO) catalog of *Gaia* DR3 (Gaia Collaboration et al. 2023a) on the *Gaia* data archive².

2.1. Completeness and robustness of *Gaia* DR3 binary candidate solutions

The documentation of the *Gaia* DR3 TBO stresses that the reported systems are 'only' binary system candidates. To better understand the completeness, robustness, and quality metrics of the orbital solutions provided in the catalog, particularly for the outliers, we explore the TBO inventory for a well-known sample of binaries. A commonly chosen gold-star sample is SB9, created and curated by the team of Pourbaix et al. (2004), which we used to assess the quality and completeness of the *Gaia* DR3 solutions. In this subsection, we only review the takeaway results of our comparison. For details of the full analysis, we refer to Appendix A.

In the SB9, we identified the 3413 unique objects. Because the efficiency of the methods for detecting binaries is dependent on the (integrated) object's magnitude (see Fig. 10 in Gaia Collaboration et al. 2023a), we constructed a magnitude-limited sample between the *Gaia* magnitudes $4 \leq G [\text{mag}] \leq 13$ to assess a completeness factor, bias corrected for objects outside the detection range of *Gaia*. Because many SB9-systems have orbits longer than the baseline of *Gaia* DR3, we further limited the sample to $P_{\text{orb,SB9}} \leq 1\,100$ d. From the 2343 systems in the period-magnitude-limited SB9 sample 668 were identified as binary systems (Fig. 2, middle panel). This corresponds to a completeness factor of 28.5%. Additional 241 SB9 systems are present in the catalog of non-linear solutions (Gaia Collaboration et al. 2023a), whose orbital elements could not be resolved from the current data in *Gaia* DR3 and most likely indicate systems with orbital periods longer than the baseline of *Gaia* DR3. Indeed the comparison in Fig. 2 (top panel) confirms this expectation. Taking these detections into account increases the overall completeness factor to 38.8%.

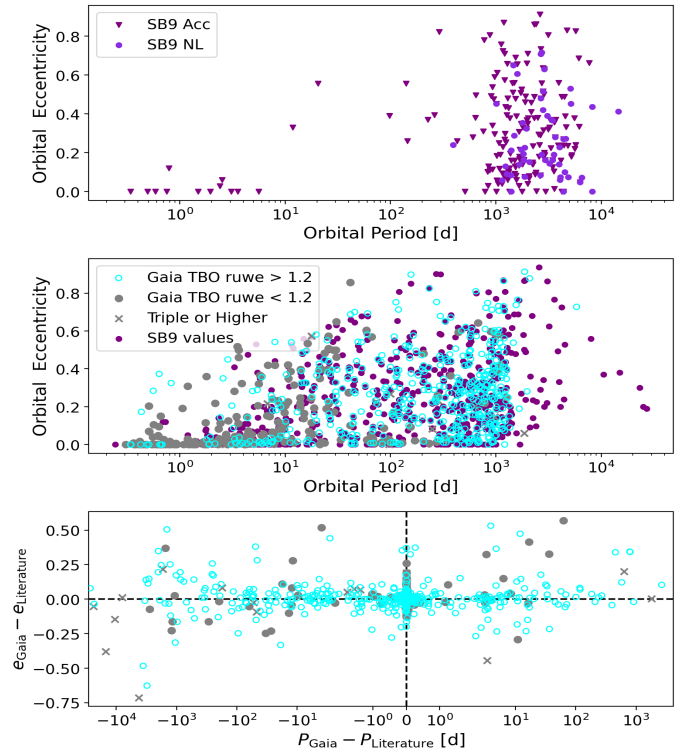


Fig. 2. Comparison of period and eccentricity from *Gaia* DR3 TBO and the SB9 catalog. The top panel depicts the SB9 values of the orbital parameters of systems for which only non-linear (violet dots) or acceleration solutions (purple triangles) are reported in the *Gaia* TBO. The middle panel shows 715 systems that have a full solution for the orbital parameters in both catalogs. The solution reported in the SB9 catalog is shown in purple. The DR3 solutions for the same set of systems are separated based on their ruwe value (ruwe < 1.2: grey dots; ruwe > 1.2: cyan circles). Triple or higher order systems are marked with a cross. The bottom panel depicts the absolute residuals for the period and eccentricity between the two sets of solutions.

The middle panel of Fig. 2 shows the e - P plane of all 715 systems for which both parameters (the eccentricity and period) are provided in the SB9 and the *Gaia* DR3 catalog. We consider a solution reliable, if the residual between the values listed in SB9 and *Gaia* DR3 (bottom panel of Fig. 2) differ by less than 10%. For such solutions, we find a good agreement for the eccentricities with a mean residual of 0.011 and a standard deviation of 0.104.

A more complex picture is found for the orbital periods. In the range of $P_{\text{orb,SB9}} \leq 250$ d, and $250 \leq P_{\text{orb,SB9}} [\text{d}] \leq 500$, we find that $\sim 90\%$ and $\sim 99\%$ of all systems have periods with residuals better than 10%, respectively. Interestingly, with a completeness factor of 41.0% the longer period range yields a higher detection rate than the short periodic range with 24.9%. The borders of the intervals were chosen to resemble one-fourth and half of the timebase covered by *Gaia* DR3. The lower percentage of reliable solutions in the short periodic range can be explained with a larger number of short-periodic solutions for long periodic systems (Fig. A.1). For $P_{\text{orb,DR3}} \geq 500$, the number of reliable solutions drops to $\sim 74\%$, which contains a significant number of significantly underestimated orbital periods of systems with $P_{\text{orb,SB9}} \geq 1\,100$ d. The comparison of the orbital elements in the SB9 and *Gaia* DR3 catalog are depicted in the bottom panel of Fig. 2, Fig. A.2, and discussed in more detail in App. A.

The ruwe parameter presents the renormalized unit weight error (ruwe) of a star's astrometry (for details see Gaia Collab-

² <https://gea.esac.esa.int/archive/>

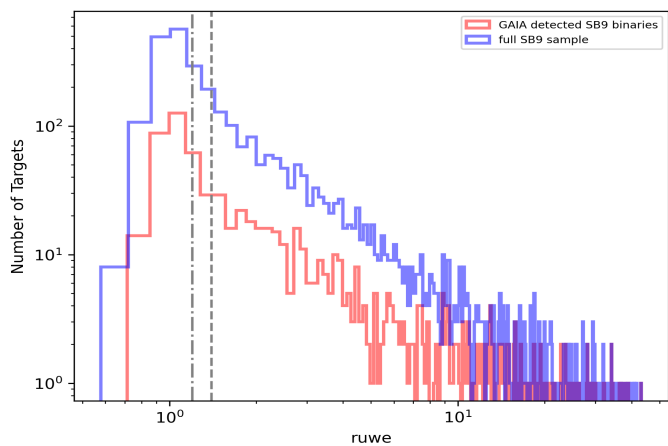


Fig. 3. *Gaia* astrometric detected SB9 binaries, based on the *ruwe* values for all *Gaia* sources of the SB9 sample (blue) and the binary candidates in the TBO catalog (red). The grey dash-dotted and dashed vertical lines mark the *ruwe* suggested threshold values of 1.2 and 1.4, respectively.

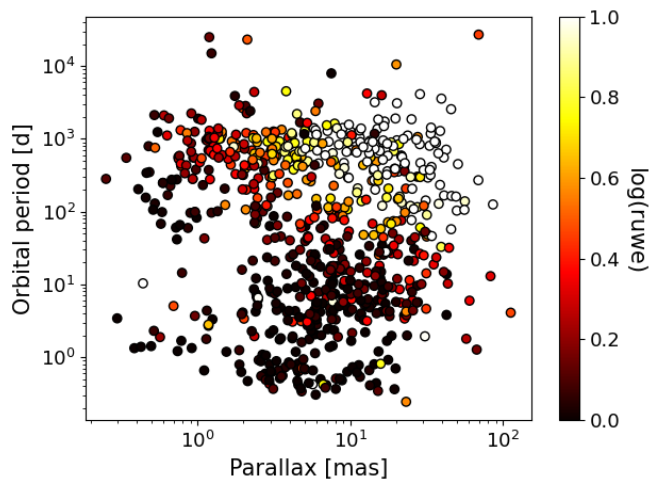


Fig. 4. Distribution of *ruwe* value of the SB9 systems in *Gaia* in logarithmic scale as a function of the *Gaia* parallax and orbital period from SB9 catalog.

oration et al. 2023a). The analysis of the SB9 sample taught us that $\sim 40\%$ of all systems in the period-magnitude limited sample have *ruwe* values below the threshold value of ~ 1.4 (Fig. 3), which is often discussed as a good general indicator for a binary detection. As shown in Fig. 4, these systems are typically far away and their components' displacement is therefore small, with respect to the astrometric precision of the *Gaia* satellite.

2.2. Solar-like oscillators in *Gaia* DR3 binary candidates

To guide our search for solar-like oscillators in binary star systems, we compiled a list of known solar-like oscillators whose global seismic parameters were reported in the literature (Table 1). Due to their characteristic shape, the PSD of solar-like oscillations are typically described through the center frequency of the excess of oscillation power, ν_{\max} . This quantity correlates with the stellar surface gravity, $\log g$, and the stellar luminosity, L . The structure of oscillation modes in the power excess is very regular (Tassoul 1980; Mosser et al. 2011b). The average frequency separation between modes of the same spherical de-

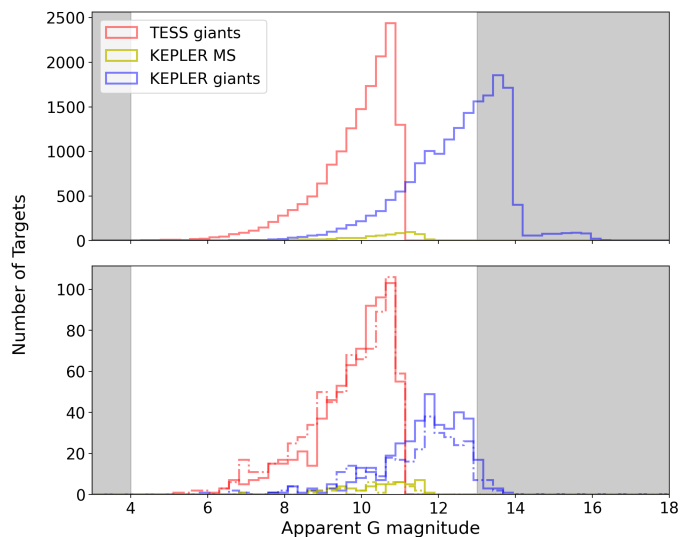


Fig. 5. Distribution of the apparent G magnitude in the input samples for the search (top panel) and found binary candidate systems (bottom panel). The bin size is one-fourth of a magnitude. The grey-shade regions mark magnitudes outside the magnitude-limited sample. The dash-dotted lines indicate the reported candidates with acceleration and non-linear solutions for the respective samples.

gree, ℓ , but consecutive radial orders is described through the large-frequency separation, $\Delta\nu$. The large-frequency separation is a proxy of the average speed of sound in the oscillating stars. We refer to the review by Aerts (2021) for a recent overview of the two global-seismic parameters.

The largest input sample comprises over eighteen thousand oscillating red giants, measured and identified from *Kepler* photometry. The *Kepler* giant sample was compiled from Yu et al. (2018). Because of the long timebase of *Kepler* photometry, the frequency resolution allows for a clear identification of the mixed-mode pattern. Evolutionary states were extracted from seismology by Vrad et al. (2016). In this sample, 17 544 systems have valid astrometric solutions listed in the *Gaia* DR3 catalog. The second sample is the *TESS* giant sample provided by the giants in the *TESS* mission's Southern Continuous Viewing Zone (SCVZ). Of the fifteen thousand giants identified from photometric and spectroscopic calibration, Mackereth et al. (2021) detected oscillations in about two-thirds of the stars. It has been a matter of discussion in the literature (e.g., Silva Aguirre et al. 2020) that while individual and well-proven asteroseismic pipelines agree on the position of the power excess within a few percent, there is an increased scatter on the determined large-frequency separation from *TESS* data. Therefore, we also accepted stars with missing or uncertain $\Delta\nu$ values into our catalog. We considered oscillations to be detected in a giant if at least two of the three pipelines used by Mackereth et al. (2021) report a power excess. For our analysis, we use the mean value of ν_{\max} reported in their paper. For 12 016 oscillating giants, an astrometric solution exists in *Gaia* DR3. We follow the evolutionary states for this sample, determined by Vrad et al. (2021).

Main sequence solar-like stars and subgiants with solar-like oscillations complement the giants samples (hereafter referred to as the MS+SG sample). Here, we have compiled a list of stars observed by *Kepler* (compiled by Mathur et al. 2022). Of the 624 oscillating dwarfs, an astrometric solution exists for 595 stars in *Gaia* DR3.

The distribution of the 30 155 oscillating stars from the *Kepler*, *TESS*, and MS+SG samples (Table 1), with an astrometric

Table 1. Input samples for oscillating main-sequence and red-giant stars and the corresponding binary yields.

Input samples		Oscillators <i>Gaia</i> DR3	Magnitude limited	NSS TBO		Binary fraction		Astrom. Inclin.	NSS TBO Acc+NL
Name	Size			Uni.	Alt.	Full	Mag lim.		
Kepler giants	18 824	17 544	10 374	376	3	2.2%	3.6%	31	257
TESS giants	15 405	12 016	12 016	549	18	4.6%	4.6%	105	633
MS + SG	624	595	595	45	1	8.1%	8.1%	14	28
Lit. giants	190	190	53	53	1	27.9%	100%	1	116
SB9 sample	3 413	–	2 343*	668	0	19.6%	28.5%*	68	241

Notes. The first four columns describe the input sample and construction of subsamples.

1 and 2: The name of the sample and the input samples for the search and the number of all targets in the catalog;

3: number of oscillating targets within this sample that have a *Gaia* DR3 solution;

4: number of targets in the magnitude limited sample within $4 \leq G$ [mag] ≤ 13 .

The next 7 columns present the results of the search of the Non-Single-Star (NSS) catalog in *Gaia* DR3.

5: gives the number of unique solutions returned by the ADQL query for the sample of oscillators with *Gaia* solutions (col. 3);

6: gives the number of alternative orbital solutions in case TBO contains multiple solutions;

7: presents the binary detection fraction, calculated from the sample of all oscillating targets with a *Gaia* DR3 solution (col. 3);

8: presents the binary detection, calculated from the magnitude limited sample (col. 4) and binaries within the magnitude limit;

9: presents the number of systems hosting an oscillating component with inclination reported in TBO;

10: number of sources with acceleration and non-linear solutions in TBO could point to longer-period binary systems.

★: Because the SB9 sample extends significantly further in period than the *Gaia* TBO sample, the magnitude limited sample for SB9 has been further corrected for a cut-off period of $P \leq 1100$ days.

solution in *Gaia* DR3 in the seismic Hertzsprung-Russell diagram (HRD) is depicted as the probability density map shown in the grey-scale of Fig. 1. The orbital and seismic parameters of the detected binary candidates are presented in Table B.1. For reference and orientation, we show evolutionary tracks for a star of the solar metallicity of 1, 2, and $3 M_{\odot}$, calculated with the MESA evolutionary code (Paxton et al. 2018; Jermyn et al. 2023, and references therein).

For our queries of the *Gaia* data archive, we produced cross-identifier tables between the solution identifier of *Gaia* DR3, the target input catalogs for the *Kepler* and TESS missions (KIC and TIC, resp.), and the Two-Micron All Sky Survey (2MASS). For the entire sample of oscillating stars in *Gaia* DR3, we found 970 unique orbital solutions for binary system candidates in the *Gaia* DR3 TBO catalog (Table 1). Between the input sample and the literature sample, we find a cross-section of 44 systems, of which 16 are detected. These are listed in the bottom panel of Table B.1. Therefore, we report the detection of 954 solar-like oscillators in binary systems.

The position of these binary systems in the seismic HR diagram is shown in Fig. 1. For 22 candidate systems, the *Gaia* catalog provides multiple solutions of the DR3 data productions that did not converge to a single solution. We have chosen not to keep them in our final sample.

2.3. Potentially long-periodic systems

Our search of the acceleration and non-linear solutions in TBO sub-catalogs delivered in total 918 results for the giants- and dwarf-star samples (see Table 1 and Fig. 5). These solutions could indicate additional binary systems. However, no orbital parameters are given, as the orbital periods of these systems could substantially exceed the timebase covered by *Gaia* DR3. Under the assumption that all these detections represent actual binaries, we would roughly double the binary detection rate.

Confirming these suggested binary detections will require more extended timebases of *Gaia* observations with forthcoming data releases or ground-based RV monitoring. Both are beyond the scope of this paper. Therefore, we only list these systems in

Table B.2 and we do not further explore their binary characteristics.

2.4. Binary detection rates

Differences between the input samples are found in the detection rate. Interestingly, the sample for giants seismically characterized with *Kepler* (2.2%) and TESS (4.6%) differ by about a factor of 2. Several observational aspects can explain these differences. The main difference between the samples is the distribution of the apparent magnitude of their targets. Figure 5 compares these data sets by depicting the distributions of the mean *Gaia* G band magnitude for the three input catalogs (Table 1). Indeed, the peak of the *Kepler* giant sample is about 3.5 magnitudes fainter than that of the TESS giants. The *Kepler* main-sequence sample peaks at about 11.5 mag.

Therefore, we corrected the fractional count of the yields in Table 1, calculated from the subsample of targets within the brightness limits ($4 \leq G$ [mag] ≤ 13) described in Appendix A. As shown in Fig. 5, correcting the sample sizes for the magnitude range mainly affects the sample size of the *Kepler* giant sample, as about 40% of all targets are fainter than 13th mag. Because the TESS telescope also shows significant saturation effects around 4th mag and the sample of Mackereth et al. (2021) was limited to TESS magnitudes brighter than 11th mag, all targets fall into the magnitude-limited range.

To make the comparison of the binary rate more compatible between the space telescopes, we recalculated the fractional yields for a magnitude-limited sample, which leads to 3.6% and 4.6% for the *Kepler* and TESS sample, respectively. Therefore, the corrected yields bring the results from the two giant samples into a closer agreement. The remaining difference could originate from the differences in the scanning law of the *Gaia* satellite. As shown by Gaia Collaboration et al. (2023a, in their Fig. 7), the *Kepler* field of view has been substantially less intensively covered than the southern CVZ of TESS.

The *Kepler* main-sequence sample achieves the highest detection rate with 8.1%. At first glance, this is surprising, as their distribution mainly ranges between the bright TESS and the fainter *Kepler* giant sample and suffers from the same lower

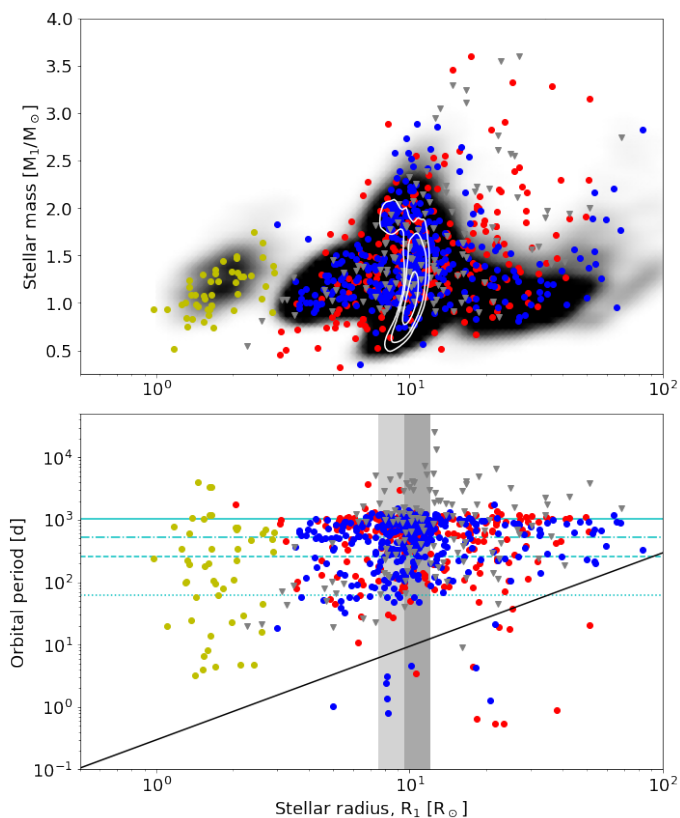


Fig. 6. Characterisation of the set of binary candidates from *Gaia* DR3. Top panel shows the distribution of the binary candidates in the radius-mass plane. The probability density map in the background shows the distribution of all oscillating stars in the *Kepler* sample. Bottom panel provides a test of the feasibility of the orbital period as a function of the stellar radius. The black line resembles the estimated minimum period for a system to fill the Roche lobe of its giant. The dark and light shaded area mark the ranges in which RC and 2RC stars are expected, respectively. The meanings of the yellow, blue, and red symbols are similar to those of Fig. 1 for the dwarfs and giants from the *Kepler* sample and giants from the TESS sample, respectively. The literature sample is represented by grey triangles. The horizontal lines (from top to bottom) indicate the full, half, one fourth of the timebase, and the ~ 63 day precession period of *Gaia* DR3.

number of scanning events as the *Kepler* giants. This sample contains more stars on shorter orbital periods that are easily detected by the *Gaia* satellite. These orbital periods are also located at periods untypical or physically impossible for giants in binary systems due to their extended radii. Therefore, the difference could already point to a different binary fractions as a function of the evolutionary state.

As discussed in the literature, based on the analysis of the large samples from the SB9 catalog and APOGEE data (e.g., Van Eylen et al. 2016; Badenes et al. 2018; Beck et al. 2022), most systems in the red giant phase are found at periods longer than several hundred to a few thousand days, which is beyond the baseline of *Gaia* DR3. Because we do not know the initial distribution of orbital periods, we cannot compile a magnitude-period limited sample, as done for the SB9 comparison in Appendix A.2 and correct the yields. However, we can estimate the approximate detection rates by including the 890 and 28 acceleration and non-linear solutions for giants and dwarfs (see Table 1), respectively, in the calculation of the magnitude-corrected binary yields. Therefore, we gain tentative binary detection rates

of $\sim 6.6\%$ for the *Kepler* giants, $\sim 11.0\%$ for the TESS giants, and $\sim 14.1\%$ for the *Kepler* dwarfs.

These numbers are still low when compared with the expected binary fraction for the mass range of solar-like stars of about $\sim 50\%$ known from stellar population studies (see the reviews by Moe & Di Stefano 2017; Offner et al. 2022, and references therein). In Appendix A.2, we showed that the binary yields are at least a factor of 3 too low. We argue that this high fraction of nondetections is due to insufficient data or the extensive orbital periods expected for these binaries. Correcting these binary fractions by this factor for incompleteness puts us into the ballpark of about $\sim 30\%$ to $\sim 40\%$, which approaches the expected value.

3. General properties of the sample

From searching the catalogs in Table 1, we find a total of 954 new binary-system candidates hosting a solar-like oscillating red giant (909) or either a main-sequence or a subgiant (45) star in the TBO. We note that Gaia Collaboration et al. (2023a) also presented a study of red giant binaries. The *Gaia* sample was drawn from a cut of all TBO solutions, whereby the giants were identified from their 2MASS colors ($J-K > 0$ mag, and $M_K < 0$ mag). Because our sample was selected on the premise of detected oscillations, the sample's "purity", size, and distribution are different in these two works. The detection of oscillation in the target source has predetermined our sample. This additional selection criterion allows us to select giants with high accuracy and apply seismic techniques to exploit the properties of the sample.

3.1. Masses and radii from asteroseismology

We calculate the mass and radius of an oscillating star in the binary candidates with the standard asteroseismic scaling relations (Brown et al. 1991; Kjeldsen & Bedding 1995). Using the solar values as a base reference, this homological formalism allows us to estimate the masses and radii from their measured global seismic parameters, the peak frequency of the global power excess, ν_{\max} , and the large frequency separation, $\Delta\nu$, and spectroscopically measured effective temperature:

$$\frac{R_{\star}}{R_{\odot}} = \left(\frac{\nu_{\max}}{\nu_{\max,\odot}} \right)^3 \cdot \left(\frac{\Delta\nu}{\Delta\nu_{\odot}} \right)^{-4} \cdot \left(\frac{T_{\text{eff},\star}}{T_{\text{eff},\odot}} \right)^{3/2}, \quad (1)$$

$$\frac{M_{\star}}{M_{\odot}} = \left(\frac{\nu_{\max}}{\nu_{\max,\odot}} \right) \cdot \left(\frac{\Delta\nu}{\Delta\nu_{\odot}} \right)^{-2} \cdot \left(\frac{T_{\text{eff},\star}}{T_{\text{eff},\odot}} \right)^{1/2}. \quad (2)$$

We use the reference values of the A2Z pipeline (Mathur et al. 2010) $\nu_{\max,\odot} = 3100 \mu\text{Hz}$, $\Delta\nu_{\odot} = 135.2 \mu\text{Hz}$, and $T_{\text{eff},\odot} = 5777$ K to describe the oscillations in the Sun.

The seismic scaling relations assume the star's oscillations to be in the asymptotic regime of high radial-order modes, where oscillation modes are equally spaced in frequency by $\Delta\nu$ (Tassoul 1980). It has been shown that with the decreasing frequency of the excess oscillation power, the stars oscillate in lower radial orders. Additionally, non-adiabatic effects in the stellar atmosphere have a stronger impact on the oscillation modes with increasing luminosity and decreasing density as the star approaches the luminous regime of the red giant branch (RGB). These effects lead to a departure of the measured global seismic properties with respect to the asymptotic assumptions built into the scaling relations. To correct for these effects, numerous techniques have been developed (e.g., Sharma et al. 2017). For the giants, we use the formalism of Mosser et al. (2013), with the suggested value

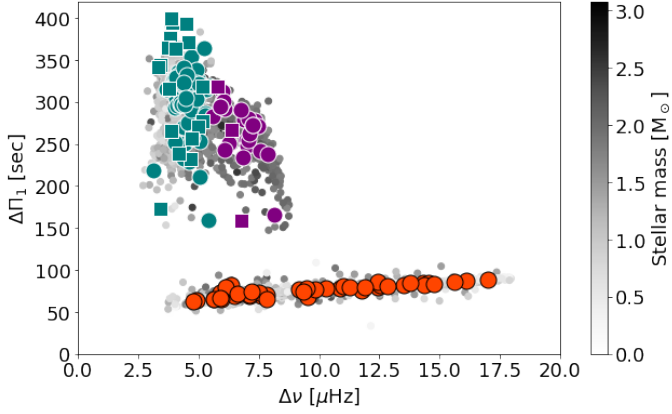


Fig. 7. Identification of the evolutionary stage of the primary of the system. Teal, purple, and orange indicate RC, 2RC, and RGB stars, respectively. Dots indicate stars observed with the *Kepler* mission. Squares mark stars observed by TESS. The points in grey mark the full input sample by [Vrard et al. \(2021\)](#), whereby the greyscale value indicates the mass of the star, determined by seismology.

of $\zeta=0.038$ to correct for the observed a large frequency separation ($\Delta\nu_{\text{obs}}$) for its asymptotic value of:

$$\Delta\nu_{\text{asy}} = (1 + \zeta)\Delta\nu_{\text{obs}}. \quad (3)$$

For stars on the main sequence, we use the uncorrected value as their structural properties and, consequently, their global seismic parameters are close to the solar reference values.

The top panel of Fig. 6 shows the binary candidates' distribution of the obtained masses and radii. From the comparison with the masses and radii for giants and dwarfs from the *Kepler* mission (Table 1), we see that stars reported from the TESS mission that have radii larger than the clump show an excess of massive stars ($2 \lesssim M/M_{\odot} \lesssim 4$). This trend is more pronounced if ν_{max} and $\Delta\nu$ values from a single pipeline are used. For TESS giants, we therefore use the mean values reported by [Mackereth et al. \(2021\)](#). We understand this as a problem of accurately determining the large frequency separation from TESS data if ν_{max} is low. In such circumstances, it is challenging to resolve the comb-like pattern of the power excess due to the contaminating signal from the granulation background, systematic effects introduced through multiple sectors with multiple CCD and pixel combinations, along with a smaller number of modes excited in the power excess as well as a lower frequency resolution due to the shorter timebase to resolve them.

3.2. Evolutionary states from asteroseismology

The evolution of a solar-like star includes several structurally distinct phases. It is straightforward to separate main sequence stars and subgiants from the red giant stars based on the peak frequency of their excess oscillation power.

The red giant phase, however, is an apposition of several structurally distinct phases (e.g., [Kippenhahn et al. 2013](#); [Pinsonneault & Ryden 2023](#), and references therein). The first phase is the RGB. Once a star has consumed its core hydrogen content, the core will contract, and the envelope will expand. In this phase, the only energy source of the star is the fusion of hydrogen in a shell around the He core. Consequently, its luminosity will rise until the inert He-core ignites. Depending on the star's mass, this will happen under degenerate conditions (for stars with $M_{\star} \lesssim 2 M_{\odot}$) and settle for quiescent core-He burning

in the red clump. For more massive stars, the ignition temperature of He will be reached before forming a degenerate core. Core helium ignition then proceeds under non-degenerate conditions, with the star settling on the less luminous secondary clump (2RC). These phases are followed by the asymptotic giant branch (AGB) once the helium in the core has been exhausted.

These structural readjustments force substantial changes in the stellar radius and luminosity. We discuss the impact of the radius on the tidal forces in detail in Sect. 4. Figures 1 and 6 indicate the location of the MS, RGB, RC, and 2RC in the respective parameter space. Because the frequency pattern of mixed modes is sensitive to the density contrast between the surface and the stellar core, these modes can use the spacing in the dipole forest to unambiguously determine the evolutionary state of a giant ([Bedding et al. 2011](#)). The approach of [Mosser et al. \(2015\)](#) reconstructs the value of the asymptotic-period spacing of dipole-gravity modes, $\Delta\Pi_{\ell=1}$ ([Tassoul 1980](#)).

To identify binary candidates whose primaries have a determined evolutionary state, we correlated the published values of $\Delta\Pi_1$ for *Kepler* and TESS giants ([Vrard et al. 2016, 2021](#)) with the binary candidate lists. The identification of RGB stars from TESS data was quite uncertain due to similar problems as discussed for the $\Delta\nu$ for the same mission. Therefore, we excluded any H-shell burning stars identified in the TESS sample. In total, we have four samples composed of 45 stars on the main sequence and 41 on the RGB (H-shell burning). For the He-core burning phase, we get 80 stars in the RC and 25 in the 2RC. The colored dots in Fig. 7 illustrate the identified stars in binary candidates from *Gaia* DR3. Because the RGB evolution is a continuous process, we believe the gap of binary candidates between $8 \lesssim \Delta\nu [\mu\text{Hz}] \lesssim 9$ is purely a statistical artifact as it is not found in the larger sample of single stars.

3.3. Validation and distribution of orbital parameters

From the seismically inferred radius, we can test if the orbital period reported for the binary candidate in the *Gaia* DR3 TBO is physical, as larger stellar radii require wider binary systems, and a very short period ($P_{\text{orb}} \lesssim 10$ d) for a giant indicates a possible problematic solution for the period. If it is too short, the giant star would eventually fill up its Roche lobe, the boundary within which the material is gravitationally bound to the star. Mass transfer and a Roche-lobe overflow (RLOF) would lead to alternated orbital evolution on very short time scales ([Soberman et al. 1997](#)). As a red giant branch star further expands its envelope, RLOF would soon be followed by a common envelope phase, which ends in the ejection of the common envelope on even shorter time scales ([Han et al. 2002](#)).

To identify such non-physically short-periodic binary systems, in Fig. 6, we show the Roche-lobe limit in the radius-period plane in the formulation of [Gaia Collaboration et al. \(2023a\)](#),

$$\log\left(\frac{P_d^{\text{Roche}}}{365.25}\right) = \frac{3}{2} \log R_1 - \frac{1}{2} \log(M_1 + M_2) - \frac{3}{2} \log\left(0.38 + 0.2 \log \frac{M_1}{M_2}\right), \quad (4)$$

whereby R_1 is the radius of a primary and M_1 and M_2 are the primary and secondary masses, respectively. In Fig. 6 (bottom panel), this criterion is depicted for a hypothetical system of $M_1=1.3 M_{\odot}$ and $M_2=1 M_{\odot}$. For the primary's potential radius we assumed a range from less than 1 to $100 R_{\odot}$.

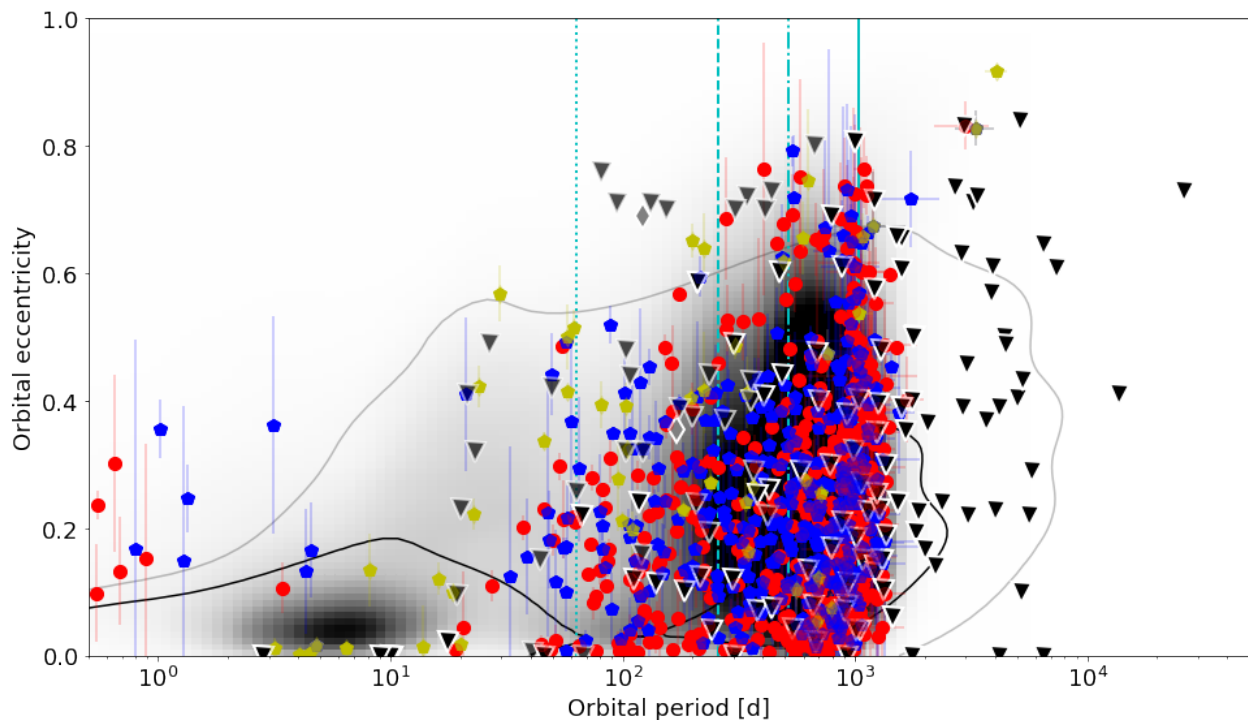


Fig. 8. Distribution of the sample of binary-candidate systems from *Gaia* DR3, hosting evolved stars as their primary stellar component. Colored dots mark systems with detected solar-like oscillations in the components primaries (blue and red mark stars from the sample of giants in *Kepler* and TESS; yellow indicates main sequence stars observed with *Kepler*). Systems from the published *Kepler* sample with an oscillating red giant primary are depicted as black triangles. Systems hosting two oscillating red giant components (PB2) are shown as grey diamonds. The background density plot represents the distribution of all systems in *Gaia* DR3 TBO with full orbital solutions. The thin and thick black contour lines show the isocontour regions of densely populated regions and the envelope of the distribution of SB9 binary systems, respectively. The vertical solid, dash-dotted, dashed, and dotted lines represent the 1034 d baseline of *Gaia* DR3 as well as one half and one-fourth of it and the ~ 63 day precession period of the satellite.

While [Gaia Collaboration et al. \(2023a\)](#) finds systems close to the Roche limit, the periods of most binary-candidate systems in our sample are substantially longer than the indicative Roche lobe limit shown in Fig. 6. This selection effect is explained by the selection criterion, as each primary component of systems depicted in the diagram oscillates. As shown in numerous papers ([Gaulme et al. 2014](#); [Beck et al. 2018b](#); [Tayar et al. 2022](#)), strong tidal interaction and the induced stellar activity suppress oscillation modes. Tidal forces get enhanced as a star increasingly fills its Roche-lobe, leading to the shown selection effect.

A few systems fall below the Roche-lobe limit. While systems with orbits of less than 10 days are close to the limit of being realistic (but short-lived), they would have an orbital trajectory inside or very close to the giant. While these systems, on average, have a lower *ruwe* value, this parameter is insufficient to identify these problematic systems. The documentation of the TBO reports an excess of orbital periods around four days, which could be connected to aliases that induce a spurious period, while the binary detection is valid. Therefore, we list these systems in the paper but flag them as unreliable and exclude them from our additional analysis.

Figure 8 presents the orbital period and eccentricity of binary candidates that host a main-sequence or a red giant star. The same figure also compares the distribution of the full TBO catalog. From the *Gaia* systems, we find the same distribution as in the SB9 sample with two clear overdensities, whereby the one at shorter periods is populated with hot main sequence stars ([Torres et al. 2010](#)). It was shown by [Beck et al. \(2022\)](#) that os-

illating giants mainly fall into the second overdensity between 500 and 1000 days.

3.4. Metallicity, distance, and space velocities

The numerous detections provided by *Gaia* allow us to view the rich dataset of the binary candidates in the much broader context of galactic archaeology. A standard tool to study the membership of stars to a particular galactic structure is the Toomre diagram. It projects the distribution of the Galactic space velocities U , V , and W , where V describes the absolute value of the velocity, $|V|$, in the direction of the rotation of the Milky Way. The velocity, U , represents the component of the motion in the direction from the sun toward the Galactic center, and W is the component perpendicular to the Galactic plane. To illustrate U , V , W in two dimensions, we calculate $\sqrt{U^2 + W^2}$, corresponding to the velocity perpendicular to V , which is the vector pointing away from the Galactic center. To collapse the diagram into one quadrant, we show $|V|$. Here, U , V , W were corrected for the local standard of rest (LSR) ($U_{\odot} = -8.63$, $V_{\odot} = 4.76$, $W_{\odot} = 7.26$ in km s^{-1}) taken from [Ding et al. \(2019\)](#). The total velocity, which we refer to as $X = \sqrt{V^2 + U^2 + W^2}$, describes the radial distance to the origin of the plot and indicates if a star tends to belong to the younger thin disk, the older thick disk, or the halo of the galaxy.

The left and right panels of Figure 9 depict the position of the binary candidates and the distribution of the TESS and *Kepler* input sample as the background density map, respectively, in the parameter space of the Toomre diagram. As input parameters, we used the astrometry provided by *Gaia* DR3 and the radial

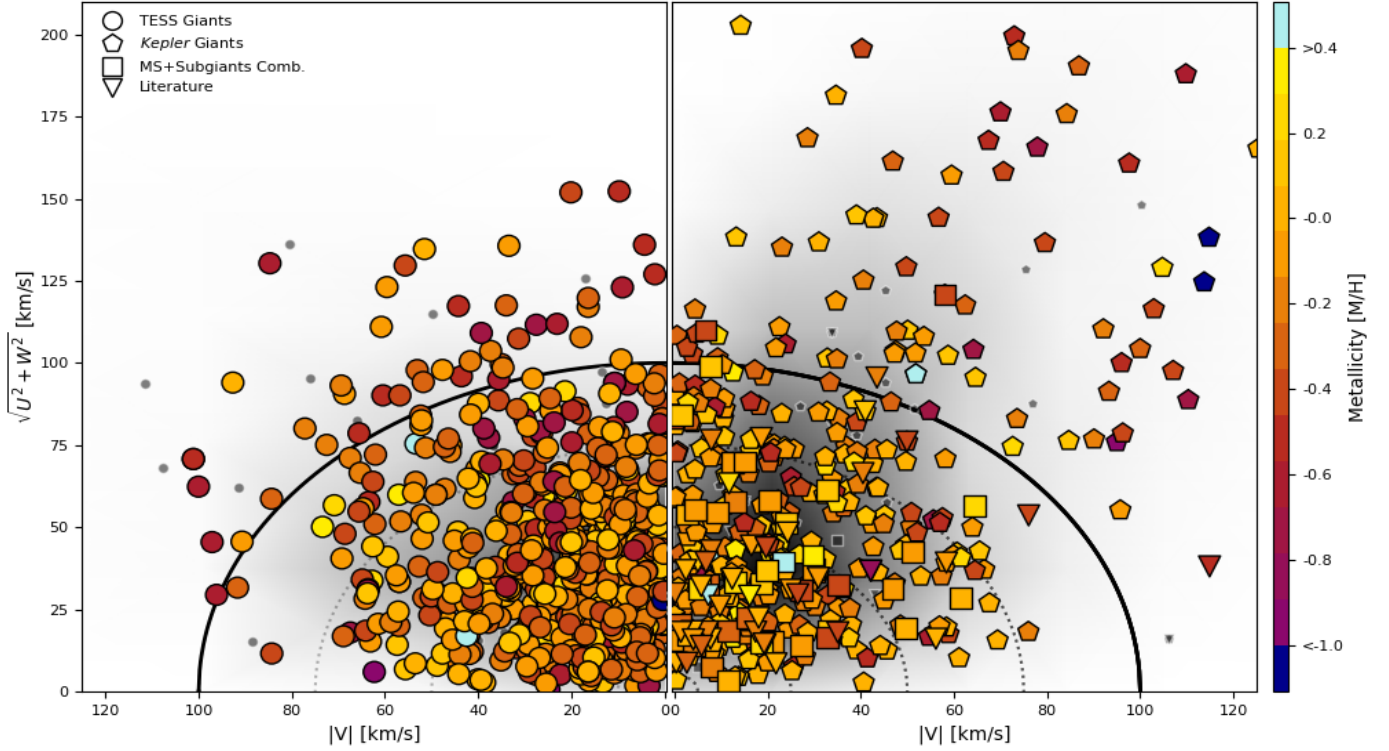


Fig. 9. Distributions of the Galactic space velocities U , V , and W for the red giants in the TESS, and red giants as well as main sequence stars in the *Kepler* and literature samples are shown in the left and right Toomre diagram, respectively. The color of the markers indicates the metallicity. We note that 9 candidate systems have velocity values outside the shown space velocity range in the left panel and 11 in the right panel. The small grey symbols represent the stars without a solution for the metallicity in the *Gaia* DR3. The thick black line marks the approximative separation between the galactic thin ($X \lesssim 100$ km/s) and thick disk ($X \gtrsim 100$ km/s). The form of the markers corresponds to the different samples as presented in Fig. 1. The grey scale in the background shows the distribution of all stars with seismic values in the *Kepler* and TESS samples.

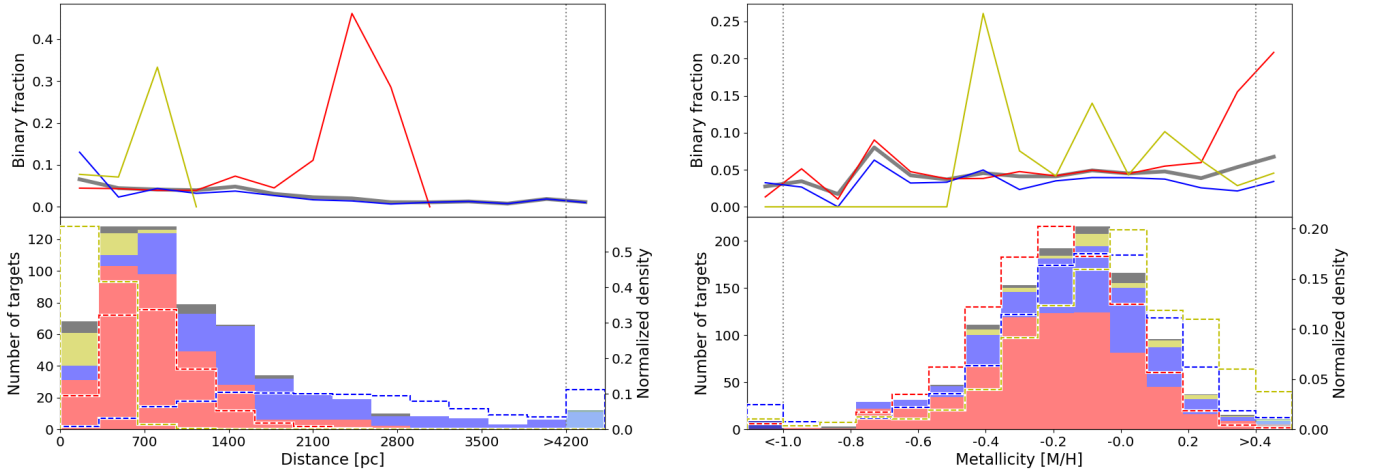


Fig. 10. Binary fractions and distribution of the samples as a function of the distance (left panel) and metallicity (right panel). The top panels visualize the ratio of the number of binary candidates over the whole sample for each bin of the histogram in the bottom panel. The colors represent the samples of giants detected with TESS and the giants, and main sequence stars observed with *Kepler* as red, blue, and yellow, respectively. The thick grey line indicates the total binary fraction. The bottom panels depict the distribution of the distances and metallicities in a histogram. The filled bars correspond to the number of binary solutions of the samples. The samples have the same color as in the top panel, and the black bars represent the literature sample. For comparison, the dashed lines show the normalized density of the corresponding input samples in the same color. The first and last bar of the histogram in the bottom left panel represents all stars with a metallicity lower than -1 and bigger than 0.4 dex, respectively. For the histogram of the distance, the last bar indicates all systems with a distance higher than 4200 pc

velocity determined from spectra taken with the *Gaia* Radial Velocity Spectrometer (RVS, [Gaia Collaboration et al. 2023b](#); [Katz et al. 2023](#), respectively). We note that the published RVS velocities are the average from all visits and are not the true systemic velocity. For simplicity, we used the inverse of the parallax as

the proxy for the distance. Most binary candidates are located in the thin disk ($X \lesssim 100$ km/s). This result is in agreement with the location of the input sample and other ensemble studies (e.g., [Hon et al. 2021](#)). We note that a particular bias is set through the selection criterion of oscillations. Because detecting modes

requires good signal-to-noise ratios (S/N) in the frequency analysis, the sample is biased toward closer and bright objects. The larger mirror size of *Kepler* allows for the detection of oscillations in fainter stars, resulting in a richer population of stars located in the halo. In total, 159 binary candidates are located in the range of $100 \lesssim X \text{ [km/s]} \lesssim 200$, which indicates membership to the thick disk. We also find 22 candidate systems that are likely halo stars ($X \gtrsim 200 \text{ kms}$). Giants in the halo are typical of spectral type K to produce the amplitudes needed to be detectable over such large distance (Mathur et al. 2016; Hon et al. 2021).

The binary yields as a function are depicted in Fig. 10. As expected, we find a clear trend in the binary detection rate (top panel) as a function of the distance (left panels in Fig. 10). As described before, this is connected to the decreasing integrated brightness of the source. This trend is best seen in the combined and *Kepler* sample. The large increase in the binary yields from TESS and *Kepler* dwarfs is due to small number statistics. The histograms of the binary detection (bottom panel) also shows that, as expected from the apparent magnitudes (Fig. 5), the TESS sample contains stars generally closer to earth (within $\sim 1 \text{ kpc}$) while the *Kepler* giant sample is rich in stars in the kiloparsec range. Naturally, dwarfs have a low luminosity. Therefore, all dwarfs that are bright enough to allow for the detection of solar-like oscillations are known to be close ($\lesssim 700 \text{ pc}$).

Previous works have reported a strong trend in the binary occurrence rate as a function of the stellar metallicity, whereby metal poor F, G, and K stars are more likely to be found in binary systems (e.g., Moe & Di Stefano 2017; Badenes et al. 2018; Offner et al. 2022, and references therein). For further interpretation of the sample, we used the metallicity ($[M/H]$) derived from the *Gaia* RVS spectra (mh_gspspec Recio-Blanco et al. 2023; Creevey et al. 2023; Fouesneau et al. 2023). The right panels of Fig. 10 show the binary yields and the histograms of the detection (top and bottom, respectively). For the *Kepler* giants, a weak trend towards higher binary rates with lower metallicities is found, with the peak at $[M/H] \simeq -0.7 \text{ dex}$. For TESS, we find the same low-metallicity peak as for the *Kepler* giants. However for the TESS giants, we find a flat distribution. The increase for $[M/H] \gtrsim 0.2 \text{ dex}$ is likely due to small number statistics. The binary yields of the *Kepler* dwarf sample appear particularly noisy, again due to small number statistics. Therefore, we do not find the expected trend as clearly as it was described in the literature.

4. Orbital evolution through tidal interaction and stellar activity

Stars in binary systems provide many constraints that simplify the ill-constrained parameter space for stellar modeling. However, for a detailed analysis, the effects of the interaction between the two stars need to be considered. The dissipation of tidal energy in the stellar structure influences the parameters of the system and the interior of its stellar components (for comprehensive reviews of tidal theory, see Zahn 2013; Ogilvie 2014; Mathis 2019, and references therein). The tidal forces lead to the circularization of the orbit and the alignment and synchronization of the orbital and rotational spins. In the case of a strong tidal interaction, the additional heat induced by dissipating the kinetic energy of the tides into the stellar structure might lead to an inflation of the stellar radius (Mathis 2013). From the first principles of physics, such extra heat will force the star to adjust its radius to stay in the thermal equilibrium and lead to the expansion of the stellar radius. Because the seismic scaling relation is based on the unperturbed solar case, such departure could

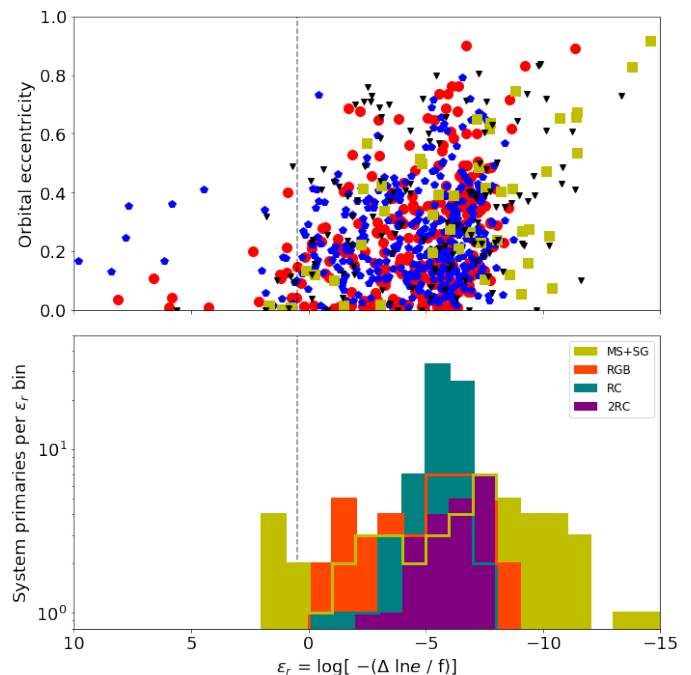


Fig. 11. Orbital eccentricity of the parameterized time scale of the tidally driven orbital circularization, ε_r . The top panel shows the position of all binary candidates in the parameter plane. The histogram in the bottom panel depicts the distribution of ε_r for the systems with an oscillating primary, for which the evolutionary state could be determined from seismology. The color distinguishes between the evolutionary states of secondary clump (2RC), red clump (RC), red giant branch (RGB) in purple, teal, and orange, respectively. Because of their small number and nearby evolutionary state, main sequence and subgiant primaries are shown as one group in yellow (MS+SG). The grey dashed line marked the proposed value of $\varepsilon_{\text{crit}}$.

lead to overestimating the seismically inferred stellar mass and radius. Therefore, it is essential to test the systems used for calibrating the seismic scaling relations for having negligible levels of tidal interaction.

4.1. Strength of the equilibrium tide

Because giant stars have deep convective envelopes and reach large stellar radii, the dominating mechanism for dissipation of tidal energy is expected to be the equilibrium tide (e.g., Mathis 2015; Remus et al. 2012; Gallet et al. 2017). It was confirmed by Beck et al. (2018b) that the dynamical tide could have a small contribution in the subgiant phase and on the very low-luminosity RGB, but is overall negligible for the orbital evolution of the binary system.

Using the formalism of Verbunt & Phinney (1995) (based on Zahn 1977; Hut 1981) to quantify the efficiency of the dissipation of the equilibrium tide, we calculated the rate of the eccentricity reduction in a binary system, which we refer to as ε_r ,

$$\varepsilon_r = \log \left[-\frac{\Delta \ln e}{f} \right]. \quad (5)$$

In this notation, the parameter f is an unknown normalization factor on the order of unity. The change in eccentricity,

$$\frac{\Delta \ln e}{f} = \frac{-1.7}{10^5} \cdot \left(\frac{M_1}{M_\odot} \right)^{-11/3} \cdot \frac{q}{(1+q)^{5/3}} \cdot I(t) \cdot \left(\frac{P_{\text{orb}}}{\text{day}} \right)^{-16/3} \quad (6)$$

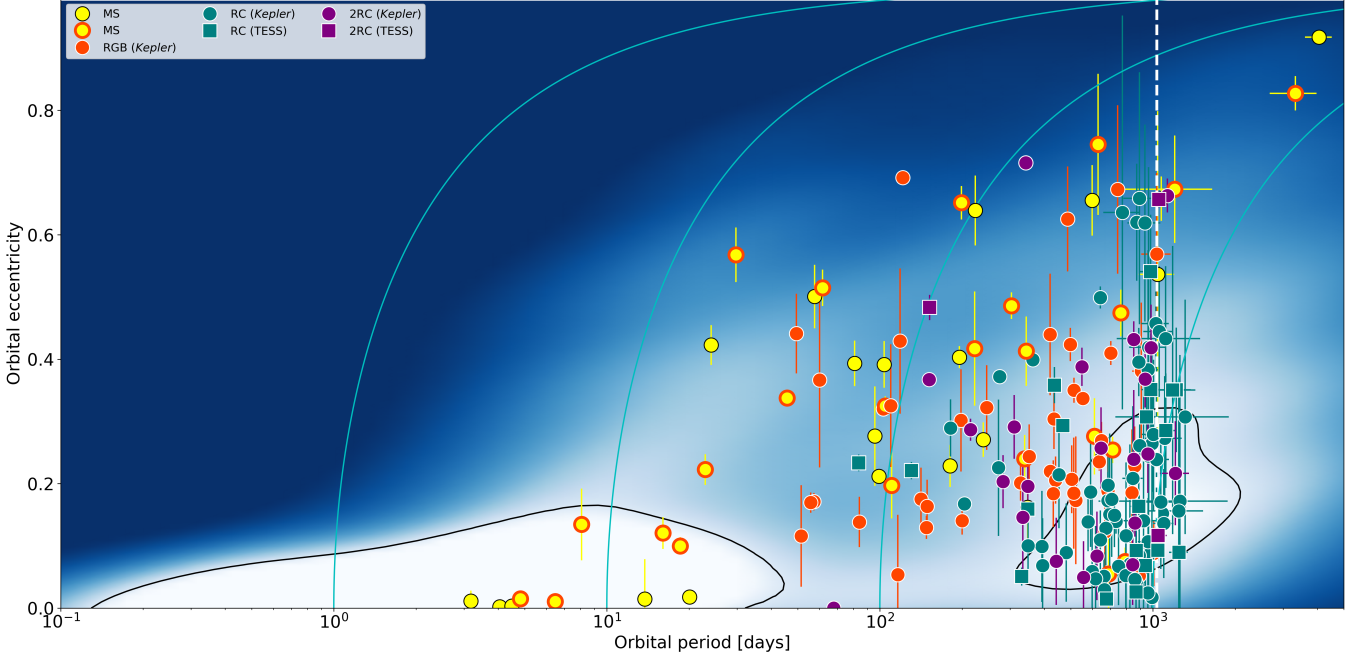


Fig. 12. Orbital periods and eccentricities of the binary systems hosting a primary with identified evolutionary stages. The particular color and the shape of the data points indicate the seismically inferred evolutionary stage and the space mission this star has been observed with, respectively. The light-blue lines indicate the arcs of constant angular momentum in the e - P plane for circular orbital periods for 1, 10, 100, and 1000 days. The background color map represents the normalized probability-density distribution of the full SB9 sample. The black lines envelop the regions with a density of at least seven times the median probability density. The white vertical dashed line represents the 1034 d timebase of *Gaia* DR3.

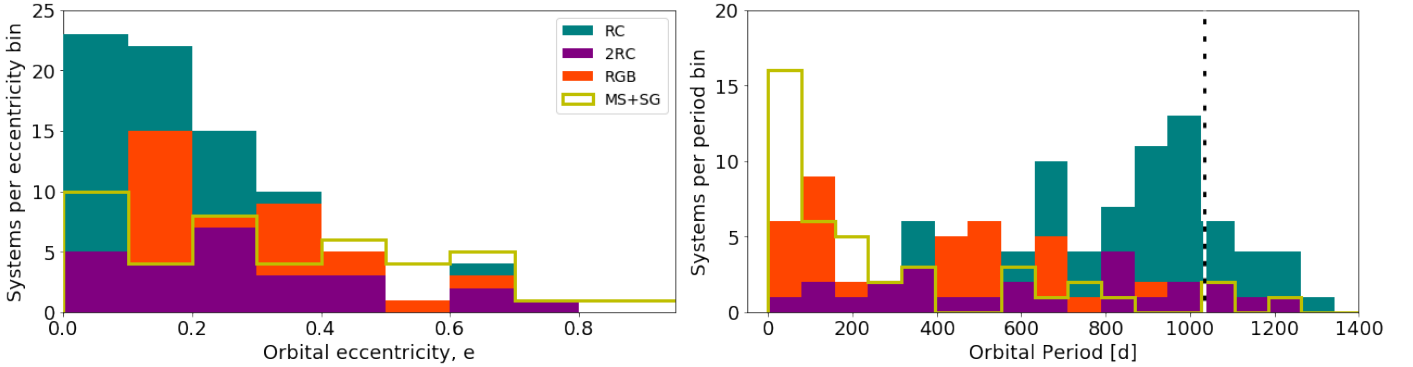


Fig. 13. Distribution of orbital eccentricities, separated by evolutionary stage and channel. The left and right panel give the number of systems per eccentricity and period bin, respectively. The color distinguishes between the evolutionary states of secondary clump (2RC), red clump (RC), red giant branch (RGB) in purple, teal, and orange respectively. Because of their small number and nearby evolutionary state, main sequence and subgiant primaries are shown as one group in yellow (MS+SG). The vertical dashed line represents the 1034 days timebase of *Gaia* DR3.

with $q=M_2/M_1$ as the mass ratio between the system's secondary and primary components, incorporates the third Keplerian law and the circularization function,

$$I(t) = \int_0^t \left(\frac{T_{\text{eff}}}{4500 K} \right)^{4/3} \cdot \left(\frac{M_{\text{env}}(t')}{M_{\odot}} \right)^{2/3} \cdot \left(\frac{R_1(t')}{R_{\odot}} \right)^8 dt' [\text{yr}]. \quad (7)$$

This function is dependent on the effective temperature (T_{eff}), the mass in its convective envelope (M_{env}), and most importantly, the stellar radius (R_1) of the primary. Because the circularization function depends on the eighth power of the primary radius, the equilibrium tide will become increasingly important as a star advances the red giant branch. Following the approach of Beck et al. (2018b), we used the asteroseismic masses and radii, calculated as described in Section 3.1, for this analysis.

The top panel of Fig. 11 depicts the distribution of the binary systems as a function of the change in eccentricity. By construc-

tion, large values of ε_r indicate strong tidal interaction in a system. Verbunt & Phinney (1995) suggested that an $\varepsilon_{\text{crit}} = 0.478$ approximates the segregation between the systems with strong and less efficient tides. As $\varepsilon_{\text{crit}}$ is not a sharp limit, eccentric binaries with values slightly above this value could be short-lived systems that are about to circularize. Kroupa (1995) coined the term "forbidden binaries" for this group. Previous studies (e.g., Verbunt & Phinney 1995; Beck et al. 2018b; Benbakoura et al. 2021) did not show eccentric systems at values of $\varepsilon_r \gtrsim 3$. These outliers are very likely unphysical and originate from significantly underestimated orbital periods in the TBO. Therefore, most of the system candidates depicted in Fig. 11 have reported periods in the TBO that are physically meaningful.

The lack of systems with values $\varepsilon_r > \varepsilon_{\text{crit}}$ in Fig. 11 is a result of the selection of only oscillating objects. Several papers have demonstrated (Gaulme et al. 2016; Beck et al. 2018b; Mathur

et al. 2019; Benbakoura et al. 2021) that the tidally driven spin of the outer stellar layers increases the dynamo action. The increased magnetic activity suppresses solar-like oscillations. Beck et al. (2018b) indeed showed that this limit also separates between system hosting giants with oscillating ($\varepsilon_r \lesssim \varepsilon_{\text{crit}}$) and non-oscillating giant primaries ($\varepsilon_r \gtrsim \varepsilon_{\text{crit}}$). Furthermore, a dependency on the orbital eccentricity can be assumed due to increased tidal strength and additional effects if the system encounters Roche-lobe overflow at the periastron. The resulting distribution of $\varepsilon_{\text{crit}}$ supports the test using the approximation of the Roche-lobe radius, shown in Fig. 6.

The main sequence stars are typically located at intermediate to shorter periods (Fig. 8). For this class of stars, the formalism presented in Eq. 5 to 7 separates well the circularized from the eccentric systems. It is interesting to note that in Fig. 11 the main-sequence dwarfs are the group of stars that extends to the lowest values of ε_r . This is a consequence of the much smaller radii and convective envelopes of solar-like dwarfs compared to red giants. In such stars, radiative structures become significant, necessitating the inclusion of the dynamical tide to accurately describe the tidal budget of the system (Ahuir et al. 2021; Barker 2022). For stellar objects cooler than the Kraft-break limit and orbital periods less than ~ 10 days, the dynamical tide is so efficient that systems are quickly circularized and synchronized (Offner et al. 2022, and references therein).

4.2. Distribution of orbital eccentricities and periods

Binary systems hosting solar-like stars are expected to be born with a flat distribution of eccentricities over a wide range of eccentricities (Moe & Di Stefano 2017; Mirouh et al. 2023). The subsequent tidal evolution is a function of dwell time and the advances in stellar evolution of both binary components. Therefore, we can study the impact of tidal forces from the distributions of the parameters in distinct evolutionary stages.

Hereby, the efficiency of the dissipation of tidal energy has been debated in the literature. In the current understanding, eccentric binaries with an evolved component should have circularized during phases of their evolution when they have expanded to large radii. Verbunt & Phinney (1995) argued that because of the high radius dependence, they expect all systems hosting a red-clump star or an AGB to be circularized. Similar behavior is expected long before the onset of RLOF (e.g., see Vos et al. 2015). Yet, contrary to this prediction, Beck et al. (2018b) pointed out the existence of red clump stars in eccentric binary systems. This finding agrees with the eccentricity distributions found in the large sample study of APOGEE time series spectroscopy by Badenes et al. (2018). Furthermore, wide hot-subdwarf binaries are almost all eccentric, even though the primary is a post-RGB star that underwent a mass-loss episode near the tip of the RGB (e.g., Vos et al. 2013, and references therein). Further examples are Ba stars, and Tc-poor S stars (e.g. Van der Swaelmen et al. 2017), symbiotic stars (e.g., Merc et al. 2019b), RV Tauri binaries (e.g., Escorza et al. 2020) or dusty post-AGB stars (e.g., Gorlova et al. 2014), all of which can occur in binary systems with significantly non-zero eccentricities, even though they should have circularized if their periods are shorter than ~ 3000 days (Pols et al. 2003). To explain the eccentricities found in red giant binary systems, Nie et al. (2017) suggested from modelling the binary evolution that the efficiency of the current formalism could be overestimated by a factor of 100.

Solar-like oscillators cover a wide range of evolutionary phases and channels. From such a sample, we can probe the distribution of the orbital eccentricities and periods as a function of

the evolutionary states to learn more about the efficiency of the equilibrium tide. Figure 12 shows the position of systems with a solar-like oscillator with a known evolutionary state in the e - P plane. The sample sizes of the various evolutionary stages, presented in Section 3.2, are sufficient to derive general conclusions. To better quantify and discuss the distributions of these four groups, we present their distribution in histograms (shown in Fig. 13).

Stars on the main sequence are significantly less evolutionarily advanced than any star in the giant phase and consequently closer to the system's initial conditions. As discussed above, these stars have smaller radii which in wider binary systems ($P_{\text{orb}} \gtrsim 10$ d) results in lower tidal interaction compared to the equilibrium tide. This is the reason why systems with primaries in this evolutionary phase, which lasts two orders of magnitude longer than the red giant phase, retain a relatively flat eccentricity distribution between $0 \lesssim e \lesssim 0.9$, originating from the birth distribution of e .

The situation changes for systems hosting a post-main sequence star. Even considering that the eccentricities have rather large error bars compared to typical values from ground-based RV monitoring, a general trend is found to show that red giant stars have lower eccentricities than main sequence stars. Overall, RGB stars are found between $0.1 \lesssim e \lesssim 0.7$. The lack of circularized systems ($e \lesssim 0.1$) with RGB primaries is in agreement with previous studies (Beck et al. 2014, 2022; Gaulme et al. 2014; Benbakoura et al. 2021). Clear differences are found among the two stages of the quiescent helium-core burning, which occupy different regions in the HRD. While the RC stars have their highest occurrence rate below $e \lesssim 0.2$, the more massive 2RC stars show a flat distribution between $0 \lesssim e \lesssim 0.8$, similarly to the main sequence stars.

These differences in the distributions are likely to be the product of the accumulated tidal history along the stellar evolution. If the mass of a star is $M_{\star} \lesssim 2 M_{\odot}$, the inert core will degenerate before it reaches the ignition temperature of He. To obtain the energy to again lift the core degeneracy, the star needs to reach a high luminosity, which forces the star to keep expanding (see Hekker et al. 2020, and references therein) until the core ignites and the star's envelope readjusts. Due to the degeneration, all cores of RGB stars of a given luminosity are similar independent of their mass and metallicity ($\log(L/L_{\odot}) \approx 3.4$, Serenelli et al. 2017). At the tip of the RGB, a star has $\sim 175 R_{\odot}$. In stars with masses $M_{\star} \gtrsim 2 M_{\odot}$, the core reaches the ignition temperature before the central regions degenerate. Consequently, such a star will ignite He in its core much earlier and at smaller radii ($\sim 30 R_{\odot}$), thus settling in the less luminous secondary clump.

The important aspect between RC and 2RC in the context of the tidal analysis is the difference in their maximum radius on the RGB. Because the equilibrium tide depends strongly on the stellar radius, systems hosting 2RC stars are expected to be far less circularized than those hosting RC primaries. Another effect that could lead to lower eccentricities is mass transfer if the system had episodes of RLOF.

The range of higher eccentricities in the RGB sample results from an observational bias. By selecting oscillating giants with resolved seismic parameters and evolutionary states, we limit ourselves to giants on the lower part of the RGB with radii $4 \lesssim R/R_{\odot} \lesssim 12$ (see Fig. 1 and 6). Therefore, the stars in the RGB sample are preferentially smaller and observed prior to maximal tidal interactions.

While many systems are expected to be found between 1 000 and 2 000 d, the pronounced peak of periods of 1000 days is likely to be an artifact of the *Gaia* DR3 solutions because pe-

Table 2. Rotation and photospheric activity for primaries of detected binary systems.

KIC	P_{orb} [d]	e	P_{rot} [d]	$P_{\text{orb}}/P_{\text{rot}}$	Type	ν_{max} [μHz]	$\Delta\nu$ [μHz]	S_{ph} [ppm]	Ref
4914923	99.24±0.07	0.21±0.01	24.5±3.8	4.04	ASB1	1825±107	88.57±2.46	125.3±3.7	[1]
5516982	24.12±0.02	0.42±0.03	24.5±2.0	0.98	SB1	1699±109	85.0±1.91	134.0±4.6	[1]
5696625	611.35±7.2	0.28±0.06	10.6±1.3	57.89	ABS1	696±4	39.24±3.22	105.1±5.9	[1]
5814512	222.54±1.34	0.42±0.09	5.6±0.7	39.39	ORB	995±21	53.35±1.66	82.5±6.5	[1]
(h) 7206837	4.05±0.0	0.0±0.01	4.0±0.3	1.0	SB1	1645±120	79.17±1.76	234.2±16.1	[1]
(b) 7668623	4.82±0.0	0.01±0.01	5.5±0.4	0.88	–	822±45	46.82±1.51	843.1±46.9	[1]
8016496	711.7±11.52	0.25±0.02	10.9±0.8	65.23	ASB1	1045±29	53.99±1.5	93.6±5.3	[1]
8414062	791.36±7.68	0.07±0.02	11.0±0.8	71.94	ASB1	1100±13	72.74±2.27	104.2±5.3	[1]
8677016	347.4±4.32	0.16±0.06	29.6±2.5	11.74	SB1	1882±53	92.64±2.37	78.5±2.7	[1]
9025370	239.12±0.45	0.27±0.03	23.2±3.5	10.3	ORB	3045±75	131.43±3.42	250.9±6.5	[1]
9098294	20.1±0.0	0.02±0.01	19.9±1.3	1.01	SB1	2368±102	110.0±3.16	223.8±7.0	[1]
9209245	22.92±0.0	0.22±0.02	22.6±1.4	1.02	SB1	1017±19	53.86±1.5	155.2±5.3	[1]
9225600	343.75±2.01	0.41±0.06	9.0±0.7	38.24	ASB1	1192±29	64.01±1.77	32.7±2.7	[1]
(f) 9328372	95.9±0.58	0.28±0.08	3.9±0.7	24.47	SB1	1379±48	68.66±1.82	307.2±22.2	[1]
(c) 9390670	1041.87±156.35	0.54±0.26	3.6±0.2	293.48	SB1	1351±26	71.07±1.97	705.4±49.1	[1]
9702369	195.76±0.3	0.4±0.02	11.6±0.9	16.88	ASB1	2039±118	94.05±2.36	50.5±2.5	[1]
(e) 9898385	13.78±0.01	0.01±0.06	3.4±0.3	4.1	SB1	1352±33	69.29±1.92	368.9±27.5	[1]
(g) 10355856	4.49±0.0	0.0±0.01	4.5±0.3	1.0	SB1	1320±79	67.41±1.31	299.8±19.6	[1]
(a) 10775748	6.48±0.0	0.01±0.01	6.4±0.5	1.01	SB1	997±10	60.88±1.82	843.2±43.8	[1]
11862497	598.79±7.41	0.66±0.06	4.6±0.4	129.89	ORB	1888±47	90.7±2.09	88.6±7.0	[1]
12317678	80.84±0.06	0.39±0.04	3.7±0.7	21.97	ORB	1244±79	63.49±1.18	51.4±4.2	[1]
3942719	339.26±1.41	0.24±0.04	38.0±5.0	8.94	ASB1	788±27	45.2±1.66	532.8±6.45	[2]
3952580	45.74±0.02	0.34±0.01	89.8±7.6	0.51	SB1	636±22	37.09±1.11	140.6±1.16	[2]
6587236	688.01±17.57	0.05±0.09	17.9±2.2	38.46	ASB1	499±2	32.09±1.57	89.8±2.28	[2]
8408931	18.57±0.0	0.1±0.01	18.4±1.3	1.01	SB1	609±4	33.98±1.54	192.34±3.4	[2]
(d) 9163769	3.17±0.0	0.01±0.02	3.2±0.2	1.0	SB1	1573±11	80.62±1.88	451.47±17.89	[2]
10732098	199.15±0.46	0.65±0.03	25.6±6.0	7.79	ASB1	1055±42	60.11±1.85	85.65±1.76	[2]
11709205	57.9±0.02	0.41±0.01	58.0±3.3	1.0	SB1	271±12	18.95±0.87	224.65±2.28	[2]
3437031	623.74±10.24	0.08±0.07	138.8±7.2	4.49	ASB1	63±3	5.6±0.18	–	[3]
4358067	139.5±0.58	0.34±0.06	67.5±4.4	2.07	ASB1	4±0	0.71±0.04	–	[3]
4758020	290.39±6.41	0.18±0.18	124.2±4.7	2.34	SB1	92±6	7.5±0.14	–	[3]
5087190	959.44±106.84	0.33±0.15	66.1±9.5	14.51	SB1	70±3	6.08±0.13	–	[3]
5382824	653.29±4.31	0.11±0.02	92.2±7.9	7.08	SB1	100±4	8.0±0.23	–	[3][4]
5439339	98.04±0.07	0.03±0.02	60.4±5.3	1.62	SB1	99±5	7.89±0.28	–	[3][4]
5534910	851.96±38.35	0.24±0.11	94.8±6.7	8.99	SB1	112±5	8.26±0.24	–	[3]
5707338	885.17±14.19	0.27±0.07	60.4±4.3	14.65	SB1	81±4	6.49±0.18	–	[3]
6032639	979.76±45.02	0.29±0.07	123.4±4.1	7.94	SB1	46±2	4.73±0.15	–	[3][4]
6933666	48.34±0.11	0.18±0.08	99.2±2.6	0.49	SB1	34±2	3.83±0.12	–	[3][4]
7661609	106.58±0.08	0.19±0.01	104.6±3.1	1.02	SB1	23±1	2.7±0.4	–	[3]
8365782	702.84±5.19	0.07±0.02	116.0±4.1	6.06	SB1	81±3	6.3±0.13	–	[3]
8825444	128.52±0.21	0.04±0.02	83.7±7.6	1.54	SB1	83±4	6.57±0.15	–	[3]
8936339	796.03±54.97	0.05±0.12	103.2±5.0	7.71	SB1	44±2	4.62±0.62	–	[3]
9086060	453.2±11.43	0.21±0.09	81.0±4.0	5.59	SB1	48±2	4.77±0.16	–	[3]
9240941	254.08±11.04	0.13±0.04	125.2±6.3	2.03	SB1	110±5	8.34±0.18	–	[3]
9469212	992.55±141.7	0.26±0.14	68.4±6.7	14.5	SB1	45±2	4.31±0.12	–	[3]
9898373	617.06±16.97	0.05±0.08	128.6±6.8	4.8	SB1	45±3	4.73±0.63	–	[3]
10148118	388.24±2.65	0.06±0.03	89.7±9.1	4.33	SB1	62±3	5.46±0.19	–	[3]
10935853	882.61±17.57	0.3±0.07	62.6±5.6	14.11	SB1	65±3	5.76±0.13	–	[3]
11650041	107.17±0.29	0.04±0.05	53.0±7.9	2.02	SB1	8±0	1.41±3.07	–	[3]
12314910	69.53±0.06	0.02±0.02	104.5±3.7	0.67	SB1	24±1	2.91±0.08	–	[3][4]

Notes. The star’s identifier in the *Kepler* input catalog is given in the first column. The next columns report the period P_{orb} and eccentricity e of the orbit as reported in the *Gaia* DR3 TBO catalog. The next column corresponds to the period of the surface rotation P_{rot} of the primary, determined from the light curve analysis. $P_{\text{orb}}/P_{\text{rot}}$ reports the ratio between the orbital and rotation period, whereby $P_{\text{orb}}/P_{\text{rot}}=1$ suggests that orbit and surface rotation are synchronized. The next three columns give the global seismic parameters of the power excess and large frequency separation as well as the photospheric activity indicator S_{ph} . The last column reports the main references for the target, where [1] refers to Santos et al. (2021), [2] to García et al. (2014b), [3] to Ceillier et al. (2017), and [4] to Beck et al. (2022).

riods longer than that are often underestimated (Fig. 2, and 6). However, Fig. 12 strongly indicates that the excess of giants in system periods around 1 000 days results from He-core burning stars. We interpret the reduced eccentricity scatter for RC pri-

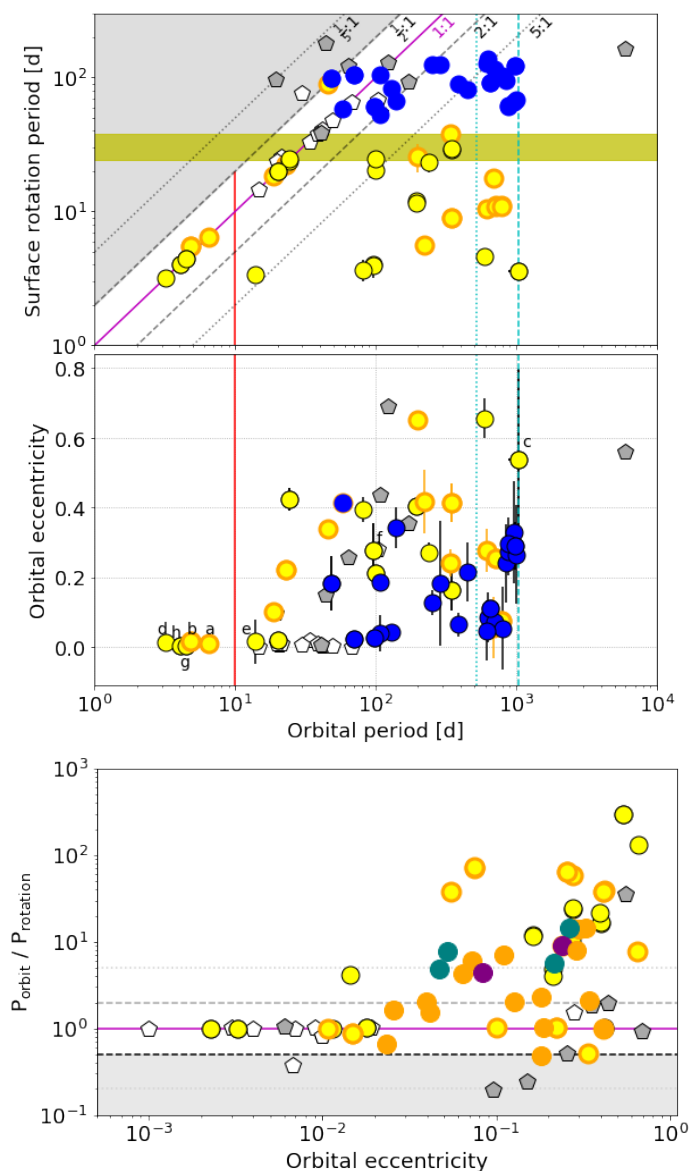


Fig. 14. Synchronization and circularization of binary systems, hosting solar-like oscillators. The top and middle panel show the surface rotation periods of the primary and orbital eccentricities for binary systems as a function of their orbital period, respectively. The bottom panel presents the ratio $P_{\text{orbit}}/P_{\text{rotation}}$ as a function of the orbital eccentricity. Yellow, orange, and blue dots indicate dwarfs, subgiants and red giants, observed with *Kepler*, respectively. Grey pentagons indicate systems reported previously in the literature. Filled and open symbols denote oscillating and non-oscillating primaries, respectively. The inclined lines represent the resonance ratios $P_{\text{orb}} : P_{\text{rot}}$ as indicated to the right of the line. The solid magenta line indicates the synchronization of the surface rotation with the orbit ($P_{\text{orb}} = P_{\text{rot}}$). The grey shaded area depicts the region in which the dynamical tide cannot be excited ($2 \cdot P_{\text{orb}} < P_{\text{rot}}$). The yellow shaded area indicates the range of the solar sidereal surface rotation. The solid vertical red line indicates the limiting period for synchronization and circularization on the main sequence ($P_{\text{circ}} \approx 10$ d). The vertical dashed and dotted lines indicate the length and half the length of the *Gaia* DR3 mission timebase.

maries ($0.1 \leq e \leq 0.5$) compared to RGB primaries to be the result of tidal interactions.

The effect of the radius dependence on the tidal strength is also seen in the period distributions as a function of the four evolutionary stages. Because RC stars have already reached their

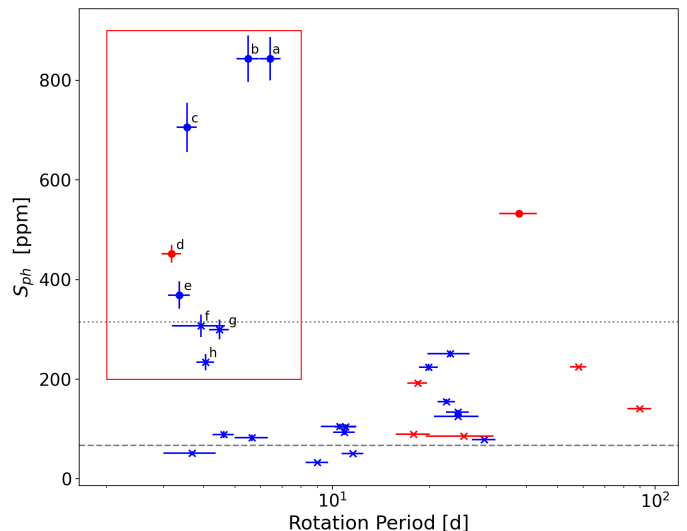


Fig. 15. Photospheric activity of main sequence stars in binary candidates of *Gaia* DR3 as a function of the rotational period. Red and blue markers indicate rotation periods reported by García et al. (2014b) and Santos et al. (2021), respectively. If measurements in both references are given, the Santos et al. (2021) value is shown. For comparison, the minimum and maximum S_{ph} value of solar cycle 23 are shown as dashed horizontal lines. The red box frames the distinct group stars of short rotation periods and mostly super-solar levels of stellar activity. The labels a-h provide cross identification with the stars in Fig. 14 and Table 2.

maximum radius on the RGB, many systems with periods below ~ 500 days could have undergone a common-envelope phase, potentially leading to the destruction of the giant primary. Therefore, we only see RC systems at longer periods, while RGB, 2RC, MS, and SG are also found at short periods. This is also seen in the typical tidal strength ε_t for both evolutionary stages. Figure 11 depicts that the remaining RC systems, because of their smaller radii and wider orbits have indeed much lower tidal interaction than RGBs.

4.3. Surface rotation and stellar activity

The rotational behavior of stellar components of a binary system is strongly connected to tides (Zahn 2013; Ogilvie 2014). The subsequent phases of pseudo-synchronization and full synchronization of the stellar rotation with the orbital motion of the binary are steps of the evolutionary path to the equilibrium state. Particularly for red giant stars, with their slow rotation period, the tidal spin-up of the envelope will give rise to strong magnetic fields through the triggered dynamo action. Lately, from photometric and chromospheric-emission measurements, Gaulme et al. (2020) and Gehan et al. (2022) showed that red giants belonging to binary systems in a configuration of spin-orbit resonance display an enhanced magnetic activity compared to single stars with the same rotation rate. Therefore, stellar rotation and activity are key observables of stars that provide information about tidal interaction.

The level of activity and the rotational period can be estimated from the rotationally modulated flux signal introduced by dark stellar spots being rotated in and out of the line of sight of the observer (Mathur et al. 2019, and references therein). For the solar-like main-sequence and red giant stars in our binary candidate sample, rotation periods were derived from the dominant period of the brightness modulation, determined through auto-correlation and wavelet analysis of the *Kepler* photometry

by [García et al. \(2014a\)](#), [Ceillier et al. \(2017\)](#) and [Santos et al. \(2021\)](#). We assume that the spots originate from the more luminous, oscillating component. The values are reported in Table 2.

The full new picture of the extended sample is shown in Fig. 14. As a reference, the range of the equatorial and polar rotation of the Sun is shown in this picture (27 and 35 days, respectively). Most of the main-sequence primaries with determined rotation periods spin significantly faster than the Sun or at least with solar-like rotation rates. Depending on the orbital period of the systems, we find three distinct forms of appearance related to the interplay between rotation and orbital eccentricity. As expected from theoretical predictions, the surface rotation of stars in systems with orbital periods below ten days is synchronized and the orbit is circularized ([Ogilvie & Lin 2007](#); [Barker 2022](#)). Dwarf-hosting systems with periods up to ~ 30 days are still pseudo-synchronized but have a wider range of eccentricities. For these groups, the rotational period is influenced by the tidal interaction. Therefore, the age of the primary cannot be determined from the relation between the surface rotation period and stellar age, known as gyrochronology ([Barnes 2007](#)). We do not see any relation between the rotational and orbital periods for systems with orbits longer than the solar rotation rate. Given that these stars have rotation periods shorter than the solar rate, we can estimate that these systems are typically younger than the Sun.

The analysis depicted in Fig. 14 also reveals a fundamental difference between dwarfs and giants. As mentioned above, no oscillations are found in giants in circularized and synchronized systems (typically with $P_{\text{orb}} \lesssim 20$ days [Gaulme et al. 2014](#); [Beck et al. 2018b](#)). The eight dwarfs and subgiants in circularized and synchronized systems on much shorter periods (stars a-h), however, do oscillate. A detailed analysis of this finding is beyond the scope of this paper.

For 28 of the main sequence stars, the catalogs by [García et al. \(2014a\)](#) and [Santos et al. \(2021\)](#) provide an estimate of the average photospheric activity. The S_{PH} value is the mean, standard deviation of the photometric variation in a sliding boxcar, with a timescale of five times the rotation period ([Mathur et al. 2014](#); [García et al. 2014b](#)). The top panel of Fig. 15 compares these values with the minimum and maximum value of S_{PH} from solar cycle 23, determined by [Salabert et al. \(2017\)](#). As can be seen from this depiction, about 80% of the systems exhibit a solar-like activity level. These are typically longer periodic systems. One separate group of eight highly active stars at short periods stands out. To better reference individual members of this group, we labeled them with letters from *a* to *h* in Fig. 15 (see red box).

To separate if this activity is caused by tides or is simply a young, rapidly spinning star, we present these primaries in the context of their orbital parameters in the middle panel of Fig. 14. If tides are efficient and lead to a tidal spin up this leads to more efficient excitation (and dissipation) of tidal inertial modes and thus a more efficient synchronisation and circularisation. Six of the eight active stars are indeed found in short periodic and circularized systems ($e \approx 0$, $P_{\text{orb}} \lesssim 11$ days). For these stars, the reason for the enhanced activity is very likely rooted in the tidal interaction. Two stars from this active group are found in wide orbits. If the orbital period listed in the TBO catalog of $\sim 1\,000$ days for star *c* is correct, even at such high eccentricity ($e \approx 0.55$) for such wide orbits, tides will not produce a lasting effect on the rotation. Similar can be assumed for star *f* with a period of ~ 100 days, and an eccentricity of 0.3. Because no significant tidal interaction is present in these systems, their high activity is likely an effect of young and rapidly rotating stars ([Skumanich 1972](#)). All

other stars showing solar-like activity values are at orbital periods longer than 11 days.

For the red giants, the picture is a different one. For the new systems, the orbital periods range from 30 to 1000 days, while their primaries rotate with periods between 50 to about 200 days. These rotation periods are typical for giants on the less-luminous part of the RGB. Typically, giants have low spot-filling factors. Only a few systems show the signature of spots in their light curves ([Ceillier et al. 2017](#)). The rapid rotators among them could be the product of stellar mergers (e.g., [Tayar et al. 2015](#); [Patton et al. 2023](#)). In the bottom panel of Fig. 14, we show the ratio of the orbital period to the surface rotation period as a function of the orbital eccentricity. This form shows that hardly any of the systems are synchronized. Only a few systems with shorter periods and stronger equilibrium tides are nearly pseudo-synchronized. Also, their measured spot signature could originate from internal processes that trigger the dynamo ([Charbonnel et al. 2017](#)).

5. Orbital inclinations and eclipsing binaries

The mass of a star is the single most fundamental parameter for understanding its structure and evolution. Depending on the type of star, different techniques can be applied to determine the stellar mass (see [Serenelli et al. 2021](#), for a review). While many mass-determination techniques report high precision, the question of how accurate is the mass can only be answered from the cross-calibration of independent techniques.

The most basic technique is the derivation of the dynamical masses of the stellar components in a binary system (for details see [Prša 2018](#), and references therein). The precision of this technique relies on well-determined orbital parameters, radial-velocity amplitudes for both components (SB2), and the orbital inclination. The method's bottleneck is the knowledge of the inclination, which is traditionally determined through modeling eclipsing binary systems. Only for 17 eclipsing systems hosting an oscillating component dynamical masses are available from the literature ([Gaulme et al. 2016](#); [Benbakoura et al. 2021](#)). From such an analysis, [Gaulme et al. \(2016\)](#) suggested that the seismic scaling relations overestimate mass and radius by 15% and 5%, respectively. New systems with known orbital inclinations are needed to solve this dichotomy between seismic and dynamical masses. To increase the sample size, we tested whether *Gaia* DR3 contains oscillators in yet unknown eclipsing systems or systems with determined orbital inclinations.

5.1. *Gaia* epoch and TESS time series photometry

The probability, θ_{Ecl} , of a randomly orientated binary system to show eclipses is a function of the sum of the radii of the components (R_1 , and R_2) and the average distance a (assuming $e=0$) between ([Deeg & Alonso 2018](#)). Using Kepler's third law, we can express this as a function of the orbital period and the sum of the mass of the components (M_1 , and M_2):

$$\theta_{\text{Ecl}} = \frac{R_1 + R_2}{a} = \frac{R_1 + R_2}{\sqrt[3]{(M_1 + M_2) P_{\text{orb}}^2}}. \quad (8)$$

The maximum radius of a solar-like star is less than 1AU. Due to the high dependence on the mass difference between both components, it is unlikely, that both targets reach the maximum expansion simultaneously. Typical binary systems are found with values of a up to several thousand AU (corresponding to orbital

Table 3. Candidates from the eclipsing binary *Gaia* DR3 catalog with at least one oscillating component.

TIC	Frequency (geom.) [d^{-1}]	ν_{max} [μHz]	$\Delta\nu$ [μHz]	Reference for seismic values	Data	Comment
235050452	0.09336 ± 0.00002	98 ± 10	9.2 ± 0.1	Mackereth et al. (2021)	6S	Surface or synchronized rotation?
272357503	0.99314 ± 0.00001	51 ± 13	5.7 ± 0.2	Mackereth et al. (2021)	23S	
293937699	0.26058 ± 0.00006	47 ± 4	6 ± 20	Mackereth et al. (2021)	16S	Eclips.Bin., actual period: 65.112 d
33767523	0.04607 ± 0.00003	–	–	–	18S	$P_{\text{orb}} = 49.63 \pm 0.02$, $e = 0.33 \pm 0.01$
268157208	0.02770 ± 0.00008	47.49	4.804	Yu et al. (2018)	1Q, 3S	= KIC 8646982

Notes. The first column reports the identifier of the eclipsing binary candidate in the *TESS Input Catalogue* (TIC). The column 'Frequency' specifies the frequency of geometric model of the eclipsing binary light curve. The third and fourth column report the mean seismic parameters ν_{max} and $\Delta\nu$ from Mackereth et al. (2021), respectively. Those seismic parameters were extracted from the references shown on the next columns. The column 'Data' reports how many Sectors (S) of TESS, or Quarters (Q) of data was available for these systems at the time of the analysis. Comments on the system are provided in the last column: the priode reported for TIC 293937699 was redetermined from TESS data; the orbital parameters for TIC 33767523 are reported in the TBO catalog by Gaia Collaboration et al. (2023a).

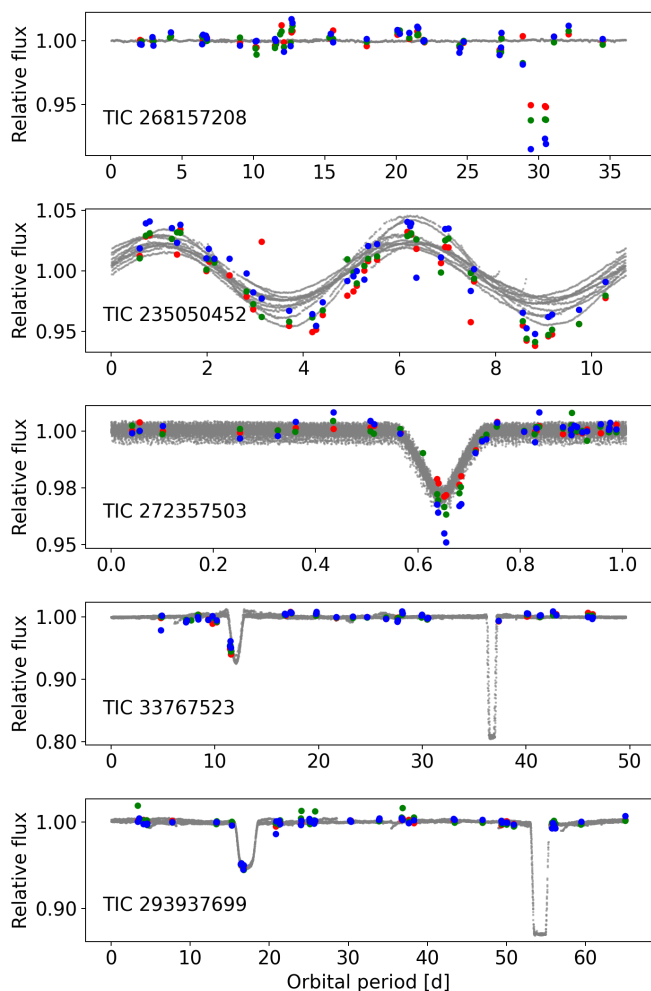


Fig. 16. Phase-folded TESS light curves of the *Gaia* DR3 eclipsing binary system candidates, TIC 268157208 (top panel), TIC 235050452 (second panel), TIC 272357503 (third), TIC 33767523 (fourth), and TIC 293937699 (bottom). Relative *Gaia* epoch photometry in the G , G_{BP} , and G_{RP} passbands are shown in green, blue, and red, respectively. For TIC 268157208, TIC 235050452, TIC 272357503 the period from the *Gaia* DR3 eclipsing binary catalog was used to fold the light curve. For TIC 3376752 the orbital period from the SB1 solution, provided in the TBO catalog is used. For TIC 293937699 we used our orbital period, determined from the TESS data.

periods of tens of thousands of years), which provides very low probabilities for detecting eclipsing binary systems.

Finding eclipsing binaries becomes increasingly challenging with longer orbital periods, as the projected surface that is eclipsed is becoming smaller and requires a nearly perfect alignment at 90 degrees. On the contrary, observing a binary system through RV monitoring, a few well-spread spectroscopic measurements are sufficient to confirm the object's binary nature and even fit the orbital parameters. However, an eclipsing binary can only be detected during the eclipsing phases through direct observations of the eclipses in the photometry or the Rossiter-McLaughlin effect on the radial velocities. The successful photometric search for yet unknown eclipsing binary systems requires continuous monitoring. Consequently, almost all systems hosting an oscillating red giant detected in the *Kepler* data have periods shorter than the mission duration of four years.

As discussed by Beck et al. (2022), such photometric detection strategy introduces a bias where eclipsing systems identified by satellites tend to have short periods. Such relatively short-period binary systems are not wide enough for luminous red giants at the tip of the red giant branch to remain in a detached configuration. Therefore, the previous literature sample is strongly biased toward the assumption of young RGB stars as the primary component, thus hardly containing RC stars.

The quasi-random single-epoch observing strategy of *Gaia*, originating from the scanning law, is not optimal for detecting long-periodic eclipsing binaries and explains why hardly any such eclipsing binaries have been found by the mission (see Fig. 4 in Gaia Collaboration et al. 2023a). See Appendix A of Eyer et al. (2017) for more details on the time sampling of *Gaia*. During a field-of-view transit of a star three photometric measurements are obtained within less than a minute: a broadband visual G , and two narrower blue G_{BP} and red G_{RP} passbands (Riello et al. 2018, 2021). The latter two are derived from integrating low-resolution photo-spectroscopic measurements of the BP and RP instrument, respectively (for more details see Sect. 3.3.6 of Gaia Collaboration et al. 2016). This data is quasi-randomly sampled over the mission duration. Mowlavi et al. (2023) provided a catalog (vari_eclipsing_binary) of 2.2 million eclipsing binary candidates in *Gaia* DR3, of which a subset of 86918 stars were fitted for astrophysical parameters and published in `gaiadr3.nss_two_body_orbit` with `nss_solution_type` set to 'EclipsingBinary' (EB). The search of the catalog of eclipsing binaries for the full seismic sample returned five candidates, which are presented in Table 3 and Fig. 16.

To validate these candidates, we extracted light curves from space photometry. All four targets were observed in multiple sectors by the TESS Mission. At the time of the analysis, data up to Sector 53 was available. The data were extracted from the full-frame images (FFI) using mostly the point-spread function fitting module of the ELEANOR package (Feinstein et al. 2019). These observations provide a cadence of 30 and 10 minutes, depending on which sector they were taken from. The *Gaia* multi-color epoch photometry (Riello et al. 2021) and monochromatic space photometry from and TESS mission for these four candidates is shown in Fig. 16. For the target TIC 268157208 (= KIC 8646982), a sub-quarter of *Kepler* data exists, which is ~ 1.5 times the length of the proposed orbit. Due to the crowded field in which the target is located, we prefer the *Kepler* data due to its smaller pixel plate scale. The *Kepler* light curve was taken from the KEPSEISMIC database on the MAST archive³ (for details see García et al. 2011, 2014b).

TIC 268157208 (= *Gaia* DR3 2079109044266147328) is reported in *Gaia* DR3 as an eclipsing binary system with a period of 36.1 d. The clear eclipse in the *Gaia* epoch photometry of about $\sim 10\%$ is not found in *Kepler* and TESS data and is clearly an artifact. For TIC 235050452 (= *Gaia* DR3 4797117284359411712), the *Gaia* and TESS light curves show a good agreement in phase and amplitude of the long periodic variations with a period of 10.7 days. The sinusoidal flux modulation with variable amplitude in TESS data indicates rotational-modulated spots. For TIC 272357503 (= *Gaia* DR3 5214824569250240128), the *Gaia* epoch photometry suggests a binary with a period of nearly 1 day and eclipses of about ~ 2 to $\sim 4\%$ in the red and the blue passband, respectively. The shape of the feature indicates a partial eclipse. The analysis of the TESS photometry does not exclude that the primary and secondary eclipses are very similar, and the system's period is ~ 2 days. Such a system is too small to host a red giant. To determine more information about the components, radial velocities for this system are required.

From *Gaia* epoch photometry, the system TIC 293937699 (= *Gaia* DR3 5490280956749756928) shows a clear drop of the flux of about 5%. From TESS data, we can confirm the presence of the 5% eclipse, which is actually the secondary eclipse. In contrast, the well-pronounced primary eclipse with an eclipse depth of $\sim 15\%$ was missed by chance by the sparse sampling of the epoch photometry. However, the period of 65.112 ± 0.05 days, determined from a period analysis of the TESS data, does not agree with the geometrical period of ~ 3.8 d, reported in the *Gaia* DR3 eclipsing star catalog. This system is similar to the cases with large residuals comparing the literature values for period and eccentricity from the SB9 catalog. TIC 293937699 is one of the few systems hosting an oscillating red giant in an eclipsing binary system. Because radial velocities have yet to be obtained for this system, we have postponed a deeper analysis of this system for a later paper.

Similarly, TIC 33767523 (= *Gaia* DR3 4627969652492312320) is an eclipsing binary for which also the TBO catalog presents an orbital solution of $P_{\text{orb}} = 49.63 \pm 0.02$, and $e = 0.33 \pm 0.01$. Typically, such systems are wide enough to allow for an RGB star to oscillate. However, no oscillations are detected. This is probably due to the faintness of the ($V \approx 11$ mag) target.

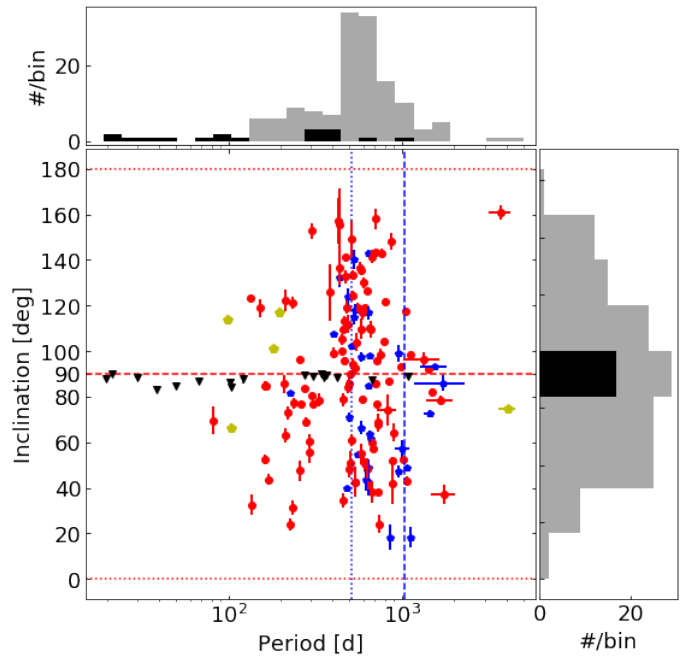


Fig. 17. Distributions of the inclinations and orbital period of astrometric binaries hosting a solar-like oscillating primary. The red dots indicate oscillating giants, observed by TESS; blue and yellow symbols mark oscillating giants and main-sequence stars observed by *Kepler*. Black triangles indicate giants in eclipsing binary systems from the *Kepler* literature sample. The vertical dashed and dotted blue lines mark the full and half length of the *Gaia* DR3 timebase, respectively. The horizontal dashed line marks the inclination for the edge-on orientation, while the dotted lines indicate the plane-on orientation of an orbit. The grey and black histogram indicate the distribution of the sample of astrometric binaries from *Gaia* DR3 and the literature sample of eclipsing binaries from *Kepler*.

5.2. Inclinations from astrometric solutions

For systems that do not have edge-on orientations ($i \approx 90^\circ$), the orbital inclination cannot be determined from the light curve. The precise and time-resolved astrometry of the *Gaia* mission now allows for the determination of the orbital inclination and provides photometric or spectroscopic constraints on the primary and secondary mass.

For 146 systems hosting an oscillating component, astrometric solutions were found to provide an orbital inclination. The solutions for astrometric orbits of Halbwachs et al. (2023); Holl et al. (2023) and listed in *Gaia* DR3 provide the Thiele-Innes coefficients describing the orbital solutions and implicitly contain the inclination. The conversion from these orbital elements to the elements in the Campbell formalism, which explicitly contain the inclination was performed with a python tool⁴ provided by Gaia Collaboration et al. (2023a).

As shown in Fig. 17, inclinations are found for 9 main-sequence targets, as well as 31, and 106 giants from the *Kepler* and TESS samples, respectively. We note that inclinations range from 0 to 180 (both plane-on orientations). This notation allows us to distinguish among prograde and retrograde movements with respect to the line of sight. Similarly to the dynamical masses, these systems have periods starting at about 100 days

⁴ We used the standard conversion formalism (e.g., Halbwachs et al. 2023). The NSS software tools have been developed by N. Leclerc and C. Babusiaux and are available at <https://www.cosmos.esa.int/web/gaia/dr3-nss-tools>

³ <https://archive.stsci.edu/prepds/kepseismic/>

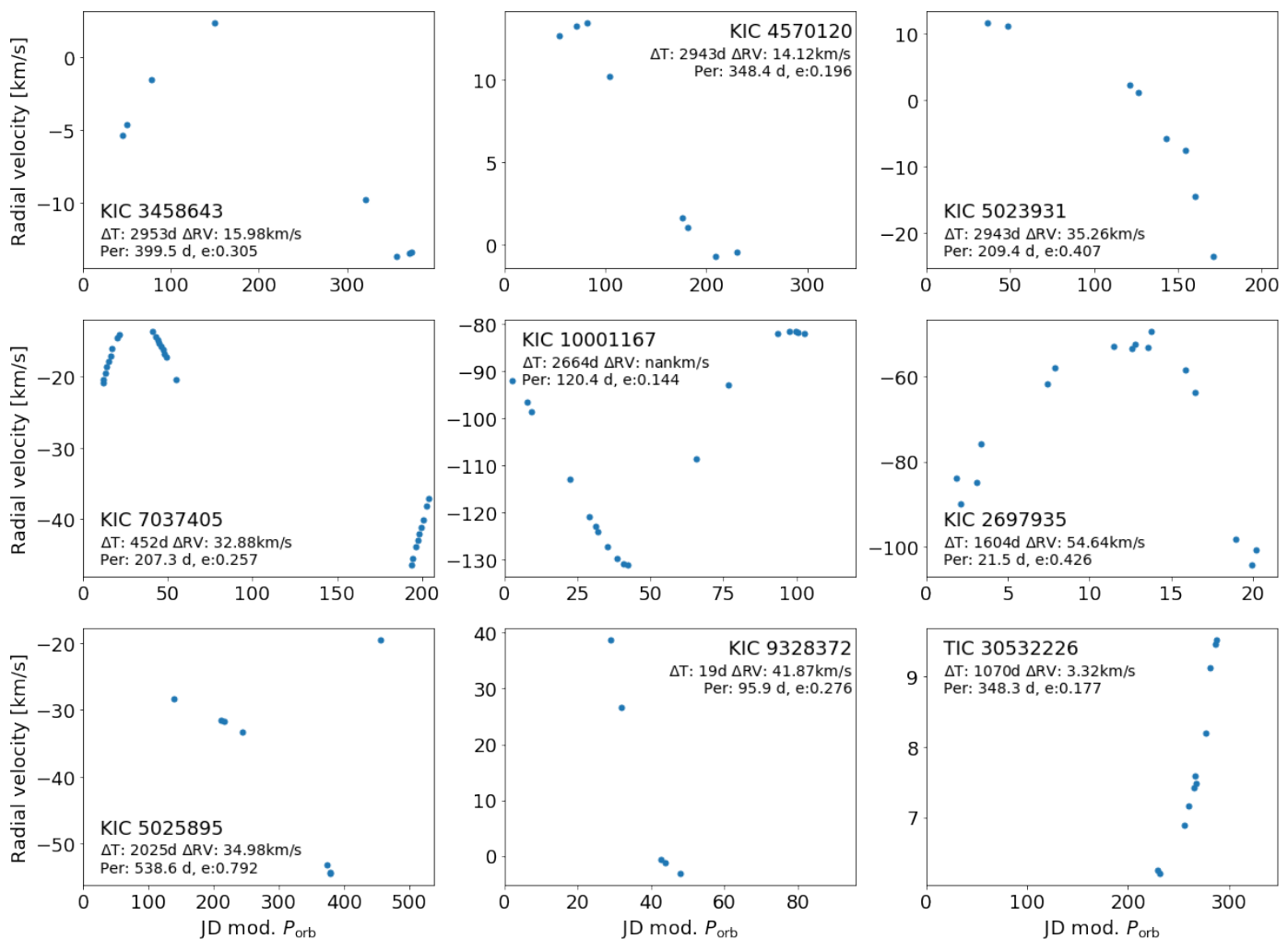


Fig. 18. Example radial-velocity curves from APOGEE spectroscopy of *Gaia* DR3 binary candidates. The panels show the RV values phasefolded with the period from *Gaia* DR3, which is also given in the annotated text.

and range beyond 1 000 days. While the analysis of the full sample by *Gaia* Collaboration et al. (2023a) shows a maximum in distribution of the inclination at 0 and 180 degrees, we find the maximum for stars in our sample around 90 degrees (Fig. 17) compared to literature. If an inclination for a system is given in *Gaia* DR3, we list it in Table B.1. Of the systems with an inclination from *Gaia* DR3, only KIC 7103951 has been previously reported in the literature (Gaulme et al. 2020), but without measured radial velocities.

Once these systems have accurate radial velocities from ground-based follow-up, these inclinations will be valuable information to extend the sample of calibrators for the scaling relations. For comparison, the *Kepler* literature sample of red giant eclipsing binary systems, is shown in Fig. 17. The wide range of orbital periods and the sheer number of targets suggest that the astrometric sample contains a sufficient number of giants in the more advanced RC or 2RC status, which will help to break the evolutionary bias for the calibration of the seismic scaling relations.

5.3. Searching for eclipses in complimentary data

From the inclinations reported in *Gaia* DR3, we identified for binaries with a quasi edge-on orientation to search for additional eclipsing systems that originally have been

missed from *Gaia* epoch photometry. From the systems with known inclinations that are hosting a solar-like oscillator, we found 6 that fall into a range of 90 ± 3 degrees, which are KIC 10732098, TIC 379953111, TIC 38843858, TIC 308539721, TIC 142053145, and TIC 237973654. These systems have periods between ~ 200 and ~ 1420 days. To search for eclipses in these targets, we extracted light curves from TESS FFIs. Given that in most cases the orbital period exceeds the timebase of TESS data, it is not surprising that no eclipses are found.

Next, we searched the *All-Sky Automated Survey for Supernovae* (ASAS-SN, Kochanek et al. 2017, and references therein)⁵. ASAS-SN began surveying the entire sky in V-band in 2014 with 2-3 day cadence and swapped to nightly monitoring in the g-band in 2018. The existing timebase therefore exceeds multiple orbits for all of the candidate systems. However, most of the six targets are brighter than the ASAS-SN saturation limit at Johnson V around 10 – 11 mag. We started by cross-matching with the ASAS-SN V- and g-band variables catalogs (Jayasinghe et al. 2021; Christy et al. 2023; Rowan et al. 2023). While identifying several matches, the variability is consistent with rotational variability instead of eclipses. We then extracted the light curves of the sample mentioned above. Neither the light curve

⁵ <https://www.astronomy.ohio-state.edu/asasn/>

nor the phase curve, produced from the orbital period reported by *Gaia* DR3, revealed any signature of the eclipses. The range of three degrees around the edge-on configuration might be too wide, given the decreasing angular size of the binary components to allow for eclipses.

We conclude that these targets are most likely non-eclipsing. Given the wide orbits, the range of three degrees around the edge-on configuration might be too wide (given the decreasing angular size of the binary components) to allow for eclipses.

6. Confirmation through radial-velocity monitoring

APOGEE (Majewski et al. 2017) is an all-sky survey, consisting of two nearly identical multi-object fiber-fed spectrographs mounted on the northern 2.5 m Sloan Foundation Telescope at Apache Point Observatory and the southern 2.5 m Irénée du Pont Telescope of Las Campanas Observatory to perform near-infrared spectroscopy in the H-Band with a resolution of $R \sim 22\,500$. It typically visits a source multiple times in the course of the project. Several papers have utilized the millions of single, homogeneous spectra to successfully search for large quantities of binaries in the red giant phase from RV variations (e.g., Badenes et al. 2018; Gaulme & Guzik 2019; Daher et al. 2022)

To test the binary-candidate detection from *Gaia* DR3, we searched for significant radial-velocity variations in the spectra contained in APOGEE DR17 (Ahumada et al. 2020). Hereafter, we adopt the simple significance criterion of Patton et al. (2023), which flags a source as potential binary if the scatter around the average radial velocity (VSCATTER) is greater than three times the average uncertainty of its RV measurement (VERR_MED) for a target with at least two visits.

From the 382 giant oscillators in the *Kepler* sample with orbit solutions in the TBO, 181 were visited multiple times, leading to 149 binary detections. DR17 is the first APOGEE data release to include a substantial set of observations of TESS targets in the Southern Continuous Viewing Zone. However, most targets were only visited once yet. Therefore, we only could test 7 binary candidates for RV variations, of which 5 exceed the significance limit for RV; for the 45 dwarfs and subgiants observed by the *Kepler* mission and reported orbital parameters from *Gaia* DR3, 27 sources had at least two spectra, of which 25 showed significant RV variations.

All systems with at least two spectroscopic observations by the APOGEE project are listed in Table B.3. In the last column, we indicate if a candidate system exceeded our significance threshold for a binary candidate. Because of the limited number of spectra typically only the binary nature can be confirmed. For systems that are particularly rich in RVs, we folded the APOGEE RVs with the period reported in *Gaia* DR3. As illustrated by the selected systems in Fig. 18 for which a good agreement was found.

A non-detection of significant RV variation from APOGEE data does not prove a proposed binary candidate from *Gaia* DR3 wrong. In many cases the multiple visits of a source in APOGEE occur in close temporal proximity, within a few nights. Therefore, the timebase for the spectroscopic observations can be short, compared to orbital periods of several hundred to thousands of days, leading to insignificant results from the RV variations. In particular, the RV variation over small ranges in phase can hardly show any variation for eccentric systems.

An additional source of RVs is provided by Beck et al. (2017), who reported six binary systems with an oscillating solar-analog primary from RV monitoring with the HERMES spectrograph (Raskin et al. 2011), mounted on the 1.2 m *Merca-*

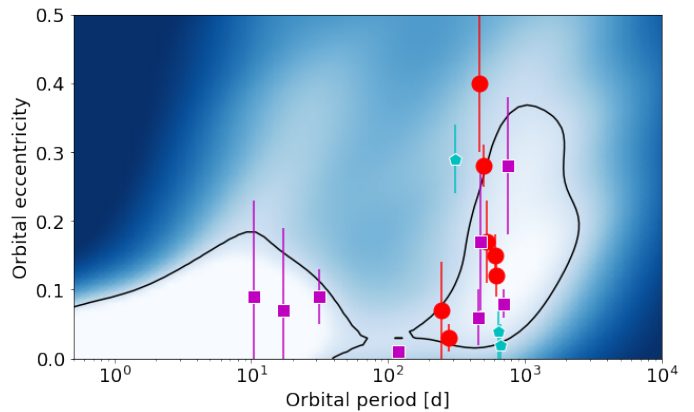


Fig. 19. Orbital parameters of systems hosting symbiotic stars and red giants that exhibit anomalous peaks in the PSD (cyan pentagrams). For the symbiotic systems, red dots and magenta squares depict the confirmed and candidate symbiotic stars, respectively. The background density map depicts the distribution and mark the most common combinations of orbital solutions in the SB9.

tor telescope on La Palma. The two systems KIC 4914923, and KIC 9098294 were reported to have a peak to peak RV amplitude of 2.11, and 41.35 km/s. KIC 4914923 is also confirmed as binary from APOGEE spectroscopy. The star KIC 3241581 is found in the non-linear solution. Indeed, the RV time series of Beck et al. (2016) points to an orbital period of ~ 1500 d.

7. Extended science cases for this dataset

This data set can also be used to test science cases, related to red giant stars in binary systems.

7.1. Symbiotic binaries

Symbiotic stars are interacting binary systems composed of a cool red giant star and a hot white dwarf or, in some cases, even a neutron star. Such systems move on orbits typically between hundreds and a few thousands of days embedded in an environment of circumstellar gas. The spectra of these systems are often showing strong emission lines due to the photoionization of the nebula by the radiation of the hot component (Munari 2019, and references therein). Because these systems are highly photometrically variable (Merc et al. 2023), it is interesting to test how known or suspected symbiotic binaries perform in *Gaia* DR3. We conducted a crossmatch, as described in Sect. 2, between the *Gaia* DR3 database and the catalog of symbiotic binaries, published by Merc et al. (2019b,c).

Out of 141 confirmed galactic symbiotic systems within the range of the magnitude-limited sample ($4 \leq G$ [mag] ≤ 13), seven targets ($\sim 5\%$) were found in the *Gaia* DR3 with orbital solutions (Table 4 and Fig. 19). For the six systems for which literature values for the orbital parameters exist, a good agreement is found. Only for AG Dra, a K-type giant and a hot white dwarf on a well-established circular orbit and an orbital period of ~ 550 days (Fekel et al. 2000), *Gaia* DR3 underestimates the orbital period by $\sim 9\%$. During the time covered by *Gaia* DR3, AG Dra was in its active stage, showing at least two outbursts at the time when the data for *Gaia* DR3 were collected (see Merc et al. 2019a; Gális et al. 2019).

Although the majority of symbiotic systems are found on orbits of 200 to 500 days (Merc et al. 2019b,c), which are suited for *Gaia*, the detection rate for this class of

Table 4. Reported orbital parameters for confirmed and candidate symbiotic binary stars in *Gaia* DR3.

Star identifier	2MASS	<i>Gaia</i> DR3	e	P [d]	Type	e_{Lit}	P_{Lit} [d]	Ref
StHA 32	J04374563-0119118	3229441606998725888	0.12 ± 0.03	618.47 ± 10.60	SB1	–	612	[1]
IV Vir	J14163429-2145500	6276714894852124032	0.03 ± 0.02	279.98 ± 1.13	SB1	0	281.6 ± 1.2	[2]
AG Dra	J16014101+6648101	1642955252784454144	0.28 ± 0.03	502.77 ± 6.01	SB1	0	548.65 ± 0.97	[3]
Hen 3-1213	J16351508-5142274	5934206543151802752	0.17 ± 0.06	530.11 ± 3.76	SB1	0.183 ± 0.034	533 ± 2	[4]
YY Her	J18143419+2059213	4528063078197198848	0.15 ± 0.03	607.73 ± 8.37	SB1	–	589.5 ± 0.3 ^a	[5]
StHA 176	J20224225-2107546	6859282948915521664	0.07 ± 0.07	246.64 ± 1.43	SB1	–	–	
LT Del	J20355722+2011275	1817300516637652352	0.40 ± 0.10	462.81 ± 6.88	SB1	–	465.6	[6]
TYC 1371-69-1	J07573112+2017347	670455944074475008	0.01 ± 0.01	119.13 ± 0.06	SB1	0.024 ± 0.015	119.18 ± 0.07	[7]
GaSS 1-4	J11121548-3207193	5403474822973970816	0.06 ± 0.04	458.92 ± 4.25	SB1	–	235 ^a	[8]
SkySyC 1-3	J15265734-7003104	5796098502440628864	0.08 ± 0.02	701.13 ± 3.81	SB1	–	482.78 ^{a,b}	[9]
IGR J15293-5609	J15292939-5612133	5883707000513657216	0.09 ± 0.04	31.50 ± 0.03	SB1	–	–	
GaSS 1-20	J16005485-1628325	6250366095129668992	0.09 ± 0.14	10.51 ± 0.00	SB1	–	–	
SS 295	J17073816-0744485	4360702354583742080	0.17 ± 0.10	471.11 ± 13.94	SB1	–	471.00 ^{a,b}	[10]
<i>Gaia</i> DR3 217...	J21180196+5721343	2178988199495779456	0.28 ± 0.10	753.92 ± 26.14	SB1	–	–	
<i>Gaia</i> DR3 533...	J11240425-6013342	5339026227414066432	0.07 ± 0.12	17.15 ± 0.02	SB1	–	–	
CGCS 5926	J23454464+6252511	2016034975622911360	–	–	–	–	–	–
<i>Gaia</i> DR3 553...	J08070625-4308520	5533253788183484672	–	–	–	–	–	–

Notes. Confirmed symbiotic systems are presented in the top panel of the table. Candidate systems for symbiotic stars with orbital solution and non-linear or acceleration solutions are reported in the middle and bottom panel, respectively. The first three columns report the commonly used identifier as well as the identifiers in the 2MASS and *Gaia* DR3 catalog. The next three columns report the orbital parameter and type of solution, presented in the TBO catalog ([Gaia Collaboration et al. 2023a](#)). The last three columns report the most recent values in the literature and their reference. ^a Period obtained from photometric variability. ^b Orbital origin of the photometric variability with this period was suggested by [Merc et al. \(2019b\)](#). References in the Table: 1: [Mürset & Schmid \(1999\)](#), 2: [Smith et al. \(1997\)](#), 3: [Fekel et al. \(2000\)](#), 4: [Fekel et al. \(2015\)](#), 5: [Mikołajewska et al. \(2002\)](#), 6: [Munari & Jurdana-Šepić \(2002\)](#), 7: [Tang et al. \(2012\)](#), 8: [Munari et al. \(2021\)](#), 9: [Pojmanski \(2002\)](#), 10: [Jayasinghe et al. \(2020\)](#).

interacting-binary systems is nearly an order of magnitude lower than for non-interacting, giant-hosting systems (Sect. 2). Because of the large variations that influence the photocenter as well as the stellar spectrum, these targets are difficult to determine in an automated way.

In addition to the confirmed symbiotic stars, the crossmatch revealed that another eight out of 744 galactic symbiotic candidates have orbital solutions listed in *Gaia* DR3. Half of the eight candidates have periods reported in the literature. For those systems for which orbital periods are known, we again find good consistency between the literature values and the periods reported by *Gaia* DR3. For one system the period of the spectroscopic solution in the TBO catalog is twice the photometric period, reported in the literature. Such a difference between the photometric and spectroscopic orbital period is often seen in the case when the giant fills or nearly fills its Roche radius and is ellipsoidally distorted. As a consequence, two minima per orbital period are observable in the light curve and the period search might return half the value of the true period. Three sources in the sample of candidates have rather short *Gaia* orbital periods (10 to 32 days) that are substantially shorter than the minimum periods of ~200 d found for symbiotic stars ([Merc et al. 2019b,c](#)). If they are true orbital periods of these systems, this would rule out the symbiotic classification of these targets.

Among the candidates from the New Online Database of Symbiotic Variables, there are also 337 targets newly identified as possible symbiotic stars from a supervised machine-learning classification by [Rimoldini et al. \(2023\)](#) of the color and variability in *Gaia* DR3 of 12.4 million sources. Only three of the *Gaia* symbiotic candidates are reported in *Gaia* DR3 as binary candidates, whereby one of them has a period of ~17 d. Also these numbers show a very low detection rate and that it is very

challenging to identify symbiotic binaries from the existing observational data in *Gaia* DR3.

Comparing these 15 systems with the distribution of the orbital period shows that they mostly follow the distribution of other red giant stars. As for the other red giant binaries (see Fig. 8), the systems are found with periods less than 1 000 days. Searching the non-linear and acceleration solutions as well, we find two additional systems, listed in the bottom panel of Table 4.

7.2. Testing giants with anomalous peaks in the PSD

[Colman et al. \(2017\)](#) published a collection of 168 oscillating red giant stars, in which the power-spectral density (PSD) reveals anomalous peaks. These peaks occur with frequencies very different and outside of the classical power excess. Furthermore, the shape of these peaks in the PSD do not resemble a Lorentz profile but seem to resemble a delta function. This suggests that these peculiar peaks are not stochastically excited but correspond to a periodic variation.

For about half of the cases, contamination with background stars was found as the most likely explanation. However, in 81 cases the source of the peculiar frequencies appears to coincide with the giant star. The authors suggested that such frequencies could be produced by the presence of close stellar components within the convective envelope of the red giant or due to a close binary in a hierarchical triple system.

We searched the *Gaia* DR3 TBO catalog for these systems to test if these are actually binary systems, where the found period indeed coincides with the anomalous peak. In total we found seven objects with peculiar peaks to be binary candidates in *Gaia*, which are listed in Table 5 and shown in Fig. 19. In two of these systems the peaks were identified as contamination and in two additional ones contamination could not be excluded.

Table 5. Binaries from *Gaia* DR3 in the sample of stars with anomalous peaks, reported by Colman et al. (2017).

KIC	P_{peak} [d]	P_{orb} [d]	e
Possible physical associations			
2449020	0.83	310 ± 2	0.29 ± 0.05
10936814	4.45	665 ± 6	0.02 ± 0.03
7596350	0.26	647 ± 11	0.04 ± 0.04
presumed chance alignments			
5556726	0.48	172 ± 1	0.24 ± 0.02
12117138	4.40	685 ± 18	0.39 ± 0.03
confirmed chance alignments			
2167774	0.35	137.0 ± 0.2	0.21 ± 0.06
1872210	0.67	540 ± 6	0.20 ± 0.07

Notes. The period and eccentricity of the orbit is taken from *Gaia* DR3 TBO. P_{peak} is the period of the dominant anomalous peak, reported by Colman et al. (2017). The categorisation of the anomalous peak, given by the authors is reported.

Three system were found to be possible physical associations. For all seven objects, the period of the anomalous peak is below 4.5 days, while all orbital periods are reported to be between 137 and 685 days on moderately eccentric orbits ($0.03 \leq e \leq 0.39$). These periods are also too long to excite tidal forces. We therefore suggest that these anomalous frequencies are unlikely to be excited by binary interaction.

8. Discussion and conclusions

In this work, we presented the successful search for solar-like oscillating stars in binary systems, revealed through photometric, spectroscopic, and astrometric solutions in the *Gaia* DR3 catalog of Two-Body-Orbit solutions, and tested it for completeness and purity.

To test the TBO, we used the SB9 catalog of orbital solutions. We introduced a magnitude-limited sample to account for observational biases due to partial saturation ($4 \leq G \text{ [mag]} \leq 13$). Because the sample contains systems with periods of several ten-thousand days, which are too long to be resolved by the *Gaia* DR3 baseline of 1034 days, we limited our sample further in periods ($P_{\text{orb}} \leq 1100$ days). We found an overall completeness factor of 28.3% for the complete SB9 catalog.

The ruwe measures the astrometric likelihood for a source to be a single star. About 40% of the detected binaries from the SB9 sample had ruwe values below 1.4, a conservative limit for the astrometric binary detection, and were detected by other means.

Performing the same searches of the TBO catalog for the lists of identified solar-like oscillators from the NASA *Kepler*, and in the Southern Continuous Viewing Zone of the NASA TESS mission, we identified 970 binary system candidates that host solar-like oscillating stars, among which 954 systems are newly detected systems. The sample presented in this work increases the binary stars with oscillating components by an order of magnitude. The full wealth of asteroseismic information allows for a comprehensive study of the system and its oscillating component.

From the search results, we obtained a magnitude-limited completeness factor of about 4% for the full red giant star sample. Taking into account the unresolved binaries and the completeness factor, determined from our comparison of the SB9,

we arrive at a binary yield similar to the expected value in the literature of 30-40% (Moe & Di Stefano 2017; Offner et al. 2022).

We assessed the mass and stellar radii ranges using the asteroseismic scaling relations. Our analysis shows that TESS suffers from noise and the limited length of the photometric time series, leading to an underestimated large-frequency separation. As a result, the masses for stars with radii larger than the typical radius of the red clump ($\nu_{\text{max}} \lesssim 30 \mu\text{Hz}$, see Fig. 6, top panel) can be overestimated, leading to an excess of stars with $M_{\star} \gtrsim 2 M_{\odot}$.

To test whether the orbits reported in the TBO catalog are physically plausible, we compared the orbital periods and the seismically inferred radii with the radius limit for the Roche-lobe overflow (Fig. 6, bottom panel). Except for a few reported systems with periods $P_{\text{orb}} \leq 10$ days where the orbit would be smaller than the radius of the primary, all reported values were found to be physically possible. However, these systems could be actual binaries with a significantly underestimated period. An additional argument for the realistic orbital periods comes from the location of the datapoints in the parameter plane, which are all well separated from the Roche-lobe limit. This gap is expected because systems were selected based on the criterion that the primary is oscillating. As a system approaches the limit for the RLOF, increased strength of tidal interactions starts to suppress the oscillations.

Because of the robust residuals centered at zero found in the comparison of the TBO catalog with the SB9, the large fraction of physically reasonable orbital periods, and the approximate agreement of the expected binary fractions for stars of about $1 M_{\odot}$, we consider most of the binary candidates reported in *Gaia* DR3 TBO catalog as reliable new binary systems.

The large amount of binary systems opens the door to studying binary star interaction and related activity. Using the seismically determined evolutionary stages, we could view the distribution of the orbital eccentricity and period as a function of stellar evolution. We showed that red clump stars have lower eccentricities and are biased towards longer periods than systems hosting the less evolved RGB stars. We attribute the lower eccentricities as a result of the increased strength of the tidal interaction due to the larger radii at the tip of the RGB. The lack of periods below 500 d originates from phases of intense star-star interaction, such as the RLOF or common envelope phase.

For the oscillating dwarfs, we showed the correlation between high photospheric activity and tidal circularization and synchronization. We used the asteroseismic inferences for the oscillating giants to analyze the distribution of the orbital period and eccentricity as a function of the evolutionary state. Indeed, we could show differences that agree with the predictions for the tidally driven evolution of binary as they converge to the equilibrium state of circularized systems.

For 146 systems, the inclinations angles are reported in *Gaia* DR3. We converted the notation of the value and associated it with oscillating primaries. If the RVs for both components are reported from ground-based observations, these systems will provide additional valuable benchmark systems for calibrating the scaling relations. If in those systems rotational splitting of non-radial modes is measured, the inclination of the rotation axis can be measured and test the spin-orbit alignment. A first work in this direction, based on *Gaia* DR3 was presented by Ball et al. (2023)

With an increasing orbital period, the probability of detecting transits in a binary system decreases for geometrical reasons, which explains the small number of eclipsing binary systems found in the vast datasets of space photometry. From our search of the *Gaia* variability catalog, we found one previously

unknown eclipsing binary system hosting an oscillating red giant primary.

Analyzing the radial velocities derived from APOGEE and HERMES spectroscopy, we could independently confirm 149 binaries out of 181 systems, proposed by *Gaia* DR3 and with multiple APOGEE spectra. This low number of the sample viewed in APOGEE originates from the limited sampling in the APOGEE observations and is expected to be improved with forthcoming DRs. For most of the systems, which had RV measurements, binarity could be confirmed. Therefore, we see the majority of the binary candidates reported in *Gaia* DR3 as bona fide candidates.

Given the numbers, this work is a first encouraging step into binary ensemble seismology. The work presented was only based on a subsample of well-characterized stars. Forthcoming data from the TESS mission will soon provide new detections of solar-like oscillations systems. With the launch of the ESA PLATO (Rauer et al. 2014, and Rauer et al. 2023 subm.), scheduled for 2026, we will increase the sample of binary systems with a component characterized by seismology. Given the mission goals of observing bright stars (Nascimbeni et al. 2022), the expected yield of the seismic detection for the *Gaia* binaries should be similar to those of the K2 mission described in this work, namely, offering an increased number of potential binary systems with seismic characterization.

The forthcoming data releases of the *Gaia* mission⁶ will allow for a more complete census of the binary population and therefore a closer estimate of the actual binary occurrence rate. The 66 months or ~2000 days of DR4, which is projected to be made public before 2026, will double the current timebase, allowing for the detection of wider systems and substantially improving the residuals of the orbital parameters beyond 500 days. Furthermore, DR5 is planned to cover all data collected during the entire mission duration. Such extended baseline will increase the number and reliability of orbital solution around 1 000 days. Because most systems with a He-core burning giant (RC) have orbital periods in this regime, this binary census extension will help reduce the current selection bias that produces an abundance of H-shell burning (RGB) primaries. The data set of the ESA *Gaia* mission are truly a Rosetta stone for studying the evolution of binary systems and tidal interactions with evolved stellar components.

Acknowledgements. We thank the referee for useful comments that allowed us to improve the article. The authors thank the people behind the ESA *Gaia*, NASA *Kepler*, and NASA TESS missions. PGB acknowledges support by the Spanish Ministry of Science and Innovation with the *Ramón y Cajal* fellowship number RYC-2021-033137-1 and the number MRR4032204. Substantial research work for this paper was performed during a summer sabbatical research stay of PGB at the *Ohio State University* (OSU), Columbus, Ohio, generously supported by the *NAWI Graz Mobility Grant 2022*. PGB thanks OSU for the hospitality and scientific exchange during his stay. PGB, DG, LS, LSS, and NM acknowledge the financial support by *NAWI Graz*. JM acknowledges support from the Instituto de Astrofísica de Canarias (IAC) received through the IAC early-career visitor program. SM acknowledges support by the Spanish Ministry of Science and Innovation with the *Ramón y Cajal* fellowship number RYC-2015-17697. SM and DGR acknowledge support from the Spanish Ministry of Science and Innovation with the grant no. PID2019-107187GB-I00. RAG and StM acknowledge support from the PLATO CNES grant. PG was supported by the German space agency (Deutsches Zentrum für Luft- und Raumfahrt) under PLATO data grant 500O1501. PG and JJ acknowledge NASA grant NNX17AF74G for partial support. KH acknowledges support through NASA ADAP grants (80NSSC19K0594). LS acknowledges financial support through the *Marshall Plan Foundation Austria* with contract number 2056139429282022). MV acknowledges support from NASA grant 80NSSC18K1582. This work has made use of data from the European Space Agency (ESA) mission *Gaia* (<https://www.cosmos.esa.int/gaia>), processed by the *Gaia*

Data Processing and Analysis Consortium (DPAC, <https://www.cosmos.esa.int/web/gaia/dpac/consortium>). Funding for the DPAC has been provided by national institutions, in particular the institutions participating in the *Gaia* Multilateral Agreement. This paper includes data collected with the *Kepler* & TESS missions, obtained from the MAST data archive at the Space Telescope Science Institute (STScI). Funding for these missions is provided by the NASA Science Mission Directorate and by the NASA Explorer Program respectively. STScI is operated by the Association of Universities for Research in Astronomy, Inc., under NASA contract NAS 5-26555.

Software: Python (Van Rossum & Drake 2009), numpy (Oliphant 2006; Harris et al. 2020), matplotlib (Hunter 2007), scipy (Virtanen et al. 2020), Astroquery (Ginsburg et al. 2019). This research made use of Astropy (Astropy Collaboration et al. 2013, 2018), a community-developed core Python package for Astronomy.

References

- Aerts, C. 2021, *Reviews of Modern Physics*, 93, 015001
- Aerts, C., Christensen-Dalsgaard, J., & Kurtz, D. W. 2010, *Asteroseismology*
- Ahuir, J., Mathis, S., & Amard, L. 2021, *A&A*, 651, A3
- Ahumada, R., Allende Prieto, C., Almeida, A., et al. 2020, *ApJS*, 249, 3
- Astropy Collab., Price-Whelan, A. M., Sipőcz, B. M., et al. 2018, *AJ*, 156, 123
- Astropy Collaboration, Price-Whelan, A. M., Sipőcz, B. M., et al. 2018, *AJ*, 156, 123
- Astropy Collaboration, Robitaille, T. P., Tollerud, E. J., et al. 2013, *A&A*, 558, A33
- Badenes, C., Mazzola, C., Thompson, T. A., et al. 2018, *ApJ*, 854, 147
- Baglin, A., Auvergne, M., Barge, P., et al. 2006, in *ESA Special Publication*, Vol. 1306, *ESA Special Publication*, ed. M. Fridlund, A. Baglin, J. Lochar, & L. Conroy, 33
- Ball, W. H., Triaid, A. H. M. J., Hatt, E., Nielsen, M. B., & Chaplin, W. J. 2023, *MNRAS*, 521, L1
- Barker, A. J. 2022, *ApJ*, 927, L36
- Barnes, S. A. 2007, *ApJ*, 669, 1167
- Beck, P. G., Allende Prieto, C., Van Reeth, T., et al. 2016, *A&A*, 589, A27
- Beck, P. G., Bedding, T. R., Mosser, B., et al. 2011, *Science*, 332, 205
- Beck, P. G., do Nascimento, Jr., J.-D., Duarte, T., et al. 2017, *A&A*, 602, A63
- Beck, P. G., Hambleton, K., Vos, J., et al. 2014, *A&A*, 564, A36
- Beck, P. G., Hambleton, K., Vos, J., et al. 2015, *EjConf* 101, 06004
- Beck, P. G., Kallinger, T., Pavlovski, K., et al. 2018a, *A&A*, 612, A22
- Beck, P. G., Mathis, S., Gallet, F., et al. 2018b, *MNRAS*, 479, L123
- Beck, P. G., Mathur, S., Hambleton, K., et al. 2022, *A&A*, 667, A31
- Beck, P. G., Montalbán, J., Kallinger, T., et al. 2012, *Nature*, 481, 55
- Bedding, T. R., Mosser, B., Huber, D., et al. 2011, *Nature*, 471, 608
- Benbakoura, M., Gaulme, P., McKeever, J., et al. 2021, *A&A*, 648, A113
- Borucki, W. J., Koch, D., Basri, G., et al. 2010, *Science*, 327, 977
- Brogard, K., Hansen, C. J., Miglio, A., et al. 2018, *MNRAS*, 476, 3729
- Brown, T. M., Gilliland, R. L., Noyes, R. W., & Ramsey, L. W. 1991, *ApJ*, 368, 599
- Ceillier, T., Tayar, J., Mathur, S., et al. 2017, *A&A*, 605, A111
- Charbonnel, C., Decressin, T., Lagarde, N., et al. 2017, *A&A*, 605, A102
- Christy, C. T., Jayasinghe, T., Stanek, K. Z., et al. 2023, *MNRAS*, 519, 5271
- Colman, I. L., Huber, D., Bedding, T. R., et al. 2017, *MNRAS*, 469, 3802
- Creevey, O. L., Sordo, R., Pailler, F., et al. 2023, *A&A*, 674, A26
- Daher, C. M., Badenes, C., Tayar, J., et al. 2022, *MNRAS*, 512, 2051
- De Ridder, J., Barban, C., Baudin, F., et al. 2009, *Nature*, 459, 398
- Deeg, H. J. & Alonso, R. 2018, in *Handbook of Exoplanets*, ed. H. J. Deeg & J. A. Belmonte, 117
- Ding, P.-J., Zhu, Z., & Liu, J.-C. 2019, *Research in Astronomy and Astrophysics*, 19, 068
- Eggleton, P. 2006, *Evolutionary Processes in Binary and Multiple Stars*
- Escorza, A., Siess, L., Van Winckel, H., & Jorissen, A. 2020, *A&A*, 639, A24
- Eyer, L., Mowlavi, N., Evans, D. W., et al. 2017, *arXiv e-prints*, arXiv:1702.03295
- Feinstein, A. D., Montet, B. T., Foreman-Mackey, D., et al. 2019, *PASP*, 131, 094502
- Fekel, F. C., Hinkle, K. H., Joyce, R. R., & Skrutskie, M. F. 2000, *AJ*, 120, 3255
- Fekel, F. C., Hinkle, K. H., Joyce, R. R., & Wood, P. R. 2015, *AJ*, 150, 48
- Fouesneau, M., Frémat, Y., Andrae, R., et al. 2023, *A&A*, 674, A28
- Frandsen, S., Lehmann, H., Hekker, S., et al. 2013, *A&A*, 556, A138
- Gaia Collaboration, Arenou, F., Babusiaux, C., et al. 2023a, *A&A*, 674, A34
- Gaia Collaboration, Prusti, T., de Bruijne, J. H. J., et al. 2016, *A&A*, 595, A1
- Gaia Collaboration, Vallenari, A., Brown, A. G. A., et al. 2023b, *A&A*, 674, A1
- Gális, R., Merc, J., & Leedjäv, L. 2019, *CoSka*, 49, 197
- Gallet, F., Bolmont, E., Mathis, S., Charbonnel, C., & Amard, L. 2017, *A&A*, 604, A112
- García, R. A., Ceillier, T., Salabert, D., et al. 2014a, *A&A*, 572, A34
- García, R. A., Hekker, S., Stello, D., et al. 2011, *MNRAS*, 414, L6

⁶ <https://www.cosmos.esa.int/web/gaia/release>

- García, R. A., Mathur, S., Pires, S., et al. 2014b, *A&A*, 568, A10
- Gaulme, P. & Guzik, J. A. 2019, *A&A*, 630, A106
- Gaulme, P., Jackiewicz, J., Appourchaux, T., & Mosser, B. 2014, *ApJ*, 785, 5
- Gaulme, P., Jackiewicz, J., Spada, F., et al. 2020, *A&A*, 639, A63
- Gaulme, P., McKeever, J., Jackiewicz, J., et al. 2016, *ApJ*, 832, 121
- Ge, J., Zhang, H., Zang, W., et al. 2022, arXiv e-prints, arXiv:2206.06693
- Gehan, C., Gaulme, P., & Yu, J. 2022, *A&A*, 668, A116
- Ginsburg, A., Sipócz, B. M., Brasseur, C. E., et al. 2019, *AJ*, 157, 98
- Gorlova, N., Van Winckel, H., Vos, J., et al. 2014, arXiv e-prints, arXiv:1403.2287
- Halbwachs, J.-L., Pourbaix, D., Arenou, F., et al. 2023, *A&A*, 674, A9
- Han, Z., Podsiadlowski, P., Maxted, P. F. L., Marsh, T. R., & Ivanova, N. 2002, *MNRAS*, 336, 449
- Handberg, R., Brogaard, K., Miglio, A., et al. 2017, *MNRAS*, 472, 979
- Harris, C. R., Millman, K. J., van der Walt, S. J., et al. 2020, *Nature*, 585, 357–362
- Hekker, S., Angelou, G. C., Elsworth, Y., & Basu, S. 2020, *MNRAS*, 492, 5940
- Hekker, S., Debosscher, J., Huber, D., et al. 2010, *ApJ*, 713, L187
- Holl, B., Sozzetti, A., Sahlmann, J., et al. 2023, *A&A*, 674, A10
- Hon, M., Huber, D., Kuszlewicz, J. S., et al. 2021, *ApJ*, 919, 131
- Hon, M., Kuszlewicz, J. S., Huber, D., Stello, D., & Reyes, C. 2022, *AJ*, 164, 135
- Howell, S. B., Sobeck, C., Haas, M., et al. 2014, *PASP*, 126, 398
- Huber, D., Pinsonneault, M., Beck, P., et al. 2023, arXiv e-prints, arXiv:2307.03237
- Hunter, J. D. 2007, *Computing in Science Engineering*, 9, 90
- Hut, P. 1981, *A&A*, 99, 126
- Jayasinghe, T., Kochanek, C. S., Stanek, K. Z., et al. 2021, *MNRAS*, 503, 200
- Jayasinghe, T., Stanek, K. Z., Kochanek, C. S., et al. 2020, *MNRAS*, 491, 13
- Jermyn, A. S., Bauer, E. B., Schwab, J., et al. 2023, *ApJS*, 265, 15
- Johnson, S. A., Penny, M., Gaudi, B. S., et al. 2020, *AJ*, 160, 123
- Johnston, C., Aymar, N., Abdul-Masih, M., et al. 2021, *MNRAS*, 503, 1124
- Katz, D., Sartoretti, P., Guerrier, A., et al. 2023, *A&A*, 674, A5
- Kippenhahn, R., Weigert, A., & Weiss, A. 2013, *Stellar Structure and Evolution* Kjeldsen, H. & Bedding, T. R. 1995, *A&A*, 293, 87
- Kochanek, C. S., Shappee, B. J., Stanek, K. Z., et al. 2017, *PASP*, 129, 104502
- Kroupa, P. 1995, *MNRAS*, 277, 1507
- Kumar, P., Ao, C. O., & Quataert, E. J. 1995, *ApJ*, 449, 294
- Li, T., Bedding, T. R., Huber, D., et al. 2018, *MNRAS*, 475, 981
- Mackereth, J. T., Miglio, A., Elsworth, Y., et al. 2021, *MNRAS*, 502, 1947
- Majewski, S. R., Schiavon, R. P., Frinchaboy, P. M., et al. 2017, *AJ*, 154, 94
- Mathis, S. 2013, in *Lecture Notes in Physics*, Berlin Springer Verlag, Vol. 865, Lecture Notes in Physics, Berlin Springer Verlag, ed. M. Goupil, K. Belkacem, C. Neiner, F. Lignières, & J. J. Green, 23
- Mathis, S. 2015, *A&A*, 580, L3
- Mathis, S. 2019, in *EAS Pub. Series*, Vol. 82, EAS Pub. Series, 5–33
- Mathur, S., García, R. A., Ballot, J., et al. 2014, *A&A*, 562, A124
- Mathur, S., García, R. A., Breton, S., et al. 2022, *A&A*, 657, A31
- Mathur, S., García, R. A., Bugnet, L., et al. 2019, *FrASS*, 6, 46
- Mathur, S., García, R. A., Huber, D., et al. 2016, *ApJ*, 827, 50
- Mathur, S., García, R. A., Régulo, C., et al. 2010, *A&A*, 511, A46
- Merc, J., Beck, P., Mathur, S., & Garcia, R. 2023, *A&A* (subm.)
- Merc, J., Gális, R., & Teyssier, F. 2019a, *CoSka*, 49, 228
- Merc, J., Gális, R., & Wolf, M. 2019b, *RNAAS*, 3, 28
- Merc, J., Gális, R., & Wolf, M. 2019c, *Astronomische Nachrichten*, 340, 598
- Mikolajewska, J., Kolotilov, E. A., Shugarov, S. Y., & Yudin, B. F. 2002, *A&A*, 392, 197
- Mirouh, G. M., Hendriks, D. D., Dykes, S., Moe, M., & Izzard, R. G. 2023, arXiv e-prints, arXiv:2307.02678
- Moe, M. & Di Stefano, R. 2017, *ApJS*, 230, 15
- Mosser, B., Barban, C., Montalbán, J., et al. 2011a, *A&A*, 532, A86
- Mosser, B., Belkacem, K., Goupil, M. J., et al. 2011b, *A&A*, 525, L9
- Mosser, B., Michel, E., Belkacem, K., et al. 2013, *A&A*, 550, A126
- Mosser, B., Vrad, M., Belkacem, K., Deheuvels, S., & Goupil, M. J. 2015, *A&A*, 584, A50
- Mowlavi, N., Holl, B., Lecoer-Taïbi, I., et al. 2023, *A&A*, 674, A16
- Munari, U. 2019, arXiv e-prints, arXiv:1909.01389
- Munari, U. & Jurdana-Šepić, R. 2002, *A&A*, 386, 237
- Munari, U., Traven, G., Masetti, N., et al. 2021, *MNRAS*, 505, 6121
- Mürset, U. & Schmid, H. M. 1999, *A&AS*, 137, 473
- Nascimbeni, V., Piotto, G., Börner, A., et al. 2022, *A&A*, 658, A31
- Nie, J. D., Wood, P. R., & Nicholls, C. P. 2017, *ApJ*, 835, 209
- Offner, S. S. R., Moe, M., Kratter, K. M., et al. 2022, arXiv e-prints, arXiv:2203.10066
- Ogilvie, G. I. 2014, *ARA&A*, 52, 171
- Ogilvie, G. I. & Lin, D. N. C. 2007, *ApJ*, 661, 1180
- Oliphant, T. 2006, *NumPy: A guide to NumPy*, USA: Trelgol Publishing
- Patton, R. A., Pinsonneault, M. H., Cao, L., et al. 2023, arXiv e-prints, arXiv:2303.08151
- Paxton, B., Schwab, J., Bauer, E. B., et al. 2018, *ApJS*, 234, 34
- Pinsonneault, M. & Ryden, B. 2023, *Stellar Structure and Evolution* (Cambridge University Press)
- Pojmanski, G. 2002, *Acta Astron.*, 52, 397
- Pols, O. R., Karakas, A. I., Lattanzio, J. C., & Tout, C. A. 2003, in *Astronomical Society of the Pacific Conference Series*, Vol. 303, *Symbiotic Stars Probing Stellar Evolution*, ed. R. L. M. Corradi, J. Mikolajewska, & T. J. Mahoney, 290
- Pourbaix, D., Tokovinin, A. A., Batten, A. H., et al. 2004, *A&A*, 424, 727
- Prša, A. 2018, *PHOEBE 2 - Modeling and Analysis of Eclipsing Binary Stars*
- Raskin, G., van Winckel, H., Hensberge, H., et al. 2011, *A&A*, 526, A69
- Rauer, H., Catala, C., Aerts, C., et al. 2014, *Experimental Astronomy*, 38, 249
- Rawls, M. L., Gaulme, P., McKeever, J., et al. 2016, *ApJ*, 818, 108
- Recio-Blanco, A., de Laverny, P., Palicio, P. A., et al. 2023, *A&A*, 674, A29
- Remus, F., Mathis, S., & Zahn, J.-P. 2012, *A&A*, 544, A132
- Ricker, G. R., Winn, J. N., Vanderspek, R., et al. 2014, in *SPIE*, Vol. 9143, *SPIE* 914320, 914320
- Riello, M., De Angeli, F., Evans, D. W., et al. 2018, *A&A*, 616, A3
- Riello, M., De Angeli, F., Evans, D. W., et al. 2021, *A&A*, 649, A3
- Rimoldini, L., Holl, B., Gavras, P., et al. 2023, *A&A*, 674, A14
- Rowan, D. M., Jayasinghe, T., Stanek, K. Z., et al. 2023, *MNRAS*, 523, 2641
- Salabert, D., García, R. A., Jiménez, A., et al. 2017, *A&A*, 608, A87
- Santos, A. R. G., Breton, S. N., Mathur, S., & García, R. A. 2021, *ApJS*, 255, 17
- Serenelli, A., Weiss, A., Aerts, C., et al. 2021, *A&A Rev.*, 29, 4
- Serenelli, A., Weiss, A., Cassisi, S., Salaris, M., & Pietrinferni, A. 2017, *A&A*, 606, A33
- Sharma, S., Stello, D., Huber, D., Bland-Hawthorn, J., & Bedding, T. R. 2017, *ApJ*, 835, 163
- Silva Aguirre, V., Stello, D., Stokholm, A., et al. 2020, *ApJ*, 889, L34
- Skumanich, A. 1972, *ApJ*, 171, 565
- Smart, R. L., Sarro, L. M., Rybizki, J., et al. 2021, *A&A*, 649, A6
- Smith, V. V., Cunha, K., Jorissen, A., & Boffin, H. M. J. 1997, *A&A*, 324, 97
- Soberman, G. E., Phinney, E. S., & van den Heuvel, E. P. J. 1997, *A&A*, 327, 620
- Tang, S., Grindlay, J. E., Moe, M., et al. 2012, *ApJ*, 751, 99
- Tassoul, M. 1980, *ApJS*, 43, 469
- Tayar, J., Ceillier, T., García-Hernández, D. A., et al. 2015, *ApJ*, 807, 82
- Tayar, J., Moyano, F. D., Soares-Furtado, M., et al. 2022, *ApJ*, 940, 23
- Thiemeßl, N., Hekker, S., Southworth, J., et al. 2018, *MNRAS*, 478, 4669
- Torres, G., Andersen, J., & Giménez, A. 2010, *A&Ar*, 18, 67
- Van der Swaelmen, M., Boffin, H. M. J., Jorissen, A., & Van Eck, S. 2017, *A&A*, 597, A68
- Van Eylen, V., Winn, J. N., & Albrecht, S. 2016, *ApJ*, 824, 15
- Van Rossum, G. & Drake, F. L. 2009, *Python 3 Reference Manual* (Scotts Valley, CA: CreateSpace)
- Verbunt, F. & Phinney, E. S. 1995, *A&A*, 296, 709
- Virtanen, P., Gommers, R., Oliphant, T. E., et al. 2020, *Nature Methods*, 17, 261
- Vos, J., Østensen, R. H., Marchant, P., & Van Winckel, H. 2015, *A&A*, 579, A49
- Vos, J., Østensen, R. H., Németh, P., et al. 2013, *A&A*, 559, A54, Paper II
- Vrad, M., Mosser, B., & Samadi, R. 2016, *A&A*, 588, A87
- Vrad, M., Pinsonneault, M., Hon, M., et al. 2021, in *Posters from the TESS Science Conference II (TSC2)*, 141
- Yu, J., Huber, D., Bedding, T. R., et al. 2018, *ApJS*, 236, 42
- Zahn, J.-P. 1977, *A&A*, 57, 383
- Zahn, J.-P. 2013, in *Lecture Notes in Physics*, Vol. 861, 301, 301

- 1 Instituto de Astrofísica de Canarias, E-38200 La Laguna, Tenerife, Spain e-mail: paul.beck@iac.es
- 2 Departamento de Astrofísica, Universidad de La Laguna, E-38206 La Laguna, Tenerife, Spain
- 3 Institut für Physik, Karl-Franzens Universität Graz, Universitätsplatz 5/II, NAWI Graz, 8010 Graz, Austria
- 4 Department of Astrophysics and Planetary Science, Villanova University, 800 East Lancaster Avenue, Villanova, PA 19085, USA
- 5 Department of Astronomy, The Ohio State University, Columbus, OH 43210, USA
- 6 Center for Cosmology and AstroParticle Physics, The Ohio State University, 191 West Woodruff Avenue, Columbus, OH 43210
- 7 Astronomical Institute, Faculty of Mathematics and Physics, Charles University, V Holešovičkách 2, 180 00 Prague, Czechia
- 8 Université Paris-Saclay, Université Paris Cité, CEA, CNRS, AIM, 91191, Gif-sur-Yvette, France
- 9 Thüringer Landessternwarte, Sternwarte 5, 07778 Tautenburg, Germany
- 10 Department of Astronomy, The University of Texas at Austin, 2515 Speedway, Stop C1400, Austin, TX 78712, USA

- ¹¹ Institute for Astronomy, University of Edinburgh, Royal Observatory, Edinburgh EH9 3HJ, UK
- ¹² INAF - Osservatorio Astrofisico di Catania, Via S. Sofia 78, I-95123, Catania, Italy
- ¹³ Université Côte d'Azur, Observatoire de la Côte d'Azur, CNRS, Laboratoire Lagrange, Bd de l'Observatoire, CS 34229, 06304 Nice Cedex 4, France
- ¹⁴ Department of Astronomy, University of Geneva, Chemin Pegasi 51, CH-1290 Versoix, Switzerland
- ¹⁵ Department of Physics and Astronomy, California State University Long Beach, Long Beach, CA 90840, USA

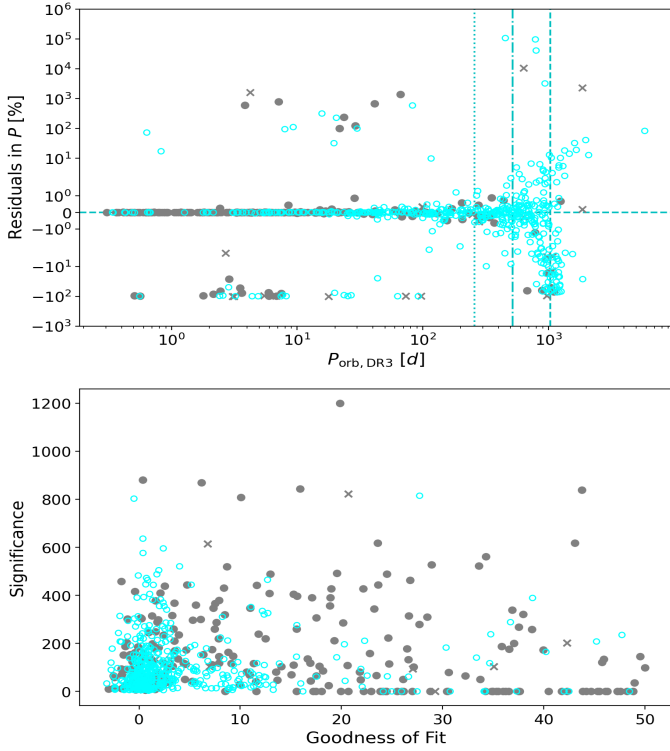


Fig. A.1. Fractional residuals of the period from the comparison of *Gaia* DR3 and SB9 in percent is shown in the top panel. The bottom panel shows the goodness-of-fit and significance parameters originating from the binary solutions in *Gaia* DR3 plotted against each other. The vertical lines from left to right indicate the precession period of the *Gaia* satellite of 69 days, as well as the one-fourth, half, and full duration of the *Gaia* DR3, ~ 250 , ~ 500 , and 1035 days, respectively. The meaning of the used symbols and colors is similar to Fig. 2.

Appendix A: Characteristics of the TBO solutions for SB9

A.1. Definition of a magnitude-limited sample

The current version of the SB9 (Pourbaix et al. 2004, version 2022/03) lists 4021 systems ($2.85 \leq G [\text{mag}] \leq 18.77$) and provides 5042 orbital solutions from ground-based radial-velocity monitoring. We limited the selection to one orbit solution per system to obtain a sample of unique stellar identifiers. For multiple entries for the same orbit of an object, we took the one with the highest SB9 grade. If two solutions had the same grade, we adopted the one with the more recent bibliographic code. The remaining sample was then screened for triples, where we adopted the orbit closer to the *Gaia* value for the residual calculation. By excluding alternative solutions for binaries and the solutions for triple and quadruple systems, we arrive at 3413 unique stellar identifiers in the "full sample."

The *Gaia* catalog of Nearby Stars (GCNS) is a clean catalog of 331 312 sources within 100 pc (Smart et al. 2021). Among the stars in the GCNS, the most common solutions in our sample are the orbital, the astrometric-spectroscopic SB1, and SB solution (see Fig. 10 in Gaia Collaboration et al. 2023a). The latter two, of which most of the solutions for our binaries consist, are abundant for magnitudes brighter than $G [\text{mag}] \leq 13$. The fainter limit is set by the brightness limit of the spectrograph and radial-velocity (RV) measurements. On the bright end of the GCNS distribution ($4 \leq G [\text{mag}]$), *Gaia* observations are limited by saturation effects.

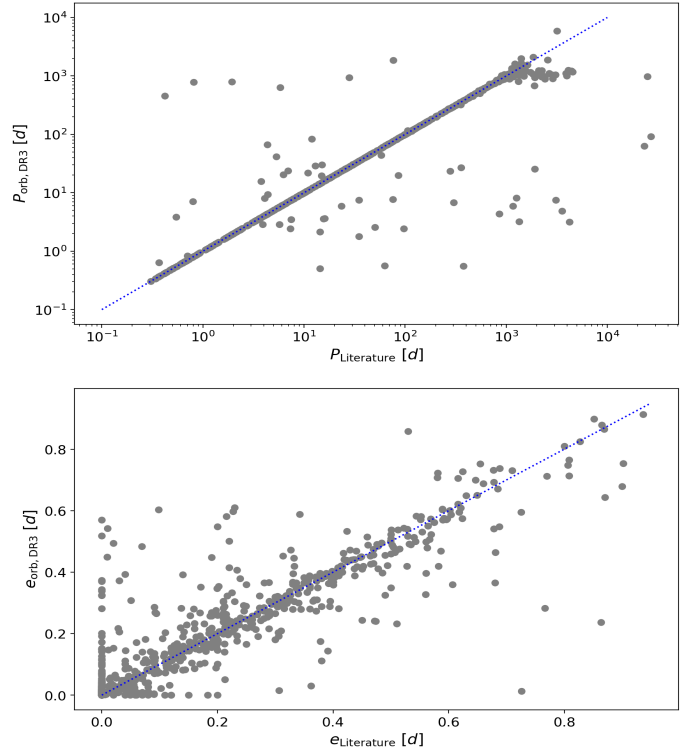


Fig. A.2. Direct comparison of the orbital period (top) and eccentricity (bottom) of the orbital elements from *Gaia* DR3 and SB9. The dotted line represents the 1:1 ratio.

To obtain the realistic corrected binary yield for the SB9 sample, we calculated the sample size within the magnitude limitations ($4 \leq G [\text{mag}] \leq 13$). The SB9 magnitude limited sample contains 2964 systems. Because the SB9 is compiled from decades of ground-based RV monitoring, it contains systems with periods up to several ten thousand days to which *Gaia* DR3 is not sensitive. Therefore, we corrected the SB9 magnitude-limited sample with a maximum value for the orbital period of $P_{\text{orb,SB9}} \leq 1\,100$ d. This magnitude-period-limited sample contains 2 343 unique DR3 source identifiers.

A.2. *Gaia* DR3 TBO completeness factor and residuals

The SB9 catalog literally provides the ground(-based) truth. We can assess the completeness and reliability of the solutions provided in the *Gaia* DR3 TBO. The crossmatch of the TBO catalog with the SB9 catalog returned 743 matches for the full sample and 668 for the magnitude-period limited sample, corresponding to a corrected binary yield of 21.7% and 28.5%, respectively. Because all the searched sources are confirmed binary systems, we can estimate the overall completeness factor of *Gaia* DR3 TBO catalog to be $\sim 30\%$.

Because the binary fraction is a strong function of the primary's mass (e.g., Offner et al. 2022), we cannot compare these numbers to those from binary population studies. This is therefore a purely systematic yield of the mission.

This sample is also sufficiently large to test the reliability of the provided values for the orbital parameters. From the full sample, we find the period and eccentricity for 743 and 715 systems (magnitude corrected: 668 and 640), respectively. These numbers show that for about 95% a complete set of period and eccentricity are reported. The middle panel of Fig. 2 shows the e - P plane of all 715 systems for which both parameters, eccentricity

and period are provided in the SB9 and the *Gaia* DR3 catalog. Consequently, such a system is represented by two data points. This comparison presents an overall good agreement between the SB9 and *Gaia* DR3 solutions. From the eccentricities' residuals of the full sample (see bottom panel of Fig. 2), we find a mean value of 0.011 ± 0.104 . Accounting only for systems where the period residual between TBO and SB9 is less than 10%, the mean residual in eccentricity reduces to 0.004 ± 0.060 .

A more complex picture is found for the orbital periods (Fig. A.1, top panel). The periods reported in the *Gaia* DR3 are quite consistent with the periods in the SB9 up to $P_{\text{orb}} \lesssim 250$ d, which is one-fourth of the timebase of *Gaia* DR3 of 1035 d (dashed and dash-dotted cyan vertical lines in Fig. A.1, respectively). In Fig. A.1, it can be seen that the general scatter in the residuals increases with the increasing orbital period. As these large residuals in the long-periodic regime of the data set would dominate any overall metric, we split the period range into three different regions.

To test the reliability of the *Gaia* periods we show in Fig. A.1 the fractional residuals as the function of the *Gaia* period, $P_{\text{orb,DR3}}$. First we inspected the region of $P_{\text{orb,DR3}} \leq 250$ days. Following a sigma-clipping approach, we excluded 54 solutions from the magnitude-unconstrained sample with period deviations between TBO and SB9 larger than 10%. From this comparison, we conclude that $\sim 90\%$ of the periods in DR3 below 250 days are reliable. For the remaining systems, the typical errors (mean and standard deviation) in period and eccentricity are 0.006 ± 0.610 d, and 0.006 ± 0.057 , respectively.

From the magnitude-unconstrained sample in the range of $250 \leq P_{\text{orb,DR3}} [\text{d}] \leq 500$, 76 out of the 77 systems have period residuals, better than 10%. This leads us to the conclusion that 99% of the solutions between $250 \leq P_{\text{orb,DR3}} [\text{d}] \leq 500$ are reliable. To avoid skewing the distribution by rejecting too many solutions, we report the mean residual values in the unclipped sample. In this period range we find a mean residual of 5 ± 52 days and -0.003 ± 0.075 for the orbital period and eccentricities, respectively.

For all systems with periods in DR3 longer than 500 days – half of the timebase of *Gaia* DR3, a mean period scatter of -273 ± 1818 d is found. Only 74%, 147 out of 198 systems with $P_{\text{orb}} \geq 500$ days have residuals, better than 10%.

As it can be seen from Fig. 2 many periods with SB9-periods longer than $P_{\text{orb,DR3}} \geq 1100$ are largely underestimated in DR3, which leads to the escalating residuals around and above 1000 days. We look forward to the forthcoming data releases, DR4 and DR5, by the *Gaia* mission, with extended timebases.

In the range of $P_{\text{orb,SB9}} \leq 250$ days the SB9 magnitude limited sample contains 1855 unique systems, of which *Gaia* DR3 TBO catalog reported 461 as candidates. This corresponds to a completeness factor of 24.9%. In the period range between $250 \leq P_{\text{orb,SB9}} [\text{d}] \leq 500$ of the magnitude-limited sample, contains 41.0 %. Therefore, the completeness in the shorter periodic regime is lower than the completeness factor for the overall period-limited sample.

A.3. Potentially long-periodic systems

The non-single star (NSS) acceleration catalog reports solutions for objects for which a solution for the proper motion with a higher-order term fits significantly better than a linear solution. As the trajectory of binary systems with long orbital periods is perceived as a parabolic arc, adding constant acceleration to the linear single-star model would enable the detection of such objects as binaries, as discussed in *Gaia* DR3 documentation. For

binary systems with slightly shorter periods, the time derivation of the acceleration has to be considered an additional parameter, as described in the *Gaia* DR3 documentation. This results in the solution types of constant acceleration (Acceleration7) and variable acceleration (Acceleration9), as seen in the *Gaia* DR3 documentation.

Figure 2 depicts the distribution of the 241 systems found with acceleration and non-linear solutions. As it can be seen, they mostly populate the regime of orbital periods, which extends from periods just a little longer than the timebase of *Gaia* DR3 to more than 10 000 day orbits. Interestingly, a few very short-periodic and circularized systems ($P_{\text{orb}} < 10$ days) are also found among these solutions.

Including these systems with both orbital parameters unresolved in the count of detected systems gives exactly 1 000 systems out of the 3529 unique stellar identifiers comprised in SB9, which were reported in the *Gaia* DR3 TBO. However, we do not include these systems in the comparison of the fractional binary yields, as the magnitude-period-limited sample of the SB9 was constructed to account for this bias.

A.4. Quality metrics in *Gaia* DR3 TBO

The TBO catalog provides numerous measures to describe the quality of a solution. The main two parameters are the goodness of fit (GoF) and significance (s). The GoF parameter describes how well a model's prediction matches the observed data (Halbwachs et al. 2023). Due to its definition in Eq. 1 in Halbwachs et al. (2023), combining the χ^2 -metrics and the degrees of freedom, values range from (small) negative to large positive values, whereby larger GOF values ($\text{GOF} \geq 25$) are considered as unreliable. The significance s describes the S/N of the semi-amplitude for spectroscopic binaries and the semi-major axis for astrometric orbits, respectively, as described in Gaia Collaboration et al. (2023a). We also used the SB9 sample to improve our understanding of the quality metrics in the *Gaia* DR3. The bottom panel of Fig. A.1 shows the quality metrics used to select the systems accepted for the catalog entries of confirmed binaries. We find most systems with single-digit GoF values and a wide range of significance.

Filtering data based on the GoF and s parameter has already been done in the post-processing of the *Gaia* DR3 catalog. Binary solutions possessing a $\text{GoF} < 50$ and a $s > 5$ were accepted into the catalog with the exception of binaries possessing the *OrbitalTargetedSearch** solution, which were accepted possessing a $\text{GoF} < 50$ and a $s > 2$, as is discussed in Gaia Collaboration et al. (2023a). In our further search for red giant binaries, we adopted all solutions provided in *Gaia* DR3 without further filtering on these parameters.

Another parameter that was reported to be a good indicator for identifying binary stars is the ruwe of the astrometry. By definition, a $\text{ruwe} \approx 1$ suggests that the astrometric solution satisfies a single star model, while a larger value suggests a binary star solution. We tested this metric based on the SB9 magnitude- and period-limited sample. For the TBO-SB9 comparison we find 59% with $\text{ruwe} \geq 1.4$ (dashed vertical line in Fig. 3), a solid threshold for binary detection from the proper motions, according to Gaia Collaboration et al. (2023a). A less conservative limit of $\text{ruwe} \geq 1.2$ still includes 65% of all confirmed binaries. The distribution peak is located at a $\text{ruwe} \approx 1.0$, while the maximum value is found at $\text{ruwe} \approx 40$.

While it shows that ruwe is a good indicator, we find that a significant number of the confirmed binaries are found with low ruwe values suggesting (likely) single-star objects. As shown in

Fig. 4, these systems are likely to be distant systems in shorter orbits, where the projected motion of the stellar component due to their binarity is small compared to the proper motion of the system. A small ruwe also means that the astrometry is very accurate, providing a good parallax for this system which provides better constraints for the stellar model.

A.5. Known oscillating giants in binaries

In addition to the SB9 sample, the second comparison sample consists of binary systems with an oscillating red giant binary component. This catalog, referred to here as the "literature sample," was recently published by Beck et al. (2022) and contains eclipsing binaries reported by Hekker et al. (2010), Frandsen et al. (2013), Gaulme et al. (2014, 2016, 2020), Rawls et al. (2016), Handberg et al. (2017), Brogaard et al. (2018), Theßel et al. (2018), Gaulme & Guzik (2019), and Benbakoura et al. (2021), as well as the catalogs of red giant heartbeat stars, compiled by Beck et al. (2014, 2015). In addition to those 81 systems, Beck et al. (2022) identified 99 systems, previously unknown to host an oscillating giant components from *Kepler*, TESS and BRITTE data, using the inventory of the SB9 catalog. Both samples are presented in the bottom panel of Table 1. The position of the red giant binaries in the literature sample is also shown in Fig. 1.

Of these 190 systems 53 are located in the magnitude limited sample. All systems in this limited sample were identified as binaries by *Gaia* DR3. Additionally, 116 were listed as possible binaries in the non-linear and acceleration solutions. Since half of them are also listed in the SB9, it is challenging to distill these detection rates into an independent metric.

Appendix B: Tables of orbital and seismic values

This section presents a limited version of the online tables for the full binary sample in *Gaia* DR3. In addition to the values provided in Tables B.1 and B.2, the online version of this table, in a machine-readable format on CDS (if available) contains the effective temperature and metallicity from apogee.

B.1. Systems with orbital parameters in *Gaia* DR3

Table B.1 presents the catalog of binary-system candidates that host a solar-like oscillator, for which the orbital period or eccentricity are reported in *Gaia* DR3. The first three identifiers for the star in the relevant catalogs are provided. The first column reports the source ID in the *Gaia* DR3 catalog. The second column indicates the stars identifier in the *Kepler* or TESS input catalog (KIC or TIC, respectively). The 2MASS identifier is given in the third column.

The next four columns report values from the TBO *Gaia* DR3 catalog for the binary-system candidate. The ruwe indicates the astrometric error. The P_{orb} and e values give the period and eccentricity of the orbit. The inclination of the orbit is given after the conversion of the Thiele-Innes coefficients to the Campbell formalism⁴.

The type of the TBO catalog solution is listed in the next column, whereby SB1 stands for Single Lined Spectroscopic binary model, ASB1 (= *AstroSpectroSB1* in the official documentation⁷) for combined astrometric + single lined spectroscopic

orbital model, ORB (= *Orbital*) for an orbital model for an astrometric binary, and OTS (= *OrbitalTargetedSearch*) for orbital model for a priori known systems, with a subset containing the suffix Validated.

The final three columns report the asteroseismic parameters. The global seismic parameters ν_{max} and $\Delta\nu$ describe the mean frequency of the excess of oscillation power and the mean large frequency separation between consecutive modes of the same spherical degree, ℓ . The asymptotic period spacing between pure gravity dipole ($\ell=1$) modes, $\Delta\Pi_1$ is given in the last column.

B.2. Systems with non-linear and acceleration solutions in *Gaia* DR3

Table B.2 presents the catalog of binary-system candidates that host a solar-like oscillator, for which no orbital elements are reported in *Gaia* DR3. Because the found solution for the star's proper motion does not agree with that of a single star, these are flagged as acceleration and non-linear solutions in the non-single star catalog of *Gaia* DR3.

The type of the TBO catalog solution is listed in the next column, whereby ACC7 (= *Acceleration7* in the official documentation) and ACC9 (= *Acceleration9*) stand for an acceleration model⁸ with 7 and 9 parameters, respectively. FSB1 (= *FirstDegreeTrendSB1*), and SSB1 (= *SecondDegreeTrendSB1*) stand for specialized solutions⁹. Similarly to Table B.1, we report the three relevant source identifiers, the ruwe of the source and the key asteroseismic parameters ν_{max} , $\Delta\nu$, and $\Delta\Pi_1$.

B.3. Confirmed *Gaia* DR3 binary systems from APOGEE radial velocities

Table B.3 presents the catalog of binary-system candidates in the *Kepler* field of view, that have been confirmed or supported through RV-variations, derived from single epoch spectroscopy of the APOGEE project, released in the DR16. The first and second column report the source identifiers in the *Kepler* and 2MASS input catalog. The orbital period for the system candidate, as reported in *Gaia* DR3 is given. The next three columns indicate the number of spectra taken, the timebase between the first and the last observation, and the mean uncertainty of the RV measurements. The next column reports the mean difference between spectra in the time series. If the source is indeed a binary, according to our significance criterion it is marked with an "x."

chap_datamodel/sec_dm_non-single_stars_tables/
ssec_dm_nss_two_body_orbit.html

⁸ https://gea.esac.esa.int/archive/documentation/GDR3/Gaia_archive/chap_datamodel/sec_dm_non-single_stars_tables/ssec_dm_nss_acceleration_astro.html

⁹ https://gea.esac.esa.int/archive/documentation/GDR3/Gaia_archive/chap_datamodel/sec_dm_non-single_stars_tables/ssec_dm_nss_non_linear_spectro.html

⁷ the more detailed documentation is found https://gea.esac.esa.int/archive/documentation/GDR3/Gaia_archive/

Table B.1. Orbital parameters of binary systems reported in *Gaia* DR3, and the seismic parameter of solar-like oscillating primary.

Gaia DR3	KIC/TIC	2MASS	ruwe	P_{orb} [d]	e	i [deg]	Type	ν_{max} [μHz]	$\Delta\nu$ [μHz]	$\Delta\Pi_1$ [s]
2050236453034915840	KIC 1026084	J19241348+3642145	0.93	393 \pm 6	0.10 \pm 0.09	–	SB1	41 \pm 1	4.4 \pm 0.1	251
2051023943874834688	KIC 1569823	J19222790+3711159	2.25	283.5 \pm 1.5	0.42 \pm 0.10	–	SB1	44 \pm 5	5.4 \pm 0.5	–
2051764945994896000	KIC 1572049	J19242968+3711000	1.19	361.3 \pm 4.1	0.01 \pm 0.05	–	SB1	52 \pm 3	5.19 \pm 0.05	–
2051723679950384256	KIC 1872210	J19291111+3718547	1.71	549.7 \pm 6.5	0.39 \pm 0.04	–	SB1	72 \pm 2	6.24 \pm 0.04	251
2051786760127550208	KIC 2016676	J19274515+3727100	1.31	842.5 \pm 29.3	0.07 \pm 0.10	–	SB1	81 \pm 2	6.95 \pm 0.05	255
2051797450308126336	KIC 2161731	J19270486+3734137	7.93	1066.0 \pm 12.6	0.42 \pm 0.01	49 \pm 1	ASB1	102 \pm 2	8.1 \pm 0.1	–
2051656918979678592	KIC 2167774	J19321701+3731246	1.39	137.0 \pm 0.2	0.24 \pm 0.02	–	SB1	60 \pm 1	5.79 \pm 0.01	–
2099089472639454208	KIC 2283075	J19040434+3737566	1.28	57.35 \pm 0.03	0.17 \pm 0.02	–	SB1	69 \pm 1	6.47 \pm 0.02	69
2052551401745695872	KIC 2303289	J19260333+3737527	1.32	941 \pm 35	0.17 \pm 0.10	–	SB1	1.95 \pm 0.03	0.42 \pm 0.03	–
2051105616974704256	KIC 2438368	J19211415+3746578	1.34	645.9 \pm 11.3	0.26 \pm 0.07	–	SB1	85 \pm 1	7.03 \pm 0.03	248
2052556040310373248	KIC 2711573	J19252964+3744385	0.91	182 \pm 1	0.29 \pm 0.05	–	SB1	42 \pm 1	4.52 \pm 0.04	337
2051864657954441344	KIC 2449020	J19304378+3745086	1.28	310.2 \pm 2.5	0.29 \pm 0.10	–	SB1	68 \pm 1	5.99 \pm 0.05	313
2052042946336958976	KIC 2585190	J19335608+3752239	0.97	349.2 \pm 4.3	0.10 \pm 0.05	–	SB1	48 \pm 2	4.8 \pm 0.1	334
2099180938261820288	KIC 2695592	J19064544+3754106	1.96	823.6 \pm 74.4	0.07 \pm 0.20	–	SB1	37 \pm 1	4.2 \pm 0.1	308
2052621328112787328	KIC 3454626	J19242875+3758587	2.38	688.5 \pm 8.8	0.38 \pm 0.10	–	SB1	352 \pm 3	23.5 \pm 0.2	–
2099534465609245184	KIC 3222519	J19111347+3820199	1.11	638 \pm 19	0.08 \pm 0.07	–	SB1	3.1 \pm 0.2	0.55 \pm 0.02	–
2051386576554694400	KIC 3437031	J19181953+3830139	1.63	624 \pm 10	0.08 \pm 0.10	43 \pm 5	ASB1	63 \pm 1	5.57 \pm 0.05	283
2052876169989763968	KIC 3439353	J19205281+3830283	1.69	522.2 \pm 14.4	0.17 \pm 0.10	–	SB1	85 \pm 1	7.58 \pm 0.02	69
2052170219113341824	KIC 3454626	J19363912+3834080	1.04	57.6 \pm 0.1	0.22 \pm 0.10	–	SB1	121 \pm 1	10.15 \pm 0.03	–
2099577209123927680	KIC 3532734	J19111567+3838265	1.0	49.5 \pm 0.1	0.44 \pm 0.10	–	SB1	147 \pm 3	11.77 \pm 0.02	75
2052283297009453440	KIC 3553435	J19344010+3840524	1.08	113.0 \pm 0.4	0.15 \pm 0.04	–	SB1	42.2 \pm 0.4	4.81 \pm 0.02	–
2052148847355741184	KIC 3558705	J19394056+3838367	3.02	401.9 \pm 0.4	0.116 \pm 0.004	107 \pm 1	ASB1	46 \pm 2	4.57 \pm 0.03	–
2073161236122435072	KIC 3663047	J19423515+3846510	1.4	276 \pm 2	0.22 \pm 0.04	–	SB1	54 \pm 1	5.67 \pm 0.02	–
2100051236074556032	KIC 3730801	J19042876+3848423	1.18	57.6 \pm 0.1	0.50 \pm 0.10	–	SB1	1482 \pm 26	76.1 \pm 2.4	–
2100048036318151296	KIC 3833819	J19032549+3856334	1.43	327.3 \pm 2.2	0.20 \pm 0.03	–	SB1	154 \pm 1	12.44 \pm 0.03	80
2099624934800877952	KIC 3836911	J19083005+3854427	1.23	105.2 \pm 0.2	0.21 \pm 0.03	–	SB1	57 \pm 3	5.5 \pm 0.6	–
2052866686700421760	KIC 3847697	J19224762+3859230	1.88	890 \pm 20	0.20 \pm 0.05	–	SB1	46 \pm 1	4.87 \pm 0.02	–
2052760828651350528	KIC 3850089	J19253546+3857039	1.24	1105.6 \pm 169.9	0.27 \pm 0.10	–	SB1	38 \pm 1	4.21 \pm 0.03	332
2052723956352547072	KIC 3852512	J19281028+3854056	1.57	940 \pm 80	0.21 \pm 0.15	–	SB1	32 \pm 3	3.4 \pm 0.1	–
2052301954347374208	KIC 3857864	J19334713+3854105	1.73	1277 \pm 147	0.15 \pm 0.06	–	SB1	44 \pm 1	4.51 \pm 0.02	–
2052206773569470720	KIC 3862485	J19381848+3858427	1.76	705.9 \pm 27.6	0.23 \pm 0.10	–	SB1	65 \pm 1	5.94 \pm 0.02	–
2073175598494019584	KIC 3869326	J19440792+3856121	2.2	732 \pm 6	0.14 \pm 0.02	–	SB1	48 \pm 2	4.60 \pm 0.04	229
2099684961263219840	KIC 3942719	J19115818+3902135	2.69	339 \pm 2	0.24 \pm 0.04	49 \pm 3	ASB1	788 \pm 28	45.2 \pm 1.7	–
2052957744310350976	KIC 3952580	J19240489+3900592	1.07	45.74 \pm 0.02	0.34 \pm 0.02	–	SB1	636 \pm 23	37 \pm 1	–
2053092228327403520	KIC 3958615	J19303237+3901286	1.2	4.344 \pm 0.001	0.13 \pm 0.10	–	SB1	10.2 \pm 0.3	1.63 \pm 0.03	–
2052389567376526720	KIC 3963755	J19354697+3905234	1.31	732 \pm 37	0.13 \pm 0.10	–	SB1	36 \pm 2	4.0 \pm 0.2	–
2100402598758481664	KIC 4042863	J19084656+3908428	1.15	183.8 \pm 1.8	0.13 \pm 0.10	–	SB1	64 \pm 1	6.46 \pm 0.02	–
2052965234733414528	KIC 4055294	J19241086+3907357	3.5	774 \pm 8	0.12 \pm 0.03	–	SB1	121 \pm 1	9.67 \pm 0.02	–
2052954475833401472	KIC 4056014	J19245972+3911026	1.44	798 \pm 27	0.12 \pm 0.12	–	SB1	45 \pm 1	4.32 \pm 0.03	318
2053153319943390080	KIC 4058998	J19281100+3911320	1.04	544 \pm 10	0.27 \pm 0.05	–	SB1	1.1 \pm 0.2	0.21 \pm 0.02	–
2052356242735632768	KIC 4064179	J19332703+3909019	2.28	611 \pm 19	0.20 \pm 0.08	–	SB1	11 \pm 1	1.56 \pm 0.03	–
2052446196529927808	KIC 4065254	J19342059+3911303	2.05	1256 \pm 314	0.22 \pm 0.10	–	SB1	86 \pm 2	7.22 \pm 0.05	–
2076176234438775936	KIC 4072847	J19414610+3909441	1.34	838 \pm 24	0.46 \pm 0.08	–	SB1	15 \pm 1	1.98 \pm 0.03	–
2076195819490063872	KIC 4073771	J19422940+3909088	1.2	890 \pm 65	0.07 \pm 0.10	–	SB1	36 \pm 1	4.26 \pm 0.05	–
2100222897327764608	KIC 4135933	J18584130+3917235	0.98	151 \pm 1	0.24 \pm 0.05	–	SB1	51 \pm 3	5.3 \pm 0.7	–
2100263579256869504	KIC 4139473	J19034869+3914505	1.54	772 \pm 65	0.19 \pm 0.20	–	SB1	39.7 \pm 0.5	4.26 \pm 0.02	–
2053155587686210304	KIC 4159982	J19284176+3917395	1.04	1002 \pm 240	0.56 \pm 0.20	–	SB1	42.0 \pm 0.4	4.75 \pm 0.02	–
2073282251119558656	KIC 4283451	J19452429+3921440	1.14	225.9 \pm 3.1	0.21 \pm 0.14	–	SB1	76 \pm 2	6.41 \pm 0.02	–
2100280342512106624	KIC 4346953	J19023044+3924283	1.37	1129 \pm 187	0.36 \pm 0.04	–	SB1	27 \pm 1	3.04 \pm 0.02	–
2101010834849710080	KIC 4358067	J19182905+3924303	1.01	139.5 \pm 0.6	0.34 \pm 0.06	–	SB1	3.59 \pm 0.06	0.71 \pm 0.03	–
2100312095207809280	KIC 4446300	J19012602+3933549	1.91	104.7 \pm 0.1	0.32 \pm 0.02	–	SB1	842 \pm 34	51.5 \pm 1.6	–
2053219840395711232	KIC 4470280	J19325679+3931207	5.74	702 \pm 4	0.41 \pm 0.02	–	SB1	80 \pm 1	7.11 \pm 0.02	70
2076211418811777920	KIC 4480938	J19430914+3932335	1.7	924 \pm 243	0.14 \pm 0.20	–	SB1	36 \pm 2	3.95 \pm 0.04	328
2100336902938929664	KIC 4543371	J19011769+3938293	2.64	3.115 \pm 0.001	0.36 \pm 0.20	–	SB1	94 \pm 1	7.70 \pm 0.04	–
2053182177821920000	KIC 4563149	J19282666+3941506	1.13	325 \pm 6	0.18 \pm 0.07	–	SB1	1.54 \pm 0.03	0.29 \pm 0.03	–
2052474298488093056	KIC 4568872	J19344311+3936355	0.91	79.9 \pm 0.2	0.23 \pm 0.10	–	SB1	46.3 \pm 0.5	5.11 \pm 0.02	–
2052484267120834816	KIC 4570120	J19355625+3939394	1.22	348.4 \pm 3.1	0.20 \pm 0.05	–	SB1	88 \pm 2	7.35 \pm 0.03	278
2073256687473394176	KIC 4585322	J19485961+3938059	1.12	858.1 \pm 29.1	0.10 \pm 0.05	–	SB1	6.8 \pm 0.4	1.1 \pm 0.1	–
2101230354919523840	KIC 4644949	J19151456+3947520	1.32	217.4 \pm 0.8	0.11 \pm 0.03	–	SB1	61 \pm 1	6.27 \pm 0.02	–
2076459324320451968	KIC 4664716	J19374983+3943195	1.47	513 \pm 7	0.18 \pm 0.09	–	ORB	149 \pm 1	12.54 \pm 0.03	82
2076277075966246016	KIC 4669400	J19420788+3947570	0.92	1065.3 \pm 344.3	0.47 \pm 0.30	–	SB1	45.2 \pm 0.4	4.91 \pm 0.02	–
2076453826762716416	KIC 4758020	J19392385+3952379	1.06	290 \pm 7	0.18 \pm 0.18	–	SB1	96 \pm 3	7.4 \pm 0.1	–
2076327275543672448	KIC 4852408	J19442124+3955537	1.65	667 \pm 17	0.12 \pm 0.08	–	ORB	165 \pm 2	12.42 \pm 0.04	86
2101240083023021952	KIC 4914923	J19163489+4002501	5.14	99.2 \pm 0.1	0.21 \pm 0.01	114 \pm 2	ASB1	1825 \pm 108	88.6 \pm 2.5	–
2053263477264248192	KIC 4930617	J19345069+4004116	0.99	1024.5 \pm 118.4	0.46 \pm 0.08	–	SB1	49 \pm 1	4.70 \pm 0.03	354
2073482430962320384	KIC 4949422	J19515497+4001290	0.94	965 \pm 146	0.42 \pm 0.29	–	SB1	49 \pm 2	4.60 \pm 0.05	335
2101147925907927168	KIC 5005508	J19202288+4009407	3.0	1234.7 \pm 249.6	0.34 \pm 0.04	–	SB1	44 \pm 1	4.32 \pm 0.02	–
2076388852501354624	KIC 5025895	J19421683+4008114	1.68	539 \pm 5	0.79 \pm 0.03	118 \pm 3	ASB1	130 \pm 2	10.23 \pm 0.02	–
2103380694721252736	KIC 5080332	J18592342+4015598	4.53	993 \pm 84	0.26 \pm 0.03	–	SB1	86 \pm 1	6.71 \pm 0.05	–
2100556800967018368	KIC 5087190	J19115123+4013021	1.37	959 \pm 107	0.33 \pm 0.15	–	SB1	70 \pm 2	6.1 \pm 0.1	–
2053442938176										

Table B.1. Orbital and seismic parameters of *Gaia* DR3 binary systems. (cont.)

Gaia DR3	KIC/TIC	2MASS	ruwe	P_{orb} [d]	e	i [deg]	Type	ν_{max} [μHz]	$\Delta\nu$ [μHz]	$\Delta\Pi_1$ [s]
2073688073986690816	KIC 5123659	J19505795+4016194	1.08	801.0 ± 84.8	0.05 ± 0.10	–	SB1	47 ± 2	4.9 ± 0.2	–
2103662384718180992	KIC 5252229	J18522890+4026027	1.4	1739 ± 567	0.72 ± 0.08	86 ± 4	ASB1	9.0 ± 0.3	1.41 ± 0.02	–
2076399847618000640	KIC 5290071	J19431995+4025391	1.32	1006 ± 67	0.28 ± 0.10	–	SB1	38 ± 2	4.4 ± 0.1	270
2101501801151469568	KIC 5360757	J19250988+4030412	1.01	57.1 ± 0.2	0.10 ± 0.10	–	SB1	38 ± 1	4.18 ± 0.02	–
2077293544406754944	KIC 5369569	J19352717+4033204	1.03	260.0 ± 2.6	0.25 ± 0.05	–	SB1	6 ± 1	1.0 ± 0.1	–
2075041126129307904	KIC 5395743	J19582034+4032579	0.98	199.6 ± 1.9	0.13 ± 0.10	–	SB1	1.8 ± 0.1	0.39 ± 0.03	–
2101337939558758656	KIC 5439189	J19153859+4040529	1.1	611.4 ± 11.7	0.19 ± 0.10	–	SB1	2.52 ± 0.06	0.47 ± 0.03	–
2101506645874572672	KIC 5446355	J19244093+4037109	1.0	822 ± 46	0.11 ± 0.12	–	SB1	8.0 ± 0.4	1.27 ± 0.03	–
2053572268231601024	KIC 5449290	J19282423+4041569	1.07	995.8 ± 78.6	0.09 ± 0.09	–	SB1	3.2 ± 0.1	0.64 ± 0.02	–
2053521347098854400	KIC 5450413	J19294602+4037219	0.99	705 ± 15	0.24 ± 0.08	–	SB1	4.80 ± 0.06	0.84 ± 0.02	–
2103619323103701248	KIC 5513771	J18571125+4042333	1.86	1034 ± 128	0.57 ± 0.10	–	SB1	173 ± 2	14.3 ± 0.1	85
2103639423550660992	KIC 5514079	J18575250+4044558	1.48	200.3 ± 0.4	0.14 ± 0.03	–	SB1	87 ± 1	7.81 ± 0.02	71
2100777463504599936	KIC 5516982	J19033956+4042178	1.47	24.12 ± 0.02	0.42 ± 0.04	–	SB1	1699 ± 110	85 ± 2	–
2100639882814366720	KIC 5520879	J19102359+4043483	1.23	368.5 ± 5.9	0.16 ± 0.10	–	SB1	19.2 ± 0.3	2.62 ± 0.02	–
2053573470824578048	KIC 5534910	J19285814+4046073	2.27	852 ± 38	0.24 ± 0.10	–	SB1	114 ± 2	8.15 ± 0.03	166
2076759594075651712	KIC 5553963	J19481244+4046338	1.3	911 ± 52	0.19 ± 0.10	–	SB1	7.4 ± 0.5	1.16 ± 0.02	–
2073748886419358080	KIC 5556726	J19502892+4045468	1.0	172.0 ± 1.1	0.21 ± 0.06	–	SB1	178 ± 2	14.44 ± 0.02	–
2103782085185469184	KIC 5603153	J19035686+4049356	1.33	1234 ± 392	0.18 ± 0.15	–	SB1	45 ± 2	4.64 ± 0.05	–
2100876728789365248	KIC 5603916	J19051840+4051499	1.34	722 ± 7	0.31 ± 0.03	–	SB1	40 ± 2	4.01 ± 0.03	–
2076657854889834624	KIC 5630215	J19391015+4049146	0.96	286 ± 4	0.31 ± 0.14	–	SB1	93 ± 3	7.50 ± 0.02	–
2075107779718925824	KIC 5650920	J19570728+4050462	1.11	530.3 ± 16.7	0.24 ± 0.13	–	SB1	39 ± 2	4.19 ± 0.05	–
2101350480864569600	KIC 5696625	J19155268+4054243	2.59	611.4 ± 7.2	0.28 ± 0.10	94 ± 2	ASB1	696 ± 5	39 ± 3	–
2101583508609740544	KIC 5701850	J19222458+4059345	1.23	4.579 ± 0.002	0.17 ± 0.10	–	SB1	43 ± 1	4.59 ± 0.02	–
2053578414322587392	KIC 5706724	J19285078+4054466	1.2	462 ± 7	0.51 ± 0.10	–	SB1	98 ± 2	8.50 ± 0.02	–
2053580548928810624	KIC 5707338	J19293455+4054186	1.77	885.2 ± 14.2	0.27 ± 0.07	–	SB1	82 ± 2	6.42 ± 0.04	–
2053555565096596736	KIC 5708328	J19304518+4059191	0.98	927.6 ± 50.6	0.73 ± 0.10	–	SB1	0.8 ± 0.2	0.24 ± 0.03	–
2103826787205344384	KIC 5773063	J19011386+4100430	1.09	247.4 ± 1.6	0.37 ± 0.05	–	SB1	48.5 ± 0.4	5.10 ± 0.02	–
2100883257139719936	KIC 5775365	J19052614+4103172	0.88	47.6 ± 0.2	0.22 ± 0.20	–	SB1	75 ± 1	6.66 ± 0.02	–
2053559963143105024	KIC 5793427	J19302545+4105344	5.73	1097.4 ± 94.9	0.29 ± 0.07	–	SB1	103 ± 1	8.87 ± 0.02	–
2077379443754039424	KIC 5795626	J19330865+4103865	3.52	672.9 ± 29.6	0.13 ± 0.06	–	SB1	38 ± 1	4.5 ± 0.1	311
2076808449315837952	KIC 5808444	J19460744+4103253	1.04	491 ± 15	0.20 ± 0.08	–	SB1	39 ± 1	4.28 ± 0.05	–
2073864270727630720	KIC 5814512	J19511453+4105051	1.48	223 ± 1	0.42 ± 0.10	–	ORB	995 ± 22	53.4 ± 1.7	–
2104030948471415168	KIC 5857618	J18583415+4110232	1.24	440 ± 4	0.21 ± 0.04	–	SB1	72 ± 1	6.33 ± 0.02	83
2103831524550631936	KIC 5878947	J19011396+4109061	2.91	648 ± 6	0.27 ± 0.03	98 ± 2	ASB1	169 ± 1	14.53 ± 0.02	84
2073818121288491776	KIC 5903484	J19544774+4106066	0.97	1141 ± 231	0.34 ± 0.07	–	SB1	30 ± 1	3.40 ± 0.03	–
2075131767121611520	KIC 5905600	J19562716+4107029	1.24	478.2 ± 3.9	0.38 ± 0.03	–	SB1	25 ± 1	3.2 ± 0.1	–
2103890730678335744	KIC 5944521	J19041021+4115215	2.05	288 ± 1	0.35 ± 0.01	–	SB1	26 ± 1	3.1 ± 0.2	–
2076825526105843584	KIC 5956252	J19450026+4116054	1.1	690 ± 17	0.22 ± 0.05	–	SB1	2.77 ± 0.04	0.49 ± 0.03	–
2077577184045787776	KIC 6047277	J19331843+4119533	1.2	259 ± 1	0.03 ± 0.03	–	SB1	15.1 ± 0.4	2.07 ± 0.02	–
2104434198659211392	KIC 6100454	J18501226+4127020	2.02	557.6 ± 5.3	0.31 ± 0.06	–	ORB	114 ± 1	10.17 ± 0.02	–
2101483384332074624	KIC 6116806	J19184248+4125258	1.2	129.6 ± 1.9	0.10 ± 0.20	–	SB1	37.6 ± 0.4	4.20 ± 0.02	–
2101656832290462208	KIC 6122562	J19260235+4126329	1.62	694 ± 34	0.15 ± 0.13	–	SB1	33 ± 2	4.01 ± 0.03	294
2101657480823132416	KIC 6122831	J19262277+4128265	1.11	1.016	0.36 ± 0.05	–	SB1	164 ± 2	12.95 ± 0.02	–
2077449812496895360	KIC 6131901	J19372371+4126341	1.05	826 ± 48	0.55 ± 0.10	–	SB1	24 ± 1	3.4 ± 0.1	–
2073887493600315264	KIC 6148227	J19525271+4127446	1.87	723.9 ± 22.7	0.15 ± 0.10	–	SB1	58 ± 1	4.99 ± 0.04	326
2104440142893990144	KIC 6181933	J18503555+4130292	4.78	859 ± 15	0.14 ± 0.03	–	SB1	65 ± 2	6.0 ± 0.1	300
2104098843314446336	KIC 6185855	J18580529+4135521	3.53	650.0 ± 5.5	0.46 ± 0.03	64 ± 2	ASB1	53.3 ± 0.6	5.61 ± 0.02	–
2103960721465404800	KIC 6188269	J19024815+4135564	1.44	898 ± 108	0.15 ± 0.20	–	SB1	65 ± 1	5.65 ± 0.03	–
2077420705493842560	KIC 6211965	J19355461+4135577	2.05	1182 ± 181	0.13 ± 0.07	–	SB1	71 ± 1	6.78 ± 0.02	–
2076903011623188224	KIC 6227242	J19504089+4133247	1.07	88.3 ± 0.2	0.52 ± 0.03	–	SB1	144 ± 3	11.10 ± 0.03	–
2104442307558409984	KIC 6263054	J18505497+4136047	1.23	941.0 ± 24.7	0.55 ± 0.10	–	SB1	21 ± 1	2.4 ± 0.2	–
2100923561113199744	KIC 6271732	J19075561+4136535	1.66	1136 ± 153	0.36 ± 0.13	–	SB1	32 ± 1	4.05 ± 0.03	–
2076861328957750144	KIC 6302852	J19465188+4140126	1.64	396 ± 7	0.28 ± 0.08	–	SB1	69 ± 2	6.03 ± 0.02	–
2102242700188455936	KIC 6357581	J19183626+4147482	1.05	987.8 ± 140.2	0.13 ± 0.16	–	SB1	42.2 ± 0.4	4.67 ± 0.02	–
2077621675604329472	KIC 6368959	J19333162+4146595	1.16	296 ± 2	0.11 ± 0.05	–	SB1	28.7 ± 0.5	3.26 ± 0.02	–
2104121387601791360	KIC 6423690	J18562944+4153250	1.55	662 ± 12	0.05 ± 0.04	–	SB1	34 ± 1	4.1 ± 0.1	305
2076914552192280448	KIC 6456563	J19514687+4154566	1.76	892 ± 70	0.29 ± 0.10	–	SB1	30 ± 3	4.8 ± 0.4	–
2104149012831597312	KIC 6458516	J18574335+4204449	1.97	868.2 ± 82.2	0.12 ± 0.14	–	SB1	64 ± 1	5.89 ± 0.02	–
2104091043653848320	KIC 6458723	J19002129+4203315	2.86	688.0 ± 17.6	0.05 ± 0.09	–	SB1	499 ± 3	32.1 ± 1.6	–
2101701706110031872	KIC 6606904	J19281499+4205159	1.06	482 ± 11	0.09 ± 0.08	–	SB1	46 ± 1	4.80 ± 0.02	306
2077725515035808640	KIC 6612265	J19342447+4204085	0.95	101.6 ± 0.4	0.41 ± 0.06	–	SB1	27 ± 1	3.17 ± 0.02	–
2105441278291399808	KIC 6676125	J19064459+4209479	1.47	546.4 ± 8.5	0.72 ± 0.10	–	ORB	169 ± 1	14.1 ± 0.1	–
2102506548618822272	KIC 6851499	J19122254+4223498	1.92	434.3 ± 4.3	0.30 ± 0.05	132 ± 4	ASB1	52 ± 1	5.62 ± 0.02	65
2125736995932614272	KIC 6866251	J19305929+4222477	0.91	371 ± 3	0.43 ± 0.05	–	SB1	95 ± 2	7.14 ± 0.04	–
2077562752958818560	KIC 6871557	J19370506+4221265	1.59	451.0 ± 8.1	0.15 ± 0.10	–	SB1	58 ± 1	6.03 ± 0.02	–
2105473993062697856	KIC 6933899	J19065834+4226082	13.14	4063.7 ± 455.1	0.92 ± 0.01	75 ± 1	ASB1	1377 ± 90	72 ± 2	–
2125788157584801280	KIC 6947945	J19262433+4229049	1.64	110.6 ± 0.3	0.20 ± 0.10	–	SB1	733 ± 31	44 ± 2	–
2125737678826723584	KIC 6951289	J19303877+4225194	1.61	552.9 ± 11.9	0.12 ± 0.10	–	SB1	111 ± 2	9.28 ± 0.02	–
210546670449777280	KIC 7018515	J19055785+4230512	2.19	498.3 ± 4.3	0.42 ± 0.03	71 ± 2	ASB1	103 ± 1	9.17 ± 0.03	77
2102562108315581952	KIC 7020972	J19101321+4235287	1.06	606 ± 9	0.20 ± 0.05	–	SB1	4.2 ± 0.2	0.77 ± 0.02	–
2102698207235956096	KIC 7025377	J19164706+4231499	1.35	1196 ± 148	0.17 ± 0.10	–	SB1	16 ± 1	2.59 ± 0.05	–
2102673124631301248	KIC 7026573	J19181979+4232040	1.18	867.7 ± 65.6	0.04 ± 0.10	–	SB1	37 ± 1	4.2 ± 0.1	313
2101960842953106432	KIC 7032190	J19252144+4232507	1.18	773.5 ± 115.3	0.64 ± 0.32	–	SB1	44 ± 1	4.64 ± 0.04	307
2077754235474155776	KIC 7041744	J19364761+4235320	0.89	893 ± 114	0.66 ± 0.20	–	SB1	31 ± 1	3.67 ± 0.04	316

Table B.1. Orbital and seismic parameters of *Gaia* DR3 binary systems. (cont.)

Gaia DR3	KIC/TIC	2MASS	ruwe	P_{orb} [d]	e	i [deg]	Type	ν_{max} [μHz]	$\Delta\nu$ [μHz]	$\Delta\Pi_1$ [s]
2078506065218151424	KIC 7138406	J19490877+4239031	3.96	638.0 \pm 6.3	0.42 \pm 0.03	–	ORB	245 \pm 2	18.3 \pm 0.2	–
2102543450978006784	KIC 7188950	J19121918+4244132	1.18	130.0 \pm 0.4	0.34 \pm 0.04	–	SB1	41.7 \pm 0.6	4.48 \pm 0.02	–
2102705938181969408	KIC 7191496	J19160765+4246319	1.15	803.5 \pm 26.5	0.11 \pm 0.10	–	SB1	16.2 \pm 0.3	2.45 \pm 0.03	–
2125797537791963520	KIC 7200133	J19265290+4245078	1.87	640.5 \pm 4.1	0.47 \pm 0.05	49 \pm 4	ASB1	40 \pm 1	4.23 \pm 0.02	–
2077773790469159680	KIC 7206837	J19350373+4244165	0.99	4.050	0.00 \pm 0.02	–	SB1	1645 \pm 121	79.2 \pm 1.8	–
2105536764004280576	KIC 7265649	J19035086+4253088	1.05	20.99 \pm 0.04	0.41 \pm 0.12	–	SB1	11.3 \pm 0.3	1.6 \pm 0.2	–
2102593513117206016	KIC 7350968	J19113234+4256584	1.89	355.7 \pm 1.3	0.31 \pm 0.02	–	SB1	14 \pm 1	2.0 \pm 0.1	–
2125850206971011072	KIC 7366321	J19313409+4255245	1.27	749.1 \pm 14.5	0.07 \pm 0.10	–	SB1	43 \pm 1	4.56 \pm 0.03	298
2078011486835316992	KIC 7374869	J19410937+4258421	3.4	787 \pm 61	0.20 \pm 0.08	–	SB1	145 \pm 1	11.56 \pm 0.02	–
2078007986445543552	KIC 7375177	J19412604+4254039	1.15	734.1 \pm 37.5	0.15 \pm 0.10	–	SB1	76 \pm 2	6.12 \pm 0.05	–
2078012762449199360	KIC 7457184	J19410681+4303056	1.17	148.2 \pm 0.2	0.13 \pm 0.02	–	SB1	66 \pm 1	5.91 \pm 0.02	73
2078541627548979328	KIC 7467630	J19501503+4305506	1.36	1210 \pm 148	0.22 \pm 0.10	–	SB1	73 \pm 2	6.06 \pm 0.03	292
2116826072661485312	KIC 7499531	J18414542+4308496	1.0	116 \pm 1	0.05 \pm 0.10	–	SB1	70 \pm 1	6.11 \pm 0.02	80
2105730488509329920	KIC 7510397	J19023940+4307029	4.28	61.63 \pm 0.05	0.51 \pm 0.03	–	SB1	1196 \pm 96	62.6 \pm 1.4	–
2125869521443115776	KIC 7530403	J19303177+4311093	1.13	220 \pm 1	0.02 \pm 0.04	–	SB1	1.98 \pm 0.03	0.41 \pm 0.02	–
2125867975254885120	KIC 7530451	J19303555+4309367	1.44	963.7 \pm 52.4	0.09 \pm 0.07	99 \pm 4	ASB1	50 \pm 1	4.92 \pm 0.02	339
2125879588848285952	KIC 7531332	J19313658+4309553	0.95	81.9 \pm 0.2	0.20 \pm 0.03	–	SB1	89 \pm 1	7.88 \pm 0.02	–
2078064881868792192	KIC 7539174	J19400036+4310168	1.7	1540.0 \pm 268.9	0.38 \pm 0.10	93 \pm 2	ASB1	46.1 \pm 0.5	5.04 \pm 0.02	–
2077275363805920000	KIC 7534672	J19441996+4307421	0.92	234.9 \pm 1.9	0.22 \pm 0.10	–	SB1	18.7 \pm 0.5	2.19 \pm 0.02	–
2102616259264055680	KIC 7595572	J19095280+4316024	1.31	685 \pm 14	0.17 \pm 0.05	–	SB1	51 \pm 2	4.89 \pm 0.04	323
2102976143158442240	KIC 7596350	J19111479+4315088	1.25	647 \pm 11	0.04 \pm 0.05	–	SB1	43.92 \pm 0.04	4.68 \pm 0.02	–
2102803416758915328	KIC 7602732	J19205861+4316421	1.04	109.6 \pm 0.7	0.33 \pm 0.10	–	SB1	56 \pm 1	5.92 \pm 0.02	65
2078021799060789888	KIC 7619818	J19412321+4315247	1.55	508.7 \pm 9.2	0.11 \pm 0.10	–	ORB	187 \pm 2	14.91 \pm 0.04	–
2105208632802645248	KIC 7661609	J18495226+4320427	1.06	106.6 \pm 0.1	0.19 \pm 0.01	–	SB1	23 \pm 1	2.72 \pm 0.02	–
2105655240682758784	KIC 7669332	J19062757+4322023	0.98	16.060 \pm 0.004	0.12 \pm 0.03	–	SB1	463 \pm 8	32 \pm 4	–
2078784409155413504	KIC 7767409	J19452669+4325554	8.63	858 \pm 44	0.23 \pm 0.10	–	SB1	119 \pm 2	9.51 \pm 0.03	68
2126047126931253248	KIC 7820868	J19250515+4335467	1.2	989 \pm 194	0.12 \pm 0.20	–	SB1	27 \pm 1	3.83 \pm 0.05	–
2103003493515093248	KIC 7880509	J19104476+4340425	2.08	2.425	–	–	SB1C	58 \pm 1	6.02 \pm 0.02	–
2103010979637374720	KIC 7880893	J19112795+4336547	1.28	130.2 \pm 0.5	0.45 \pm 0.03	–	SB1	133 \pm 2	11.01 \pm 0.01	–
2078195345796733056	KIC 7898413	J19372026+4339146	2.44	996 \pm 129	0.32 \pm 0.10	–	SB1	36.4 \pm 0.5	3.92 \pm 0.02	–
2078102372648860672	KIC 7901381	J19405956+4341186	1.0	420 \pm 9	0.39 \pm 0.13	–	SB1	32 \pm 1	3.68 \pm 0.02	–
2078793342681913216	KIC 7905696	J19460178+4337388	1.96	887 \pm 43	0.28 \pm 0.10	–	SB1	45 \pm 1	4.58 \pm 0.02	–
2078837666746964096	KIC 7909775	J19501324+4339539	1.36	913 \pm 12	0.46 \pm 0.02	–	SB1	1.44 \pm 0.03	0.31 \pm 0.02	–
2078993282002686720	KIC 7938221	J19544857+4343055	1.02	331.8 \pm 3.9	0.14 \pm 0.10	–	SB1	84 \pm 2	6.91 \pm 0.03	–
2106019247750146816	KIC 8016496	J19072417+4348317	3.37	712 \pm 12	0.25 \pm 0.03	120 \pm 2	ASB1	1045 \pm 30	54 \pm 2	–
20781216441161462016	KIC 8039063	J19410522+4353322	0.99	60.2 \pm 0.2	0.37 \pm 0.20	–	SB1	80 \pm 1	7.53 \pm 0.02	74
2126862827118663680	KIC 8093934	J19215733+4359243	1.54	675.0 \pm 21.9	0.18 \pm 0.10	–	ORB	86 \pm 1	8.45 \pm 0.03	–
2125976139712014848	KIC 8098590	J19284090+4355434	1.77	837.5 \pm 49.4	0.19 \pm 0.10	–	SB1	127 \pm 1	10.87 \pm 0.02	78
2078864467342860544	KIC 8114988	J19491528+4357277	1.1	675.8 \pm 12.8	0.01 \pm 0.04	–	SB1	1.46 \pm 0.03	0.34 \pm 0.02	–
2076036115424231680	KIC 8127707	J20015409+4358014	1.29	118.7 \pm 0.4	0.43 \pm 0.12	–	SB1	224 \pm 2	16.99 \pm 0.03	89
2105852293782390272	KIC 8149637	J18590692+4401028	1.8	929 \pm 469	0.49 \pm 0.20	–	SB1	139 \pm 1	11.45 \pm 0.02	–
2126210473126264448	KIC 8163250	J19233187+4405575	2.21	846 \pm 51	0.03 \pm 0.10	–	SB1	55 \pm 1	5.73 \pm 0.02	–
2078350072000091904	KIC 8172666	J19365024+4404058	0.95	394 \pm 5	0.07 \pm 0.08	–	SB1	56 \pm 2	5.14 \pm 0.03	320
2078126390106069376	KIC 8175438	J19402226+4401212	1.15	992.9 \pm 36.4	0.02 \pm 0.10	–	SB1	42 \pm 1	4.40 \pm 0.05	317
2078911578848824320	KIC 8181509	J19473900+4404373	3.1	1039.3 \pm 119.4	0.08 \pm 0.12	–	SB1	33 \pm 2	3.25 \pm 0.03	–
2076015327786778240	KIC 8192056	J19580204+4401225	1.17	883.3 \pm 18.8	0.19 \pm 0.04	–	SB1	3.29 \pm 0.06	0.66 \pm 0.02	–
2106608238086027520	KIC 8217125	J18574847+4410284	1.31	862.6 \pm 61.8	0.32 \pm 0.13	–	SB1	53.7 \pm 0.6	5.44 \pm 0.02	–
2106601267358233728	KIC 8217206	J18575907+4406340	1.02	966 \pm 58	0.69 \pm 0.20	–	SB1	21 \pm 2	2.5 \pm 0.1	–
2103086644080983552	KIC 8225926	J19163464+4409268	1.15	1085.4 \pm 114.5	0.31 \pm 0.10	–	SB1	29 \pm 2	2.9 \pm 0.2	–
2126210644924922496	KIC 8230578	J19231486+4406148	1.11	557.6 \pm 10.7	0.05 \pm 0.06	–	SB1	90 \pm 1	7.5 \pm 0.1	272
2126339695802448640	KIC 8235448	J19302386+4406026	1.27	255.3 \pm 1.4	0.11 \pm 0.04	–	SB1	32.0 \pm 0.5	3.71 \pm 0.02	–
2078912128603392128	KIC 8248948	J19474543+4407197	1.46	227.7 \pm 0.4	0.25 \pm 0.02	–	SB1	30 \pm 2	3.35 \pm 0.01	–
2076097271451099648	KIC 8260453	J19592289+4408304	0.93	1313.2 \pm 584.1	0.31 \pm 0.19	–	SB1	43 \pm 1	4.61 \pm 0.02	310
2076079305616028288	KIC 8328348	J20012933+4417205	1.62	579.2 \pm 13.4	0.14 \pm 0.05	66 \pm 3	ASB1	52 \pm 2	5.08 \pm 0.03	312
2126921612329489920	KIC 8358665	J19170268+4422390	0.98	148.0 \pm 0.9	0.13 \pm 0.08	–	SB1	17.8 \pm 0.4	2.24 \pm 0.02	–
2126219647176597120	KIC 8363272	J19235349+4418479	1.86	937.5 \pm 34.7	0.37 \pm 0.05	–	SB1	91 \pm 1	7.56 \pm 0.05	241
2126549053987387008	KIC 8365782	J19273691+4423124	2.11	702.8 \pm 5.2	0.07 \pm 0.02	–	SB1	83 \pm 2	6.31 \pm 0.03	–
2079601075715743360	KIC 8378481	J19445982+4421035	2.29	596.0 \pm 11.3	0.31 \pm 0.03	–	SB1	62.1 \pm 0.5	6.17 \pm 0.02	–
2117369471924207232	KIC 8408931	J18440812+4426509	1.02	18.571 \pm 0.004	0.10 \pm 0.02	–	SB1	609 \pm 5	34 \pm 2	–
2117404656294880000	KIC 8410006	J18470819+4426322	1.28	437 \pm 17	0.15 \pm 0.10	–	SB1	31.4 \pm 0.4	3.85 \pm 0.02	–
2106673315430481280	KIC 8414062	J18561527+4427183	6.38	791.4 \pm 7.7	0.07 \pm 0.03	133 \pm 2	ASB1	1100 \pm 14	72.7 \pm 2.3	–
2076131120102611456	KIC 8458459	J20003730+4426278	2.77	890.5 \pm 29.3	0.05 \pm 0.06	–	SB1	209 \pm 2	16.11 \pm 0.03	87
2105405307945593984	KIC 8475872	J18492457+4432239	1.91	852.5 \pm 9.2	0.03 \pm 0.03	–	SB1	32.2 \pm 0.5	4.05 \pm 0.04	–
2126565924618897280	KIC 8494839	J19263774+4434325	1.0	233.6 \pm 1.7	0.06 \pm 0.05	–	SB1	1.56 \pm 0.03	0.38 \pm 0.03	–
2106293507181579648	KIC 8547279	J19043616+4441299	2.86	492 \pm 3	0.62 \pm 0.03	133 \pm 3	ASB1	366 \pm 16	26 \pm 4	–
2126579458058892544	KIC 8561238	J19291104+4441085	1.47	966 \pm 84	0.24 \pm 0.10	–	SB1	57 \pm 1	5.32 \pm 0.02	315
2079656910290968320	KIC 8570823	J19430724+4437348	1.15	599 \pm 20	0.06 \pm 0.10	–	SB1	37 \pm 2	4.00 \pm 0.05	329
2076139877526679040	KIC 8587948	J20011735+4439452	1.67	214.7 \pm 0.6	0.29 \pm 0.02	–	SB1	82 \pm 2	6.82 \pm 0.04	234
2126948004910921472	KIC 8619322	J19190884+4446426	2.63	984 \pm 30	0.42 \pm 0.07	–	SB1	78 \pm 2	6.9 \pm 0.1	279
2126572242512906752	KIC 8625289	J19275253+4445017	1.36	388 \pm 2	0.18 \pm 0.03	–	SB1	2.01 \pm 0.04	0.39 $\$	

Table B.1. Orbital and seismic parameters of *Gaia* DR3 binary systems. (cont.)

Gaia DR3	KIC/TIC	2MASS	ruwe	P_{orb} [d]	e	i [deg]	Type	ν_{max} [μHz]	$\Delta\nu$ [μHz]	$\Delta\Pi_1$ [s]
2106316150250297472	KIC 8677016	J19050879+4448309	4.54	347 ±4	0.16 ±0.06	–	SB1	1882 ±54	92.6 ±2.4	–
2126960752373840256	KIC 8683589	J19184517+4449131	1.22	1338 ±636	0.18 ±0.19	–	SB1	16.7 ±0.4	2.36 ±0.02	–
2126626260320170624	KIC 8752893	J19261819+4459436	2.26	370.0 ±1.1	0.21 ±0.02	–	SB1	68 ±1	6.61 ±0.02	–
2078410682579606400	KIC 8759207	J19360805+4454226	1.66	959 ±44	0.25 ±0.10	–	SB1	82 ±1	7.08 ±0.02	280
2082118063992336768	KIC 8784382	J20051982+4459585	1.38	1255.7 ±623.1	0.17 ±0.20	–	SB1	55 ±1	5.46 ±0.05	319
2127014937679781760	KIC 8816007	J19225418+4500004	1.25	246 ±3	0.32 ±0.07	–	SB1	205 ±2	15.62 ±0.03	86
2126649586280860544	KIC 8818802	J19270676+4503429	1.26	1214 ±201	0.50 ±0.08	–	SB1	2.04 ±0.05	0.38 ±0.02	–
2079911893908124416	KIC 8824732	J19362457+4500275	1.2	429 ±6	0.33 ±0.06	–	SB1	53 ±1	5.30 ±0.02	–
2079915600456768256	KIC 8825444	J19372696+4503329	1.36	128.5 ±0.3	0.04 ±0.03	–	SB1	81 ±3	6.58 ±0.04	–
2082178395390565632	KIC 8914923	J20031610+4509192	1.55	1305 ±348	0.15 ±0.08	–	SB1	62 ±13	6.6 ±0.2	–
2106768079588474624	KIC 8936339	J18575109+4516185	1.5	796 ±55	0.05 ±0.12	–	SB1	44 ±1	4.6 ±0.1	275
2126514453732259584	KIC 8956226	J19321605+4513571	1.25	868 ±32	0.12 ±0.04	–	SB1	2.13 ±0.04	0.48 ±0.02	–
20821791556608496256	KIC 8984355	J20032129+4513187	1.0	51.5 ±0.2	0.12 ±0.10	–	SB1	188 ±1	14.37 ±0.04	83
2106992311244648448	KIC 9002884	J18540578+4520474	1.1	585 ±16	0.03 ±0.10	–	SB1	4.8 ±0.2	0.90 ±0.02	–
2126516412237386880	KIC 9025370	J19321460+4518384	5.16	239.1 ±0.5	0.27 ±0.03	–	ORB	3045 ±76	131 ±4	–
2079978998476343296	KIC 9031549	J19403884+4521015	1.32	141.4 ±0.6	0.18 ±0.10	–	SB1	73 ±1	7.11 ±0.02	71
2127414507076699648	KIC 9086060	J19231055+4527206	0.92	453 ±12	0.21 ±0.09	–	SB1	47 ±1	4.71 ±0.05	258
2079984805272568192	KIC 9098294	J19402120+4529209	1.64	20.101 ±0.003	0.02 ±0.02	–	SB1	2368 ±103	110.0 ±3.2	–
2127323350690676736	KIC 91477335	J19142703+4535380	0.95	1056 ±133	0.44 ±0.10	–	SB1	50 ±1	4.98 ±0.03	322
2127418973843085184	KIC 9151578	J19222634+4532326	1.9	873.2 ±39.1	0.62 ±0.10	–	SB1	26 ±1	3.11 ±0.04	219
2127417049697428864	KIC 9152245	J19232912+4533427	2.48	504 ±9	0.21 ±0.10	–	SB1	129 ±1	11.02 ±0.02	80
2126539467621880320	KIC 9157260	J19313671+4532500	4.01	675.0 ±30.4	0.30 ±0.04	–	SB1	233 ±2	18.10 ±0.03	–
2079988275606270720	KIC 9163769	J19411858+4532375	1.05	3.175	0.01 ±0.02	–	SB1	1573 ±12	80.6 ±1.9	–
2107175315507604352	KIC 9204313	J18590801+4540561	5.08	1073 ±69	0.66 ±0.04	–	ORB	1354 ±31	73 ±2	–
2106471902943000960	KIC 9206941	J19050068+4539045	2.19	1008.4 ±97.7	0.09 ±0.10	57 ±4	ASB1	43.3 ±0.4	4.92 ±0.03	65
2130237262663056512	KIC 9209245	J19102283+4541405	0.86	22.921 ±0.005	0.22 ±0.03	–	SB1	1017 ±20	54 ±2	–
2080048954904573056	KIC 9225600	J19383293+4541328	1.6	344 ±2	0.41 ±0.06	51 ±5	ASB1	1192 ±30	64.0 ±1.8	–
2080035760764475776	KIC 9225958	J19390626+4536122	1.1	198.1 ±1.9	0.30 ±0.10	–	SB1	171 ±2	13.51 ±0.02	82
2079427009281199488	KIC 9237611	J19532144+4538467	1.34	700 ±24	0.36 ±0.08	–	SB1	38 ±3	4.2 ±0.5	–
2085243318408612608	KIC 9240941	J19571060+4537363	1.37	254 ±1	0.13 ±0.04	–	SB1	107 ±3	8.33 ±0.04	–
2127247037712503040	KIC 9273251	J19131848+4545298	1.83	488 ±6	0.63 ±0.10	124 ±4	ASB1	169 ±1	13.76 ±0.02	84
2107404288802819712	KIC 9326421	J18543641+4550541	2.23	775.3 ±79.9	0.37 ±0.09	–	SB1	68 ±1	6.80 ±0.02	–
2107178682759063296	KIC 9328372	J18584987+4550576	1.22	95.9 ±0.6	0.28 ±0.08	–	SB1	1379 ±49	69 ±2	–
2130263513502675072	KIC 9340290	J19102759+4553438	1.21	394 ±2	0.39 ±0.02	–	SB1	24.4 ±0.4	2.96 ±0.02	–
2128033944442073984	KIC 9346607	J19340574+4549361	1.45	876.9 ±124.7	0.12 ±0.14	–	SB1	43.3 ±0.5	4.66 ±0.02	–
2107174387794486528	KIC 9390670	J18594346+4557377	8.84	1041.9 ±156.4	0.54 ±0.30	–	SB1	1351 ±27	71 ±2	–
2085308400058034816	KIC 9430039	J20015898+4554344	1.35	0.797	0.17 ±0.30	–	SB1	57 ±1	5.87 ±0.02	–
2128063768695712256	KIC 9469212	J19341942+4604596	1.78	993 ±142	0.26 ±0.20	–	SB1	46 ±2	4.37 ±0.05	232
2107095222956882688	KIC 9509251	J18504770+4609166	0.85	220 ±1	0.22 ±0.04	–	SB1	7.0 ±0.5	1.21 ±0.02	–
2127681550963320576	KIC 9521696	J19192803+4609448	1.15	824.2 ±25.9	0.37 ±0.10	–	SB1	4.3 ±0.4	0.85 ±0.02	–
2128259103806871168	KIC 9590062	J19304122+4614122	0.95	90.89 ±0.04	0.35 ±0.02	–	SB1	140 ±1	10.69 ±0.03	–
2128080776766136704	KIC 9591529	J19330295+4613427	1.09	89.9 ±0.3	0.07 ±0.06	–	SB1	26 ±1	3.2 ±0.1	–
2080405432886650880	KIC 9597524	J19415343+4614449	1.18	960 ±82	0.38 ±0.20	–	SB1	37 ±1	4.26 ±0.04	322
2107491287660520832	KIC 9693187	J18510009+4625209	1.7	103.8 ±0.2	0.39 ±0.04	66 ±2	ASB1	1527 ±75	80 ±2	–
2107295780749712128	KIC 9696716	J18591290+4626283	1.17	249.9 ±2.1	0.41 ±0.08	–	SB1	24 ±1	3.31 ±0.03	–
2130384528501056000	KIC 9702369	J19124093+4624012	4.84	195.8 ±0.3	0.40 ±0.02	117 ±3	ASB1	2039 ±119	94.0 ±2.4	–
2130386177768568704	KIC 9702609	J19131244+4629496	1.01	119.6 ±0.5	0.09 ±0.10	–	SB1	45.8 ±0.5	4.96 ±0.02	–
2080098536007525120	KIC 9718024	J19394402+4627390	1.89	960.6 ±79.9	0.11 ±0.10	–	SB1	35 ±1	4.1 ±0.1	336
2080271429909797504	KIC 9724859	J19490511+4626307	0.96	194 ±3	0.12 ±0.10	–	SB1	33 ±1	3.57 ±0.02	–
2119130923909851904	KIC 9753178	J18491645+4632307	1.23	935.7 ±129.5	0.62 ±0.16	–	SB1	30 ±1	4.1 ±0.2	332
2107318870494224640	KIC 9757624	J18594776+4635013	1.09	32.6 ±0.2	0.12 ±0.20	–	SB1	112 ±2	10.03 ±0.03	–
2119134630463422720	KIC 9813102	J18482411+4637472	1.79	996 ±101	0.27 ±0.12	–	SB1	30 ±1	4.01 ±0.04	–
2127764083055345664	KIC 9824516	J19151761+4636526	1.73	726.4 ±15.1	0.03 ±0.06	–	SB1	186 ±2	14.09 ±0.03	–
2128178594640028800	KIC 9835672	J19351093+4639586	1.9	361.4 ±0.6	0.37 ±0.01	–	SB1	4.0 ±0.2	0.80 ±0.02	–
2128177873085526400	KIC 9835853	J19352912+4638019	1.03	107.7 ±0.2	0.35 ±0.03	–	SB1	23.1 ±0.5	2.81 ±0.03	–
2080337748505913728	KIC 9843910	J19470909+4636499	1.21	323.3 ±3.4	0.03 ±0.05	–	SB1	51.3 ±0.4	5.13 ±0.02	–
2130547221862394880	KIC 9880324	J19061670+4642036	2.22	1439 ±95	0.45 ±0.04	73 ±2	ASB1	50 ±1	5.02 ±0.02	–
2127721850636523904	KIC 9886274	J19193154+4642230	1.41	352.7 ±2.8	0.24 ±0.10	–	SB1	42.5 ±0.5	4.76 ±0.02	63
2128157742579607296	KIC 9896877	J19370831+4643235	1.21	859.5 ±33.4	0.45 ±0.10	–	SB1	8.8 ±0.5	1.52 ±0.03	–
2128519894220750464	KIC 9897838	J19383112+4647332	1.66	630.0 ±12.2	0.75 ±0.10	–	ORB	513 ±18	30 ±1	–
2128517484740285312	KIC 9898240	J19390668+4646496	1.42	970.9 ±182.5	0.24 ±0.20	–	SB1	36 ±1	3.74 ±0.02	–
2128517244222116992	KIC 9898373	J19392003+4646168	1.16	617 ±17	0.05 ±0.10	–	SB1	46 ±2	4.69 ±0.05	291
2128516458246962688	KIC 9898385	J19392138+4644069	1.23	13.78 ±0.01	0.01 ±0.10	–	SB1	1352 ±34	69 ±2	–
2080525146519838592	KIC 9902962	J19454831+4645271	0.96	333.7 ±5.8	0.15 ±0.10	–	SB1	77 ±1	6.76 ±0.05	290
2130629096818869760	KIC 9941713	J19080214+4649540	1.07	345.6 ±1.6	0.12 ±0.03	–	SB1	48.6 ±0.4	4.84 ±0.02	–
2127739236664163968	KIC 9961623	J19182488+4653323	2.94	431.5 ±4.2	0.18 ±0.10	–	SB1	111 ±1	9.84 ±0.03	77
2127633511750746112	KIC 9947848	J19212528+4653377	1.48	561.0 ±6.2	0.27 ±0.03	–	SB1	3.8 ±0.1	0.74 ±0.02	–
2085573485440615808	KIC 9969732	J19540321+4653037	1.14	1114 ±377	0.43 ±0.12	–	SB1	50 ±1	5.05 ±0.03	253
2107566707285611136	KIC 9995162	J18534324+4657405	4.88	636.6 ±2.2	0.24 ±0.02	143 ±2	ASB1	55 ±1	5.63 ±0.02	65
2129090776976049920	KIC 10011329	J19263640+4658023	1.45	534 ±4	0.26 ±0.03	115 ±4	ASB1	36 ±1	3.78 ±0.02	–
2086307443809615488	KIC 10028634	J19512811+4659150	2.2	1070 ±80	0.05 ±0.10	–	SB1	94 ±2	8.28 ±0.02	–
2107394839875949184	KIC 10059338	J18574084+4701539	1.69	1057 ±95	0.12 ±0.10	–	SB1	9.7 ±0.3	1.5 ±0.1	–
2130616830392969728	KIC 10062594	J19041307+4704305	1.1	384.5 ±4.1	0.44 ±0.04	–	SB1	42.8 ±0.5	4.78 ±0.02	–
2085581422540208768	KIC 10094550	J19535070+4702380	3.49	1199.3 ±105.4	0.40 ±0.05	–	SB1	57 ±2	4.8 ±0.1	–

Table B.1. Orbital and seismic parameters of *Gaia* DR3 binary systems. (cont.)

Gaia DR3	KIC/TIC	2MASS	ruwe	P_{orb} [d]	e	i [deg]	Type	ν_{max} [μHz]	$\Delta\nu$ [μHz]	$\Delta\Pi_1$ [s]
2128545079909313792	KIC 10148118	J19375110+4709246	1.05	388 \pm 3	0.06 \pm 0.04	–	SB1	62 \pm 3	5.5 \pm 0.1	–
2080552325071338496	KIC 10153182	J19443431+4710071	1.06	1096.0 \pm 94.7	0.14 \pm 0.09	–	SB1	35 \pm 1	4.19 \pm 0.04	324
2080378499156480256	KIC 10155387	J19470990+4710521	1.09	1166.8 \pm 264.7	0.20 \pm 0.10	–	SB1	49.5 \pm 0.4	5.46 \pm 0.02	–
2085585816283421696	KIC 10160940	J19531756+4708591	0.92	272 \pm 4	0.23 \pm 0.11	–	SB1	57 \pm 2	5.29 \pm 0.05	287
2129109576049777280	KIC 10206457	J19251020+4713306	1.15	1042 \pm 313	0.48 \pm 0.28	–	SB1	21.8 \pm 0.4	2.82 \pm 0.04	–
2128370772957380096	KIC 10208303	J19281257+4714039	1.04	8.086 \pm 0.002	0.13 \pm 0.06	–	SB1	1118 \pm 38	63.1 \pm 1.7	–
2128556590421963392	KIC 10215903	J19394466+4717334	1.17	784.8 \pm 10.6	0.27 \pm 0.05	–	SB1	3.9 \pm 0.1	0.78 \pm 0.02	–
2080571875762719744	KIC 10286616	J19460016+4720165	1.41	892 \pm 108	0.08 \pm 0.10	–	SB1	33 \pm 1	4.05 \pm 0.05	330
2119602717477409792	KIC 10318734	J18442402+4728147	2.68	906 \pm 66	0.38 \pm 0.10	–	SB1	107 \pm 1	9.48 \pm 0.02	78
2080574139202017280	KIC 10352615	J19462274+4726595	2.32	821.3 \pm 8.7	0.21 \pm 0.02	–	SB1	62 \pm 2	5.72 \pm 0.02	–
2086375781025481856	KIC 10355764	J19500831+4725247	2.15	1069.8 \pm 209.6	0.17 \pm 0.11	–	SB1	33 \pm 1	4.11 \pm 0.04	295
2086399420525476352	KIC 10355856	J19501427+4728252	1.12	4.486	0.00 \pm 0.02	–	SB1	1320 \pm 80	67 \pm 1	–
2085675121545993856	KIC 10361019	J19555417+4726384	1.46	267.6 \pm 0.3	0.38 \pm 0.01	–	SB1	51 \pm 3	4.44 \pm 0.04	–
2085698005131997184	KIC 10426854	J19564169+4733296	3.17	959 \pm 18	0.02 \pm 0.10	–	SB1	40 \pm 1	4.36 \pm 0.04	341
2131453082003911168	KIC 10454887	J18580811+4739078	3.15	1157 \pm 115	0.22 \pm 0.05	–	SB1	36 \pm 1	3.80 \pm 0.02	–
2080590704899412096	KIC 10482598	J19452990+4736587	1.36	1.294	0.15 \pm 0.30	–	SB1	9.4 \pm 0.4	1.51 \pm 0.03	–
2130758770472767616	KIC 10587702	J19044603+4753567	2.11	531.6 \pm 4.6	0.25 \pm 0.04	140 \pm 5	ASB1	46.5 \pm 0.5	4.89 \pm 0.02	–
2130888272326733568	KIC 10591093	J19120791+4752590	1.22	142 \pm 1	0.29 \pm 0.04	–	SB1	164 \pm 2	12.68 \pm 0.02	–
2130923392277894400	KIC 10592818	J19152552+4752055	1.79	257.9 \pm 1.9	0.09 \pm 0.03	–	SB1	3.1 \pm 0.2	0.60 \pm 0.04	–
2086610458041800576	KIC 10614382	J19480780+4750357	5.7	851.0 \pm 17.4	0.43 \pm 0.03	18 \pm 6	ASB1	95 \pm 1	7.88 \pm 0.04	239
2131499051034743936	KIC 10651991	J19014937+4755571	1.11	993.6 \pm 276.2	0.61 \pm 0.24	–	SB1	31.7 \pm 0.5	3.85 \pm 0.02	–
2128867786571861376	KIC 10668443	J19320112+4755406	1.64	38.7 \pm 0.1	0.16 \pm 0.10	–	SB1	125 \pm 2	10.81 \pm 0.03	–
2128825180495948544	KIC 10669568	J19335097+4757481	1.7	1244.1 \pm 283.5	0.16 \pm 0.20	–	SB1	45 \pm 1	4.54 \pm 0.04	305
2128835381037146880	KIC 10670371	J19350588+4754151	2.74	303.7 \pm 0.9	0.49 \pm 0.03	126 \pm 2	ASB1	540 \pm 17	31.4 \pm 1.4	–
2086474191620375680	KIC 10684837	J19535439+4756543	1.23	443 \pm 8	0.08 \pm 0.10	–	SB1	87 \pm 2	7.07 \pm 0.04	255
2085720579480250880	KIC 10685892	J19550617+4754033	4.11	1052.8 \pm 35.7	0.26 \pm 0.03	–	SB1	18 \pm 2	2.2 \pm 0.1	–
2129259899906063488	KIC 10732098	J19284730+4802154	2.05	199.1 \pm 0.5	0.65 \pm 0.03	92 \pm 2	ASB1	1055 \pm 43	60 \pm 2	–
2086616166058986112	KIC 10745554	J19474735+4800540	1.04	283 \pm 2	0.20 \pm 0.05	–	SB1	87 \pm 1	7.10 \pm 0.03	262
2119834851869352448	KIC 10775748	J18445125+4806250	0.99	6.476	0.01 \pm 0.01	–	SB1	997 \pm 11	61 \pm 2	–
2119729569334276096	KIC 10777098	J18475055+4808509	1.04	64.6 \pm 0.4	0.29 \pm 0.10	–	SB1	42.0 \pm 0.5	4.88 \pm 0.02	–
2129404932360528896	KIC 10794816	J19232646+4806195	2.24	943.6 \pm 115.7	0.13 \pm 0.13	–	SB1	330 \pm 4	22.5 \pm 0.1	–
2129299512386602496	KIC 10796857	J19264357+4807193	1.14	149 \pm 1	0.16 \pm 0.05	–	SB1	89 \pm 1	7.82 \pm 0.02	65
2086629909953579264	KIC 10810905	J19472187+4808403	1.24	857.2 \pm 35.6	0.08 \pm 0.14	–	SB1	16.3 \pm 0.5	2.23 \pm 0.02	–
2086515010991869056	KIC 10815065	J19520255+4806035	2.74	512 \pm 10	0.33 \pm 0.10	–	SB1	21 \pm 1	2.44 \pm 0.03	–
2129503544809296896	KIC 10858780	J19225371+4817014	3.0	224 \pm 2	0.64 \pm 0.06	–	ORB	1323 \pm 42	74 \pm 3	–
2129316211219234432	KIC 10859779	J19244413+4817090	3.61	1225.1 \pm 340.4	0.42 \pm 0.20	–	SB1	81 \pm 1	7.29 \pm 0.02	–
2129305216103166592	KIC 10860202	J19252971+4817309	2.49	731.6 \pm 11.1	0.27 \pm 0.03	–	SB1	33.7 \pm 0.4	3.92 \pm 0.02	–
2128895789759142016	KIC 10922167	J19311901+4822074	1.44	586.3 \pm 4.6	0.30 \pm 0.03	97 \pm 3	ASB1	87 \pm 2	7.24 \pm 0.02	–
2086542150882274688	KIC 10935853	J19523172+4818406	1.1	882.6 \pm 17.6	0.30 \pm 0.10	–	SB1	66 \pm 7	5.7 \pm 0.2	–
2086501988644207872	KIC 10936814	J19535355+4823527	3.16	664.7 \pm 5.6	0.03 \pm 0.03	61 \pm 2	ASB1	37 \pm 1	4.2 \pm 0.1	297
2086501988651116032	KIC 10936833	J19535560+4823354	1.71	888 \pm 21	0.40 \pm 0.10	–	SB1	37 \pm 1	4.2 \pm 0.1	300
2143726105669980288	KIC 11014468	J18512777+4833261	2.82	643 \pm 4	0.50 \pm 0.02	117 \pm 3	ASB1	51 \pm 2	4.74 \pm 0.04	258
2131044402976539520	KIC 11129945	J19115842+4845466	1.44	641.9 \pm 7.7	0.11 \pm 0.05	42 \pm 6	ASB1	50 \pm 2	4.92 \pm 0.03	304
2129572882762263552	KIC 11134475	J19204772+4842357	1.18	511 \pm 18	0.11 \pm 0.10	–	SB1	36 \pm 1	3.93 \pm 0.03	–
2129538351225139712	KIC 11135910	J19240131+4847212	2.92	961 \pm 23	0.19 \pm 0.03	47 \pm 3	ASB1	29.3 \pm 0.3	3.67 \pm 0.02	–
2129669055669429120	KIC 11138542	J19292894+4844341	1.75	970 \pm 49	0.27 \pm 0.06	–	SB1	15 \pm 1	1.96 \pm 0.03	–
2129010104607554048	KIC 11140732	J19335319+4844510	1.19	806.3 \pm 26.1	0.17 \pm 0.07	–	SB1	46 \pm 2	4.9 \pm 0.4	–
2134747665519893632	KIC 11146152	J19425889+4846276	1.57	1251 \pm 135	0.28 \pm 0.05	–	SB1	32 \pm 1	3.56 \pm 0.03	–
2134744126466917632	KIC 11146813	J19435374+4842309	1.24	354.6 \pm 8.9	0.07 \pm 0.11	–	SB1	189 \pm 5	13.8 \pm 0.1	–
2129532853666622336	KIC 11188067	J19220808+4850043	1.97	860 \pm 8	0.05 \pm 0.03	–	SB1	39 \pm 1	4.3 \pm 0.1	298
2134749864543225984	KIC 11199046	J19431669+4852248	1.22	351.4 \pm 6.8	0.08 \pm 0.10	–	SB1	58 \pm 1	5.86 \pm 0.02	–
2086939834794981760	KIC 11260007	J19533465+4856312	1.07	337.0 \pm 2.5	0.41 \pm 0.10	–	SB1	42 \pm 2	4.50 \pm 0.05	–
2143765855589398272	KIC 11282383	J18511176+4903317	1.37	305.2 \pm 2.2	0.04 \pm 0.05	–	SB1	76 \pm 1	7.21 \pm 0.02	–
2132740713199620608	KIC 11289615	J19110961+4904423	2.35	832.6 \pm 16.3	0.05 \pm 0.05	–	SB1	101 \pm 2	8.14 \pm 0.03	–
2129922080782260992	KIC 11295820	J19245594+4901599	0.97	82.2 \pm 0.3	0.17 \pm 0.06	–	SB1	78 \pm 1	7.13 \pm 0.02	–
2129700666629150464	KIC 11297585	J19284253+4903436	1.09	963.3 \pm 83.4	0.52 \pm 0.13	–	SB1	35 \pm 2	3.33 \pm 0.05	–
2134769209075917824	KIC 11305250	J19424145+4900432	1.68	627.7 \pm 23.1	0.27 \pm 0.08	–	SB1	92 \pm 2	7.59 \pm 0.03	–
2132000119099480320	KIC 11339247	J19020865+4907009	1.86	311 \pm 1	0.07 \pm 0.03	–	SB1	10.0 \pm 0.2	1.49 \pm 0.03	–
2132744973807252608	KIC 11343185	J19120805+4908507	1.11	291.4 \pm 2.2	0.26 \pm 0.03	–	SB1	3.6 \pm 0.2	0.69 \pm 0.03	–
2131256887898248576	KIC 11394905	J19093999+4913392	1.29	591.2 \pm 13.8	0.19 \pm 0.09	–	SB1	38.9 \pm 0.5	4.41 \pm 0.04	298
2086842661151252736	KIC 11413158	J19460458+4916004	1.55	204.2 \pm 0.3	0.17 \pm 0.01	–	SB1	59 \pm 1	5.02 \pm 0.03	211
2129947988025131520	KIC 11453721	J19240608+4922533	6.11	1064 \pm 77	0.65 \pm 0.04	–	SB1	60.9 \pm 0.5	6.11 \pm 0.02	–
2087161210284820480	KIC 11467720	J19494396+4919431	1.19	552 \pm 15	0.41 \pm 0.10	–	SB1	34.3 \pm 0.5	3.88 \pm 0.02	–
2132620694633811456	KIC 11502218	J19162237+4925280	5.71	226.23 \pm 0.04	0.370 \pm 0.002	81 \pm 1	ASB1	23 \pm 2	2.7 \pm 0.1	–
2129761895682980224	KIC 11507653	J19280539+4924572	2.06	180.9 \pm 0.4	0.23 \pm 0.04	101 \pm 2	ASB1	1350 \pm 39	70 \pm 2	–
2134919842168119424	KIC 11515377	J19422614+4927364	3.6	514 \pm 3	0.35 \pm 0.02	102 \pm 2	ASB1	192 \pm 1	14.78 \pm 0.04	83
2132206006950066560	KIC 11546913	J18570613+4932187	1.29	834.2 \pm 29.4	0.14 \pm 0.07	–	SB1	176 \pm 2	13.30 \pm 0.03	–
2134881050023624064	KIC 11567572	J19432356+4934101	1.09	1030.1 \pm 115.8	0.24 \pm 0.15	–	SB1	57 \pm 1	5.26 \pm 0.03	284
2132113785412645632	KIC 11600413	J19030418+4939499	1.01	56.94 \pm 0.02	0.01 \pm 0.01	–	SB1	79 \pm 6	6.7 \pm 0.2	–
2132641718496922496	KIC 11607216	J19193319+								

Table B.1. Orbital and seismic parameters of *Gaia* DR3 binary systems. (cont.)

Gaia DR3	KIC/TIC	2MASS	ruwe	P_{orb} [d]	e	i [deg]	Type	ν_{max} [μHz]	$\Delta\nu$ [μHz]	$\Delta\Pi_1$ [s]
2132653989220503936	KIC 11657306	J19170208+4942536	1.68	982 \pm 116	0.30 \pm 0.11	–	SB1	180 \pm 1	14.07 \pm 0.03	–
2132642921087764480	KIC 11658270	J19191603+4943201	1.71	480 \pm 2	0.30 \pm 0.02	–	SB1	26.3 \pm 0.4	3.08 \pm 0.02	–
2132140242411526784	KIC 11702480	J19031815+4950070	1.95	687 \pm 29	0.10 \pm 0.10	–	SB1	38 \pm 2	3.89 \pm 0.02	–
2133022222535674496	KIC 11709205	J19191607+4952206	1.52	57.90 \pm 0.02	0.41 \pm 0.01	–	SB1	271 \pm 13	18.9 \pm 0.9	–
2133039272320064000	KIC 11718785	J19391236+4948558	2.09	437 \pm 1	0.37 \pm 0.01	–	SB1	27 \pm 1	2.86 \pm 0.03	–
2132134435615664384	KIC 11752358	J19004872+4956146	1.42	421 \pm 10	0.44 \pm 0.10	–	SB1	65.4 \pm 0.5	6.59 \pm 0.03	72
2132144807957844480	KIC 11823838	J19023911+4958135	2.37	1022 \pm 143	0.40 \pm 0.10	–	SB1	65 \pm 1	6.07 \pm 0.02	–
2135137992146308736	KIC 11769801	J19403430+4959350	0.81	29.73 \pm 0.02	0.57 \pm 0.05	–	SB1	770 \pm 40	45.2 \pm 2.3	–
2133591563399816704	KIC 11805217	J19070228+5003188	1.34	683.7 \pm 25.3	0.19 \pm 0.07	–	SB1	61 \pm 1	5.90 \pm 0.02	67
2132723872629209472	KIC 11808139	J19141503+5004136	1.62	936 \pm 137	0.24 \pm 0.15	–	SB1	160 \pm 2	12.25 \pm 0.03	–
2135277767562458624	KIC 11823838	J19455292+5002304	1.47	894.5 \pm 13.9	0.26 \pm 0.04	–	SB1	43 \pm 1	4.51 \pm 0.03	332
2130038697734970624	KIC 11862497	J19235402+5006454	4.33	599 \pm 8	0.66 \pm 0.06	–	ORB	1888 \pm 48	90.7 \pm 2.1	–
2135150292932789376	KIC 11869694	J19384144+5009175	1.59	706.1 \pm 26.5	0.17 \pm 0.10	–	SB1	40 \pm 1	4.4 \pm 0.2	323
2132165702977781888	KIC 11903733	J19014318+5013078	1.35	881.3 \pm 38.8	0.38 \pm 0.04	–	SB1	4.2 \pm 0.3	0.85 \pm 0.03	–
2133046205633198976	KIC 11910960	J19191473+5014527	1.14	84.1 \pm 0.2	0.14 \pm 0.05	–	SB1	71 \pm 1	7.20 \pm 0.02	74
2132984766121731584	KIC 12104686	J19111329+5038119	1.36	151.6 \pm 0.2	0.37 \pm 0.01	–	SB1	71 \pm 4	6.0 \pm 0.1	301
2130169264740410496	KIC 12110240	J19244302+5037490	1.2	114.1 \pm 0.2	0.20 \pm 0.02	–	SB1	35 \pm 3	4.0 \pm 0.3	–
2135194445196787584	KIC 12117138	J19393497+5036085	1.44	685.1 \pm 18.5	0.20 \pm 0.10	–	SB1	41 \pm 1	4.46 \pm 0.04	305
2135337549207262720	KIC 12169924	J19463770+5043313	1.16	469.3 \pm 14.5	0.16 \pm 0.10	–	SB1	45 \pm 1	4.45 \pm 0.02	–
2130194755367500288	KIC 12257460	J19234876+5058321	1.16	953.5 \pm 41.9	0.16 \pm 0.06	–	SB1	12.7 \pm 0.2	1.75 \pm 0.02	–
2136138822604578432	KIC 12258572	J19262929+5059005	1.19	617.4 \pm 24.5	0.31 \pm 0.10	–	SB1	12.6 \pm 0.5	1.88 \pm 0.04	–
2135400122591847168	KIC 12266731	J19432174+5056396	1.05	979 \pm 123	0.65 \pm 0.10	–	SB1	95 \pm 4	7.3 \pm 0.1	–
2136186410842184064	KIC 12307366	J19255330+5101382	2.38	365.0 \pm 2.9	0.27 \pm 0.04	–	SB1	327 \pm 15	21.7 \pm 1.2	–
2135483028339642368	KIC 12317678	J19463773+5101135	3.93	80.8 \pm 0.1	0.39 \pm 0.04	–	ORB	1244 \pm 80	63.5 \pm 1.2	–
4665935617200432000	TIC 25117590	J04060420-7040102	1.47	1181 \pm 250	0.35 \pm 0.20	–	SB1	30 \pm 4	3.7 \pm 0.2	366
4667997716898783872	TIC 29759742	J04164946-6857334	0.98	203 \pm 1	0.26 \pm 0.03	–	SB1	6 \pm 1	1.03 \pm 0.03	–
4655973457739127296	TIC 29761457	J04180788-6919506	3.61	992.2 \pm 2.5	0.24 \pm 0.01	–	SB1	17 \pm 2	2.2 \pm 0.4	–
4655884878333686528	TIC 29832154	J04260443-6953295	1.63	1140.8 \pm 161.3	0.37 \pm 0.17	–	SB1	20 \pm 3	3 \pm 1	–
4655890444611210368	TIC 29834079	J04272852-6945156	3.9	535.1 \pm 1.8	0.01 \pm 0.02	42 \pm 2	ASB1	42 \pm 6	4.6 \pm 0.1	–
4662917595232874496	TIC 29990017	J04522376-6614274	2.72	652.5 \pm 3.4	0.02 \pm 0.03	110 \pm 2	ASB1	4.3 \pm 0.4	0.8 \pm 0.4	–
4661550180745632640	TIC 30316155	J04571326-6801330	2.03	669 \pm 10	0.29 \pm 0.10	38 \pm 5	ASB1	31 \pm 3	4.75 \pm 0.02	–
4654692801588119040	TIC 30399782	J04565078-7055303	3.66	303.7 \pm 0.5	0.02 \pm 0.01	80 \pm 2	ASB1	65 \pm 5	5.6 \pm 0.5	–
4655152500553182080	TIC 30532226	J04591653-6949088	1.75	348.3 \pm 2.7	0.18 \pm 0.03	–	SB1	42 \pm 3	4.5 \pm 0.7	–
4654676446349157632	TIC 30630877	J05003258-7041569	4.27	721 \pm 1	0.646 \pm 0.004	96 \pm 1	ASB1	37 \pm 3	4.1 \pm 0.4	–
4659044325008819456	TIC 31313861	J05533961-6901194	3.89	611 \pm 1	0.28 \pm 0.01	119 \pm 2	ASB1	11 \pm 2	1.6 \pm 0.2	–
4657534351948625920	TIC 31314164	J05525602-6914083	1.01	362.6 \pm 1.8	0.09 \pm 0.03	–	SB1	127 \pm 3	10.98 \pm 0.04	–
4657436117451600256	TIC 31531197	J05583171-6951235	0.99	30.6 \pm 0.2	0.36 \pm 0.15	–	SB1	11 \pm 3	1.8 \pm 0.2	–
4646578680633774464	TIC 31701594	J03110677-6812596	3.52	702.1 \pm 5.1	0.04 \pm 0.02	–	SB1	52 \pm 5	5 \pm 1	–
4670545835095919488	TIC 31746687	J03174864-6807127	1.58	584 \pm 7	0.64 \pm 0.10	55 \pm 5	ASB1	159 \pm 9	12 \pm 1	–
4642936136049811456	TIC 31779457	J03200803-7124318	1.65	1218 \pm 161	0.35 \pm 0.10	–	SB1	34 \pm 3	3.9 \pm 0.2	266
4646207492380073344	TIC 31782079	J03212604-6936545	1.41	86.5 \pm 0.1	0.15 \pm 0.03	–	SB1	19 \pm 3	2.6 \pm 1.8	–
4642741178894231808	TIC 31795900	J03225471-7140569	2.16	883.653 \pm 30.988	0.09 \pm 0.07	–	SB1	86.14	7.58	–
4670421830800091008	TIC 31927492	J03351495-6751460	2.9	448 \pm 1	0.04 \pm 0.01	100 \pm 2	ASB1	48 \pm 3	4.8 \pm 0.2	–
4670828924980416256	TIC 31927660	J03352062-6720224	1.35	122.8 \pm 0.1	0.06 \pm 0.01	–	SB1	39 \pm 3	4 \pm 1	–
4642839344666809984	TIC 31946252	J03384398-7051545	4.42	832.4 \pm 11.6	0.02 \pm 0.02	–	SB1	28 \pm 3	3.3 \pm 0.2	–
4666913078741798400	TIC 31963236	J03412379-7009257	2.51	176 \pm 1	0.13 \pm 0.05	–	SB1	15 \pm 2	1.9 \pm 0.2	–
4666083020478183936	TIC 32035118	J03452877-7108332	1.86	348.5 \pm 1.2	0.16 \pm 0.02	–	SB1	43 \pm 4	4.6 \pm 0.2	233
4666680536328166528	TIC 32152529	J03572194-6918326	1.42	81.473 \pm 0.018	0.26 \pm 0.01	70 \pm 6	SB1	42.72	4.37	–
4652603660758350848	TIC 33878549	J04243976-7337516	2.14	922.3 \pm 12.7	0.12 \pm 0.04	–	SB1	9 \pm 1	1.4 \pm 0.3	–
4680147251666241664	TIC 38396389	J04002981-6021170	0.9	385 \pm 12	0.09 \pm 0.11	–	SB1	78 \pm 21	7.1 \pm 0.1	–
4670213232829114624	TIC 38423834	J04020842-6346459	5.04	226.9 \pm 0.3	0.11 \pm 0.02	24 \pm 3	ASB1	177 \pm 20	14.1 \pm 0.3	–
4680019777037419776	TIC 38460200	J04045315-6037403	1.46	170.2 \pm 0.2	0.31 \pm 0.01	–	SB1	7 \pm 1	1.2 \pm 0.2	–
467932333854885760	TIC 38460752	J04043614-6220286	1.45	142.5 \pm 0.3	0.14 \pm 0.02	–	SB1	29 \pm 5	3.4 \pm 0.1	–
4669721579333353856	TIC 38508895	J04090307-6537046	2.89	106.64 \pm 0.03	0.31 \pm 0.01	–	SB1	138 \pm 3	9.9 \pm 0.1	–
4676974645225234560	TIC 38518731	J04122615-6046091	2.33	699.3 \pm 5.5	0.21 \pm 0.03	–	SB1	59 \pm 4	5.7 \pm 0.3	–
4674948348375131008	TIC 38761245	J04283489-6514372	1.22	1189 \pm 190	0.16 \pm 0.20	–	SB1	32 \pm 6	3.5 \pm 0.1	–
4675781056634164864	TIC 38762182	J04283659-6239437	3.88	808 \pm 6	0.34 \pm 0.03	122 \pm 2	ASB1	16.9 \pm 0.2	2.3 \pm 0.3	–
4674939586641954944	TIC 38825397	J04322917-6451122	6.83	754 \pm 9	0.04 \pm 0.03	–	SB1	34.6 \pm 0.1	4.3 \pm 0.2	–
4677064873898524800	TIC 38843858	J04344960-6249136	5.01	847.1 \pm 0.9	0.57 \pm 0.01	87 \pm 1	ASB1	129 \pm 14	11.3 \pm 0.1	–
4677872980583538304	TIC 38905542	J04370633-6036578	1.8	484 \pm 3	0.39 \pm 0.04	119 \pm 3	ASB1	84 \pm 9	7 \pm 1	–
5283888055699607680	TIC 41230355	J06062355-6725160	2.26	982 \pm 62	0.17 \pm 0.02	–	SB1	6.0 \pm 0.3	1.27 \pm 0.04	–
5302847381369384832	TIC 45059078	J08385952-5812587	1.87	540.3 \pm 2.9	0.20 \pm 0.04	–	SB1	92 \pm 6	8.22 \pm 0.01	–
5302847828045603584	TIC 45466902	J08425172-5854500	1.18	1070 \pm 59	0.45 \pm 0.18	–	SB1	60 \pm 11	5.6 \pm 0.3	–
4633962437540777856	TIC 50378733	J02124160-7702508	2.07	946.2 \pm 37.7	0.40 \pm 0.04	–	SB1	45 \pm 5	4.4 \pm 0.1	–
4643237299156751232	TIC 50441124	J02231707-7449486	2.34	783 \pm 13	0.08 \pm 0.04	–	SB1	60 \pm 6	6 \pm 1	–
4664323630078954880	TIC 55299740	J05080556-6404105	1.4	899 \pm 15	0.29 \pm 0.10	64 \pm 4	ASB1	8 \pm 2	1.1 \pm 0.2	–
4761257154999649024	TIC 55389898	J05103973-6017556	3.39	963 \pm 15	0.06 \pm 0.03	–	SB1	44 \pm 3	4.7 \pm 0.9	–
4663217074702729088	TIC 55399173	J04411241-6518438	1.93	139.6 \pm 0.2	0.02 \pm 0.02	–	SB1	91 \pm 6	8.3 \pm 0.1	–
4761183010980405632	TIC 55401630	J05112059-6031167	1.66	634.5 \pm 9.8	0.08 \pm 0.05	–	SB1	102 \pm 9	7.9 \pm 0.5	–
4663238549539408000	TIC 55453443	J04435097-6503265	1.33	609.7 \pm 7.6	0.02 \pm 0.05	–	SB1	9 \pm 1	1.2 \pm 0.1	

Table B.1. Orbital and seismic parameters of *Gaia* DR3 binary systems. (cont.)

Gaia DR3	KIC/TIC	2MASS	ruwe	P_{orb} [d]	e	i [deg]	Type	v_{max} [μHz]	Δv [μHz]	$\Delta\Pi_1$ [s]
5314431664078092288	TIC 89787362	J08314689-5859130	2.81	525 \pm 2	0.27 \pm 0.03	125 \pm 2	ASB1	88 \pm 18	9.2 \pm 0.3	–
5315143391701747328	TIC 118306543	J08343664-5719303	1.58	122.7 \pm 0.4	0.14 \pm 0.11	–	SB1	150 \pm 27	12 \pm 1	–
4653533946377667328	TIC 140527554	J04271764-7224231	2.77	469.0 \pm 2.9	0.03 \pm 0.05	113 \pm 2	ASB1	69 \pm 6	5.8 \pm 0.2	–
4653156474592041984	TIC 140576110	J04305341-7223120	3.02	818 \pm 6	0.29 \pm 0.03	–	SB1	181 \pm 4	15.7 \pm 0.1	–
4652467561839539968	TIC 140630116	J04464170-7341243	2.7	577.850 \pm 3.811	0.49 \pm 0.01	–	SB1	27.24	3.40	345
4649903500731567616	TIC 140830011	J05023476-7314063	2.82	468.1 \pm 1.2	0.29 \pm 0.01	96 \pm 2	ASB1	41 \pm 4	4.5 \pm 0.1	372
4649065844660928384	TIC 140997423	J05120231-7521372	1.62	62.33 \pm 0.02	0.21 \pm 0.01	–	SB1	118 \pm 7	9.6 \pm 0.2	–
4648905934434970240	TIC 141028728	J05153743-7552573	1.2	195.7 \pm 0.5	0.03 \pm 0.04	–	SB1	43 \pm 5	4.2 \pm 0.2	–
4648642202040982400	TIC 141187997	J05273711-7524100	3.82	980.2 \pm 22.1	0.46 \pm 0.02	–	SB1	68 \pm 7	6.0 \pm 0.1	–
4648642223446712704	TIC 141279868	J05305576-7518067	1.13	718 \pm 20	0.12 \pm 0.06	–	SB1	44 \pm 5	4.7 \pm 0.1	–
4648740698458629248	TIC 141430018	J05391804-7448537	1.6	869 \pm 40	0.09 \pm 0.04	–	SB1	36 \pm 5	4 \pm 1	239
4647819548225633408	TIC 141436183	J05394310-7717017	1.61	929 \pm 19	0.10 \pm 0.03	–	SB1	8 \pm 2	1.3 \pm 0.6	–
4647941147340202752	TIC 141473442	J05450816-7645289	1.49	237.3 \pm 0.2	0.09 \pm 0.01	–	SB1	3.1 \pm 0.2	0.55 \pm 0.03	–
4648505471686976256	TIC 141479796	J05471496-7515291	2.48	934 \pm 14	0.06 \pm 0.03	–	SB1	83 \pm 7	7.9 \pm 0.3	–
5260668225534015744	TIC 142053145	J06303663-7612044	3.88	502.0 \pm 0.9	0.56 \pm 0.01	90 \pm 1	ASB1	3.5 \pm 0.3	1 \pm 1	–
5261799966596528640	TIC 142084127	J06324623-7436289	1.14	45.50 \pm 0.01	0.23 \pm 0.01	–	SB1	67 \pm 7	4.7 \pm 0.1	–
5260410871093882496	TIC 142109353	J06381494-7635072	2.7	680.8 \pm 4.1	0.01 \pm 0.02	–	SB1	46 \pm 4	4.9 \pm 0.3	–
4644066206924790400	TIC 149253821	J05135106-6428084	1.66	293 \pm 2	0.06 \pm 0.04	56 \pm 5	ASB1	91 \pm 9	7.7 \pm 0.2	–
4759478802317150080	TIC 149252615	J05295617-6055270	5.96	1199.7 \pm 78.2	0.35 \pm 0.03	–	SB1	7 \pm 1	1.4 \pm 1	–
4757052175860319488	TIC 149269000	J05310011-6353000	1.22	313 \pm 1	0.17 \pm 0.01	–	SB1	1.9 \pm 0.2	0 \pm 1	–
4759266867156545536	TIC 149346975	J05342598-6122023	2.65	1025 \pm 75	0.30 \pm 0.04	–	SB1	37 \pm 2	5.0 \pm 0.2	–
4759292568239351296	TIC 149347890	J05350609-6053301	1.71	1167 \pm 143	0.46 \pm 0.07	–	SB1	3.4 \pm 0.3	0.65 \pm 0.02	–
4759428911976861056	TIC 149391651	J05364566-6013493	1.4	48.77 \pm 0.02	0.01 \pm 0.01	–	SB1	20 \pm 3	2.27 \pm 0.03	–
4758613722889241600	TIC 149497617	J05420416-6032356	1.37	178.1 \pm 0.5	0.30 \pm 0.02	–	SB1	64 \pm 4	6.7 \pm 0.6	–
4756815304122927360	TIC 149574318	J05470830-6255360	1.59	844.6 \pm 45.8	0.06 \pm 0.10	–	SB1	11 \pm 1	1.5 \pm 0.3	–
475666449235164288	TIC 149575038	J05463619-6355143	2.39	817.4 \pm 32.6	0.19 \pm 0.10	–	SB1	95 \pm 10	10.0 \pm 0.1	–
4756683289707564032	TIC 149628632	J05493358-6342136	0.94	957 \pm 27	0.65 \pm 0.07	–	SB1	8 \pm 1	1.3 \pm 1.7	–
4756786510662352384	TIC 149628824	J05495536-6324338	2.0	1099.6 \pm 83.4	0.41 \pm 0.10	–	SB1	40 \pm 6	5 \pm 1	–
4756641753084850816	TIC 149663985	J05505334-6253542	1.26	1078 \pm 36	0.10 \pm 0.03	–	SB1	3.6 \pm 0.3	0.6 \pm 0.1	–
4758760855584222208	TIC 149935879	J05590418-6056540	2.2	850 \pm 35	0.10 \pm 0.06	–	SB1	43 \pm 6	4.8 \pm 0.1	–
5482040426336645376	TIC 150030461	J06043123-6116388	1.27	1176 \pm 61	0.09 \pm 0.03	–	SB1	2.7 \pm 0.2	0.52 \pm 0.03	–
5478365544942771328	TIC 150274967	J06193549-6226178	2.99	754 \pm 12	0.03 \pm 0.03	–	SB1	33 \pm 4	3.6 \pm 0.2	–
5477240405247171456	TIC 150298382	J06204539-6355505	7.85	473.0 \pm 0.6	0.231 \pm 0.005	141 \pm 2	ASB1	16 \pm 2	2.1 \pm 0.1	–
5478085173774116096	TIC 150347899	J06201401-6308338	2.57	996 \pm 142	0.12 \pm 0.10	–	SB1	39 \pm 3	4.2 \pm 0.1	–
5477319363925766784	TIC 150324174	J06232440-6319594	2.43	675.9 \pm 3.2	0.01 \pm 0.02	–	SB1	35 \pm 5	4 \pm 6	400
5477307058842123136	TIC 150324211	J06231402-6324134	1.23	130.26 \pm 0.05	0.02 \pm 0.01	–	SB1	224 \pm 1	16 \pm 999	–
5481501665639174784	TIC 150358763	J06241087-6110284	0.93	55.6 \pm 0.2	0.21 \pm 0.10	–	SB1	51 \pm 4	5.2 \pm 0.2	–
5478565591636064896	TIC 150431942	J06292367-6118301	1.97	76.90 \pm 0.03	0.007 \pm 0.005	–	SB1	4.8 \pm 0.4	0.8 \pm 0.1	–
4801071746648212992	TIC 151586409	J05535180-4634391	1.63	611 \pm 12	0.36 \pm 0.07	–	SB1	76 \pm 7	6.4 \pm 0.1	–
5552320762907540480	TIC 156831685	J06335766-4718423	3.83	302 \pm 1	0.01 \pm 0.01	153 \pm 4	ASB1	53 \pm 5	5.5 \pm 0.1	–
5552289701704157312	TIC 156882305	J06353928-4726006	1.15	206 \pm 3	0.25 \pm 0.20	–	SB1	29 \pm 2	3.4 \pm 0.9	–
5552091102416382464	TIC 156915469	J06364027-4732016	6.37	1028 \pm 26	0.00 \pm 1	–	ORB	32 \pm 3	4.6 \pm 0.3	–
5282989544235048960	TIC 167007869	J06191319-6735532	4.03	732 \pm 3	0.90 \pm 0.05	69 \pm 5	ASB1	91 \pm 2	8.30 \pm 0.01	–
5279599994707557120	TIC 167087865	J06230003-6910200	1.79	1218.4 \pm 137.8	0.33 \pm 0.10	–	SB1	55 \pm 7	5.1 \pm 0.2	–
5283522566852452352	TIC 167365998	J06355114-6618452	1.57	1087 \pm 99	0.76 \pm 0.10	–	ORB	29 \pm 4	3.2 \pm 0.1	–
5280333403315940480	TIC 167367427	J06371428-6746161	3.21	929 \pm 18	0.02 \pm 0.03	–	SB1	51 \pm 6	4.98 \pm 0.05	–
5286417276028070656	TIC 167572930	J06461257-6345489	1.55	757.5 \pm 11.2	0.00 \pm 0.04	99 \pm 3	ASB1	20 \pm 3	2.5 \pm 0.4	–
5480342058829420800	TIC 167723530	J06542479-6001577	1.15	64.67 \pm 0.05	0.02 \pm 0.02	–	SB1	7 \pm 1	1 \pm 1	–
5286685247627959936	TIC 167811654	J06595005-6305598	2.6	219.6 \pm 1.8	0.17 \pm 0.04	–	SB1	49 \pm 7	5.0 \pm 0.9	–
5285889063771129216	TIC 167890671	J07010059-6346540	4.78	1089.7 \pm 66.4	0.03 \pm 0.05	–	SB1	21 \pm 2	3 \pm 1	–
5286750462411071360	TIC 167894973	J07023777-6234153	1.94	235.9 \pm 0.2	0.13 \pm 0.01	121 \pm 3	ASB1	176 \pm 3	12.02 \pm 0.03	–
526198107677468288	TIC 176871629	J06421823-7426366	5.02	674 \pm 3	0.65 \pm 0.06	–	ORB	35 \pm 5	4 \pm 1	–
5262305982463154304	TIC 176872208	J06423072-7323139	1.3	1358.5 \pm 125.4	0.43 \pm 0.06	–	SB1	6 \pm 1	0.9 \pm 0.2	–
5260793806080913280	TIC 176875517	J06440552-7624296	1.97	1256 \pm 70	0.23 \pm 0.05	–	SB1	20 \pm 3	2.4 \pm 0.3	–
5266513607305185920	TIC 176930920	J06412266-7119027	4.38	640.0 \pm 2.5	0.23 \pm 0.02	41 \pm 2	ASB1	84 \pm 13	6.6 \pm 0.1	–
5280114359983202048	TIC 176958889	J06445914-6749333	1.58	520 \pm 4	0.03 \pm 0.02	–	SB1	75 \pm 6	6.5 \pm 0.1	–
5266658777198978560	TIC 177077420	J06523675-7030361	1.51	211.1 \pm 0.3	0.02 \pm 0.02	86 \pm 5	ASB1	5 \pm 1	0.79 \pm 0.05	–
5268463866053986688	TIC 177112605	J06540338-6914471	1.52	105.98 \pm 0.04	0.01 \pm 0.01	–	SB1	5 \pm 1	1 \pm 1	–
5268369617292407680	TIC 177113064	J06544086-7002118	4.16	460 \pm 1	0.65 \pm 0.01	35 \pm 4	ASB1	15 \pm 2	1.9 \pm 0.2	–
5262295395367212288	TIC 177242602	J06451618-7327077	3.64	559 \pm 2	0.24 \pm 0.02	119 \pm 2	ASB1	56 \pm 4	5.6 \pm 0.1	–
4660451699926636928	TIC 179439961	J05195749-6647140	0.96	415.9 \pm 2.2	0.12 \pm 0.03	–	SB1	50 \pm 5	5 \pm 1	–
4800860984012486784	TIC 180968208	J05570836-4742344	1.19	1042 \pm 91	0.39 \pm 0.12	–	SB1	41 \pm 6	4.1 \pm 0.3	–
4723083524328257408	TIC 197787143	J03242950-5950538	2.28	1063.3 \pm 10.5	0.24 \pm 0.02	–	SB1	164 \pm 3	12.48 \pm 0.05	–
4728953713829893888	TIC 197843938	J03383772-5903255	2.7	405.0 \pm 2.2	0.76 \pm 0.20	99 \pm 3	ASB1	180 \pm 24	13.0 \pm 0.2	–
4731378858523716352	TIC 197880085	–	3.52	1302.9 \pm 328.4	0.04 \pm 0.20	–	SB1	178 \pm 31	13.95 \pm 0.04	–
4680349252568173952	TIC 198006618	J03595446-5922191	2.67	967 \pm 28	0.52 \pm 0.05	–	SB1	47 \pm 9	6.0 \pm 0.2	–
4683612908021230080	TIC 198011389	J04025861-5536059	1.54	1136 \pm 332	0.39 \pm 0.20	–	SB1	16 \pm 2	1.9 \pm 0.3	–
4779533482090644736	TIC 198037452	J04061767-5514389	9.38	1050.5 \pm 18.9	0.66 \pm 0.02	118 \pm 1	ASB1	74 \pm 7	6.7 \pm 0.2	159
4680077570117053184	TIC 198038410	J04061669-5955199	1.15	83.22 \pm 0.03	0.04 \pm 0.01	–	SB1	18 \pm 1	2.3 \pm 0.2	–
4682596340801303168	TIC 198051979	J04115404-5616236	1.14	86.7 \pm 0.1	0.17 \pm 0.02	–	SB1	44 \pm 1	4.1 \pm 0.1	–

Table B.1. Orbital and seismic parameters of *Gaia* DR3 binary systems. (cont.)

Gaia DR3	KIC/TIC	2MASS	ruwe	P_{orb} [d]	e	i [deg]	Type	ν_{max} [μHz]	$\Delta\nu$ [μHz]	$\Delta\Pi_1$ [s]
4794264390985596032	TIC 219151553	J05590183-4952464	5.19	1153.7 ±144.6	0.37 ±0.10	–	SB1	52 ±3	5.0 ±0.2	–
5549645822915406848	TIC 219160960	J06020665-5159404	3.41	234.1 ±0.4	0.31 ±0.02	31 ±4	ASB1	85 ±4	7.9 ±0.2	–
5554151106169931520	TIC 219163316	J06022864-4851454	2.49	733.1 ±18.7	0.32 ±0.03	–	SB1	41 ±5	4.56 ±0.02	–
5548758207794149760	TIC 219171820	J06045004-5256163	1.95	948.9 ±52.2	0.26 ±0.10	–	SB1	35 ±3	4 ±1	–
5548847474394289536	TIC 219172129	J06044491-5218036	1.73	1314 ±163	0.13 ±0.06	–	SB1	43 ±3	4.5 ±0.3	–
5553334237749992064	TIC 219173413	J06050445-4928456	1.47	541.9 ±6.3	0.02 ±0.04	43 ±7	ASB1	116 ±3	10.6 ±0.1	–
5554180174508531840	TIC 219173837	J06050579-4836226	3.37	554.194 ±4.146	0.58 ±0.04	–	SB1	35.24	4.55	–
5550014910928613760	TIC 219193524	J06085194-5040301	1.63	611.221 ±11.741	0.36 ±0.07	–	SB1	83.70	7.35	–
5553120756398988032	TIC 219202611	J06104905-4949138	1.54	103.06 ±0.03	0.005 ±0.005	–	SB1	182 ±28	16.1 ±0.4	–
5553148832601816704	TIC 219210404	J06123760-4923214	1.52	213.1 ±0.5	0.15 ±0.03	63 ±4	ASB1	65 ±2	8.00 ±0.01	–
4779347870784038912	TIC 219252929	J04224690-5338467	2.46	1061.7 ±29.6	0.04 ±0.03	–	SB1	34 ±4	4.1 ±1.3	–
4782298753834720128	TIC 219253671	J04234748-5039516	3.85	896 ±17	0.07 ±0.03	–	SB1	37 ±3	4.2 ±0.2	–
4771408950154415616	TIC 219372670	J05041476-5224484	2.19	905 ±47	0.04 ±0.03	–	SB1	33 ±5	4.1 ±0.8	–
4785112575889072256	TIC 219376062	J05052170-5042054	2.81	1069.7 ±17.8	0.35 ±0.02	–	SB1	25 ±3	2.9 ±0.3	–
4770717426060381184	TIC 219389784	J05090869-5342431	12.66	701 ±4	0.37 ±0.02	144 ±1	ASB1	74 ±11	6.6 ±0.2	–
4773799352856641536	TIC 219391354	J05090448-4836485	2.56	1129.7 ±193.2	0.43 ±0.05	–	SB1	33 ±3	3.4 ±3.3	–
4771231172868437504	TIC 219393876	J05103104-5251423	3.42	587 ±3	0.19 ±0.02	136 ±3	ASB1	84 ±6	7.5 ±0.1	–
4773543270700610176	TIC 219400718	J05123709-5010152	4.66	1119 ±30	0.72 ±0.02	98 ±1	ASB1	71 ±6	7.2 ±0.1	–
4772903461334926464	TIC 219405568	J05142806-5128155	1.57	578.5 ±3.5	0.02 ±0.02	–	SB1	9 ±2	1.5 ±0.2	–
4773411092109807360	TIC 219416620	J05173719-5014404	2.75	619.4 ±5.6	0.13 ±0.02	–	SB1	45 ±5	4.2 ±0.6	–
4771936475218040064	TIC 219419279	J05181459-5246374	3.37	554 ±4	0.58 ±0.05	–	ORB	90 ±6	7.58 ±0.05	–
4678061542532048608	TIC 220392312	J04334830-5948535	1.72	1339 ±204	0.21 ±0.06	–	SB1	77 ±6	6.7 ±0.4	–
4775977691550813824	TIC 220394135	J04344279-5502139	3.24	767 ±10	0.06 ±0.04	–	SB1	44 ±5	5 ±2	–
4678107313999241088	TIC 220395161	J04344418-5909063	3.56	519.2 ±2.2	0.06 ±0.03	133 ±3	ASB1	126 ±6	10.5 ±0.4	–
4774217721327537920	TIC 220401179	J04375341-5829041	1.44	120.1 ±0.2	0.10 ±0.02	–	SB1	42 ±5	4.6 ±0.2	–
477432822246003840	TIC 220402024	J04380754-5812136	2.75	619.413 ±5.553	0.13 ±0.02	–	ASB1	111.35	8.65	–
4774296813149242368	TIC 220407585	J04410339-5807041	2.63	492.9 ±3.5	0.09 ±0.03	–	SB1	180 ±4	12.4 ±0.3	–
4774287123702682624	TIC 220411942	J04431241-5809165	1.93	1133 ±105	0.13 ±0.10	–	SB1	24 ±2	2.9 ±0.2	–
4776823834466591744	TIC 220459133	J04582618-5409168	5.26	921 ±49	0.10 ±0.06	–	SB1	14.4 ±0.4	2.4 ±0.2	–
4770738694738527360	TIC 220479888	J05041708-5447279	2.68	1042 ±51	0.09 ±0.02	–	SB1	28 ±2	3.3 ±0.2	343
4720064952592830464	TIC 220556986	J02563292-6523089	1.08	95.8 ±0.2	0.02 ±0.02	–	SB1	4.2 ±0.3	0.78 ±0.02	–
4723494535519505280	TIC 220569225	J03061795-6021371	4.9	133.23 ±0.05	0.27 ±0.01	123 ±2	ASB1	119 ±2	9.2 ±0.1	–
4639269505289755520	TIC 229809739	J02593349-7527506	1.49	258 ±1	0.46 ±0.02	48 ±5	ASB1	33 ±2	3.7 ±0.1	–
4662651891366718080	TIC 231090667	J04354455-6654331	1.18	141.5 ±0.2	0.06 ±0.03	–	SB1	44 ±4	4 ±1	–
4655657897904202496	TIC 231096138	J04363511-7007372	2.42	661 ±3	0.07 ±0.02	–	SB1	19 ±2	2.4 ±0.1	–
4771803228152766848	TIC 231725585	J05251366-5240368	5.46	1319.8 ±178.1	0.32 ±0.10	–	OTS	79 ±5	7.1 ±0.4	–
4658206669015976576	TIC 231794283	J05123681-6933414	1.2	988 ±54	0.29 ±0.10	–	SB1	3.5 ±0.3	0.8 ±0.2	–
5553758168202389248	TIC 232025525	J06243488-4748420	1.6	152.1 ±0.3	0.48 ±0.03	119 ±5	ASB1	43 ±5	6.3 ±3.3	268
4695359476072682880	TIC 234334347	J02260975-6808292	1.22	1201.5 ±661.2	0.44 ±0.30	–	SB1	33 ±2	3.7 ±0.1	–
4693566103888368768	TIC 234335789	J02272369-6913351	1.31	642 ±6	0.05 ±0.03	–	SB1	8 ±1	1.3 ±1.7	–
4645250745465039232	TIC 234339025	J02293941-7036230	2.15	331.1 ±0.3	0.34 ±0.01	–	SB1	70 ±8	6.33 ±0.03	–
4695077520059619968	TIC 234340071	J02310843-6855579	2.58	1124.4 ±90.7	0.44 ±0.10	–	SB1	42 ±5	5.0 ±0.4	–
4696709092235972864	TIC 234346798	J02362601-6613438	2.15	1001 ±43	0.04 ±0.05	–	SB1	6 ±2	1.1 ±0.2	–
4797117284359411968	TIC 235050452	J05304214-4815050	1.38	10.708 ±0.002	–	–	SB2C	98 ±11	9.2 ±0.2	–
4679294236801599488	TIC 237939849	J03591614-6247134	7.09	591 ±2	0.35 ±0.02	79 ±1	ASB1	192 ±23	14.9 ±0.2	–
5502901941487180544	TIC 237951824	–	–	219.1 ±0.4	0.20 ±0.02	73 ±3	ASB1	137 ±12	10.7 ±0.2	–
5503163865772809728	TIC 237952246	J06461075-4944066	2.23	674 ±2	0.46 ±0.02	–	SB1	6.8 ±0.3	1.24 ±0.02	–
5551403873289774336	TIC 237954155	J06472275-4833488	7.82	804.7 ±5.5	0.23 ±0.02	–	SB1	235 ±8	16.2 ±0.6	–
5498443421835895168	TIC 237969773	J06475449-5322478	2.06	799 ±21	0.10 ±0.05	–	SB1	31 ±3	4.3 ±0.2	–
5551424970168908160	TIC 237973654	J06480312-4811550	1.69	534 ±4	0.33 ±0.02	93 ±3	ASB1	56 ±3	5.3 ±0.2	–
5502272260626398976	TIC 238024014	J06525854-4945561	1.27	1042 ±45	0.31 ±0.05	–	SB1	5.0 ±0.5	0.95 ±0.05	–
5498766265938483712	TIC 238028476	J06531292-5224366	1.03	44.73 ±0.02	0.02 ±0.02	–	SB1	94 ±9	9.8 ±0.4	–
5501901901302078080	TIC 238039424	J06550775-5109536	1.59	313.8 ±0.6	0.09 ±0.01	–	SB1	181 ±3	12.2 ±0.2	–
5508185919492904576	TIC 238040122	J06545194-5019015	1.45	273 ±2	0.05 ±0.05	–	SB1	166 ±3	11.74 ±0.05	–
5497669846686934016	TIC 238058759	J06555552-5344122	1.14	974 ±44	0.56 ±0.12	–	SB1	29 ±3	3.5 ±0.2	–
5507985842736012288	TIC 238065989	J06573093-5024165	3.08	572 ±2	0.43 ±0.02	137 ±3	ASB1	21 ±3	2.5 ±0.3	–
5504809761664304256	TIC 238067214	J06570748-5150180	1.15	1163.1 ±487.6	0.30 ±0.34	–	SB1	6.2 ±0.4	1.0 ±0.5	–
5508037790364084992	TIC 238082975	J06594348-4953484	1.23	1097 ±254	0.39 ±0.20	–	SB1	10 ±1	1.5 ±0.3	–
5504922221086250496	TIC 238092933	J07004127-5055278	1.9	435.7 ±2.5	0.36 ±0.03	136 ±8	ASB1	43 ±3	4.4 ±0.2	394
5505032657583535104	TIC 238136275	J07034963-5027177	2.33	860 ±16	0.33 ±0.06	–	SB1	54 ±2	6.3 ±0.1	–
5508440387715185152	TIC 238144215	J07033134-4836444	1.26	1264.6 ±326.4	0.30 ±0.12	–	SB1	59 ±3	6.0 ±0.2	–
5504771386133773568	TIC 238164588	J07060343-5111107	1.68	385.7 ±2.1	0.53 ±0.13	126 ±13	ASB1	8 ±1	1.19 ±0.01	–
4627361760001541504	TIC 238186782	J03395957-7611524	5.23	711 ±2	0.24 ±0.01	86 ±1	ASB1	26 ±2	3 ±1	–
4641654174211281792	TIC 238189546	J03434257-7236328	5.93	378 ±1	0.03 ±0.02	–	SB1	48 ±3	5.1 ±0.1	–
4628676569749373184	TIC 238198771	J03501908-7553443	2.48	173.1 ±1.3	0.06 ±0.10	–	ORB	30 ±4	3.41 ±0.04	–
4629548276312264832	TIC 238202102	J03530918-7327300	3.46	734 ±3	0.46 ±0.02	68 ±2	ASB1	112 ±7	8.6 ±7.3	–
5512467108536017408	TIC 238369822	J08022776-5326441	2.06	596 ±3	0.12 ±0.03	117 ±4	ASB1	11 ±1	1.6 ±0.1	–
4640220926445059200	TIC 238870035	J02325431-7516467	0.96	927 ±48	0.64 ±0.13	–	SB1	70 ±8	7.0 ±0.2	–
4644147076309428224	TIC 238870840	J02324229-7222504	1.04	519 ±7	0.02 ±0.03	–	SB1	3.8 ±0.5	0.70 ±0.02	–
4643827335048974208	TIC 238875766	J02365628-7652397	1.48	774.0 ±7.8	0.12 ±0.03	–	SB1	56 ±2	5.91 ±0.02	–
4643393876484581632	TIC 238877134	J02393350-7401182	1.22	74.5 ±0.1	0.08 ±0.03	–	SB1	17 ±3	2 ±1	–
5550495126928283136	TIC 238896664	J06140695-4943208	1.27	53.70 ±0.04	0.30 ±0.03	–	SB1	249 ±25	16.0 ±0.6	–
5550130570104465152	TIC 238899260	J06144945-5059563	1.37	106.0 ±0.1	0.03 ±0.02	–	SB1	125 ±3	9.8 ±0.1	–
5500944084938022016	TIC 238914325	J06154782-5253353	1.68	1091 ±161	0.34 ±0.10	–	SB1	26 ±4	2.9 ±0.1	–

Table B.1. Orbital and seismic parameters of *Gaia* DR3 binary systems. (cont.)

Gaia DR3	KIC/TIC	2MASS	ruwe	P_{orb} [d]	e	i [deg]	Type	ν_{max} [μHz]	$\Delta\nu$ [μHz]	$\Delta\Pi_1$ [s]
5549024976803262926	TIC 238919268	J06162790-5219118	1.17	862.9 \pm 32.9	0.69 \pm 0.09	–	SB1	38 \pm 2	4.0 \pm 0.3	–
5553684981960079732	TIC 255556532	J06232532-4815593	1.79	1349 \pm 495	0.49 \pm 0.10	–	SB1	72 \pm 2	7 \pm 1	–
5500837260512210688	TIC 255567751	J06260573-5232400	1.44	1093 \pm 42	0.05 \pm 0.05	–	SB1	39 \pm 3	4.8 \pm 0.4	–
5500769060733535232	TIC 255587723	J06271121-5256212	1.25	1064.5 \pm 310.4	0.60 \pm 0.18	–	SB1	66 \pm 5	5.8 \pm 0.2	–
5551069140717987840	TIC 255613880	J06294763-4925148	1.46	198 \pm 1	0.22 \pm 0.07	–	SB1	20 \pm 2	2.3 \pm 0.2	–
5502797590961348352	TIC 255699681	J06353458-5017460	2.53	799.4 \pm 2.7	0.06 \pm 0.02	–	SB1	97 \pm 3	9.96 \pm 0.04	–
5501494326085031296	TIC 259444007	J06353656-5232059	1.75	216.4 \pm 0.2	0.37 \pm 0.01	–	SB1	3.9 \pm 0.2	0.61 \pm 0.01	–
5551991527895001728	TIC 255742317	J06370016-4818590	2.21	226.0 \pm 0.2	0.210 \pm 0.004	–	SB1	6.1 \pm 0.4	1.2 \pm 0.2	–
5550868131952051200	TIC 255743422	J06371228-4953548	1.14	333 \pm 1	0.02 \pm 0.02	–	SB1	11 \pm 2	1.8 \pm 1.2	–
5502511030743706752	TIC 255744271	J06370109-5109536	1.39	924.5 \pm 36.5	0.23 \pm 0.05	–	SB1	34 \pm 4	3.9 \pm 5.1	–
4778208639299087616	TIC 259444007	J04392443-5211559	1.27	93.30 \pm 0.04	0.02 \pm 0.01	–	SB1	161 \pm 3	11.3 \pm 0.2	–
4784398202568692864	TIC 259476124	J04424127-5046002	0.94	37.37 \pm 0.02	0.20 \pm 0.02	–	SB1	17 \pm 2	1.86 \pm 0.01	–
4784811653300397696	TIC 259512588	J04434356-5010333	5.28	957.4 \pm 8.3	0.42 \pm 0.02	–	SB1	186 \pm 25	15.4 \pm 0.2	–
4784178849999179392	TIC 259514295	J04443574-5121165	2.06	707 \pm 5	0.04 \pm 0.03	–	SB1	40 \pm 2	4.3 \pm 0.1	–
4783369128404125952	TIC 259593290	J04512703-5143319	3.47	432.344 \pm 2.538	0.07 \pm 0.03	157 \pm 10	ORB	16.22	2.43	–
4783707571827634688	TIC 259698601	J04562062-5126287	2.08	673.1 \pm 7.6	0.10 \pm 0.03	–	SB1	5.7 \pm 0.5	1.1 \pm 0.2	–
4646933887312754688	TIC 259886074	J02435497-6917440	1.15	106.63 \pm 0.05	0.01 \pm 0.01	–	SB1	4.7 \pm 0.2	0.75 \pm 0.03	–
4647086929883657472	TIC 259886201	J02434971-6850338	2.95	1049.1 \pm 90.2	0.29 \pm 0.10	–	SB1	116 \pm 7	11.1 \pm 0.2	–
4695790106673649408	TIC 259961732	J02522488-6629172	1.16	213.0 \pm 0.5	0.21 \pm 0.04	–	SB1	3.5 \pm 0.3	0.7 \pm 0.3	–
4695610680119692416	TIC 259961947	J02522207-6718256	5.46	1069.6 \pm 94.3	0.60 \pm 0.07	–	SB1	115 \pm 11	9.7 \pm 0.1	–
4644048979256241920	TIC 259963142	J02523299-7151386	1.78	238.8 \pm 0.3	0.41 \pm 0.01	77 \pm 3	ASB1	14 \pm 2	1.76 \pm 0.04	–
4647463061643696768	TIC 259975708	J02542640-6808472	1.43	544 \pm 3	0.33 \pm 0.02	104 \pm 5	ASB1	7 \pm 1	1.1 \pm 0.2	–
4646842666503383552	TIC 259975922	J02535621-6908509	2.33	881 \pm 47	0.09 \pm 0.09	–	SB1	45 \pm 3	4.4 \pm 0.3	–
4646759172339191808	TIC 259976011	J02542795-6935446	2.08	1185 \pm 132	0.15 \pm 0.10	–	SB1	11 \pm 1	1.45 \pm 0.03	–
4645541119614245888	TIC 259976592	J02560657-7145367	1.97	512 \pm 5	0.06 \pm 0.04	149 \pm 8	ASB1	45 \pm 5	4.6 \pm 0.1	–
5498940091853977856	TIC 260074858	J06065296-5642364	3.18	851 \pm 66	0.31 \pm 0.10	–	SB1	97 \pm 7	8.5 \pm 0.2	–
5495580362276327936	TIC 260075417	J06064633-5802569	7.4	2987.9 \pm 802.2	0.83 \pm 0.04	–	ORB	56 \pm 4	5.5 \pm 0.2	–
5499041075125301504	TIC 260080114	J06085012-5626099	1.42	76.40 \pm 0.04	0.09 \pm 0.01	–	SB1	27 \pm 2	3.2 \pm 0.4	–
5494557747743359872	TIC 260160104	J06100846-5912561	2.15	425.2 \pm 1.3	0.01 \pm 0.02	–	SB1	4.1 \pm 0.3	0.74 \pm 0.02	–
5495997145903080576	TIC 260189950	J06121566-5640453	5.16	3.421	0.11 \pm 0.04	–	SB1	46 \pm 4	4.7 \pm 0.3	–
5496053289715459200	TIC 260192462	J06130599-5620253	1.25	17.899 \pm 0.002	0.01 \pm 0.01	–	SB1	5 \pm 2	1.0 \pm 0.1	–
5499170576979230592	TIC 260243101	J06150268-5519481	4.46	1115.2 \pm 85.9	0.29 \pm 0.10	–	SB1	31 \pm 4	4.0 \pm 0.2	365
5496009515408751104	TIC 260243618	J06152944-5619379	1.13	1053 \pm 100	0.42 \pm 0.10	–	SB1	27 \pm 3	3.2 \pm 0.1	–
5482943812577924096	TIC 260296755	J06172048-5857239	2.04	776.3 \pm 11.3	0.03 \pm 0.04	–	SB1	20 \pm 2	2.4 \pm 0.3	–
5499846948428524416	TIC 260353403	J06193571-5411217	1.18	488.8 \pm 3.5	0.27 \pm 0.03	–	SB1	128 \pm 3	10.5 \pm 0.1	–
5495016656409201152	TIC 260419840	J06233831-5805339	2.34	865 \pm 12	0.16 \pm 0.03	–	SB1	67 \pm 1	5.9 \pm 0.5	–
5499611687300171136	TIC 260504408	J06261576-5441047	2.09	920 \pm 26	0.10 \pm 0.05	–	SB1	24 \pm 2	3 \pm 2	–
5483128599250644096	TIC 260640311	J06312228-5736473	2.76	1104 \pm 26	0.13 \pm 0.02	–	SB1	68 \pm 4	6.1 \pm 0.1	–
5497009967911120128	TIC 260657912	J06333115-5551308	1.44	981.9 \pm 74.1	0.35 \pm 0.10	–	SB1	56 \pm 6	5.1 \pm 0.4	319
4622434161202432000	TIC 260969670	J04585308-8022377	0.89	102.3 \pm 0.1	0.13 \pm 0.02	–	SB1	22 \pm 1	2.7 \pm 0.3	–
4621252804677820288	TIC 260981689	J05005439-8122445	0.93	50.26 \pm 0.04	0.18 \pm 0.03	–	SB1	55 \pm 7	5.3 \pm 0.3	–
462385221964746752	TIC 261090072	J05301739-7812269	2.14	308.5 \pm 0.9	0.30 \pm 0.03	77 \pm 2	ASB1	72 \pm 7	7 \pm 1	–
5210796439681854336	TIC 261400159	J06182824-7958597	1.14	282.6 \pm 2.2	0.53 \pm 0.06	–	SB1	31 \pm 2	3.6 \pm 0.1	–
5210707963355764608	TIC 261400453	J06180401-8034368	2.82	162.4 \pm 0.2	0.46 \pm 0.01	53 \pm 3	ASB1	21.3 \pm 0.3	2.42 \pm 0.01	–
5485525225362257536	TIC 262496793	J07191488-5939080	1.59	963 \pm 78	0.51 \pm 0.13	–	SB1	88 \pm 7	7.4 \pm 0.1	–
5209981529767621888	TIC 2627110991	J07534899-7755164	0.98	943 \pm 75	0.33 \pm 0.19	–	SB1	64 \pm 3	6.16 \pm 0.04	–
4673717273307522304	TIC 262874415	J03302612-6407209	1.4	48.771 \pm 0.011	0.01 \pm 0.01	–	ORB	112.47	9.68	–
5488209098888310528	TIC 264923715	J07505309-5535459	3.55	1223.5 \pm 183.9	0.27 \pm 0.12	–	SB1	37 \pm 3	4 \pm 1	–
5488229302414171392	TIC 264924112	J07510199-5515492	1.79	0.324	0.13 \pm 0.08	–	SB1	54 \pm 3	6.17 \pm 0.03	–
4643842236710517120	TIC 267115716	J02473686-7252300	1.89	660 \pm 16	0.26 \pm 0.08	–	SB1	53 \pm 4	5.8 \pm 0.1	–
5489175569607741312	TIC 267459880	J07344214-5355093	2.2	894.6 \pm 17.7	0.15 \pm 0.02	–	SB1	44 \pm 2	4.92 \pm 0.03	–
5492384150695978624	TIC 267461409	J07355272-5234028	0.96	1015 \pm 48	0.67 \pm 0.05	–	SB1	26.3 \pm 0.2	2.95 \pm 0.01	–
5492415349338349696	TIC 267759318	J07391679-5213389	2.52	883 \pm 38	0.15 \pm 0.03	–	SB1	30 \pm 2	4 \pm 6	–
5492868382489940352	TIC 268343886	J07460909-5133027	1.42	1045 \pm 59	0.56 \pm 0.04	–	SB1	7.4 \pm 0.4	1.1 \pm 0.2	–
5488746416476541312	TIC 269074621	J07532893-5314289	1.0	4.449	0.04 \pm 0.01	–	SB2	10.0 \pm 0.4	1.781 \pm 0.004	–
5488684122271133568	TIC 269331924	J07554279-5329029	1.19	441 \pm 3	0.10 \pm 0.04	–	SB1	15 \pm 2	2 \pm 1	–
4622798305709556864	TIC 269763500	J04273555-7913380	5.97	1358 \pm 101	0.27 \pm 0.03	–	SB1	58 \pm 6	6.1 \pm 0.3	–
4632394671398391936	TIC 270309486	J02085391-7923591	1.41	826.8 \pm 103.7	0.66 \pm 0.10	74 \pm 7	ASB1	87 \pm 3	6.6 \pm 0.2	–
4794596512217333120	TIC 270576246	J05474221-4859327	2.52	1034.0 \pm 115.7	0.38 \pm 0.11	–	SB1	55 \pm 6	5.6 \pm 1.4	–
4795023676780493952	TIC 270625322	J05484395-4803213	4.38	376.3 \pm 1.2	0.30 \pm 0.01	–	SB1	62 \pm 4	5.8 \pm 0.5	–
4768097972749950208	TIC 270677487	J05505162-5324488	2.41	712.5 \pm 8.8	0.03 \pm 0.03	–	SB1	26 \pm 3	2.7 \pm 0.2	–
5261308416177125760	TIC 271574685	J07034184-7417523	4.03	461 \pm 1	0.12 \pm 0.01	109 \pm 2	ASB1	56 \pm 10	5.7 \pm 0.2	–
5263914293096915840	TIC 271594930	J07134647-7220475	1.55	584.5 \pm 5.7	0.75 \pm 0.20	110 \pm 5	ASB1	9 \pm 2	1.4 \pm 0.2	–
5262559660411478144	TIC 271638912	J07143948-7423011	1.66	1149 \pm 196	0.38 \pm 0.20	–	SB1	69 \pm 12	6.5 \pm 0.2	–
5211488376093233408	TIC 271699161	J07220932-7756274	1.73	295.6 \pm 1.1	0.04 \pm 0.03	61 \pm 3	ASB1	104 \pm 2	7.86 \pm 0.03	–
5214430806648518912	TIC 271721824	J07211482-7514502	2.99	593.1 \pm 4.7	0.10 \pm 0.03	–	SB1	24 \pm 3	2.9 \pm 0.4	–
5263842064630939776	TIC 271796911	J07251787-7202027	2.32	631.8 \pm 10.1	0.05 \pm 0.04	–	SB1	74 \pm 10	6.0 \pm 0.2	–
5213360122841527808	TIC 272003288	J07403190-7625334	2.69	260.3 \pm 0.6	0.19 \pm 0.02	77 \pm 2	ASB1	83 \pm 6	7.1 \pm 0.2	–
5213512542641305216	TIC 272434321	J08023704-7614278	1.13	357.6 \pm 0.9	0.19 \pm 0.02	–	SB1	42.4 \pm 0.4	5.04 \pm 0.01	–
521397773498413184	TIC 272466541	J08021981-7447215	3.44	1089 \pm 213	0.15 \pm 0.09	–	SB1	38 \pm 3	6.1 \pm 1.4	–

Table B.1. Orbital and seismic parameters of *Gaia* DR3 binary systems. (cont.)

Gaia DR3	KIC/TIC	2MASS	ruwe	P_{orb} [d]	e	i [deg]	Type	ν_{max} [μHz]	$\Delta\nu$ [μHz]	$\Delta\Pi_1$ [s]
5211401171077351424	TIC 278180628	J07153439-7825519	1.34	80.0 \pm 0.1	0.13 \pm 0.03	–	SB1	264 \pm 13	19.2 \pm 0.6	–
5209939576526903168	TIC 278408360	J07444186-7756049	4.52	1046 \pm 77	0.12 \pm 0.03	–	SB1	60 \pm 5	5.74 \pm 0.05	320
5194840636177373056	TIC 278416495	J07491086-8207047	3.65	1179 \pm 208	0.24 \pm 0.05	–	SB1	43 \pm 6	4.6 \pm 0.2	–
5194895298225520384	TIC 278476656	J07575123-8127146	1.22	986 \pm 290	0.62 \pm 0.30	–	SB1	240 \pm 2	19.9 \pm 0.2	–
5208423831028609664	TIC 278539735	J08054375-8053440	4.04	200.3 \pm 0.5	0.39 \pm 0.05	–	ORB	61 \pm 4	5.9 \pm 0.1	–
5209728951331293568	TIC 278544678	J08113022-7816480	1.56	658.2 \pm 11.9	0.01 \pm 0.04	110 \pm 4	ASB1	144 \pm 3	11.5 \pm 0.1	–
5196331264707474048	TIC 278589939	J08104339-8133150	2.23	163.8 \pm 0.5	0.24 \pm 0.10	–	ORB	13 \pm 1	2 \pm 1	–
5194516658204339200	TIC 278594030	J08121358-8257178	1.93	934.196 \pm 155.710	0.14 \pm 0.09	–	ORB	66.55	7.12	–
5497050405026582912	TIC 278685116	J06361769-5531063	2.65	661 \pm 7	0.05 \pm 0.04	–	SB1	36 \pm 6	4.5 \pm 0.2	–
5497905245253821696	TIC 278723939	J06372940-5429104	1.46	116.48 \pm 0.04	0.006 \pm 0.004	–	SB1	90 \pm 14	7.5 \pm 0.1	–
5498012310199094784	TIC 278732696	J06391765-5409589	2.0	616.3 \pm 0.1	0.02 \pm 0.03	–	SB1	67 \pm 3	5.8 \pm 0.1	–
5484477562578920064	TIC 278862374	J06421520-5729236	4.47	1022 \pm 21	0.35 \pm 0.02	53 \pm 2	ASB1	42 \pm 4	4.8 \pm 0.1	–
5484715538127271680	TIC 278896350	J06435807-5640371	5.46	1319.814 \pm 178.055	0.32 \pm 0.06	–	SB1	41.15	3.84	–
5483398353260448896	TIC 278989223	J06471521-5835507	4.43	1045.6 \pm 130.1	0.06 \pm 0.10	–	SB1	52 \pm 4	4.27 \pm 0.02	–
5485113870574265088	TIC 279088460	J06503820-5620216	2.26	975.1 \pm 77.4	0.06 \pm 0.10	–	SB1	26 \pm 2	3.1 \pm 9.8	–
5480724998113187456	TIC 279252047	J06562556-5834191	0.95	0.887	0.15 \pm 0.18	–	SB1	3.4 \pm 0.2	0.7 \pm 0.6	–
5484993336612145920	TIC 279321950	J06572400-5606047	1.0	905 \pm 17	0.74 \pm 0.08	–	SB1	36 \pm 3	4.2 \pm 0.1	–
5485086314064004352	TIC 279359816	J06585924-5533190	3.26	540 \pm 3	0.69 \pm 0.10	–	ORB	11 \pm 1	1.47 \pm 0.01	–
5491391257335480320	TIC 279428181	J07005202-5415177	3.45	1038 \pm 46	0.30 \pm 0.03	–	SB1	15 \pm 4	2.1 \pm 0.2	–
5480806396333685376	TIC 279572330	J07045241-5800513	1.95	1167 \pm 46	0.35 \pm 0.03	–	SB1	11 \pm 2	1.5 \pm 0.3	–
4722093482827445504	TIC 279675292	J03212244-6226288	2.65	1025.302 \pm 75.111	0.30 \pm 0.03	–	SB1	36.24	4.10	–
4640468003027744384	TIC 280050583	J02545187-7454191	2.89	803 \pm 5	0.03 \pm 0.02	–	SB1	13 \pm 2	1.90 \pm 0.05	–
4640830021527110272	TIC 280051953	J03024087-7332570	1.73	28.342 \pm 0.005	0.013 \pm 0.005	–	SB1	132 \pm 3	10.46 \pm 0.02	–
5209481286337113984	TIC 281922368	J08375512-7731016	1.16	970 \pm 46	0.61 \pm 0.12	–	SB1	38 \pm 8	4.4 \pm 0.4	–
5209257157764085760	TIC 282052954	J08491110-7735585	2.03	85.35 \pm 0.05	0.01 \pm 0.01	–	SB1	192 \pm 4	14.9 \pm 0.2	–
5216441813416663168	TIC 282054564	J08505001-7550224	1.39	314.6 \pm 1.2	0.24 \pm 0.03	–	SB1	35 \pm 2	4.05 \pm 0.01	–
5217412407306841728	TIC 282089085	–	2.09	698.0 \pm 30.9	0.23 \pm 0.14	–	SB1	49 \pm 1	4.8 \pm 0.2	–
5280689232764455680	TIC 284194969	J07025602-6800509	6.26	714 \pm 4	0.46 \pm 0.01	77 \pm 1	ASB1	79 \pm 15	7.3 \pm 0.1	–
5210580626166619520	TIC 287723398	J08250952-7602474	2.03	572.3 \pm 2.2	0.10 \pm 0.02	–	SB1	4.2 \pm 0.3	0.7 \pm 0.2	–
5209384357515088896	TIC 287768836	J08252692-7752561	1.62	649 \pm 6	0.11 \pm 0.02	–	SB1	8 \pm 1	1.10 \pm 0.02	–
5210329559557939072	TIC 287769668	J08272449-7644280	2.73	1166 \pm 130	0.31 \pm 0.05	–	SB1	59 \pm 3	5.5 \pm 0.1	–
5209442837790409600	TIC 287979908	J08475280-7738467	1.87	461.5 \pm 1.8	0.05 \pm 0.02	79 \pm 3	ASB1	95 \pm 3	11.5 \pm 0.1	–
5217098805975564288	TIC 288063038	J09051100-7337174	4.5	883 \pm 8	0.26 \pm 0.02	52 \pm 2	ASB1	44 \pm 5	5.2 \pm 0.2	–
5294949619403458560	TIC 290158475	J07582981-5707538	2.59	704.8 \pm 10.5	0.02 \pm 0.05	–	SB1	82 \pm 8	7.3 \pm 0.7	–
5223044999219009152	TIC 290378243	J09123907-6804482	3.19	865 \pm 14	0.27 \pm 0.03	148 \pm 4	ASB1	37 \pm 16	3 \pm 1	–
4769218104516825472	TIC 290754446	J05383711-5202154	2.29	1018.6 \pm 68.9	0.25 \pm 0.08	–	SB1	24 \pm 1	3.30 \pm 0.03	–
4793052149352862080	TIC 290777864	J05391557-5154394	1.56	507.7 \pm 2.7	0.02 \pm 0.02	51 \pm 6	ASB1	13 \pm 1	1.67 \pm 0.03	–
549365353637742720	TIC 291556528	J07271659-5105165	1.09	909.9 \pm 76.9	0.13 \pm 0.11	–	SB1	14 \pm 1	1.94 \pm 0.03	–
5477399387756317824	TIC 293271416	J06353096-6255189	1.2	441.5 \pm 3.1	0.25 \pm 0.03	–	SB1	49 \pm 4	5.0 \pm 0.1	–
4620406004629522560	TIC 293437409	J03141651-7912392	2.09	633 \pm 5	0.38 \pm 0.03	48 \pm 5	ASB1	122 \pm 9	11.0 \pm 0.1	–
4615478547566867072	TIC 293465974	J03191650-8341262	1.75	245.7 \pm 2.3	0.14 \pm 0.12	–	ORB	74 \pm 2	8.7 \pm 0.1	–
5490000787443518080	TIC 294093836	J07091379-5621363	1.53	1160 \pm 21	0.35 \pm 0.02	–	SB1	141 \pm 8	9 \pm 1	–
5490835793507264384	TIC 294394572	J07172483-5407541	3.57	792 \pm 5	0.08 \pm 0.02	104 \pm 1	ASB1	93 \pm 7	8.7 \pm 1.3	–
5490831262319843712	TIC 294394610	J07171805-5410403	1.44	1009 \pm 103	0.42 \pm 0.13	–	SB1	17 \pm 1	2.13 \pm 0.02	–
4653260137927665792	TIC 294748269	J04424280-7137254	1.16	938.7 \pm 20.7	0.07 \pm 0.04	–	SB1	37 \pm 6	3.9 \pm 3.3	394
5280945281535607936	TIC 300013094	J07083736-6703484	2.17	277.6 \pm 2.3	0.69 \pm 0.10	–	ORB	11 \pm 1	1.52 \pm 0.02	–
5268639272518593280	TIC 300013829	J07091028-6812065	1.58	1053.0 \pm 70.2	0.24 \pm 0.05	–	SB1	10 \pm 3	1.9 \pm 0.3	–
5281127766107447168	TIC 300037832	J07105043-6708172	2.36	998 \pm 10	0.72 \pm 0.11	–	SB1	180.90 \pm 0.01	11.1 \pm 0.2	–
5268334054962416512	TIC 300087347	J07113842-6915453	1.45	1188 \pm 452	0.35 \pm 0.19	–	SB1	31 \pm 3	3.3 \pm 0.6	–
5268335738589611264	TIC 300087385	J07120858-6912475	2.91	1028.4 \pm 57.3	0.20 \pm 0.10	–	SB1	12 \pm 2	1.7 \pm 0.5	–
5267115074524974848	TIC 300137830	J07141944-7117255	3.04	1065 \pm 80	0.11 \pm 0.06	–	SB1	93 \pm 6	8.0 \pm 0.2	–
5268288734467593728	TIC 300139027	J07145719-6919449	1.28	214 \pm 2	0.07 \pm 0.10	–	SB1	87 \pm 3	10.11 \pm 0.05	–
5268978265697599232	TIC 300326394	J07231177-6753184	3.39	1211 \pm 49	0.37 \pm 0.02	–	SB1	56 \pm 4	5.2 \pm 0.1	–
5275213080744624768	TIC 300561571	J07314482-6628587	1.62	498 \pm 5	0.06 \pm 0.03	86 \pm 4	ASB1	73 \pm 6	6 \pm 1	–
5272418328345197184	TIC 301783936	J08430142-6616517	1.29	590 \pm 5	0.06 \pm 0.02	–	SB1	85 \pm 2	6.65 \pm 0.05	–
5223560287915772288	TIC 301859829	J08425904-6847221	2.58	136.1 \pm 0.2	0.28 \pm 0.03	33 \pm 5	ASB1	168.2 \pm 0.5	13.43 \pm 0.01	–
5272116340604356736	TIC 301868495	J08440383-6713437	4.49	1506.6 \pm 32.2	0.483 \pm 0.005	82 \pm 2	ASB1	58 \pm 11	6.57 \pm 0.05	–
5272428704986353792	TIC 301921072	J08441219-6559178	2.78	274.3 \pm 0.4	0.01 \pm 0.01	83 \pm 2	ASB1	17 \pm 2	2.3 \pm 0.3	–
5223552664352812928	TIC 301925163	J08453909-6844202	1.84	1083 \pm 211	0.30 \pm 0.10	–	SB1	107 \pm 24	9.7 \pm 0.6	–
5272457257929408000	TIC 302132642	J08484957-6605440	1.44	70.95 \pm 0.02	0.13 \pm 0.01	–	SB1	17.9 \pm 0.2	1.9 \pm 0.2	–
5223703228726620416	TIC 302449161	J08561447-6842160	2.63	1189.8 \pm 130.6	0.16 \pm 0.10	–	SB1	13 \pm 15	1.68 \pm 0.04	–
5222858460199169920	TIC 302796208	J09022885-6928487	7.44	875 \pm 9	0.10 \pm 0.04	–	SB1	162 \pm 4	16.2 \pm 0.2	–
4616069741224392576	TIC 302967127	J04071226-8217050	3.29	959.5 \pm 10.5	0.06 \pm 0.03	–	SB1	61 \pm 4	5.7 \pm 0.6	–
5208457774152835328	TIC 302992217	J08145401-8035494	3.21	965.8 \pm 25.4	0.07 \pm 0.03	–	SB1	51 \pm 4	5 \pm 1	–
5222653401281330304	TIC 303605377	J09175023-6940085	1.13	958.1 \pm 61.8	0.47 \pm 0.09	–	SB1	98 \pm 6	10.5 \pm 0.1	–
5246813588754068992	TIC 304083900	J09250226-6818092	0.92	347 \pm 3	0.06 \pm 0.04	–	SB1	19 \pm 3	2.34 \pm 0.01	–
5219233537860830592	TIC 304177037	J09255716-7122352	1.06	111.9 \pm 0.2	0.03 \pm 0.02	–	SB1	3.8 \pm 0.2	0.82 \pm 0.03	–
5246911479645277952	TIC 304213082	J09271484-6804405	2.13	1097 \pm 132	0.20 \pm 0.05	–	SB1	4.0 \pm 0.3	0.8 \pm 0.5	–
5273986335003835008	TIC 306470380	J07542569-6728336	1.14	736 \pm 17	0.11 \pm 0.10	–	SB1	43 \pm 3	5 \pm 3	–
5273982211835236736	TIC 306508123	J07544225-6733069	1.18	1011.6 \pm 300.8	0.30 \pm 0.20	–	SB1	31 \pm 3		

Table B.1. Orbital and seismic parameters of *Gaia* DR3 binary systems. (cont.)

Gaia DR3	KIC/TIC	2MASS	ruwe	P_{orb} [d]	e	i [deg]	Type	ν_{max} [μHz]	$\Delta\nu$ [μHz]	$\Delta\Pi_1$ [s]	
5271049779965156480	TIC 307160250	J08170500-6820218	1.16	1156 \pm 320	0.36 \pm 0.16	–	SB1	17 \pm 2	2.3 \pm 0.2	–	
5271068780900512000	TIC 307210739	J08171630-6813327	1.32	1271 \pm 120	0.37 \pm 0.10	–	SB1	45 \pm 1	4.5 \pm 0.4	–	
5269875325450848512	TIC 307212437	J08180682-6956008	2.6	868 \pm 25	0.03 \pm 0.06	–	SB1	47 \pm 5	5.1 \pm 0.3	277	
5271052631823579008	TIC 307217497	J08192588-6820134	1.14	1074 \pm 205	0.18 \pm 0.15	–	SB1	16 \pm 2	1.78 \pm 0.01	–	
5221441292788884736	TIC 307575440	J08285780-7144186	1.38	10,708 \pm 0.001	–	–	ORB	13.54	1.70	–	
5221785749166191616	TIC 307785023	J08332451-7044266	1.67	986.7 \pm 168.8	0.46 \pm 0.30	–	SB1	44 \pm 5	4.6 \pm 0.2	–	
5290789243502185984	TIC 308539721	J08045309-6031342	7.07	982.8 \pm 4.3	0.248 \pm 0.005	93.0 \pm 0.5	ASB1	12 \pm 1	1.6 \pm 0.1	–	
5277455740867533056	TIC 308543034	J08041873-6330451	2.55	718.3 \pm 6.8	0.06 \pm 0.05	–	SB1	9 \pm 2	1.38 \pm 0.02	–	
5277196771520878208	TIC 308661352	J08064974-6356478	1.5	83.7 \pm 0.1	0.23 \pm 0.02	–	SB1	42 \pm 5	5 \pm 1	257	
5277095101054489856	TIC 308749969	J08080476-6449211	1.72	684.6 \pm 10.4	0.49 \pm 0.20	–	ORB	40 \pm 3	3.4 \pm 0.3	–	
5290434582282788352	TIC 308925901	J08105948-6011171	3.3	974 \pm 19	0.01 \pm 0.04	–	SB1	88 \pm 3	7.8 \pm 0.2	–	
5290441385509447552	TIC 308926035	J08114082-6004325	11.47	888.9 \pm 14.5	0.33 \pm 0.04	–	SB1	42 \pm 6	4.4 \pm 0.1	–	
5277324830264215808	TIC 308989495	J08121636-6324150	4.23	941.9 \pm 3.4	0.03 \pm 0.01	–	SB1	4.6 \pm 0.3	0.87 \pm 0.02	–	
5277341426019097984	TIC 309251722	J08154801-6319463	2.16	698 \pm 6	0.10 \pm 0.03	–	SB1	51 \pm 5	4.8 \pm 0.5	–	
5278067103692506496	TIC 309290693	J08164269-6132107	1.8	1087 \pm 80	0.48 \pm 0.11	–	SB1	42 \pm 3	4.4 \pm 0.7	–	
5195179217040063104	TIC 309487275	J09183639-8202582	1.54	877 \pm 30	0.29 \pm 0.11	42 \pm 10	ASB1	21 \pm 1	2.5 \pm 0.1	–	
5195814219365087744	TIC 309490601	J09195885-8101305	1.53	391 \pm 3	0.23 \pm 0.03	–	SB1	83 \pm 6	7 \pm 2	–	
5278103799894304768	TIC 309552570	J08211330-6126435	4.3	1179 \pm 50	0.21 \pm 0.05	–	SB1	85 \pm 2	6.7 \pm 0.1	–	
5276895986370219520	TIC 309627098	J08232106-6325393	1.11	414.0 \pm 0.8	0.15 \pm 0.01	–	SB1	125 \pm 3	12.2 \pm 0.1	–	
5277695571842986624	TIC 309627723	J08224994-6255419	2.34	1185 \pm 68	0.25 \pm 0.10	–	SB1	7 \pm 1	1.4 \pm 0.2	–	
4760900573931444864	TIC 309754751	J05182213-6119323	3.31	911 \pm 18	0.02 \pm 0.03	–	SB1	35 \pm 4	4.3 \pm 0.3	–	
4761126592290010112	TIC 309755356	J05190491-6001233	5.47	681 \pm 4	0.01 \pm 0.02	57 \pm 2	ASB1	26 \pm 3	3 \pm 1	–	
4661224209891819904	TIC 309790487	J05205024-6331303	2.44	331 \pm 1	0.05 \pm 0.02	–	SB1	52 \pm 4	5.0 \pm 0.3	272	
5272869609147946496	TIC 310308312	J08325722-6545307	3.3	785 \pm 33	0.16 \pm 0.10	–	SB1	41 \pm 5	4.5 \pm 0.2	–	
5273560171170589440	TIC 310309795	J08330219-6435407	2.39	1147 \pm 66	0.14 \pm 0.10	–	SB1	34 \pm 4	4.0 \pm 0.4	–	
5301088712518194560	TIC 310388119	J08333932-6217073	1.96	709 \pm 17	0.05 \pm 0.06	–	SB1	37 \pm 2	9 \pm 10	–	
5273541513832962560	TIC 310478750	J08341043-6449424	7.78	1055.8 \pm 52.5	0.40 \pm 0.03	–	ORB	46 \pm 1	4.07 \pm 0.04	–	
5277003016957792768	TIC 310481832	J08342667-6239068	1.16	128.7 \pm 0.1	0.18 \pm 0.02	–	SB1	58 \pm 2	6.85 \pm 0.05	–	
5273646242312633600	TIC 310541158	J08355960-6428354	1.03	363 \pm 1	0.17 \pm 0.03	–	SB1	105 \pm 3	11.22 \pm 0.02	–	
4641508454561459200	TIC 314827374	J03285436-7244232	1.52	72.38 \pm 0.03	0.18 \pm 0.01	–	SB1	110 \pm 24	9.9 \pm 0.2	–	
4614819974460776192	TIC 317181186	J05104949-8423076	2.24	598.9 \pm 4.5	0.04 \pm 0.03	51 \pm 3	ASB1	42 \pm 5	4.6 \pm 0.8	–	
4614592341194069888	TIC 317183131	J05162774-8452550	2.86	913.4 \pm 43.7	0.23 \pm 0.10	–	SB1	78 \pm 4	6.0 \pm 0.2	–	
5193552622729151872	TIC 317244353	J07563768-8409430	1.06	18,989 \pm 0.002	0.01 \pm 0.01	–	SB1	15 \pm 21	2 \pm 3	–	
5193229782924856064	TIC 317297785	J08143467-8507300	0.98	924.8 \pm 29.9	0.26 \pm 0.04	–	SB1	4.5 \pm 0.3	1 \pm 1	–	
4615286820226008320	TIC 317335840	J04060255-8407231	2.74	0.545	0.10 \pm 0.08	–	SB1	12 \pm 1	1.64 \pm 0.02	–	
4621869424542677376	TIC 319290269	J04473630-8155127	1.03	123.7 \pm 0.2	0.07 \pm 0.02	–	SB1	6 \pm 1	1.1 \pm 0.3	–	
5551256328275498880	TIC 319437646	J06405672-4927076	2.67	758 \pm 14	0.14 \pm 0.05	–	SB1	38 \pm 3	4 \pm 4	–	
5503212411785581312	TIC 319437757	J06412298-4937344	1.65	1052 \pm 107	0.49 \pm 0.05	–	SB1	49 \pm 8	4.7 \pm 0.4	–	
5498318867784341504	TIC 319468075	J06413506-5307278	1.18	218 \pm 1	0.03 \pm 0.03	–	SB1	29 \pm 1	3.3 \pm 0.4	–	
5551373086963769728	TIC 319476436	J06424001-4839130	2.04	649.3 \pm 2.3	0.42 \pm 0.02	–	SB1	3.0 \pm 0.2	0.54 \pm 0.04	–	
5196060475609310208	TIC 323008272	J08233867-8205569	2.61	114.2 \pm 0.1	0.11 \pm 0.01	–	SB1	117 \pm 7	9.7 \pm 0.6	–	
5209272963243529728	TIC 323065603	–	–	2.09	1173 \pm 116	0.36 \pm 0.11	–	SB1	68 \pm 10	6.2 \pm 0.2	–
5209058489756737152	TIC 323168600	J08334293-7901415	1.96	696 \pm 14	0.07 \pm 0.04	–	SB1	19 \pm 2	2.36 \pm 0.03	–	
4615628424744876160	TIC 323423503	J04282154-8401186	1.86	937.5 \pm 85.5	0.15 \pm 0.05	–	SB1	14 \pm 1	1.8 \pm 0.2	–	
4614856670661412352	TIC 323444284	J04464813-8417077	2.42	1242.3 \pm 101.1	0.26 \pm 0.07	–	SB1	14 \pm 2	1.7 \pm 0.1	–	
5197100510530297216	TIC 323515122	J08561254-7854481	2.47	1093 \pm 34	0.21 \pm 0.04	–	SB1	39 \pm 5	4 \pm 1	–	
5195973889069600256	TIC 323815681	J09252357-8023148	3.13	1113 \pm 51	0.17 \pm 0.04	–	SB1	8 \pm 1	1.1 \pm 0.2	–	
5192049147953684736	TIC 323817602	J09255485-8313589	1.38	152.6 \pm 0.1	0.248 \pm 0.005	–	SB1	86 \pm 2	8.2 \pm 0.1	–	
4614538838784619520	TIC 325607724	J05593294-8504255	3.33	770.4 \pm 6.9	0.28 \pm 0.04	–	SB1	124 \pm 2	10.6 \pm 0.1	–	
5487466241343198080	TIC 329673338	J07220414-5539100	6.2	1754 \pm 279	0.72 \pm 0.03	37 \pm 5	ASB1	106 \pm 15	16 \pm 11	–	
5486353363776983040	TIC 339773102	J07251305-5707062	1.52	139.7 \pm 0.1	0.227 \pm 0.005	–	SB1	13 \pm 2	1.9 \pm 0.1	–	
5293790051248219648	TIC 339862761	J07270748-5859564	1.71	1166.932 \pm 142.747	0.46 \pm 0.07	–	SB1	39.24	4.40	–	
5487624296139481344	TIC 339887962	J07273458-5442350	2.02	960.0 \pm 73.4	0.21 \pm 0.10	–	SB1	45 \pm 5	4.9 \pm 0.2	–	
5293516856968125952	TIC 339960404	J07302823-5933299	2.66	947 \pm 38	0.68 \pm 0.06	–	SB1	49 \pm 3	5.1 \pm 0.4	–	
5293806647002029824	TIC 339960953	J07295911-5850121	2.75	896.5 \pm 8.2	0.36 \pm 0.02	–	SB1	22 \pm 2	2.4 \pm 0.2	–	
5486012068495731584	TIC 340006114	J07312531-5756239	6.05	927.5 \pm 24.7	0.29 \pm 0.02	–	SB1	55 \pm 5	4.9 \pm 0.1	–	
5487348902836720256	TIC 340060472	J07315932-5518575	4.68	896.0 \pm 16.8	0.31 \pm 0.02	–	SB1	23 \pm 3	2.8 \pm 0.4	–	
5293551629023688064	TIC 340136613	J07332938-5911548	0.97	378.6 \pm 5.4	0.18 \pm 0.10	–	SB1	1.9 \pm 0.2	0.46 \pm 0.01	–	
5488006612650604544	TIC 340179249	J07345449-5556503	2.09	607.8 \pm 2.3	0.31 \pm 0.01	–	SB1	15 \pm 15	2.2 \pm 0.6	–	
5295485292021374208	TIC 340255470	J07392238-5715303	2.8	756 \pm 10	0.20 \pm 0.03	–	SB1	15 \pm 2	1.8 \pm 0.1	–	
5488141994318792064	TIC 340362223	J07414717-5510462	1.56	984.5 \pm 60.9	0.58 \pm 0.12	–	SB1	20 \pm 3	2.8 \pm 1.7	–	
5488575854736421376	TIC 340696282	J07463475-5414423	4.98	1146.8 \pm 69.9	0.20 \pm 0.04	–	SB1	50 \pm 4	4.9 \pm 0.1	–	
5487838700907700352	TIC 340699073	J07475279-5548478	2.43	1060 \pm 100	0.36 \pm 0.10	–	SB1	17 \pm 3	2.2 \pm 0.1	–	
5295287173769548928	TIC 341038574	J07525026-5733267	1.8	993 \pm 139	0.50 \pm 0.10	–	SB1	46 \pm 6	4.8 \pm 0.2	–	
5296072431230768128	TIC 341107993	J07543161-5526347	1.31	547.0 \pm 4.2	0.07 \pm 0.03	–	SB1	72 \pm 2	5.78 \pm 0.03	–	
5296186398184284544	TIC 341191116	J07551421-5504096	1.54	114.79 \pm 0.03	0.15 \pm 0.01	–	SB1	10 \pm 2	1.3 \pm 0.2	–	
5295778208791215360	TIC 341264608	J07565224-5628593	1.8	1178 \pm 320	0.29 \pm 0.20	–	SB1	107 \pm 11	9 \pm 1	–	
5295948044680574208	TIC 341550214	J08020411-5517363	1.08	107.36 \pm 0.05	0.12 \pm 0.01	–	SB1	8 \pm 1	1.3 \pm 0.8	–	
5295071841290178560	TIC 341551629	J08023056-5618127	1.28	157.3 \pm 0.5	0.16 \pm 0.04	–	SB1	66 \pm 9	5.7 \pm 0.2	–	
5294800708595024640	TIC 341929445	J08080552-5707025	2.82	580 \pm 5	0.25 \pm 0.07	–	ORB	15 \pm 1	2.05 \pm 0.03	–	
5319916199873949696	TIC 341932245	J08083583-5515331	2.06	1254 \pm 127	0.39 \pm 0.06	–	SB1	42 $\pm</$			

Table B.1. Orbital and seismic parameters of *Gaia* DR3 binary systems. (cont.)

Gaia DR3	KIC/TIC	2MASS	ruwe	P_{orb} [d]	e	i [deg]	Type	ν_{max} [μHz]	$\Delta\nu$ [μHz]	$\Delta\Pi_1$ [s]
5319316003966383744	TIC 342836330	J08211020-5542357	1.42	460.6 ±2.9	0.35 ±0.05	–	SB1	159 ±4	15.8 ±0.1	–
5315624668554128768	TIC 342957562	J08225316-5712490	1.27	176.5 ±0.5	0.27 ±0.05	–	SB1	55.85 ±0.03	5.45 ±0.04	–
5505385910054841088	TIC 343937772	J07094072-4959354	1.86	769 ±17	0.36 ±0.02	–	SB1	6 ±1	1.0 ±0.1	–
5503582161228109440	TIC 343965002	J07095770-5254055	2.69	1003 ±23	0.16 ±0.03	–	SB1	57 ±3	5 ±1	–
5505220880230192128	TIC 344084890	J07123078-4958304	1.05	967 ±122	0.39 ±0.20	–	SB1	8.5 ±0.5	1.3 ±0.2	–
5491488014358980224	TIC 344134552	J07122432-5329321	1.11	1136 ±77	0.27 ±0.05	–	SB1	7.8 ±0.5	1.24 ±0.03	–
5505531286107303040	TIC 344141200	J07135971-4917047	1.04	941.0 ±51.8	0.53 ±0.09	–	SB1	6.8 ±0.4	1.0 ±0.3	–
4618920396917854720	TIC 348770230	J03064863-8155105	1.04	330 ±10	0.15 ±0.10	–	SB1	11 ±1	1.62 ±0.04	–
4618654177665407360	TIC 348772362	J03091928-8257225	1.85	903 ±17	0.18 ±0.03	–	SB1	20 ±3	2.3 ±0.2	–
5498113156030848128	TIC 348843739	J06360852-5415165	1.62	689.9 ±15.1	0.07 ±0.09	–	SB1	114 ±13	10 ±1	–
5479254160793170432	TIC 348844648	J07030138-6106364	0.94	96.8 ±0.1	0.01 ±0.01	–	SB1	5 ±1	0.9 ±0.2	–
5285571476709346176	TIC 348960248	J07055421-6418188	1.88	894.5 ±5.4	0.35 ±0.02	–	SB1	2.7 ±0.2	0 ±1	–
5479369437715439744	TIC 348997612	J07083611-6040501	0.9	0.547	0.24 ±0.03	–	SB2	8 ±1	1 ±1	–
5285866936098900480	TIC 349060088	J07094423-6321436	1.3	1055.9 ±269.6	0.47 ±0.36	–	SB1	5 ±1	1.0 ±0.2	–
5286817326462230272	TIC 349060722	J07095202-6221338	1.22	212 ±1	0.01 ±0.03	–	SB1	6 ±1	1.1 ±0.3	–
5287211260862325760	TIC 349061757	J07102473-6049184	5.03	825.7 ±46.1	0.15 ±0.09	–	SB1	99 ±11	8.1 ±0.3	–
5287150409765989632	TIC 349152250	J07122301-6100104	1.3	115.8 ±0.2	0.28 ±0.03	–	SB1	28 ±3	3 ±1	–
5281544962050491776	TIC 349274962	J07171628-6546524	1.57	73.4 ±0.1	0.28 ±0.03	–	SB1	55 ±5	5.3 ±0.4	–
5292941537509309568	TIC 349306704	J07172630-6108057	2.2	668 ±8	0.02 ±0.02	60 ±2	ASB1	30 ±3	3.5 ±0.1	–
5282333552405140096	TIC 349311420	J07185146-6504463	1.54	520.9 ±3.6	0.48 ±0.03	94 ±3	ASB1	36 ±4	4.1 ±0.3	–
5292915183590061312	TIC 349371980	J07193233-6108419	4.34	646.9 ±5.8	0.47 ±0.04	–	ORB	8 ±2	1.4 ±0.2	–
5291812957543034752	TIC 349409309	J07220830-6238390	1.58	371 ±1	0.33 ±0.03	–	SB1	26 ±2	3 ±3	–
5291970904962999936	TIC 349645349	J07284798-6144456	1.42	117.0 ±0.2	0.13 ±0.02	–	SB1	10 ±2	1.3 ±0.2	–
5291998843727867008	TIC 349679149	J07295112-6132552	2.57	0.275	0.10 ±0.11	–	SB1	65 ±6	5.6 ±0.2	–
5293424429272296960	TIC 349680394	J07294862-6012426	1.19	192.6 ±0.3	0.02 ±0.02	–	SB1	54 ±7	6.4 ±0.2	–
5292702973549148800	TIC 349828202	J07332215-6003226	1.79	587 ±6	0.02 ±0.03	–	SB1	53 ±4	4.9 ±0.1	–
5288812046714487296	TIC 349902991	J07351345-6254398	3.02	1335 ±312	0.10 ±0.07	97 ±3	ASB1	5 ±1	0.9 ±0.1	–
5292338352301865216	TIC 350091478	J07402191-6113501	0.98	30.22 ±0.02	0.04 ±0.02	–	SB1	83 ±17	7.2 ±0.1	–
5288996592868969472	TIC 350098066	J07412660-6243499	0.95	95.93 ±0.03	0.01 ±0.01	–	SB1	55 ±4	4.8 ±0.1	–
4768208061351339520	TIC 350442556	J05414110-5524224	2.23	0.261	0.12 ±0.10	–	SB1	78 ±9	6.4 ±0.1	–
4768769435053119872	TIC 350446970	–	2.79	559 ±7	0.14 ±0.10	–	ORB	18 ±2	2.4 ±0.2	–
4765929087281315456	TIC 350522041	J05452332-5604040	1.31	887 ±302	0.17 ±0.26	–	SB1	3.1 ±0.2	0.6 ±0.1	–
4767560723880526848	TIC 350563396	J05465283-5511463	1.52	0.686	0.13 ±0.09	–	SB1	29 ±7	2.5 ±0.3	–
4765051402124443392	TIC 350655254	J05515824-5845521	1.42	81.47 ±0.02	0.26 ±0.01	70 ±7	ASB1	23 ±2	3 ±4	–
4765463959502856448	TIC 350711600	J05523188-5812147	4.35	1069.8 ±44.4	0.34 ±0.05	43 ±3	ASB1	78 ±9	7.2 ±0.2	–
4765491516012812544	TIC 350715119	J05540072-5746396	1.13	109.9 ±0.4	0.40 ±0.04	–	SB1	10 ±3	1.8 ±0.1	–
4767299388006839296	TIC 350716404	J05533323-5544384	1.68	491.0 ±3.4	0.31 ±0.02	84 ±3	ASB1	21 ±2	2.4 ±0.3	–
4767765787095957888	TIC 350840596	J05591987-5457229	3.47	432 ±3	0.07 ±0.04	157 ±11	ASB1	8 ±2	1.4 ±0.2	–
5500023694923029632	TIC 350859088	J06012042-5542478	2.92	788.4 ±10.2	0.24 ±0.03	–	SB1	38 ±4	4.3 ±0.2	–
5499250394651323904	TIC 350859255	J06010833-5604541	1.5	492 ±3	0.68 ±0.01	112 ±4	ASB1	7 ±1	1.2 ±0.2	–
5500323002604126976	TIC 350930032	–	1.89	1157 ±57	0.34 ±0.04	–	SB1	17 ±3	2.3 ±0.2	–
4796054881248518144	TIC 350847401	J05410570-4712052	1.21	80.0 ±0.1	0.01 ±0.03	–	SB1	5.3 ±0.4	1.21 ±0.02	–
5300754804578782592	TIC 355005481	J08390336-6311236	2.15	1018 ±32	0.22 ±0.04	–	SB1	3.8 ±0.3	0.91 ±0.02	–
5297733209188853632	TIC 355091013	J08403192-6329372	1.11	360 ±2	0.30 ±0.05	–	SB1	48 ±2	5.56 ±0.04	–
5491907168807390976	TIC 355354578	J07174935-5248437	4.38	376.273 ±1.193	0.30 ±0.01	–	SB1	63.97	6.32	–
5490974920386379136	TIC 355457903	J07225231-5323147	3.02	1240.8 ±266.8	0.15 ±0.18	–	SB1	51 ±3	5 ±5	–
5296615108939566464	TIC 356017514	J08522899-6445183	8.57	3699.4 ±546.7	0.89 ±0.02	161 ±4	ASB1	160 ±3	11.0 ±0.2	–
5301466326044927616	TIC 356096344	J08542312-6041265	2.63	602 ±6	0.34 ±0.02	130 ±3	ASB1	29 ±6	3.20 ±0.01	–
5301471239487596928	TIC 356299151	J08545436-6042094	1.35	587.6 ±2.6	0.03 ±0.02	–	SB1	6 ±1	1.2 ±0.1	–
5298220395921850112	TIC 356358845	J08560831-6213151	3.02	256.2 ±0.3	0.30 ±0.01	97 ±2	ASB1	38 ±4	4.30 ±0.02	–
5297289212653037312	TIC 357294987	J09072234-6259489	0.96	153.9 ±0.4	0.36 ±0.03	–	SB1	21 ±2	2.4 ±0.1	–
5248687053494097792	TIC 357902967	J09134178-6520253	1.31	620.5 ±7.4	0.22 ±0.03	–	SB1	67 ±6	7.15 ±0.01	–
4639539538471977600	TIC 358107812	J03235624-7458537	1.39	0.650	0.30 ±0.14	–	SB1	20 ±2	2 ±1	–
54652297893448474240	TIC 358155108	J04412859-7444483	1.45	222.7 ±1.8	0.13 ±0.12	–	SB1	135 ±9	10 ±1	–
4731140397642849920	TIC 358251302	J03480837-5627536	1.2	1018.8 ±33.7	0.20 ±0.03	–	SB1	2.6 ±0.2	0.56 ±0.01	–
4731959022706137728	TIC 358251881	J03482480-5417375	2.59	212.6 ±0.2	0.298 ±0.005	–	SB1	141 ±32	10.6 ±0.1	–
4683381735700830592	TIC 358252465	J04073399-5546116	1.08	349 ±2	0.07 ±0.03	–	SB1	30 ±3	3.4 ±0.1	–
5275923433976133504	TIC 358406093	J07555890-6407139	1.41	1122.4 ±88.6	0.74 ±0.05	–	SB1	22 ±2	2.7 ±0.1	–
4665508624435523200	TIC 358710790	J04492909-6150341	2.04	557 ±4	0.35 ±0.05	–	SB1	11 ±1	1.6 ±0.3	–
5248704783119495808	TIC 358869739	J09174432-6508369	2.22	330 ±1	0.35 ±0.03	–	SB1	117 ±3	9.89 ±0.04	–
5194012807001036928	TIC 362066609	J06514990-8404046	3.81	738.5 ±7.4	0.41 ±0.04	24 ±5	ASB1	35 ±2	3.5 ±0.2	–
5192876255575637504	TIC 362066609	J07163936-8535332	1.14	1100 ±203	0.29 ±0.20	–	SB1	68 ±3	5.3 ±0.2	–
4794711621636781696	TIC 363914872	J05571087-4843113	1.24	463 ±3	0.03 ±0.02	–	SB1	5.1 ±0.2	0.79 ±0.02	–
4681709623329594496	TIC 364266060	J04110325-5904227	2.42	473 ±3	0.16 ±0.03	133 ±4	ASB1	88 ±9	7 ±1	–
5289890908139518336	TIC 364399182	J07581264-6126042	5.99	762 ±6	0.13 ±0.02	143 ±2	ASB1	44 ±3	4.2 ±0.2	–
4650236034272500608	TIC 364591606	J05444444-7330396	1.21	989.535 ±90.099	0.51 ±0.11	–	ORB	58.72	5.70	–
4668610110516263040	TIC 370040560	J04231902-6703014	2.05	1072.7 ±122.9	0.09 ±0.08	–	SB1	41 ±5	4.0 ±0.1	–
4668792904325646720	TIC 370041080	J04243269-6616250	2.32	845.6 ±15.5	0.11 ±0.10	–	SB1	6.7 ±0.5	1.1 ±1.5	–
4654007011257640192	TIC 370101172	J04232912-7127296	2.46	1246 ±99	0.09 ±0.03	–	SB1	31 ±3	3.8 ±0.3	377
4620543241720792704	TIC 370237773	J02443981-7915424	2.18	495 ±3	0.04 ±0.03	48 ±4	ASB1	79 ±12	8.5 ±0.2	–
4622312974405261568	TIC 370327584	J04180673-8045124	2.43	1179 ±107	0.26 ±0.04	–	SB1	45 ±3	5 ±1	–
5219325626259859840	TIC 370329640	J09301016-7107083	2.46	416.2 ±6.7	0.13 ±0.10	–	SB1	37 ±3	4.24 ±0.04	–
5218514736434413184	TIC 371019748	J09433665-7127154	3.75	1311.0 ±153.4	0.23 ±0.10	–	SB1	122 ±24	12.4 ±0.2	–
4755911299414588544	TIC 374829302	J05531147-6534005	1.53	212 ±1	0.03 ±0.03	122 ±5	ASB1	80 ±9	8.63 ±0.01	–

Table B.1. Orbital and seismic parameters of *Gaia* DR3 binary systems. (cont.)

Gaia DR3	KIC/TIC	2MASS	ruwe	P_{orb} [d]	e	i [deg]	Type	ν_{max} [μHz]	$\Delta\nu$ [μHz]	$\Delta\Pi_1$ [s]
5480054777056960768	TIC 375033046	J06372437-6054249	2.05	1101.0 \pm 77.7	0.29 \pm 0.05	–	SB1	42 \pm 3	5 \pm 1	–
5477150928191504896	TIC 375055532	J06390160-6307352	1.34	104.4 \pm 0.2	0.01 \pm 0.03	–	SB1	97 \pm 8	8.0 \pm 0.1	–
5479765880376661632	TIC 375089891	J06411203-6138266	2.48	648 \pm 10	0.04 \pm 0.04	–	SB1	47 \pm 8	4.7 \pm 0.3	–
4794159426281391616	TIC 375145184	J05553293-5035258	0.95	395.3 \pm 9.5	0.05 \pm 0.08	–	SB1	16 \pm 2	1.90 \pm 0.04	–
4794721792119196672	TIC 375146334	J05554630-4905518	3.26	646 \pm 6	0.05 \pm 0.04	–	SB1	35 \pm 3	4.1 \pm 0.5	–
4626059040584912256	TIC 376931357	J03560671-7847296	2.18	897 \pm 53	0.02 \pm 0.05	–	SB1	75 \pm 4	8.6 \pm 0.2	–
4621818606489765888	TIC 376987461	J05094338-7949159	2.15	278.5 \pm 0.2	0.51 \pm 0.01	69 \pm 3	ASB1	15 \pm 2	2.0 \pm 0.2	–
4621149759822563968	TIC 377018491	J05114976-8202138	2.4	338 \pm 1	0.18 \pm 0.01	–	SB1	36 \pm 4	4.5 \pm 19.6	–
5505344506569228032	TIC 379953111	J07182913-4921264	3.57	1419.8 \pm 55.8	0.60 \pm 0.02	92 \pm 1	ASB1	43 \pm 7	4.87 \pm 0.03	–
5492005815617056512	TIC 380037418	J07195170-5233539	7.32	464.3 \pm 1.5	0.08 \pm 0.03	–	ORB	15 \pm 3	2.0 \pm 0.2	–
4763851319543022848	TIC 381975051	J05075321-5739339	2.75	600.0 \pm 5.9	0.23 \pm 0.04	–	SB1	74 \pm 5	7.1 \pm 0.1	–
4770682104249367680	TIC 381976111	J05083714-5407147	3.77	667.9 \pm 3.8	0.04 \pm 0.02	142 \pm 3	ASB1	36 \pm 3	3.6 \pm 0.3	–
4770663893588067712	TIC 381978003	J05095036-5419004	2.66	578 \pm 4	0.03 \pm 0.02	–	SB1	17 \pm 2	2.0 \pm 0.2	–
4770546383282420736	TIC 381978460	J05102227-5454517	1.16	1006 \pm 62	0.43 \pm 0.13	–	SB1	30 \pm 3	3.6 \pm 0.2	–
4769725872730421376	TIC 382031115	J05151466-5524592	1.33	1087.3 \pm 132.7	0.36 \pm 0.09	–	SB1	5 \pm 1	1 \pm 1	–
4763608980307581696	TIC 382042802	J05164159-5627358	3.24	968.9 \pm 61.5	0.50 \pm 0.10	–	SB1	38 \pm 6	4.4 \pm 0.2	–
4769619593763442816	TIC 382042909	J05165235-5607485	2.82	852.0 \pm 36.3	0.14 \pm 0.04	–	SB1	64 \pm 3	5.8 \pm 0.3	–
4769410347253298816	TIC 382145418	J05211212-5631080	6.11	963.3 \pm 51.2	0.21 \pm 0.03	–	SB1	30 \pm 3	3.2 \pm 0.1	–
4769470614234150272	TIC 382189444	J05255261-5624238	2.25	729.1 \pm 17.3	0.42 \pm 0.10	–	SB1	94 \pm 2	7.57 \pm 0.03	–
4769356093226280832	TIC 382201632	J05273854-5647061	1.21	989.5 \pm 90.1	0.51 \pm 0.10	–	SB1	168 \pm 3	13.5 \pm 0.1	–
4771572949186057344	TIC 382258436	J05294426-5405400	1.45	130.6 \pm 0.2	0.22 \pm 0.02	–	SB1	31 \pm 3	4 \pm 3	316
4655951845463738240	TIC 388131014	J04215507-6935504	5.28	630.2 \pm 1.8	0.27 \pm 0.02	127 \pm 2	ASB1	65 \pm 5	6.39 \pm 0.05	–
4625996132199623168	TIC 388200104	J04101804-7809304	1.28	99.7 \pm 0.2	0.02 \pm 0.03	–	SB1	71 \pm 15	6.2 \pm 0.1	–
4616055619371968896	TIC 388201707	J04102575-8227398	1.17	487.9 \pm 6.6	0.15 \pm 0.10	–	SB1	47 \pm 3	5.0 \pm 0.2	–
5193455904361683328	TIC 388244276	J08262396-8358571	1.45	723.1 \pm 9.1	0.01 \pm 0.03	–	SB1	4.8 \pm 0.2	0.85 \pm 0.01	–
4657020600829305472	TIC 389321361	J05430340-7109399	1.39	799.6 \pm 87.9	0.29 \pm 0.20	–	SB1	24 \pm 3	2.8 \pm 0.2	–
4659190800578570880	TIC 389869805	J05510331-6806503	1.04	118.3 \pm 0.2	0.05 \pm 0.03	–	SB1	41 \pm 5	4.1 \pm 0.2	–
5260949941029124352	TIC 391903220	J07062497-7528524	3.62	980 \pm 16	0.01 \pm 0.02	–	SB1	33 \pm 5	3.6 \pm 0.2	–
4775369116159613952	TIC 393490334	J04291760-5711160	3.77	171.0 \pm 0.1	0.195 \pm 0.004	44 \pm 3	ASB1	25 \pm 2	3.0 \pm 0.3	–
4633328088050950400	TIC 394276655	J02045722-7805402	3.32	817 \pm 19	0.33 \pm 0.10	–	SB1	47 \pm 4	5 \pm 3	–
4618730593723703936	TIC 394343422	J02392418-8310209	1.85	510 \pm 5	0.10 \pm 0.04	61 \pm 3	ASB1	80 \pm 4	7.9 \pm 0.2	–
4618845870645280384	TIC 394345080	J02464355-8210289	1.74	54.70 \pm 0.02	0.49 \pm 0.01	–	SB1	11.4 \pm 0.5	1.5 \pm 0.2	–
4625279766014849664	TIC 394699401	J03523455-8028015	1.56	1120 \pm 172	0.41 \pm 0.20	–	SB1	120 \pm 3	9.93 \pm 0.03	–
4615270190112641536	TIC 394720967	J04181954-8355122	1.74	331.3 \pm 2.7	0.52 \pm 0.10	79 \pm 3	ASB1	11 \pm 1	1.6 \pm 0.1	–
5194131966573758464	TIC 404707913	J06090890-8419065	2.65	764.9 \pm 9.5	0.29 \pm 0.04	–	SB1	56 \pm 9	5.8 \pm 0.1	–
5192829835569265152	TIC 405253727	J07450313-8547149	2.19	727 \pm 12	0.09 \pm 0.04	–	SB1	148 \pm 3	12.1 \pm 0.2	–
4652277311965454080	TIC 407622315	J04433582-7435050	0.98	20.47 \pm 0.02	0.04 \pm 0.09	–	SB1	4.0 \pm 0.3	0.6 \pm 0.2	–
4615180854792857216	TIC 410637115	J03592177-8432247	1.13	88.6 \pm 0.2	0.31 \pm 0.04	–	SB1	54 \pm 4	5.8 \pm 0.5	–
5290693654708705920	TIC 410449401	J07514168-6113232	1.08	51.51 \pm 0.04	0.02 \pm 0.03	–	SB1	57 \pm 2	6.25 \pm 0.01	–
5492232418092243072	TIC 445260011	J07282697-5337155	1.36	1123.6 \pm 52.3	0.14 \pm 0.04	–	SB1	174 \pm 3	11.8 \pm 0.1	–
5493502354021796096	TIC 445457466	J07305024-5109321	1.5	85.40 \pm 0.05	0.11 \pm 0.01	–	SB1	51 \pm 4	5.2 \pm 0.2	–
5488510704373214208	TIC 452667876	J07484505-5435024	2.8	757.1 \pm 9.3	0.32 \pm 0.03	–	SB1	88 \pm 3	7.4 \pm 0.1	–
5218604346628091520	TIC 452444834	J09161439-7309286	1.89	720.3 \pm 4.9	0.08 \pm 0.03	–	SB1	14.7 \pm 0.2	1.7 \pm 0.6	–
5216272694785111936	TIC 452469303	J09175579-7416057	4.49	1678 \pm 289	0.40 \pm 0.07	79 \pm 2	ASB1	21.5 \pm 0.3	2.28 \pm 0.01	–
5203697717736566144	TIC 452601856	J09341108-7631390	1.46	1109 \pm 45	0.36 \pm 0.02	–	SB1	2.6 \pm 0.2	0.52 \pm 0.02	–
5205405431093479808	TIC 452667876	J09392567-7525398	1.22	1390 \pm 385	0.36 \pm 0.10	–	SB1	12 \pm 1	1.6 \pm 0.1	–
5217681748996987520	TIC 452674990	J09405785-7325390	1.67	137.4 \pm 0.1	0.06 \pm 0.02	–	SB1	4.0 \pm 0.2	0.76 \pm 0.02	–
5203886073523999872	TIC 452677845	J09402958-7542202	2.17	452 \pm 2	0.23 \pm 0.02	105 \pm 3	ASB1	12 \pm 2	2 \pm 1	–
5203838760164269056	TIC 452677909	J09413117-7545490	2.41	949.8 \pm 27.9	0.35 \pm 0.05	–	SB1	114 \pm 3	10.5 \pm 0.1	–
5203810074078863360	TIC 452681557	–	–	61.35 \pm 0.03	0.22 \pm 0.01	–	SB1	48 \pm 5	5.2 \pm 8.4	–
5268004545071607680	TIC 453080867	J07350343-6837377	1.86	1186 \pm 189	0.28 \pm 0.07	–	SB1	18 \pm 2	2.4 \pm 0.4	–
5273748496894554752	TIC 453100125	J07444734-6848538	1.09	234 \pm 1	0.05 \pm 0.03	–	SB1	3.5 \pm 0.3	1 \pm 1	–
5274112778840834176	TIC 453101053	J07444525-6737409	6.28	729.8 \pm 1.3	0.40 \pm 0.02	38 \pm 2	ASB1	12 \pm 1	1.7 \pm 0.3	–
5218417601454570624	TIC 453240628	J09464754-7201019	2.72	927 \pm 42	0.34 \pm 0.04	–	SB1	13.6 \pm 0.4	1.75 \pm 0.01	–
5315718814234654592	TIC 457256644	J08174071-5716045	0.82	107.0 \pm 0.2	0.03 \pm 0.03	–	SB1	49 \pm 3	4.4 \pm 0.1	–
4661290313716760960	TIC 31181262	J05070045-6828344	3.06	693 \pm 8	0.32 \pm 0.02	123 \pm 2	ASB1	–	–	–
4659657607668823424	TIC 31308642	J05514623-6645171	1.24	124.9 \pm 0.1	0.010 \pm 0.005	–	SB1	–	–	–
4667738713190929408	TIC 32034170	J03461278-6804497	3.13	162.6 \pm 0.4	0.24 \pm 0.04	138 \pm 4	ASB1	–	–	–
4669439176643330688	TIC 32091578	J03545170-6623453	1.89	425 \pm 3	0.71 \pm 0.03	72 \pm 4	ASB1	–	–	–
4627969652492312320	TIC 33767523	J04101462-7555035	1.21	49.63 \pm 0.02	0.33 \pm 0.01	–	SB1	–	–	–
4627768132626702976	TIC 33837484	J04175279-7700274	1.66	812.7 \pm 30.4	0.11 \pm 0.05	–	SB1	–	–	–
4675571148695147392	TIC 38815315	J04315835-6258499	1.83	594.2 \pm 7.1	0.09 \pm 0.04	–	SB1	–	–	–
4677073601271449856	TIC 38845940	J04353558-6238537	0.97	659.6 \pm 12.3	0.42 \pm 0.08	–	SB1	–	–	–
4677103940918750208	TIC 38877648	J04370466-6225477	3.83	866 \pm 35	0.28 \pm 0.06	–	SB1	–	–	–
4658769687633857664	TIC 40970982	J05153759-6804070	0.87	29.65 \pm 0.05	0.23 \pm 0.13	–	SB1	–	–	–
5278385481032848768	TIC 41597225	J06170980-7108506	3.04	435 \pm 2	0.12 \pm 0.02	50 \pm 2	ASB1	–	–	–
5302872463981334400	TIC 45461862	J08420702-5827359	1.61	1254 \pm 131	0.44 \pm 0.12	–	SB1	–	–	–
4640146984288119808	TIC 50493505	J02305636-7532240	1.72	124.7 \pm 0.1	0.23 \pm 0.02	–	SB1	–	–	–
4665579749095086848	TIC 55501289	J04471941-6132211	1.97	220.7 \pm 0.7	0.21 \pm 0.03	110 \pm 3	ASB1	–	–	–
5314382529650775552	TIC 89399162	J08260832-5907010	1.65	683.5 \pm 3.2	0.18 \pm 0.02	–	SB1	–	–	–
5314513990012144768	TIC 89623068	J08293574-5835272	1.65	1237.3 \pm 98.3	0.16 \pm 0.10	–	SB1	–	–	–
5314889232716144512	TIC 118084798	–	–	79.5 \pm 0.2	0.05 \pm 0.04	–	SB1	–	–	–
5302779658324821888										

Table B.1. Orbital and seismic parameters of *Gaia* DR3 binary systems. (cont.)

Gaia DR3	KIC/TIC	2MASS	ruwe	P_{orb} [d]	e	i [deg]	Type	ν_{max} [μHz]	$\Delta\nu$ [μHz]	$\Delta\Pi_1$ [s]
4650023381850107392	TIC 141608755	J05542707-7434119	1.22	9.593	0.007 ± 0.004	–	SB1	–	–	–
5261433073310086144	TIC 141755674	J06055189-7553024	1.42	795.7 ± 5.4	0.33 ± 0.02	–	SB1	–	–	–
5265001366505117056	TIC 141768810	J06074155-7413362	0.99	51.92 ± 0.03	0.30 ± 0.03	–	SB1	–	–	–
5265156363282336128	TIC 141912821	J06185139-7321390	0.91	0.509	0.05 ± 0.20	–	SB1	–	–	–
5260690284486101760	TIC 142086656	J06343570-7554514	1.92	1062.5 ± 92.1	0.14 ± 0.06	–	SB1	–	–	–
4757482673322147584	TIC 149120568	J05231213-6213518	1.96	220.8 ± 0.2	0.16 ± 0.01	89 ± 2	ASB1	–	–	–
4758028477761000320	TIC 149176463	J05271679-6051215	1.43	611.5 ± 6.2	0.26 ± 0.02	43 ± 7	ASB1	–	–	–
4756597875699224576	TIC 149664368	J05510328-6328498	2.57	531 ± 1	0.41 ± 0.01	95 ± 2	ASB1	–	–	–
5482420204524665472	TIC 150099766	J06065705-6001460	1.93	934 ± 156	0.14 ± 0.09	–	SB1	–	–	–
54767923938377691392	TIC 150109061	J06093961-6425356	1.22	115.05 ± 0.05	0.00 ± 0.01	–	SB1	–	–	–
5284359436942989440	TIC 150151147	J06121684-6545409	2.12	130.1 ± 0.2	0.20 ± 0.02	55 ± 3	ASB1	–	–	–
5284507561772919168	TIC 150356481	J06240603-6534167	2.22	1021.4 ± 29.7	0.28 ± 0.03	114 ± 3	ASB1	–	–	–
5284740898751090432	TIC 150513313	J06311260-6453569	1.39	1172.6 ± 39.3	0.15 ± 0.02	–	SB1	–	–	–
5280142981644419968	TIC 167367512	J06373653-6754454	2.59	1131.3 ± 129.6	0.23 ± 0.10	–	SB1	–	–	–
5286144528424970496	TIC 167653886	J06492950-6419140	0.95	1101.1 ± 246.7	0.16 ± 0.17	–	SB1	–	–	–
5280110339893207424	TIC 176982676	J06452343-6752224	1.02	8.714 ± 0.002	0.02 ± 0.03	–	SB1	–	–	–
4658337098561947392	TIC 179213914	J05180327-6827567	1.28	336.3 ± 2.1	0.13 ± 0.03	–	SB1	–	–	–
5548507209905622784	TIC 219154947	J06005281-5347027	1.0	1118.4 ± 141.7	0.30 ± 0.14	–	SB1	–	–	–
5553357426277546368	TIC 219173590	J06051602-4907277	1.01	7.649 ± 0.001	0.05 ± 0.02	–	SB2	–	–	–
4796751765461633280	TIC 219425685	J05210061-4910237	1.58	580.9 ± 3.4	0.02 ± 0.02	78 ± 3	ASB1	–	–	–
4776834765159984768	TIC 220455606	J04573740-5410267	2.8	109.22 ± 0.03	0.008 ± 0.004	–	SB1	–	–	–
4639135261791598592	TIC 229809418	J02591815-7636352	1.04	21.704 ± 0.004	0.03 ± 0.02	–	SB1	–	–	–
4793558818054720128	TIC 231821462	J05450381-5042284	1.7	707 ± 6	0.04 ± 0.02	–	SB1	–	–	–
4693789094294131328	TIC 234331327	J02234497-6849369	3.52	974.4 ± 45.4	0.10 ± 0.10	–	SB1	–	–	–
4693786349811314688	TIC 234334233	J02262337-6838073	3.08	834 ± 23	0.07 ± 0.04	–	SB1	–	–	–
4796497022361626752	TIC 235047039	J05303031-5005594	2.7	578 ± 4	0.49 ± 0.02	–	SB1	–	–	–
4670220860690980096	TIC 237940170	J03584576-6350058	1.72	1390 ± 97	0.35 ± 0.10	–	SB1	–	–	–
5508204508111336064	TIC 238040306	J06550797-5005566	1.79	717.5 ± 4.2	0.19 ± 0.02	–	SB1	–	–	–
5509082777383488128	TIC 238062832	J06561548-4859122	1.9	565 ± 13	0.44 ± 0.10	–	ORB	–	–	–
4641689667821250944	TIC 238226341	J03534711-7242247	4.42	575.9 ± 1.7	0.63 ± 0.03	92 ± 2	ASB1	–	–	–
5549224087191024512	TIC 255554828	J06231618-5110437	5.43	541.4 ± 1.8	0.24 ± 0.02	108 ± 1	ASB1	–	–	–
5500010947461073024	TIC 255586681	J06264671-5305214	1.79	960 ± 216	0.32 ± 0.11	–	SB1	–	–	–
4778049828588148096	TIC 259444251	J04392680-5313553	1.81	895 ± 28	0.23 ± 0.04	–	SB1	–	–	–
4784031893397776128	TIC 259516310	J04452838-5158466	3.27	1212.5 ± 71.8	0.44 ± 0.02	–	SB1	–	–	–
4783787011542598272	TIC 259646046	J04533909-5050313	3.71	1038.0 ± 231.5	0.22 ± 0.12	–	SB1	–	–	–
4782957498738446464	TIC 259700972	J04563253-5301387	4.63	897.1 ± 16.2	0.02 ± 0.02	–	SB1	–	–	–
5495300811445430400	TIC 260471970	J06241556-5710432	1.3	648 ± 8	0.08 ± 0.04	–	SB1	–	–	–
5496939942764415104	TIC 260709734	J06341009-5613124	1.26	804 ± 34	0.49 ± 0.08	–	SB1	–	–	–
4624242308074644480	TIC 260984889	J05062625-7824309	0.99	320 ± 7	0.21 ± 0.10	–	SB1	–	–	–
5487656108960965760	TIC 262574106	J07384173-5704137	2.39	1129 ± 184	0.21 ± 0.08	–	SB1	–	–	–
5288191131882431232	TIC 262615103	J07463398-6301336	1.14	101.01 ± 0.02	0.006 ± 0.004	–	SB1	–	–	–
5488550286790245888	TIC 264925677	J07510253-5401474	1.03	394.4 ± 1.7	0.02 ± 0.03	–	SB1	–	–	–
5492708334828932352	TIC 267891517	J07403866-5237241	1.82	967.6 ± 40.4	0.12 ± 0.10	–	SB1	–	–	–
5492838180279235328	TIC 268118960	J07434668-5126155	2.15	245.9 ± 0.6	0.12 ± 0.02	94 ± 3	ASB1	–	–	–
5492745649504319744	TIC 268119965	J07433749-5208372	1.07	1155 ± 165	0.48 ± 0.07	–	SB1	–	–	–
5492744481273525504	TIC 268120053	J07434841-5212212	1.05	39.164 ± 0.003	0.060 ± 0.003	–	SB2	–	–	–
5492764409921474944	TIC 268125089	J07441728-5159231	1.29	297 ± 2	0.42 ± 0.03	–	SB1	–	–	–
5489767862779236736	TIC 268590132	J07482524-5225240	4.75	886 ± 53	0.38 ± 0.04	–	SB1	–	–	–
5512764148474450176	TIC 269407166	–	–	490.4 ± 9.4	0.12 ± 0.10	–	SB1	–	–	–
4622472059993948672	TIC 269854281	J04402336-8031199	3.34	290 ± 1	0.15 ± 0.04	146 ± 3	ASB1	–	–	–
5207632629333597824	TIC 270473069	J06263923-8104553	1.77	1013 ± 28	0.19 ± 0.03	–	SB1	–	–	–
5214110024129335424	TIC 271887188	J07293210-7552090	1.33	1104 ± 137	0.35 ± 0.12	–	SB1	–	–	–
5211521052204564480	TIC 278020457	J06570489-7839316	1.13	354.8 ± 1.3	0.12 ± 0.02	–	SB1	–	–	–
5207855039919798784	TIC 278050666	J07010004-8103496	3.03	797.9 ± 12.9	0.05 ± 0.03	–	SB1	–	–	–
5208031545895458432	TIC 278294347	J07323014-7956488	1.19	998 ± 108	0.42 ± 0.17	–	SB1	–	–	–
5194667600535358208	TIC 278413777	J07472967-8241176	2.17	799 ± 46	0.15 ± 0.10	–	SB1	–	–	–
5208737432360611712	TIC 278479052	J08004280-7951386	2.95	384 ± 1	0.618 ± 0.005	80 ± 2	ASB1	–	–	–
5491318930086438656	TIC 279479357	J07010117-5441073	1.13	109.877 ± 0.339	0.40 ± 0.03	–	SB1	–	–	–
5480853572252196992	TIC 279569875	J07032748-5753016	1.16	22.225 ± 0.005	0.04 ± 0.02	–	SB1	–	–	–
4640465499062979584	TIC 280054211	J03043680-7419174	1.28	224 ± 1	0.28 ± 0.04	–	SB1	–	–	–
5216787163146854016	TIC 281924214	J08380237-7455478	1.91	793 ± 9	0.03 ± 0.05	–	SB1	–	–	–
5216541147420180608	TIC 282055012	J08513978-7516291	1.32	1252.8 ± 490.5	0.20 ± 0.30	–	SB1	–	–	–
5486679884370416384	TIC 282724322	J07172986-5738148	1.89	1193.6 ± 68.1	0.12 ± 0.05	–	SB1	–	–	–
5220869478022138368	TIC 287350119	J08075861-7325040	1.67	630.9 ± 11.8	0.36 ± 0.10	147 ± 9	ASB1	–	–	–
5220053880912293376	TIC 287496627	J08155172-7339511	1.57	761.6 ± 20.2	0.01 ± 0.05	–	SB1	–	–	–
5216611378725475584	TIC 287956802	J08371093-7538065	1.32	65.93 ± 0.02	0.004 ± 0.005	–	SB1	–	–	–
5294640867091428864	TIC 290157464	J07581926-5801363	3.39	202.2 ± 0.4	0.13 ± 0.04	120 ± 2	ASB1	–	–	–
5318986940749479040	TIC 290292058	J08140315-5548357	3.21	1124 ± 239	0.16 ± 0.20	–	SB1	–	–	–
5297212727873784832	TIC 290301888	J09055533-6251429	2.69	1246 ± 126	0.08 ± 0.11	–	SB1	–	–	–
4768982568510506112	TIC 290754762	J05385690-5250089	3.89	647 ± 8	0.55 ± 0.04	55 ± 2	ASB1	–	–	–
4679140958008380416	TIC 293164704	J04254238-5816487	2.83	994 ± 93	0.45 ± 0.09	–	SB1	–	–	–
5555242027863701632	TIC 293650052	J06305702-4715273	4.13	972 ± 7	0.23 ± 0.01	–	SB1	–	–	–
5491226360654244864	TIC 294049251	J07081258-5437459	1.34	5.538	0.44 ± 0.01	–	SB2	–	–	–
5486610988797752704	TIC 294099212	J07102821-5755490	1.31	120.8 ± 0.2	0.13 ± 0.02	–	SB1	–	–	–

Table B.1. Orbital and seismic parameters of *Gaia* DR3 binary systems. (cont.)

Gaia DR3	KIC/TIC	2MASS	ruwe	P_{orb} [d]	e	i [deg]	Type	v_{max} [μHz]	Δv [μHz]	$\Delta\Pi_1$ [s]
5485762960391754112	TIC 294099926	J07105025-5851228	1.72	368 \pm 1	0.02 \pm 0.02	–	SB1	–	–	–
5487037805467014272	TIC 294276343	J07145292-5618034	1.96	536 \pm 2	0.61 \pm 0.03	73 \pm 3	ASB1	–	–	–
5268512691242626432	TIC 299899690	J07041732-6916062	1.77	315.7 \pm 0.6	0.38 \pm 0.05	114 \pm 3	ASB1	–	–	–
5264003181740256384	TIC 300085625	J07104434-7146550	1.2	23.323 \pm 0.005	0.10 \pm 0.01	–	SB1	–	–	–
5281051831085011968	TIC 300088409	J07122897-6739418	1.04	363 \pm 2	0.06 \pm 0.02	–	SB1	–	–	–
5264555961210572928	TIC 300510171	J07290078-7030027	3.01	328.7 \pm 0.7	0.02 \pm 0.01	–	SB1	–	–	–
5267670018659029504	TIC 300603298	J07334270-6953282	1.1	161.0 \pm 0.1	0.01 \pm 0.01	–	SB1	–	–	–
5264644884214094848	TIC 300654549	J07365406-7016261	6.25	809 \pm 19	0.04 \pm 0.04	–	SB1	–	–	–
5264692781689478528	TIC 300739338	J07403033-6950465	3.19	417 \pm 2	0.00 \pm –	–	ORB	–	–	–
5220689364275188224	TIC 3011863175	J08434620-7149334	2.75	599.984 \pm 5.873	0.23 \pm 0.03	–	SB1	–	–	–
5223269845046430976	TIC 302211802	J08514210-6934176	1.55	215 \pm 1	0.53 \pm 0.03	–	SB1	–	–	–
5224119977993425408	TIC 302525310	J08572274-6710307	1.38	894.8 \pm 37.6	0.22 \pm 0.10	–	SB1	–	–	–
5222859353553282432	TIC 302851752	J09025489-6923587	8.92	339.9 \pm 0.3	0.35 \pm 0.02	141 \pm 2	ASB1	–	–	–
4798649724393537792	TIC 302964395	J05331468-4711599	1.01	509.4 \pm 12.1	0.24 \pm 0.10	–	SB1	–	–	–
5223039707819145984	TIC 303304284	J09105017-6811363	2.47	843 \pm 11	0.03 \pm 0.04	–	SB1	–	–	–
5248245977526953216	TIC 303309502	J09115479-6611054	0.95	1027.0 \pm 54.5	0.61 \pm 0.10	–	SB1	–	–	–
5247608363864664960	TIC 304090728	J09253962-6648325	1.1	161.5 \pm 0.1	0.20 \pm 0.01	–	SB1	–	–	–
5269495242321492608	TIC 306573785	J07562608-7132209	1.34	353.8 \pm 0.8	0.03 \pm 0.02	–	SB1	–	–	–
5269290801875435648	TIC 306633505	J07595156-7148322	4.4	410 \pm 1	0.22 \pm 0.02	50 \pm 2	ASB1	–	–	–
5274718128713414144	TIC 306736221	J08025672-6612427	1.06	622.0 \pm 18.3	0.22 \pm 0.10	–	SB1	–	–	–
5270015620559332224	TIC 307489446	J08251466-6913556	4.01	1015.6 \pm 9.7	0.21 \pm 0.02	–	SB1	–	–	–
5221468879359841024	TIC 307780517	J08321461-7130517	1.19	406 \pm 14	0.15 \pm 0.11	–	SB1	–	–	–
5272746154608855680	TIC 307847839	J08332906-6643202	3.44	626 \pm 4	0.01 \pm 0.03	63 \pm 2	ASB1	–	–	–
5221575364487577600	TIC 307920241	J08361324-7105544	7.31	1053.3 \pm 36.4	0.55 \pm 0.03	41 \pm 2	ASB1	–	–	–
5272782438492514304	TIC 307926974	J08361843-6618327	0.99	51.52 \pm 0.02	0.01 \pm 0.02	–	SB1	–	–	–
5289828510855092480	TIC 308309337	J08010202-6141269	2.74	585 \pm 5	0.06 \pm 0.02	–	SB1	–	–	–
5289533223264812288	TIC 308456170	J08031933-6243243	2.2	567 \pm 6	0.13 \pm 0.04	–	SB1	–	–	–
5289960967647374080	TIC 308605789	J08054137-6103325	1.03	3.748 \pm 0.001	0.38 \pm 0.12	–	SB1	–	–	–
5277605033927032192	TIC 308666504	–	1.64	155.77 \pm 0.05	0.41 \pm 0.01	–	SB1	–	–	–
5277945916896945664	TIC 309250444	J08163448-6221090	1.43	1306.3 \pm 247.3	0.37 \pm 0.20	–	SB1	–	–	–
5290204062797415552	TIC 309291740	J08172863-6050173	3.11	1290.4 \pm 239.1	0.48 \pm 0.10	–	SB1	–	–	–
5195155401443650304	TIC 309438240	J09163816-8227095	0.98	1091 \pm 183	0.36 \pm 0.20	–	SB1	–	–	–
5195559098307711872	TIC 309487217	J09171034-8155196	3.33	976 \pm 45	0.36 \pm 0.10	26 \pm 7	ASB1	–	–	–
4761098554743625856	TIC 309658666	J05161475-6027109	1.25	581 \pm 7	0.05 \pm 0.03	–	SB1	–	–	–
5277704264855778560	TIC 309713854	J08235836-6245513	2.56	395 \pm 1	0.08 \pm 0.02	137 \pm 8	ASB1	–	–	–
5277909976609615232	TIC 309861809	J08270468-6139290	1.3	38.39 \pm 0.01	0.43 \pm 0.02	–	SB1	–	–	–
5302274089131700992	TIC 309928867	J08275157-6000407	1.84	592.7 \pm 1.1	0.60 \pm 0.01	82 \pm 3	ASB1	–	–	–
5277831876925129850	TIC 310023469	J08285993-6216375	2.08	312.5 \pm 0.9	0.38 \pm 0.04	–	SB1	–	–	–
4781431376599775616	TIC 311886371	J04282097-5135263	1.24	672.1 \pm 16.2	0.05 \pm 0.10	–	SB1	–	–	–
4615645364095865216	TIC 317351868	J04195400-8354408	1.81	390 \pm 2	0.11 \pm 0.04	–	SB1	–	–	–
5201997735321107968	TIC 323972404	J09392426-7944521	1.51	435.7 \pm 0.5	0.44 \pm 0.01	83 \pm 3	ASB1	–	–	–
5487339522627751808	TIC 340000762	J07303330-5531353	1.67	764 \pm 15	0.48 \pm 0.10	–	ORB	–	–	–
5293848428444555008	TIC 340174734	J07344299-5839255	11.82	2068.5 \pm 143.2	0.87 \pm 0.02	31 \pm 4	ASB1	–	–	–
5486130502216983808	TIC 340217123	J07361337-5730254	1.89	670.2 \pm 5.6	0.22 \pm 0.03	–	SB1	–	–	–
5512414057100302464	TIC 341418749	J08001789-5402304	1.41	1173.1 \pm 117.8	0.08 \pm 0.10	–	SB1	–	–	–
5291344252055379840	TIC 342312217	J08143277-5910504	2.48	964 \pm 65	0.49 \pm 0.10	–	SB1	–	–	–
5291442147248954240	TIC 342313284	J08142930-5821467	0.94	331.2 \pm 8.3	0.26 \pm 0.10	–	SB1	–	–	–
5314648439667464704	TIC 342883080	J08223681-5833044	1.07	103.6 \pm 0.1	0.04 \pm 0.02	–	SB1	–	–	–
5314674931018636416	TIC 343170476	J08254220-5843353	1.42	1159.8 \pm 78.8	0.51 \pm 0.10	–	SB1	–	–	–
4620345398347163904	TIC 348771456	J03084852-7953305	1.28	131.6 \pm 0.1	0.07 \pm 0.01	–	SB1	–	–	–
5293290563731367680	TIC 349484626	J07241488-5959248	2.24	947 \pm 81	0.13 \pm 0.08	–	SB1	–	–	–
5292690058583817472	TIC 349906032	J07362420-6007236	7.16	830 \pm 17	0.32 \pm 0.03	33 \pm 3	ASB1	–	–	–
5491970699963730688	TIC 349920934	J07160657-5234032	3.32	717 \pm 20	0.02 \pm 0.10	–	SB1	–	–	–
5273607896848635136	TIC 355003870	J08391971-6418540	4.47	1088 \pm 11	0.13 \pm 0.01	–	SB1	–	–	–
5273643218659444992	TIC 355240223	J08422386-6356210	4.48	606 \pm 3	0.46 \pm 0.02	138 \pm 2	ASB1	–	–	–
5300788442763212544	TIC 355374979	J08435431-6238311	1.93	1056.1 \pm 99.2	0.53 \pm 0.12	–	SB1	–	–	–
5297723828980335488	TIC 355376298	J08441438-6325181	1.93	175.2 \pm 0.7	0.66 \pm 0.10	–	ORB	–	–	–
5273353875302344704	TIC 355381344	J08451490-6450084	1.91	1124 \pm 33	0.60 \pm 0.02	–	SB1	–	–	–
5297491076111767296	TIC 355845851	J08494789-6348333	2.02	852.8 \pm 5.9	0.30 \pm 0.02	–	SB1	–	–	–
5297478259929413760	TIC 355859169	–	1.32	912.7 \pm 12.4	0.15 \pm 0.03	–	SB1	–	–	–
5298295592984840320	TIC 355940193	J08510571-6159390	1.3	465 \pm 5	0.27 \pm 0.05	–	SB1	–	–	–
5301357371314849792	TIC 355941844	J08511566-6112398	1.12	35.0 \pm 0.2	0.22 \pm 0.20	–	SB1	–	–	–
5297093426557255808	TIC 357190479	J09062167-6345016	2.09	180.5 \pm 0.5	0.12 \pm 0.02	–	SB1	–	–	–
5297124423344636800	TIC 357487409	J09094146-6327262	1.52	768.1 \pm 14.4	0.42 \pm 0.06	114 \pm 5	ASB1	–	–	–
5296815598014572544	TIC 357489617	J09091912-6436466	1.45	964 \pm 19	0.43 \pm 0.02	–	SB1	–	–	–
5248351908601242112	TIC 357534594	J09095866-6534252	3.62	1194 \pm 31	0.39 \pm 0.02	100 \pm 2	ASB1	–	–	–
4683227254317123200	TIC 358287572	J04073661-5640267	1.92	11.577 \pm 0.004	0.10 \pm 0.05	–	SB1	–	–	–
4615909109447769472	TIC 358500537	J04002240-8318321	1.38	340 \pm 1	0.23 \pm 0.02	–	SB1	–	–	–
5248466287868269696	TIC 359062562	J09193960-6544269	2.78	946.1 \pm 72.3	0.19 \pm 0.06	–	SB1	–	–	–
5491796874047394816	TIC 363965918	J07214229-5256359	1.22	114.6 \pm 0.1	0.01 \pm 0.01	–	SB1	–	–	–
5288129249991030144	TIC 364393973	J07454987-6325333	8.87	663.2 \pm 2.2	0.32 \pm 0.02	–	ORB	–	–	–
5218541979406720384	TIC 370885869	J09410743-7108372	1.51	398.0 \pm 8.8	0.09 \pm 0.08	–	SB1	–	–	–
5477371453288971776	TIC 372851332	J06321900-6312277	1.71	910.7 \pm 23.2	0.27 \pm 0.05	–	SB1	–	–	–
5284894349344403072	TIC 374996137	J06373668-6404551	1.22	16.054 \pm 0.002	0.01 \pm 0.01	–	SB1	–	–	–

Table B.1. Orbital and seismic parameters of *Gaia* DR3 binary systems. (cont.)

Gaia DR3	KIC/TIC	2MASS	ruwe	P_{orb} [d]	e	i [deg]	Type	ν_{max} [μHz]	$\Delta\nu$ [μHz]	$\Delta\Pi_1$ [s]
4769411618563540608	TIC 382147324	J05215739-5627057	2.16	884 \pm 31	0.09 \pm 0.07	–	SB1	–	–	–
5275118007347610752	TIC 382435583	J07492309-6549273	3.25	985 \pm 5	0.41 \pm 0.04	–	SB1	–	–	–
5275486240664958592	TIC 382626856	J07540870-6541299	1.2	15.243 \pm 0.002	0.03 \pm 0.02	–	SB1	–	–	–
4659661391549688704	TIC 389865242	J05500687-6654259	1.47	1222 \pm 98	0.16 \pm 0.10	–	SB1	–	–	–
4778952935654560000	TIC 396721315	J04230275-5525543	1.78	800.9 \pm 65.6	0.29 \pm 0.09	–	SB1	–	–	–
4615407349891806336	TIC 435869116	J03351122-8404431	1.42	658 \pm 2	0.40 \pm 0.01	–	SB1	–	–	–
5492258772011520000	TIC 445521588	J07325545-5315082	1.51	27.644 \pm 0.004	0.06 \pm 0.01	–	SB1	–	–	–
5218864278052473344	TIC 452413300	J09110138-7238580	1.72	266 \pm 1	0.05 \pm 0.03	54 \pm 4	ASB1	–	–	–
5218567512993484416	TIC 452440888	J09150316-7328493	1.36	590 \pm 8	0.04 \pm 0.04	–	SB1	–	–	–
5215889476325815552	TIC 452573117	J09292010-7533328	3.26	756 \pm 10	0.37 \pm 0.05	–	SB1	–	–	–
5205159346646988928	TIC 45320236	J09534267-7547471	0.95	79.2 \pm 0.1	0.21 \pm 0.04	–	SB1	–	–	–
5315887245673421056	TIC 457257592	J08171101-5637443	1.28	454 \pm 2	0.17 \pm 0.03	–	SB1	–	–	–
2052131736205469184	KIC 3458643	J19401962+3831015	1.27	399.5 \pm 1.7	0.31 \pm 0.03	–	SB1	68 \pm 4	5.8 \pm 0.1	–
2100306150972929664	KIC 4242873	J19005046+3921272	1.07	56.71 \pm 0.05	0.49 \pm 0.02	–	SB1	118 \pm 2	10.41 \pm 0.04	–
2100979292611673216	KIC 4360072	J19203389+3928547	1.61	845.3 \pm 71.8	0.21 \pm 0.12	–	ORB	31 \pm 1	3.9 \pm 0.1	324
2076487224429134592	KIC 5023931	J19405704+4010068	1.11	209.4 \pm 2.7	0.41 \pm 0.12	–	SB1	50 \pm 2	4.91 \pm 0.02	–
2073575786370595456	KIC 5039392	J19533622+4010197	1.23	236.0 \pm 0.7	0.41 \pm 0.02	–	SB1	6.4 \pm 0.2	1.13 \pm 0.03	–
2076733377594699264	KIC 5382824	J19475490+4032009	2.83	653 \pm 4	0.11 \pm 0.03	–	SB1	103 \pm 2	7.90 \pm 0.04	–
2101343024800284288	KIC 5439039	J19155185+4040542	1.0	98.0 \pm 0.1	0.03 \pm 0.02	–	SB1	100 \pm 2	7.9 \pm 0.1	–
2102124743207232128	KIC 6032639	J19141495+4118432	1.22	980 \pm 45	0.29 \pm 0.07	–	SB1	46 \pm 2	4.6 \pm 0.1	–
2103953196683494144	KIC 6590195	J19053056+4203223	1.07	55.86 \pm 0.03	0.17 \pm 0.02	–	SB1	112 \pm 2	9.53 \pm 0.03	75
2105486701865509504	KIC 6933666	J19063556+4228102	0.88	48.3 \pm 0.2	0.18 \pm 0.08	–	SB1	33 \pm 2	3.85 \pm 0.03	–
2105480001719302400	KIC 7103951	J19082415+4238093	3.74	643 \pm 3	0.15 \pm 0.01	–	ASB1	55 \pm 2	5.0 \pm 0.1	–
2078778709739759488	KIC 7768447	J19464078+4328213	1.14	122.3 \pm 0.2	0.32 \pm 0.02	–	SB1	57 \pm 1	5.8 \pm 0.1	–
2080263733328413696	KIC 9540226	J19480815+4611544	1.06	175.5 \pm 0.3	0.40 \pm 0.02	–	SB1	27 \pm 2	3.19 \pm 0.03	–
2130638481326861824	KIC 10001167	J19074937+4656118	1.35	120.38 \pm 0.05	0.144 \pm 0.005	–	SB1	19.9 \pm 0.5	2.78 \pm 0.04	–
2133597988670827776	KIC 11753949	J19050982+4955232	7.32	677.2 \pm 2.7	0.02 \pm 0.05	–	ORB	11.1 \pm 0.2	1.70 \pm 0.05	–
2135591403254321536	KIC 12314910	J19414879+5102085	1.0	69.5 \pm 0.1	0.02 \pm 0.02	–	SB1	24.0 \pm 0.4	2.94 \pm 0.04	–
2099147746755032448	KIC 2697935	J19095228+3757599	3.55	21.51 \pm 0.01	0.43 \pm 0.02	–	SB1	–	–	–
2052444444184805376	KIC 4663623	J19364769+3945288	1.06	359 \pm 2	0.44 \pm 0.04	–	SB1	–	–	–
2101352886044180480	KIC 5179609	J19182673+4020090	1.01	43.92 \pm 0.04	0.10 \pm 0.05	–	SB1	–	–	–
2075037346557985152	KIC 5308778	J19581857+4027305	1.11	40.54 \pm 0.04	0.02 \pm 0.03	–	SB1	–	–	–
2076767561231738240	KIC 5640750	J19484843+4053327	2.0	1017 \pm 19	0.39 \pm 0.05	–	SB1	–	–	–
2077800002648034944	KIC 7037405	J19315429+4232516	1.18	207.3 \pm 0.4	0.26 \pm 0.03	–	SB1	–	–	–
2078985967681169792	KIC 8054233	J19565846+4348517	1.27	1003.4 \pm 73.6	0.35 \pm 0.11	–	SB1	–	–	–
2117287420868639744	KIC 8143170	J18442147+4403285	1.39	28.81 \pm 0.02	0.11 \pm 0.04	–	SB1	–	–	–
2079719960410280320	KIC 8702921	J19463960+4451110	0.88	19.39 \pm 0.01	0.05 \pm 0.04	–	SB1	–	–	–
2085168830800260992	KIC 8912308	J20001640+4506058	1.14	20.168 \pm 0.003	0.22 \pm 0.01	–	SB1	–	–	–
2085557916175822336	KIC 9970396	J19545035+4649589	1.41	235.2 \pm 0.7	0.21 \pm 0.03	–	SB1	–	–	–
2128408220770539904	KIC 10015516	J19335366+4658134	1.17	67.67 \pm 0.02	0.01 \pm 0.01	–	SB1	–	–	–
2926995477518201856	TIC 49253887	J06463327-2048425	1.69	1200 \pm 34	0.56 \pm 0.02	–	SB1	–	–	–
1469958436868294144	TIC 71595072	J13274461+3337354	1.42	471.6 \pm 1.2	0.60 \pm 0.02	–	ASB1	–	–	–
429037103683886976	TIC 83620534	J00135620+5959575	4.13	1010 \pm 4	0.05 \pm 0.01	–	ASB1	–	–	–
1064389863427560064	TIC 86279245	J09254419+6356274	2.23	184.5 \pm 0.5	0.41 \pm 0.07	–	ORB	–	–	–
2030314161368193920	TIC 87306827	J19552002+2959207	5.05	295.0 \pm 0.2	0.117 \pm 0.002	–	ASB1	–	–	–
1465913780265266048	TIC 139124331	J12561787+3231514	6.33	1346 \pm 76	0.21 \pm 0.02	–	ASB1	–	–	–
240650492225895040	TIC 192775243	J03135122+4351469	1.51	45.77 \pm 0.01	0.01 \pm 0.01	–	SB1	–	–	–
1629145730337692800	TIC 198213983	J16334202+6424112	4.44	1009 \pm 49	0.20 \pm 0.03	–	SB1	–	–	–
1433356519412765696	TIC 224598071	J16592151+5641187	7.59	1018.0 \pm 56.5	0.14 \pm 0.05	–	ORB	–	–	–
2258762750242910464	TIC 229751007	J18432472+6806445	2.39	432 \pm 3	0.04 \pm 0.03	–	SB1	–	–	–
2159401155750826624	TIC 233078994	J18062588+6257082	7.27	658.1 \pm 1.5	0.03 \pm 0.01	–	ASB1	–	–	–
2188045323443081472	TIC 233829187	J20140775+5806194	2.92	542 \pm 4	0.02 \pm 0.05	–	ORB	–	–	–
457872723834950656	TIC 245663551	J02404072+5718318	1.42	1054 \pm 295	0.41 \pm 0.13	–	SB1	–	–	–
3254233055882250496	TIC 250141410	J04145883-0059507	2.5	1144.3 \pm 60.1	0.37 \pm 0.02	–	SB1	–	–	–
1408413342222248192	TIC 274676814	J17044978+4848144	21.52	785 \pm 4	0.23 \pm 0.02	–	ORB	–	–	–
597447616074699136	TIC 283768251	J08574203+0923162	5.88	912 \pm 33	0.30 \pm 0.04	–	ORB	–	–	–
841422546129913344	TIC 284596799	J11301292+5421442	6.06	955 \pm 54	0.10 \pm 0.05	–	ORB	–	–	–
837425237247462656	TIC 318232318	J10523088+5233552	1.89	300 \pm 1	0.02 \pm 0.01	–	ASB1	–	–	–
260022272200061824	TIC 354428725	J04590372+5156321	2.46	998.3 \pm 8.6	0.11 \pm 0.01	–	SB1	–	–	–
1258076808118217216	TIC 357387775	J13572882+2459541	2.61	301.2 \pm 0.8	0.46 \pm 0.01	–	ASB1	–	–	–
2040514502502017536	TIC 358152485	J18513589+2847011	1.43	215.7 \pm 0.1	0.122 \pm 0.003	–	SB2	–	–	–
1444169597796090368	TIC 383477233	J13511631+2441441	6.64	700.0 \pm 1.5	0.368 \pm 0.004	–	ASB1	–	–	–
245966562230839552	TIC 391085379	J04012603+4727013	7.26	915.1 \pm 11.8	0.38 \pm 0.01	–	ASB1	–	–	–
227988413243127936	TIC 417891254	J04190089+4132281	3.34	487.7 \pm 2.2	0.47 \pm 0.02	–	ASB1	–	–	–

Table B.2. Seismic parameters for potential binary systems in *Gaia* DR3, with non-linear and acceleration solutions.

Gaia DR3	KIC/TIC	2MASS	ruwe	Type	ν_{\max} [μHz]	$\Delta\nu$ [μHz]	$\Delta\Pi_1$ [s]
2050253151867756160	KIC 1160867	J19233983+3650426	2.34	ACC7	4.7 \pm 0.1	0.89 \pm 0.02	–
2051742028048983296	KIC 1163359	J19255838+3650557	1.34	SSB1	21.4 \pm 0.5	2.64 \pm 0.02	–
2051760410508998912	KIC 1431599	J19250117+3705112	1.16	FSB1	2.30 \pm 0.05	0.5 \pm –	–
2051751030300733440	KIC 1433593	J19264298+3704199	0.88	FSB1	69 \pm 1	6.24 \pm 0.02	–
2051714265379610624	KIC 1435467	J19281984+3703353	5.73	FSB1	1369 \pm 57	70.8 \pm 1.5	–
2051816245082293632	KIC 1725815	J19293996+3716306	4.04	ACC9/SSB1	1040 \pm 29	56 \pm 2	–
2051819062581067776	KIC 2019396	J19300833+3726004	1.01	FSB1	37 \pm 1	4.2 \pm 0.1	–
2099171691193663872	KIC 2284679	J19060736+3740100	1.82	SSB1/ACC7	198 \pm 1	16.15 \pm 0.03	–
2051102077921899776	KIC 2439233	J19215339+3743039	1.13	SSB1	2.79 \pm 0.06	0.60 \pm 0.03	–
2052548382386512000	KIC 2441436	J19240130+3747567	1.0	SSB1	3.9 \pm 0.2	0.71 \pm 0.02	–
2051886094127597056	KIC 2447046	J19285988+3745187	3.58	ACC9	170 \pm 3	13.18 \pm 0.02	–
2051844037807834880	KIC 2447604	J19292597+3743597	0.94	FSB1	54 \pm 2	5.02 \pm 0.04	295
2051852494607152128	KIC 2449558	J19311366+3745510	1.79	ACC7	90 \pm 1	7.57 \pm 0.02	75
2051856927013539200	KIC 2453018	J19315457+3747319	1.88	ACC9	136 \pm 1	11.53 \pm 0.02	–
2099944201189350912	KIC 2693967	J19044478+3757204	1.25	SSB1	84 \pm 2	7.03 \pm 0.04	229
2099155134098571392	KIC 2696955	J19083373+3754367	1.76	SSB1/ACC7	107 \pm 2	8.65 \pm 0.02	–
2052622496343870464	KIC 2850480	J19240900+3801141	1.72	ACC7	56 \pm 1	5.62 \pm 0.02	–
2099209418183813248	KIC 2973238	J19074383+3810198	1.34	FSB1	55 \pm 1	5.06 \pm 0.02	–
2051880394715133952	KIC 2996112	J19312076+3810229	1.0	FSB1	31 \pm 1	3.9 \pm 0.1	324
2052667851198093824	KIC 3119555	J19282751+3817054	2.13	ACC7	84 \pm 1	7.65 \pm 0.02	70
2051935885690224256	KIC 3120486	J19291841+3812145	1.05	SSB1	136 \pm 2	10.62 \pm 0.02	–
2052812127737361024	KIC 3231503	J19215076+3820311	1.04	FSB1	43 \pm 1	4.34 \pm 0.02	225
2052255843577676288	KIC 3241581	J19322044+3820302	6.4	ACC9 FSB1	3018 \pm 34	126 \pm 5	–
2099375654899935872	KIC 3331352	J19132263+3828033	1.44	SSB1	38 \pm 3	4.5 \pm 0.2	–
2052839611230408576	KIC 3441184	J19230440+3834096	1.46	SSB1	43.8 \pm 0.4	4.95 \pm 0.02	–
2052732859824129024	KIC 3443483	J19253516+3832018	3.83	FSB1	132 \pm 2	10.66 \pm 0.02	72
2100036667546509824	KIC 3526964	J19021974+3838207	1.53	SSB1	30 \pm 1	3.65 \pm 0.02	–
2100001689331818368	KIC 3528656	J19050492+3839005	0.9	FSB1	21.0 \pm 0.4	2.68 \pm 0.02	–
2052691314601113728	KIC 3546046	J19271321+3838527	1.37	FSB1	180 \pm 1	14.02 \pm 0.03	82
2052138883031079168	KIC 3559502	J19402099+3836566	0.99	FSB1	75 \pm 1	7.04 \pm 0.02	66
2099584562109394560	KIC 3633847	J19113506+3844375	2.61	ACC9	1056 \pm 36	61.6 \pm 1.8	–
2099666991121299968	KIC 3634720	J19124737+3847265	1.28	FSB1	37 \pm 2	3.9 \pm 0.1	292
2073161648439344896	KIC 3663200	J19424202+3847430	1.89	ACC7	92 \pm 2	7.60 \pm 0.04	274
2052865247894089216	KIC 3744408	J19225461+3853584	1.24	SSB1	43 \pm 1	4.53 \pm 0.02	–
2052158365003178880	KIC 3761250	J19401070+3852227	2.16	ACC7	56 \pm 7	6.2 \pm 0.6	–
2100149642365263232	KIC 3832396	J19010019+3854285	1.29	FSB1	32 \pm 1	3.9 \pm 0.1	–
2052784227633493632	KIC 3954327	J19260622+3901447	1.23	FSB1	25.6 \pm 0.5	2.99 \pm 0.02	–
2052355967857779200	KIC 4064398	J19334007+3910213	0.95	SSB1	2.2 \pm 0.2	0.46 \pm 0.04	–
2073274898135148672	KIC 4077835	J19454030+3908054	0.82	SSB1	22.3 \pm 0.5	2.51 \pm 0.03	–
2076234405477197312	KIC 4171788	J19393367+3912426	3.2	SSB1	92.2 \pm 0.5	8.39 \pm 0.02	73
2076231622338420864	KIC 4172283	J19395925+3912392	1.04	SSB1	60 \pm 1	5.78 \pm 0.02	–
2099711521341329920	KIC 4355160	J19150365+3924469	2.45	ACC7	197 \pm 3	14.7 \pm 0.2	–
2052466674935854720	KIC 4372082	J19334998+3928559	1.18	SSB1	79 \pm 1	6.2 \pm 0.1	254
2099722756976231168	KIC 4454123	J19140725+3933363	0.9	FSB1	29 \pm 1	3.12 \pm 0.02	–
2101015954452624512	KIC 4457351	J19181290+3933557	1.66	ACC7	1084 \pm 24	60 \pm 2	–
2073626668826201600	KIC 4489185	J19494259+3931486	1.12	FSB1	94 \pm 1	8.59 \pm 0.03	74
2076223101122787328	KIC 4577484	J19424387+3937074	2.7	ACC9	832 \pm 16	47 \pm 2	–
2073632166384337536	KIC 4585508	J19490856+3940517	2.32	ACC7	34 \pm 1	3.85 \pm 0.03	319
2053147272629176064	KIC 4658599	J19313034+3943094	1.17	FSB1	8.9 \pm 0.2	1.59 \pm 0.03	–
2076453719376920960	KIC 4758222	J19393602+3953104	3.73	SSB1	25 \pm 1	3.0 \pm 0.1	–
2100719979661614720	KIC 4818312	J19032074+3958448	1.56	SSB1/ACC7	44.6 \pm 0.5	4.89 \pm 0.02	–
2073642719130987904	KIC 4859338	J19500857+3954488	3.53	ACC7	350 \pm 51	27 \pm 4	–
2073668042259111936	KIC 4948479	J19510579+4004300	1.52	ACC7	75 \pm 1	7.31 \pm 0.02	–
2103412477479445248	KIC 4991033	J18573038+4011144	1.02	FSB1	48.5 \pm 0.4	5.26 \pm 0.02	–
2103403367852149248	KIC 4991732	J18584812+4011357	1.85	SSB1/ACC7	105 \pm 1	8.55 \pm 0.02	89
2101158405628098944	KIC 5004660	J19192385+4006451	0.92	SSB1	2.76 \pm 0.04	0.58 \pm 0.06	–
2053273849603515648	KIC 5016549	J19333315+4010306	1.53	ACC7	99 \pm 1	8.69 \pm 0.02	–
2073520325442253184	KIC 5041311	J19551276+4009321	0.92	SSB1	3.30 \pm 0.06	0.59 \pm 0.03	–
2100706648083445504	KIC 5083205	J19050067+4015299	2.08	SSB1/ACC7	137 \pm 1	11.25 \pm 0.02	–
2073544553367404032	KIC 5129011	J19553674+4016323	1.19	SSB1	42 \pm 2	4.57 \pm 0.04	308
2100601541645216000	KIC 5172229	J19075054+4018279	1.29	FSB1	40.5 \pm 0.5	4.40 \pm 0.02	–
2073537986348455040	KIC 5219666	J19571782+4022206	1.53	SSB1	55 \pm 1	5.11 \pm 0.02	–
2100576351658133120	KIC 5262788	J19113030+4029318	0.94	FSB1	40 \pm 1	4.43 \pm 0.05	272
2077291929498868608	KIC 5282288	J19353565+4025596	1.05	SSB1	51 \pm 2	5.10 \pm 0.03	321
2073555720282766976	KIC 5393453	J19564015+4035334	1.63	FSB1	128 \pm 1	10.53 \pm 0.02	75
2103439140636760064	KIC 5429911	J19001259+4036420	2.7	ACC7	470 \pm 7	27.4 \pm 1.3	–
2100639058180647168	KIC 5435689	J19101856+4040047	1.13	FSB1	5.5 \pm 0.3	0.91 \pm 0.02	–
2101515957363522432	KIC 5445379	J19232394+4039477	1.25	SSB1	33.6 \pm 0.5	3.67 \pm 0.02	–
2076570168838678400	KIC 5457182	J19372122+4038120	10.53	SSB1	31.7 \pm 0.4	3.54 \pm 0.02	–
2100641742539258112	KIC 5521210	J19105440+4047539	1.73	ACC7	23.4 \pm 0.4	2.84 \pm 0.02	–
2101191670154074240	KIC 5529992	J19222893+4043132	1.7	ACC7	95 \pm 1	8.03 \pm 0.02	–
2076621502285818112	KIC 5547077	J19421132+4045130	0.9	FSB1	53 \pm 1	5.05 \pm 0.02	312

Table B.2. Seismic parameters for potential binary systems in *Gaia* DR3, with non-linear and acceleration solutions. (continued)

Gaia DR3	KIC/TIC	2MASS	ruwe	Type	ν_{\max} [μHz]	$\Delta\nu$ [μHz]	$\Delta\Pi_1$ [s]
2073620003043206272	KIC 5563078	J19554159+4047192	1.48	SSB1	36 ±2	4.1 ±0.2	–
2073620144794639744	KIC 5563343	J19555462+4047253	1.93	ACC7	75 ±2	6.59 ±0.05	291
2100642876410617856	KIC 5607242	J19103512+4050350	2.04	ACC7/ACC7	684 ±3	40.39 ±0.01	–
2101209605937442176	KIC 5615331	J19212398+4052278	2.28	ACC7	46 ±1	4.7 ±0.1	328
2076576319232128128	KIC 5629783	J19384478+4049062	1.13	FSB1	11.3 ±0.5	1.8 ±0.1	–
2103637705563916288	KIC 5685237	J18555805+4055455	1.99	ACC7	106 ±1	9.41 ±0.02	76
2103657320675288064	KIC 5685682	J18564987+4055220	1.5	ACC7	98 ±1	9.69 ±0.03	–
2053549517782643840	KIC 5709182	J19314933+4059408	0.91	FSB1	32 ±1	4.13 ±0.03	331
2076775949311326592	KIC 5725087	J19475229+4055363	2.14	ACC7	6.0 ±0.3	1.01 ±0.03	–
2101633192790325504	KIC 5790837	J19270775+4102534	2.4	ACC7	47 ±1	4.68 ±0.02	–
2053562750585942784	KIC 5794100	J19311995+4105084	1.05	SSB1	35 ±1	4.15 ±0.05	319
2075128296787855616	KIC 5820359	J19560456+4103248	1.96	ACC7	125 ±1	10.20 ±0.02	–
2104369705429967232	KIC 5854239	J18514993+4106125	1.09	FSB1	28 ±1	3.00 ±0.02	–
2102118627173316096	KIC 5866537	J19142689+4109216	1.16	FSB1	104 ±1	8.95 ±0.02	73
2104372729087003648	KIC 5938430	J18521894+4116496	1.83	FSB1	59.0 ±0.4	5.93 ±0.02	–
2102164875381532032	KIC 5949648	J19132011+4115408	1.36	FSB1	42 ±1	4.37 ±0.02	–
2101636182087624320	KIC 5960594	J19274204+4115182	1.16	FSB1	40 ±1	4.3 ±0.1	356
2076825423026628864	KIC 5976798	J19451285+4115593	1.41	FSB1	52 ±1	5.1 ±0.1	309
2076833261356367616	KIC 5978324	J19463646+4113194	2.54	SSB1	49 ±1	4.07 ±0.03	–
2076868514445183104	KIC 5981666	J19493102+4114177	4.22	ACC9	93 ±2	7.60 ±0.03	278
2073867844140668928	KIC 5983759	J19511957+4116154	1.52	SSB1	53 ±4	4.7 ±0.5	–
2101781592499879168	KIC 6038057	J19212931+4119163	1.03	SSB1	2.58 ±0.04	0.55 ±0.03	–
2076839514828934016	KIC 6061867	J19480992+4123269	1.95	ACC9	112 ±1	9.96 ±0.03	76
2073835717784356864	KIC 6067987	J19540665+4118111	2.06	ACC7	38 ±1	4.17 ±0.04	308
2103725284237785728	KIC 6103934	J18564594+4128038	0.94	SSB1	100 ±2	8.40 ±0.02	–
2076855629546546048	KIC 6222768	J19464390+4130165	1.44	SSB1	50 ±3	5.0 ±0.3	–
2102249022380726528	KIC 6276898	J19163450+4140329	2.9	ACC7	46 ±1	4.53 ±0.05	295
2053640433652398976	KIC 6287060	J19294989+4141547	3.8	ACC7/FSB1	1587 ±21	81 ±2	–
2073902955482573952	KIC 6309307	J19524727+4139016	1.12	SSB1	72 ±2	6.30 ±0.05	291
2075349607856207616	KIC 6390781	J19550865+4144444	1.07	FSB1	24.1 ±0.4	2.78 ±0.02	–
2075376958208856320	KIC 6471060	J19563145+4152230	1.24	SSB1	41.9 ±0.5	4.52 ±0.04	310
2101693906449210624	KIC 6522553	J19272692+4156404	1.42	SSB1	57 ±1	5.68 ±0.02	–
2101737234079077888	KIC 6689943	J19252467+4207248	3.05	ACC7	1706 ±59	80.1 ±2.1	–
2077680194542729472	KIC 6695665	J19321255+4206062	1.11	SSB1	59 ±1	5.51 ±0.03	246
2104719350128236160	KIC 6836772	J18453843+4218075	1.77	FSB1	52 ±1	5.48 ±0.02	–
2102690716812671616	KIC 6854391	J19163509+4220109	2.05	ACC7	62 ±2	5.61 ±0.03	312
2077173525841741312	KIC 6881330	J19461729+4221322	4.8	ACC9	1343 ±16	83 ±5	–
2104808337551988352	KIC 6923677	J18482034+4226016	3.91	SSB1/ACC7	61 ±1	5.54 ±0.03	271
2101946141286979072	KIC 6945411	J19230209+4224592	1.83	ACC7	204 ±2	15.36 ±0.05	–
2077186685622052096	KIC 6967600	J19472104+4227387	1.41	SSB1/ACC7	41 ±1	4.35 ±0.05	264
2077800831583487104	KIC 7121674	J19315108+4237154	2.11	ACC7	64 ±1	5.84 ±0.02	70
2102724939117336704	KIC 7191945	J19164681+4242250	1.12	SSB1	58 ±1	5.49 ±0.04	264
2125797842728589696	KIC 7200117	J19265165+4246356	2.6	ACC7	58 ±1	5.55 ±0.02	–
2125798564283095168	KIC 7200574	J19272514+4246552	1.56	SSB1/ACC7	33 ±1	3.98 ±0.03	–
2077804130118429568	KIC 7204026	J19314653+4246022	2.21	SSB1/ACC7	80 ±1	7.61 ±0.02	72
2105545701837139328	KIC 7347189	J19052086+4254372	1.06	FSB1	42 ±1	4.08 ±0.02	–
2102909622709232128	KIC 7352727	J19141781+4254478	1.05	FSB1	36 ±1	4.28 ±0.05	325
2105166331665460224	KIC 7420646	J18504359+4303193	1.56	SSB1	39.5 ±0.5	4.15 ±0.02	–
2125819077046893312	KIC 7445653	J19280492+4300061	3.62	ACC7	31 ±1	3.77 ±0.04	–
2125818531592428544	KIC 7445931	J19282537+4300242	1.05	SSB1	1.1 ±0.1	0.28 ±0.04	–
2078016503357114752	KIC 7458106	J19415922+4303503	2.17	SSB1	44.5 ±0.4	4.65 ±0.02	–
2102973325664374016	KIC 7516024	J19114657+4311280	1.59	ACC7	120 ±1	10.52 ±0.02	–
2078201569212490112	KIC 7533995	J19343332+4306202	1.37	FSB1	107 ±1	9.58 ±0.03	77
2078061725077730944	KIC 7540174	J19410219+4308253	2.88	FSB1	61.1 ±0.5	6.28 ±0.02	88
2078765614373087104	KIC 7546098	J19463186+4309352	15.37	SSB1	160 ±1	13.07 ±0.03	83
2105767077331293824	KIC 7591311	J19021036+4312440	1.19	SSB1	36.5 ±0.5	3.66 ±0.02	–
2125870444853994624	KIC 7610274	J19303856+4317005	2.17	ACC7	180 ±1	14.3 ±0.1	84
2078174425018561536	KIC 7617072	J19382780+4317002	1.42	SSB1	56 ±1	5.60 ±0.02	–
2078031179269645824	KIC 7621593	J19431164+4315553	1.86	ACC7	128 ±1	10.49 ±0.02	75
2078722836498812544	KIC 7626457	J19475330+4313360	2.41	ACC7	174 ±2	13.29 ±0.02	–
2078550354922555392	KIC 7629559	J19504238+4317202	1.17	FSB1	94 ±1	8.29 ±0.02	74
2078596598819992320	KIC 7707887	J19554382+4318064	1.01	FSB1	79 ±1	6.5 ±0.1	269
2102993632270086144	KIC 7742049	J19095794+4325272	1.14	FSB1	24 ±1	3.4 ±0.1	–
2102958241739384448	KIC 7743539	J19124404+4324534	1.06	FSB1	41 ±1	4.54 ±0.04	290
2102819321017487104	KIC 7747060	J19185126+4328299	1.35	FSB1	48 ±2	4.7 ±0.1	–
2126075130117536128	KIC 7749249	J19215355+4325572	1.29	FSB1	72 ±1	6.66 ±0.02	–
2126076126549995520	KIC 7818452	J19215537+4332316	1.31	SSB1	37 ±1	4.2 ±0.2	253
2078097218687976448	KIC 7833491	J19414321+4334497	1.03	FSB1	51 ±1	4.93 ±0.04	–
2078089625185545728	KIC 7900733	J19401193+4337080	1.07	FSB1	33 ±1	3.79 ±0.05	312
2078101028313523456	KIC 7901207	J19404732+4340086	1.19	FSB1	85 ±5	6.49 ±0.05	–
2105839134002312448	KIC 7944142	J18592870+4343593	5.44	ACC9	75 ±1	6.99 ±0.02	–
2079551975648637312	KIC 8041612	J19441583+4348390	0.97	SSB1	3.8 ±0.2	0.76 ±0.05	–
2106023096040944896	KIC 8085998	J19083825+4355009	3.34	ACC7	35 ±1	4.1 ±0.1	297

Table B.2. Seismic parameters for potential binary systems in *Gaia* DR3, with non-linear and acceleration solutions. (continued)

Gaia DR3	KIC/TIC	2MASS	ruwe	Type	ν_{\max} [μHz]	$\Delta\nu$ [μHz]	$\Delta\Pi_1$ [s]
2105322397895821184	KIC 8145759	J18505689+4401414	1.0	FSB1	11.6 ±0.5	1.75 ±0.02	–
2078350072000090368	KIC 8172679	J19365126+4403421	1.91	ACC7	148 ±2	12.19 ±0.02	79
2103086781520674432	KIC 8225839	J19162397+4409115	1.18	SSB1	32 ±1	3.98 ±0.04	–
2079627597130763264	KIC 8243725	J19412709+4409097	1.11	FSB1	39 ±1	4.33 ±0.03	319
2079619625671459840	KIC 8244769	J19424807+4410432	1.39	SSB1	60 ±1	5.9 ±0.1	–
2078832203551450368	KIC 8247851	J19463143+4406467	0.93	FSB1	42 ±1	4.56 ±0.03	246
2079603618336250368	KIC 8377727	J19440539+4423418	0.97	FSB1	40 ±1	4.32 ±0.05	312
2078929961307827200	KIC 8379927	J19464129+4420547	32.79	SSB1	2803 ±164	121 ±3	–
2082088686415440512	KIC 8460634	J20030794+4429213	2.08	ACC7	36 ±1	4.3 ±0.1	297
2106709947211609472	KIC 8480205	J18585843+4432026	1.07	SSB1	49 ±1	5.25 ±0.02	–
2127114340402131328	KIC 8487905	J19155712+4430443	2.02	ACC7	51 ±2	5.2 ±0.2	–
2126235207836940288	KIC 8493800	J19250252+4432437	2.94	ACC9	1813 ±45	82 ±2	–
2079657013370134528	KIC 8506096	J19425300+4434338	1.23	SSB1	45 ±1	4.53 ±0.04	294
2078957620897687808	KIC 8510483	J19480534+4431080	1.58	SSB1	35 ±1	4.2 ±0.2	–
2106289315293364608	KIC 8547564	J19051226+4437481	1.17	SSB1	135 ±1	11.60 ±0.04	–
2079663782238517760	KIC 8569991	J19420723+4436111	0.99	FSB1	16 ±2	1.9 ±0.1	–
2079663438641171072	KIC 8570254	J19422579+4436400	1.23	SSB1	34 ±1	4.19 ±0.04	326
2079268297345363456	KIC 8579578	J19524160+4436168	5.2	ACC9/SSB1	957 ±52	51 ±1	–
2079127426723311616	KIC 8585236	J19582646+4436572	1.13	FSB1	2.31 ±0.05	0.51 ±0.02	–
2126435804290545280	KIC 8693018	J19331881+4449576	1.6	ACC7	90 ±1	7.30 ±0.04	265
2106778494889177984	KIC 8737094	J18553646+4457024	2.41	ACC7	833 ±33	45.3 ±1.4	–
2127051015405294592	KIC 8813946	J19195507+4501556	1.04	SSB1	72 ±1	6.4 ±0.1	–
2079869081674009472	KIC 8827934	J19405000+4503470	1.41	SSB1	56 ±2	5.42 ±0.02	–
2082162108874588672	KIC 8845313	J20005721+4501282	1.76	ACC7	39 ±1	4.3 ±0.1	–
2127062182320159360	KIC 8879558	J19182227+4508427	1.78	SSB1	32.7 ±0.5	3.85 ±0.02	–
2079883134807073536	KIC 8895291	J19404886+4511295	1.27	SSB1	49 ±2	4.84 ±0.04	281
2079216757737807872	KIC 8907943	J19550926+4510375	0.95	FSB1	34 ±1	3.97 ±0.04	286
2106908752656623360	KIC 8933174	J18514153+4515405	1.45	SSB1	31.9 ±0.5	3.62 ±0.02	–
2106236465716432128	KIC 8941196	J19073581+4513065	1.97	ACC7	63.4 ±0.5	6.23 ±0.02	68
2126658936431524992	KIC 8952800	J19270311+4515461	2.56	ACC7/SSB1	984 ±34	52 ±2	–
2079968690555015424	KIC 8964218	J19422862+4515280	1.34	SSB1	31.3 ±0.5	3.58 ±0.02	–
2127082866883371008	KIC 9018004	J19213304+4522372	1.11	FSB1	31.8 ±0.5	4.2 ±0.1	322
2127973230784130304	KIC 9026685	J19341193+4521415	4.28	ACC9	1109 ±37	62.4 ±1.8	–
2127960689479531264	KIC 9028221	J19361872+4519393	1.14	SSB1	68 ±2	5.70 ±0.03	–
2079245276320641280	KIC 9112472	J19554378+4527330	1.54	SSB1/ACC7	47.0 ±0.5	4.7 ±0.1	265
2107196859063021184	KIC 9139330	J18564193+4532278	1.45	FSB1	42 ±2	4.47 ±0.03	310
2107181049283909760	KIC 9266926	J18583986+4547476	1.83	ACC7	1368 ±37	76.3 ±2.6	–
2107170676942345088	KIC 9267654	J19000746+4545325	0.97	FSB1	119 ±1	10.31 ±0.02	78
2085200613558669184	KIC 9304991	J19591729+4542508	1.06	FSB1	55 ±2	4.9 ±0.2	–
2127332799619227392	KIC 9335457	J19150203+4551200	1.99	SSB1/ACC7	232 ±2	17.52 ±0.03	–
2080051634964207488	KIC 9349632	J19383551+4551079	1.61	SSB1	100 ±1	7.80 ±0.04	228
2080195567909323776	KIC 9353859	J19442278+4553519	1.69	SSB1	407 ±4	24.1 ±2.5	–
2079452912219609216	KIC 9361885	J19535162+4548487	3.42	ACC9	30 ±1	3.40 ±0.03	–
2107220769143046912	KIC 9389234	J18563217+4554559	1.27	FSB1	28 ±5	3.3 ±0.2	–
2130265712526464512	KIC 9395752	J19111509+4554019	1.88	ACC7	150 ±2	12.44 ±0.03	–
2127531227108123776	KIC 9402881	J19252841+4557014	1.11	SSB1	82 ±2	6.66 ±0.05	–
2128235773544309120	KIC 9406638	J19312786+4559033	1.23	SSB1	38 ±1	4.42 ±0.02	–
210724197339960832	KIC 9511938	J18570822+4611498	1.06	SSB1	49 ±1	4.94 ±0.01	–
2080074724708827648	KIC 9535050	J19410038+4606367	1.17	FSB1	45 ±1	4.53 ±0.04	–
2127705637139947008	KIC 9583430	J19193882+4614557	0.93	SSB1	100 ±2	7.76 ±0.03	169
2080313761107471744	KIC 9662723	J19474313+4620231	1.28	FSB1	83 ±2	7.42 ±0.02	84
2128306485885973248	KIC 9711269	J19285963+4624427	2.64	ACC7	65 ±1	6.39 ±0.02	–
2128311738625520384	KIC 9711510	J19292513+4624320	1.16	FSB1	54 ±2	5.08 ±0.04	315
2128265559137187968	KIC 9711988	J19301359+4624506	1.26	SSB1	38 ±1	4.07 ±0.05	268
2128285178547796352	KIC 9712510	J19310601+4624322	0.99	SSB1	34 ±1	3.75 ±0.02	62
2127621627579989888	KIC 9767051	J19211712+4633148	1.15	FSB1	21 ±1	2.78 ±0.02	–
2128291127083154432	KIC 9772366	J19302335+4635095	4.83	ACC9	76 ±1	6.82 ±0.02	71
2085541290366624768	KIC 9787965	J19521405+4633578	3.41	ACC7	892 ±34	53 ±2	–
2080300124592637056	KIC 9845323	J19485274+4638520	1.12	FSB1	5.5 ±0.2	0.88 ±0.05	–
2127781503442529024	KIC 9885121	J19170569+4647260	1.54	ACC7	75 ±1	7.37 ±0.02	72
2130456782730953472	KIC 9942816	J19103744+4651401	1.12	SSB1	40 ±1	4.5 ±0.1	336
2086310772400457088	KIC 9966914	J19504258+4651019	1.34	SSB1	111 ±2	8.80 ±0.05	–
2085432232557088000	KIC 9974365	J19594711+4653439	1.29	SSB1	4.0 ±0.2	0.75 ±0.04	–
2128528655954439168	KIC 10018967	J19390103+4659348	1.35	SSB1	59 ±1	5.43 ±0.02	250
2085564277030640896	KIC 10031856	J19551455+4655196	0.94	FSB1	20.6 ±0.4	2.54 ±0.01	–
2119406072397731328	KIC 10118422	J18430594+4708391	1.29	SSB1	45 ±1	4.71 ±0.04	316
2130697885015094528	KIC 10128629	J19053778+4708331	1.34	FSB1	37 ±1	4.21 ±0.03	–
2127850119841327488	KIC 10136807	J19204057+4708085	1.86	ACC7	22 ±2	2.9 ±0.1	–
2129114072878649984	KIC 10141049	J19271636+4709081	0.93	SSB1	3.11 ±0.06	0.67 ±0.04	–
2128229515770464256	KIC 10145736	J19342606+4711488	2.34	SSB1/ACC7	194 ±2	14.08 ±0.03	96
2107597459252129792	KIC 10190841	J18550107+4716208	3.56	ACC9	36 ±1	4.2 ±0.1	324
2130679335055863040	KIC 10196797	J19071356+4717043	0.96	FSB1	31 ±1	3.9 ±0.1	283
2130811860567145984	KIC 10200831	J19153178+4717403	1.52	ACC7	86 ±1	7.86 ±0.02	78

Table B.2. Seismic parameters for potential binary systems in *Gaia* DR3, with non-linear and acceleration solutions. (continued)

Gaia DR3	KIC/TIC	2MASS	ruwe	Type	ν_{\max} [μHz]	$\Delta\nu$ [μHz]	$\Delta\Pi_1$ [s]
2129118956258547456	KIC 10207623	J19270794+4714354	1.02	SSB1	41 ±1	4.2 ±0.5	–
2107605465070907520	KIC 10257419	J18551515+4722088	1.74	SSB1/ACC7	91 ±1	8.41 ±0.02	74
2119591997239080704	KIC 10319325	J18460437+4724088	0.89	SSB1	29 ±2	3.5 ±0.1	316
2130832716928596608	KIC 10396693	J19130886+4731507	0.95	SSB1	1.3 ±0.1	0.29 ±0.03	–
2129221412701321344	KIC 10405377	J19282181+4735226	1.41	SSB1	84 ±1	6.95 ±0.05	265
2129188500369799680	KIC 10468528	J19242861+4736427	1.69	SSB1/ACC7	28.7 ±0.5	3.7 ±0.1	328
2129191455307266560	KIC 10469022	J19252230+4737108	0.95	FSB1	35.4 ±0.5	4.01 ±0.02	–
2128441794535894144	KIC 10473692	J19325328+4737099	1.88	ACC7	93 ±1	8.64 ±0.02	81
2130894220860474752	KIC 10525475	J19102133+4743193	1.05	FSB1	39 ±1	4.34 ±0.03	324
2129196849785839872	KIC 10533369	J19243319+4744285	0.95	SSB1	42 ±3	4.3 ±0.2	330
2128818308548103296	KIC 10538371	J19325505+4746578	1.05	FSB1	2.66 ±0.05	0.58 ±0.03	–
2085716971707682816	KIC 10555618	J19552174+4743524	2.19	ACC7	33 ±1	4.14 ±0.02	300
2131506438378495872	KIC 10586902	J19031115+4753540	1.06	SSB1	45.1 ±0.4	4.98 ±0.02	–
2129198499053586560	KIC 10598558	J19250775+4750191	0.95	FSB1	43.5 ±0.5	4.56 ±0.03	274
2131503655239675136	KIC 10716853	J19010654+4802081	1.76	SSB1/ACC7	49 ±1	5.0 ±0.1	–
2128841157774523008	KIC 10736390	J19353947+4805008	2.04	ACC7	74 ±2	5.84 ±0.05	–
2128852943165070336	KIC 10801063	J19333700+4807422	3.29	ACC7	199 ±1	16.09 ±0.03	–
2086524047601016320	KIC 10813862	J19504319+4806541	1.1	FSB1	30 ±2	3.8 ±0.1	–
2131141572318833152	KIC 10849499	J19042591+4813575	0.85	FSB1	125 ±1	10.94 ±0.03	–
2128938528973761280	KIC 10866694	J19362512+4817342	1.31	SSB1	32 ±1	3.91 ±0.03	269
2128897129788939520	KIC 10922092	J19311099+4819453	1.02	SSB1	43.0 ±0.6	4.73 ±0.02	–
2119763967729811584	KIC 10959362	J18482584+4828027	4.09	ACC9	858 ±21	45 ±1	–
2129520930836942848	KIC 10972873	J19214232+4826361	4.35	ACC9/ACC9	1033 ±6	58.07 ±0.01	–
2086876475436251008	KIC 11046496	J19543309+4831256	2.48	ACC7	31 ±1	3.91 ±0.03	340
2086554176790676864	KIC 11098762	J19521070+4837036	1.23	FSB1	34 ±3	4.0 ±0.5	–
2131944666780188416	KIC 11126673	J19032139+4847102	1.51	FSB1	55 ±1	5.65 ±0.02	–
2129587034673659392	KIC 11133969	J19195188+4845218	1.04	FSB1	30 ±2	3.7 ±0.1	260
2086887539272570752	KIC 11153898	J19542298+4843270	1.79	ACC7	139 ±1	11.47 ±0.02	–
2131231599130749440	KIC 11182706	J19102221+4853112	1.81	SSB1	38.9 ±0.5	4.43 ±0.02	–
2129558928407670016	KIC 11241927	J19223498+4859542	1.19	SSB1	26.7 ±0.5	2.96 ±0.02	–
2134762470268558848	KIC 11252510	J19423899+4855122	1.84	ACC7	204 ±2	14.94 ±0.03	–
2129924451604211840	KIC 11295851	J19245919+4904405	1.87	ACC7	96 ±2	7.55 ±0.03	–
2134851908665475968	KIC 11306275	J19441480+4905035	1.0	FSB1	41 ±1	4.32 ±0.05	305
2132741533533785984	KIC 11342694	J19110062+4906529	1.11	FSB1	75 ±1	7.11 ±0.02	–
2129754302180758144	KIC 11350954	J19283246+4909237	1.04	FSB1	21 ±1	2.45 ±0.03	–
2129783130000893184	KIC 11352446	J19314166+4906270	2.74	SSB1/ACC7	90 ±2	7.64 ±0.02	–
2134772129653795328	KIC 11358669	J19425925+4911303	2.88	ACC7	98 ±1	8.44 ±0.02	73
2132186559337913600	KIC 11390588	J18582031+4916070	1.84	ACC7	106 ±1	9.64 ±0.02	–
2134823566182556928	KIC 11462972	J19421645+4919079	2.4	ACC7	44 ±1	4.52 ±0.03	314
2134869814389051648	KIC 11463411	J19425814+4918225	0.99	FSB1	51 ±2	4.65 ±0.04	–
2086847372737400704	KIC 11518690	J19473059+4924086	1.0	FSB1	31 ±2	3.89 ±0.05	288
2132657700072708224	KIC 11708622	J19181434+4948384	1.16	SSB1	38 ±1	4.26 ±0.03	–
2087250515546944640	KIC 11775041	J19491544+4959530	1.33	SSB1	34 ±2	4.2 ±0.1	–
2130058729462541184	KIC 11911929	J19212853+5016139	1.55	ACC7	109 ±1	9.59 ±0.02	81
2133668731075321984	KIC 11953581	J19022344+5021306	1.28	FSB1	37 ±1	4.3 ±0.1	297
2133056891511922816	KIC 11960908	J19202865+5021404	1.33	SSB1	50 ±1	5.11 ±0.02	–
2135870988444769408	KIC 11966513	J19335072+5018091	1.35	SSB1	42 ±3	4.5 ±0.2	–
2135870576127957504	KIC 11966805	J19342372+5019090	1.24	FSB1	40 ±1	4.45 ±0.02	–
2133672824181319168	KIC 12003253	J19015178+5024593	0.95	FSB1	32 ±2	3.85 ±0.05	–
2130153321821614720	KIC 12011630	J19224559+5028077	5.87	FSB1	2561 ±69	126 ±4	–
2130145552220927232	KIC 12011995	J19234442+5025201	1.24	FSB1	23.0 ±0.4	3.6 ±0.2	292
2130146033257324800	KIC 12012082	J19235844+5027243	1.07	SSB1	30 ±1	3.28 ±0.02	–
2134986568780887936	KIC 12020532	J19421354+5024406	1.62	ACC7	373 ±14	23.2 ±0.9	–
2135375692817914112	KIC 12071521	J19451479+5035233	1.24	SSB1	3.8 ±0.2	0.76 ±0.02	–
2130173349249960832	KIC 12109888	J19234800+5041131	1.1	SSB1	16.5 ±0.5	2.33 ±0.02	–
2135224613047204352	KIC 12114999	J19352533+5036463	0.91	FSB1	40 ±1	4.40 ±0.04	333
2135336076039746560	KIC 12120937	J19461603+5040551	1.56	ACC7	123 ±2	10.66 ±0.02	–
2133317647565635968	KIC 12153827	J19125385+5045510	0.95	FSB1	47 ±1	4.88 ±0.05	300
2133170072489773056	KIC 12207049	J19220307+5052296	1.6	ACC7	147 ±2	10.91 ±0.05	–
2133341149626842368	KIC 12352180	J19144496+5108424	1.62	ACC7	1032 ±68	58.3 ±1.7	–
2130202456247909632	KIC 12406610	J19230524+5112569	1.0	FSB1	2.4 ±0.1	0.53 ±0.02	–
2133217450271251456	KIC 12457780	J19195017+5120078	1.08	SSB1	7.5 ±0.4	1.20 ±0.04	–
2133441647566036352	KIC 12506130	J19154367+5124490	1.03	FSB1	38 ±1	4.3 ±0.1	232
2133226319381976832	KIC 12508433	J19205271+5128182	10.13	ACC7/ACC7	790 ±3	44.8 ±–	–
2139299501918127744	KIC 12735580	J19183698+5157382	2.33	ACC7/SSB1	1287 ±22	61 ±2	–
4665896550178539264	TIC 25080591	J04032993-7114139	1.49	FSB1	34 ±3	4.0 ±0.1	–
4654219977209475712	TIC 29760419	J04001914-6154420	4.27	ACC7/SSB1	10.7 ±0.4	1.481 ±0.005	–
4656014551985981312	TIC 29781030	J04391688-6516409	1.14	FSB1	56 ±3	4.6 ±0.3	–
4654503135828629120	TIC 30194561	J04103753-7141295	2.18	ACC7	6 ±2	1 ±24	–
4654529695911767168	TIC 30400653	J05520794-7835158	4.75	ACC9	136 ±8	10.9 ±0.2	–
4662070558983676416	TIC 30642910	J05411458-7837531	1.1	SSB1	20 ±2	2.7 ±0.2	–
4651617845529714304	TIC 30762052	J05550054-7820212	1.4	ACC7	2.2 ±0.3	0 ±1	–
4654646896974959744	TIC 30762356	J05032551-7110319	1.23	FSB1	44 ±3	5.7 ±0.2	–

Table B.2. Seismic parameters for potential binary systems in *Gaia* DR3, with non-linear and acceleration solutions. (continued)

Gaia DR3	KIC/TIC	2MASS	ruwe	Type	ν_{\max} [μHz]	$\Delta\nu$ [μHz]	$\Delta\Pi_1$ [s]
4652039886199883776	TIC 31016109	J08330987-5907274	1.09	FSB1	5.1 \pm 0.5	0.9 \pm 0.2	–
4659093287637278848	TIC 31273019	J04522693-7521338	0.95	FSB1	39 \pm 4	3.9 \pm 0.2	–
4646110082521710080	TIC 31675664	J06395061-6909256	0.9	SSB1	5.3 \pm 0.4	0.90 \pm 0.05	–
4642946340892098688	TIC 31782503	J08025715-7001484	1.9	ACC7/SSB1	92 \pm 4	8.3 \pm 0.2	–
4641943173970653440	TIC 31942864	J04545038-7145110	2.31	ACC7	44.3 \pm 0.3	3.7 \pm 0.1	–
4667335948338097024	TIC 31943791	J03224817-6416539	4.3	SSB1	11 \pm 1	1.6 \pm 0.3	–
4666841924019140992	TIC 32154421	J03372266-6840480	1.61	SSB1	39 \pm 3	5.5 \pm 0.2	–
4666842301976254720	TIC 32154434	J03225232-6533244	1.27	SSB1	33 \pm 5	3.4 \pm 0.2	–
4629229143063414144	TIC 33714066	J03184009-7335554	2.55	ACC7	38 \pm 5	4 \pm 11	–
4626238093477225088	TIC 33734517	J05290616-6417441	1.75	SSB1	13 \pm 2	1.8 \pm 0.2	–
4629392832855344896	TIC 33834132	J05004518-8145460	1.57	ACC7	5.2 \pm 0.5	0.8 \pm 0.2	–
4653778317132644736	TIC 33834943	J05032548-7124502	5.17	ACC9	31 \pm 4	3.9 \pm 0.2	320
4629291501691558144	TIC 33835925	J02160571-7546150	1.4	SSB1	5.1 \pm 0.4	0.9 \pm 0.3	–
4668009984511656192	TIC 38507264	J08400961-6119160	3.93	ACC9	28 \pm 4	3.5 \pm 0.2	–
4676628917537272448	TIC 38680205	J06120580-5916110	4.39	ACC9	32 \pm 3	3.3 \pm 0.1	–
4677501070775557760	TIC 38762657	J02460100-7340467	1.01	SSB1	8.1 \pm 0.4	1.465 \pm 0.005	–
4663435362120899200	TIC 38941661	J09410681-7252192	1.1	FSB1	30 \pm 3	3.6 \pm 0.2	–
4663266518366217728	TIC 38942180	J09492342-7255235	1.86	SSB1	75 \pm 4	7.4 \pm 0.3	–
5283051185606757248	TIC 41338480	J05144993-5740509	1.51	SSB1	75 \pm 5	7.0 \pm 0.1	–
5266249209115367168	TIC 41481508	J03364926-7143199	1.79	ACC7	63 \pm 3	4.8 \pm 0.1	–
5302843911036540928	TIC 44985274	J04205621-6853214	1.05	SSB1	92 \pm 7	8.12 \pm 0.02	–
4637169987836223104	TIC 50385569	J07321502-5121060	1.36	SSB1	93 \pm 9	8.4 \pm 0.2	143
4633858705490193024	TIC 50442240	J07274975-5206118	1.04	SSB1	30 \pm 2	3.8 \pm 0.1	–
4643271452736658944	TIC 50475841	J06150036-7510247	5.72	ACC7/SSB1	56 \pm 6	5.1 \pm 0.4	–
4663920487264015232	TIC 55269260	J05200470-6304222	1.53	ACC7	44 \pm 5	4.7 \pm 0.2	–
4760670668624915456	TIC 55272033	J05241157-5857110	0.95	FSB1	12 \pm 2	2 \pm 1	–
4664992820340914432	TIC 55478057	J09111864-6436522	1.88	ACC7/SSB1	38 \pm 3	4.2 \pm 0.2	343
4664433649961554816	TIC 55848319	J05032086-6312206	1.18	FSB1	11 \pm 2	1.5 \pm 0.3	–
4653497735509689344	TIC 140527371	J07523661-6540013	1.33	FSB1	17 \pm 3	2.2 \pm 0.2	–
4649201286447683840	TIC 140687635	J06453720-7123055	2.35	SSB1	27 \pm 3	3.2 \pm 0.1	–
4654494919539316864	TIC 140757304	J04164968-7159524	1.85	ACC7/SSB1	44 \pm 4	4.7 \pm 0.2	372
4652958734308341888	TIC 140758260	J04270340-7244056	1.07	SSB1	59 \pm 5	5.9 \pm 0.1	75
4649688855438914688	TIC 140938580	J05250648-7322247	1.76	ACC7/SSB1	37 \pm 4	4.4 \pm 0.1	–
4651392926670678016	TIC 140940299	J05225382-5648586	0.86	FSB1	1.9 \pm 0.2	0 \pm 1	–
4648130091541186176	TIC 141186362	J06194916-7122505	1.3	SSB1	34 \pm 4	4 \pm 1	–
4648600957400661632	TIC 141422621	J02521023-7537556	3.58	ACC9	70 \pm 5	6.0 \pm 0.3	–
4647869610364852736	TIC 141610781	J06245769-7706027	2.22	ACC7	80 \pm 6	7.1 \pm 0.3	298
4650146832087788416	TIC 141625696	J03583541-6820376	1.34	SSB1	37 \pm 4	3.9 \pm 0.2	–
4648317077238452864	TIC 141627237	J03533315-7518367	2.36	ACC7	77 \pm 4	7.6 \pm 0.1	–
4647865212318369280	TIC 141628215	J08390602-6250327	1.03	FSB1	45 \pm 6	4.9 \pm 0.3	–
5260610569892891904	TIC 141811001	J07000648-7238569	1.3	SSB1	8 \pm 2	1 \pm 2	–
5261678298763438336	TIC 141866758	J06522148-7247014	2.86	ACC7/SSB1	10 \pm 1	1.5 \pm 0.2	–
5260535253346530176	TIC 141909852	J06364593-7648095	2.59	ACC7/SSB1	33 \pm 5	3.8 \pm 0.2	303
5260550852667759232	TIC 141910909	J06192054-7523410	1.17	FSB1	8 \pm 2	1 \pm 1	–
5261560891536860928	TIC 141911519	J07120135-7437065	1.15	SSB1	23 \pm 3	2.8 \pm 0.3	–
5260369983004904576	TIC 141977610	J07010271-7304023	1.9	ACC7/SSB1	74 \pm 6	6.1 \pm 0.1	–
5260377335988918784	TIC 141977647	J07244833-7600578	2.68	ACC7	10 \pm 1	1.40 \pm 0.02	–
5260659292002154624	TIC 141978023	J06373790-7630511	1.76	ACC7	37 \pm 4	4.5 \pm 0.2	299
5260394412779052544	TIC 142109251	J07095096-7638544	2.08	ACC9	95 \pm 11	8 \pm 999	134
5265371283442843008	TIC 142142864	J03061148-7237128	4.65	ACC9	73 \pm 13	7 \pm 1	–
5265328093251778432	TIC 142144296	J05263853-7003491	2.38	ACC7	50 \pm 3	4.7 \pm 0.1	–
4757388115323382656	TIC 149219812	J05512892-5957114	1.06	FSB1	12 \pm 1	1.52 \pm 0.03	–
4660943387757280640	TIC 149220852	J05495532-5102200	1.34	SSB1	24 \pm 3	2.9 \pm 0.1	–
4757763869122791040	TIC 149346919	J04222566-6150057	3.97	ACC9	132 \pm 11	9.6 \pm 0.2	–
4757766690915335552	TIC 149346984	–	2.61	ACC9	48 \pm 7	5.0 \pm 0.1	–
4757122475883048064	TIC 149393493	J04445586-6318345	5.48	ACC9	91 \pm 9	8.7 \pm 0.2	–
4757082966490652672	TIC 149393720	J09092916-6516211	2.12	ACC7	37 \pm 3	4.7 \pm 0.2	–
4758467728361095808	TIC 149498425	J08314286-6109256	6.41	ACC9	44 \pm 6	5 \pm 1	–
4660076972592356480	TIC 149501150	J08222684-5901479	1.04	FSB1	22 \pm 3	3.0 \pm 0.3	–
4756840283652673280	TIC 149574243	J04320664-6039463	1.92	ACC7/SSB1	40 \pm 3	4.5 \pm 0.2	–
4756400272846337152	TIC 149933941	J06371906-4917098	1.16	FSB1	39 \pm 5	4.0 \pm 0.5	–
5482066913397844608	TIC 150064083	J06503881-5812435	1.04	SSB1	11.3 \pm 0.5	1.4 \pm 0.3	–
5481007950559542144	TIC 150098720	J06365365-5938485	1.02	FSB1	11 \pm 1	2 \pm 1	–
5476606571156022656	TIC 150150095	J07352172-6514296	4.98	ACC9	15 \pm 1	1.9 \pm 0.3	–
5477731401610570240	TIC 150187382	J08241370-5556561	0.99	SSB1	78 \pm 5	7.0 \pm 0.3	68
5476588051256813312	TIC 150298011	J06144257-6318092	1.06	SSB1	4.3 \pm 0.3	0.8 \pm 0.2	–
5478084104324927360	TIC 150298773	J06511181-6304342	2.29	ACC9	47 \pm 4	5.1 \pm 0.2	–
4801121392173433088	TIC 151586174	J09015617-6146446	1.27	SSB1	18 \pm 2	2.2 \pm 0.1	–
4800941660678042624	TIC 151628740	J08482017-6325473	1.32	SSB1	16 \pm 2	2.3 \pm 0.2	–
5552294512067493760	TIC 156888563	J06132219-4911564	1.03	FSB1	27 \pm 4	3.7 \pm 1.7	–
5566670656663653504	TIC 165187830	J09321203-8136389	1.08	SSB1	21 \pm 2	2.5 \pm 0.2	–
5266360637756153728	TIC 166975681	J06424582-7041373	0.92	FSB1	37 \pm 3	4.0 \pm 0.1	–
5283572633293059072	TIC 167085827	J08112049-6149236	1.8	ACC7	87 \pm 5	7.0 \pm 0.1	–

Table B.2. Seismic parameters for potential binary systems in *Gaia* DR3, with non-linear and acceleration solutions. (continued)

Gaia DR3	KIC/TIC	2MASS	ruwe	Type	ν_{\max} [μHz]	$\Delta\nu$ [μHz]	$\Delta\Pi_1$ [s]
5279211901453725440	TIC 167421985	J09231317-6904366	2.88	SSB1	49 ±4	5 ±5	–
5286542959654908288	TIC 167692036	J08031638-6154305	1.82	ACC7/SSB1	41 ±3	4.6 ±0.6	–
5285416376849503232	TIC 167720698	J07153842-6310473	6.47	ACC9	71 ±4	7.1 ±0.3	–
5286534030419408512	TIC 167721564	J07331222-6445571	1.46	FSB1	31 ±2	3.3 ±0.3	–
5286656419807218304	TIC 167755398	J04000907-5940186	3.24	ACC7	66 ±6	5.9 ±0.8	–
5285224683870045056	TIC 167810736	J07034896-6118337	1.06	FSB1	4 ±1	0.8 ±0.2	–
5265393338097340672	TIC 176873464	J07261121-7131398	2.49	ACC7	25 ±3	3.4 ±0.2	386
5266824421200366464	TIC 176937307	J07263172-7039155	1.11	FSB1	14 ±5	1.86 ±0.02	–
5266544805946921216	TIC 176980573	J07111507-7118320	1.01	FSB1	16 ±3	2.2 ±0.2	–
5281670753051921408	TIC 177022013	J03354079-5748367	1.05	FSB1	53 ±3	4.6 ±0.1	–
5281682778961042304	TIC 177038273	J06115061-6502530	2.12	ACC7	138 ±8	12 ±11	–
5268387656154570624	TIC 177115421	J07584722-6903073	2.99	ACC7	37 ±4	4.1 ±0.3	312
5281751326638265216	TIC 177236627	J05363967-4802544	1.06	FSB1	54 ±15	5.6 ±0.4	–
5280996511906284160	TIC 177236746	J08133742-6248051	2.48	ACC7	38 ±6	3.8 ±0.3	–
5265423127991329024	TIC 177307119	J05073424-7424493	3.02	ACC9	69 ±6	6.8 ±0.3	–
5262438026938122368	TIC 177386950	J07214221-7357489	1.37	SSB1	7 ±2	1.5 ±4.9	–
4651743877059761152	TIC 179318090	J07264649-7132280	3.89	ACC9	70 ±2	6.8 ±0.4	–
4723909291920831232	TIC 197785467	J07364029-5955341	2.98	ACC9/SSB1	66 ±3	5.8 ±0.2	–
4729272125525236352	TIC 197808795	J05452858-5729224	0.98	FSB1	36 ±4	4.1 ±0.4	–
4729886546366843136	TIC 197847423	J06082348-5736006	2.18	ACC7	39 ±3	3.99 ±0.04	–
4729601635416187520	TIC 197882677	J05130995-5423295	2.68	ACC7/SSB1	111 ±11	10.1 ±0.5	–
4682903173265254400	TIC 197908104	J03052486-7200147	3.23	ACC7	107 ±9	8 ±1	–
4680309498350830336	TIC 198006797	J07403655-5954363	3.62	ACC7	41 ±5	4.6 ±0.2	–
4683418607996178176	TIC 198034932	J09234973-7824082	1.05	FSB1	23 ±2	2.7 ±0.2	–
4683185683329746560	TIC 198035227	J08022009-5953575	2.8	ACC7	53 ±3	5.4 ±0.2	–
4778868243195813632	TIC 198075355	J04302959-5300446	1.18	FSB1	57 ±6	5.6 ±0.2	–
4678666033408510464	TIC 198079175	J05334167-6129301	2.69	ACC9	125 ±9	9.7 ±0.1	–
4682313598810541824	TIC 198081375	J04042851-5547500	1.01	FSB1	29 ±3	3.4 ±0.1	–
5553002387100157312	TIC 219175377	J08022086-8541270	1.04	SSB1	25 ±2	3.2 ±0.2	–
5548665054246731904	TIC 219183283	–	3.4	ACC7	256 ±2	16.1 ±0.3	–
5553443604797189504	TIC 219197375	J05280539-5429280	1.95	ACC7/SSB1	121 ±12	10.7 ±0.2	–
5553573141010823808	TIC 219215104	J05360612-5951282	1.04	SSB1	11 ±1	1.5 ±0.1	–
4781500851990718080	TIC 219256367	J02251396-7007304	1.49	FSB1	43 ±2	4.9 ±0.4	–
4783494197851643392	TIC 219362223	–	2.51	ACC7	9.8 ±0.4	1.51 ±0.02	–
4785175591649134720	TIC 219362727	J07235816-5143104	2.07	ACC7/SSB1	55 ±4	5.3 ±0.1	–
4782999451978900224	TIC 219365715	J02442700-6553083	1.02	FSB1	14 ±2	1.7 ±0.4	–
4772765094667497088	TIC 219401448	J05182257-4940213	2.44	ACC7	18 ±2	2.29 ±0.02	–
4772832199237630848	TIC 219414678	J04461891-5255354	1.38	FSB1	28 ±1	4.11 ±0.03	–
4796884256612908416	TIC 219426361	J05525581-5131339	4.7	ACC9/SSB1	44.7 ±0.4	4.31 ±0.01	–
4775195629544547584	TIC 220392975	J08012227-5901202	2.13	ACC7	47 ±4	5 ±1	–
4776343622763376640	TIC 220429975	J04145668-5443199	1.25	FSB1	17 ±2	2.3 ±0.2	–
4776216942704209664	TIC 220438395	J07553637-5246328	1.65	ACC7	6 ±1	1 ±1	–
4762457241877392896	TIC 220460609	J08213708-5640409	6.3	ACC9	89 ±7	7.5 ±10.5	–
4695982035875959168	TIC 220515400	J06230777-5019151	1.1	FSB1	31 ±5	3.6 ±0.2	–
4721157386114808064	TIC 220556481	J08214650-6540188	5.31	ACC9	18 ±2	2.2 ±0.3	–
4720272622851664768	TIC 220557433	J03074895-6915536	1.89	ACC7	5.9 ±0.4	1.02 ±0.04	–
4662639384421989632	TIC 231098859	J04394088-6404054	1.25	FSB1	42 ±4	4.4 ±0.2	352
4771992477295349632	TIC 231720649	J05171249-5154080	1.1	SSB1	37 ±4	4.2 ±0.1	–
4796636381164466688	TIC 231722341	J07005791-6648023	1.39	SSB1	31 ±3	3.7 ±0.2	–
4772591990306410880	TIC 231724036	J04515642-5516386	1.37	SSB1	37 ±1	3.69 ±0.05	–
4796430055231615360	TIC 231730731	J06490794-6721035	1.0	FSB1	69.99 ±0.01	6.3 ±0.2	–
4795238700023196160	TIC 231817242	J05240059-5005132	1.0	FSB1	9.2 ±0.4	1.45 ±0.03	–
4793543830073768064	TIC 231819003	J05441543-4910246	1.17	FSB1	26 ±3	3.3 ±0.2	–
4693364480943357184	TIC 234333085	J05592970-6428192	1.49	FSB1	58 ±4	5.50 ±0.02	–
4644958790768178688	TIC 234342190	J03111644-7011523	1.42	SSB1	5.6 ±0.4	0.84 ±0.04	–
4796536020665091328	TIC 235051152	J05551869-4742517	2.32	ACC7	41 ±2	4.1 ±0.1	–
4769139729953728512	TIC 235057579	J05223858-5232459	1.22	FSB1	29 ±1	3.2 ±0.1	–
4779947001541937664	TIC 237360132	J07211381-5048162	1.78	ACC7	87 ±6	9.0 ±0.4	–
5503178468661647232	TIC 237943767	J05511619-5646406	3.31	ACC9	21 ±2	2.4 ±0.3	–
5551481182700770048	TIC 237953492	J06433545-4759347	1.14	FSB1	59 ±8	6 ±1	–
5551473383040241152	TIC 237973708	J06465012-4754262	1.05	FSB1	64 ±10	6.66 ±0.04	–
5498730291291675520	TIC 237979497	J07002361-4908060	1.83	ACC7/FSB1	83 ±17	8.4 ±0.2	–
5497722142208920064	TIC 238017828	J06543307-5214113	2.04	SSB1	68 ±7	6.1 ±0.1	–
5508277002861309952	TIC 238030636	J06574194-4823130	1.23	SSB1	89 ±15	7 ±1	–
5498792619857554176	TIC 238035953	J06202454-5430574	1.01	SSB1	27 ±5	2.8 ±0.3	–
5509038792620666880	TIC 238040965	J06442246-5251599	1.79	ACC7	185 ±19	11.55 ±0.04	–
5509045527129377920	TIC 238043480	J06523575-5348539	1.89	ACC7	42 ±2	5.5 ±0.2	–
5508251271715022336	TIC 238072589	J02491397-6838531	3.74	ACC7/SSB1	136 ±3	11.77 ±0.05	–
5509162556400089856	TIC 238073682	J03585454-6823089	0.95	FSB1	62 ±4	6 ±1	–
5509188880255887232	TIC 238084356	–	3.69	ACC7	38 ±5	4.3 ±0.4	–
5508397575481610112	TIC 238086247	J02375987-8128024	4.65	ACC9	46 ±7	4.7 ±0.2	–
5503759418821655040	TIC 238089714	J06382950-8448106	1.06	SSB1	10 ±1	1.5 ±0.3	–
5503485266765897728	TIC 238122623	J06594988-5258186	1.05	FSB1	86 ±5	7.4 ±0.4	–

Table B.2. Seismic parameters for potential binary systems in *Gaia* DR3, with non-linear and acceleration solutions. (continued)

Gaia DR3	KIC/TIC	2MASS	ruwe	Type	ν_{\max} [μHz]	$\Delta\nu$ [μHz]	$\Delta\Pi_1$ [s]
5503511277087495168	TIC 238132672	J08353972-8349550	1.18	FSB1	31 \pm 2	3.5 \pm 0.3	–
4641928227484566016	TIC 238181450	J02332358-7315215	1.47	FSB1	20 \pm 3	2.6 \pm 0.3	–
4643672873264197632	TIC 238870588	J02314604-7137288	1.12	SSB1	29 \pm 4	3.2 \pm 0.3	–
4640257068594061696	TIC 238891740	J04431858-7439342	6.43	ACC9	192 \pm 16	12.0 \pm 0.2	–
4643899308235906048	TIC 238892495	J06371398-7256148	6.29	ACC9/SSB1	30 \pm 2	2.9 \pm 0.1	–
5550535357886217472	TIC 238924009	J05001464-5151278	1.75	ACC7	46 \pm 2	4.51 \pm 0.05	–
5550452795730597376	TIC 238930632	J06491119-5228415	2.59	ACC7	39 \pm 5	4.17 \pm 0.03	–
5549044286976168448	TIC 238951938	J07154845-5452026	3.94	ACC7	8.6 \pm 0.5	1.28 \pm 0.04	–
5549519275999097344	TIC 255555328	J063000431-4929174	1.26	SSB1	132 \pm 3	11.7 \pm 0.1	–
5499986483327422976	TIC 255567238	J06363183-5155480	1.1	FSB1	46 \pm 3	4.7 \pm 0.1	267
5550690084084279936	TIC 255596297	J05343467-4724235	1.63	ACC7	152 \pm 3	11.0 \pm 0.1	–
5551079551718734208	TIC 255619287	J06480193-4806246	1.01	FSB1	66 \pm 7	5.6 \pm 0.2	–
5501262810167611264	TIC 255686229	J09401589-7940471	1.64	ACC7/SSB1	6 \pm 1	1 \pm 1	–
5501665368862525312	TIC 255703095	J07011858-5354434	1.0	SSB1	6.1 \pm 0.4	1.21 \pm 0.01	–
5502705472503021184	TIC 255703658	J07020702-5328109	1.17	FSB1	83 \pm 6	8.1 \pm 0.2	–
5550957059251391104	TIC 255754842	J06442960-4820254	1.36	SSB1	12 \pm 1	2 \pm 1	–
4770622417087664768	TIC 257722263	J07342806-5403549	3.51	ACC9	62 \pm 2	6.1 \pm 0.1	–
47807402099182115584	TIC 259319622	J04251115-5112479	1.48	SSB1	19 \pm 2	2 \pm 1	–
4780741570492432384	TIC 259319624	J05213225-4832098	2.18	ACC7	10.3 \pm 0.2	1.45 \pm 0.03	–
4781389011042044288	TIC 259375305	J05015244-5304570	1.32	SSB1	125 \pm 18	10.8 \pm 0.2	–
4777674276647368192	TIC 259389905	J05504487-5540459	3.37	ACC7	49 \pm 3	5.3 \pm 0.2	–
4777939877424981504	TIC 259517082	J04081655-5408540	1.39	SSB1	39 \pm 4	4.3 \pm 0.2	–
4645825618248371712	TIC 259930936	J05591207-7716163	1.61	FSB1	47 \pm 3	5.0 \pm 0.1	–
5495858195120842880	TIC 260042176	J06195468-5542579	1.06	FSB1	28 \pm 3	3.7 \pm 0.2	–
5499029152295754112	TIC 260074589	J06261359-5329562	1.38	FSB1	29 \pm 3	4 \pm 1	–
5495734156465667840	TIC 260127465	J07542015-5329534	4.0	ACC7/SSB1	44 \pm 3	4.5 \pm 0.5	–
5494547783419181696	TIC 260188160	J07302598-5721500	1.96	ACC7	33 \pm 1	4.29 \pm 0.01	–
5495984845116841344	TIC 260241050	J06353842-5609202	1.07	SSB1	34 \pm 5	4.2 \pm 0.2	–
5496472066206657664	TIC 260354441	J06535059-4942573	1.1	SSB1	33 \pm 4	3.7 \pm 0.5	–
5484634071187872384	TIC 260658725	J04163586-7417144	2.3	SSB1	26 \pm 2	3.4 \pm 0.3	–
4624295840546956928	TIC 260972404	J07425201-7132308	3.77	ACC7	6 \pm 8	1.0 \pm 0.6	–
4621215799239630848	TIC 260981834	J05373596-8042567	2.95	ACC7	56 \pm 8	5.11 \pm 0.05	–
4620822758192568448	TIC 261061125	J04414742-8110369	1.89	ACC7	94 \pm 10	8 \pm 1	–
4621531359077506816	TIC 261139187	J02425005-7932330	2.06	ACC7	26 \pm 4	3.0 \pm 0.1	–
4623670390229752064	TIC 261207550	J04331807-8422345	2.88	ACC9	42 \pm 6	4.3 \pm 0.2	–
4623105035094343296	TIC 261235411	J06285907-7800250	5.4	ACC9	112 \pm 2	9.27 \pm 0.04	–
4623514878053740800	TIC 261237686	J06161212-7822549	3.2	ACC7	31 \pm 3	3.9 \pm 0.3	200
5211866573733506176	TIC 261258625	J08285050-7855336	4.86	ACC9	55 \pm 2	5.3 \pm 0.1	–
5210757063422428160	TIC 261329743	J07020080-7823162	2.62	FSB1	80 \pm 5	6.6 \pm 0.1	–
5211820497324450048	TIC 261333691	J05365182-6807551	1.0	FSB1	13 \pm 1	1.7 \pm 0.2	–
5212114582325142144	TIC 261396829	J07320435-7905463	2.2	ACC9	133 \pm 8	11.3 \pm 0.1	–
5493551007411377024	TIC 262494539	J07305569-5038172	1.09	FSB1	27 \pm 2	3.6 \pm 0.6	–
5488990989093828736	TIC 262571290	J07445551-5349010	1.11	FSB1	64 \pm 2	6.1 \pm 0.1	–
5289146813645216768	TIC 262609849	J07454276-5737235	3.23	ACC7/SSB1	37 \pm 4	4 \pm 1	–
5287869146774371200	TIC 262616166	J07431898-6347492	3.94	ACC9	37 \pm 5	4.3 \pm 0.1	–
5221935282747699584	TIC 262710881	J09024868-7201389	1.08	FSB1	18 \pm 3	1.8 \pm 0.1	–
5209961257522652032	TIC 262711175	J07160773-7819063	1.35	FSB1	89 \pm 3	10.82 \pm 0.02	–
4673734762414368896	TIC 262841966	J04292453-6113075	1.01	FSB1	10 \pm 2	1.5 \pm 0.2	–
4673748712467201536	TIC 262843950	J06251211-7614059	1.84	ACC7	65 \pm 2	8.0 \pm 0.1	–
5295639013192061184	TIC 264768896	J08093672-5736302	2.9	ACC7	4.5 \pm 0.3	0.87 \pm 0.03	–
5488214665165737088	TIC 264927843	J05390699-5857269	1.92	ACC7	108 \pm 3	10.9 \pm 0.2	–
4613859688492969344	TIC 267117566	J05090299-5532417	3.73	ACC9	50 \pm 4	4.6 \pm 0.2	–
4615430993689043968	TIC 267165764	J02400109-8319396	1.33	SSB1	7 \pm 1	1.5 \pm 0.2	–
5492678888531884928	TIC 267599417	J07153794-5029550	5.39	ACC9	49 \pm 5	5 \pm 1	–
5489252256245102592	TIC 267892411	J07474063-5326054	1.49	FSB1	71 \pm 2	6.19 \pm 0.03	–
5489351182231223552	TIC 268297162	J07503474-5230329	1.06	FSB1	8 \pm 1	3 \pm 3	–
5489386332243685504	TIC 268505206	J07032962-5556535	1.49	SSB1	5.7 \pm 0.3	0.97 \pm 0.04	–
5489569847606652032	TIC 268818165	J07155038-5502420	1.06	SSB1	108 \pm 7	8.6 \pm 0.1	–
5488727449902432896	TIC 269169656	J07580115-5918060	2.64	ACC7	26 \pm 2	3.2 \pm 0.2	–
5512781500142671360	TIC 269332964	J05124991-5215242	2.62	ACC9	6 \pm 1	1.0 \pm 0.2	–
4622822804203122432	TIC 269850511	J02362966-7850515	2.08	ACC7/SSB1	63 \pm 4	5.7 \pm 0.3	–
4622043216099827072	TIC 269856685	J05001323-7818003	3.06	ACC7	46 \pm 3	4.6 \pm 0.3	–
5212222574983241984	TIC 270474308	J08023211-7730320	2.87	ACC9	70 \pm 6	6.7 \pm 0.6	–
5207729867392401792	TIC 270507871	J07100462-7054240	2.05	ACC7	41 \pm 3	4.2 \pm 0.2	–
5206213400339933696	TIC 270556746	J07421558-8133559	1.25	FSB1	7 \pm 1	1.2 \pm 0.2	–
4792742121434140672	TIC 270673370	J05443094-5047517	1.05	FSB1	7.8 \pm 0.4	1.13 \pm 0.02	–
5262595360179810688	TIC 271722585	J07534453-7230143	1.18	FSB1	110 \pm 16	9.4 \pm 0.1	–
5263740359803945728	TIC 271724362	J09141447-8039342	0.89	FSB1	43 \pm 4	4.8 \pm 0.4	–
5214125726531599360	TIC 271794326	J07580733-7318462	4.23	ACC9	50 \pm 5	4.9 \pm 0.1	81
5262693594672018944	TIC 271795775	J07035096-6028091	0.95	FSB1	8 \pm 1	1.2 \pm 0.2	–
5214054082179809408	TIC 271799985	J07264654-7627538	1.07	FSB1	53 \pm 3	5.1 \pm 0.1	–
5212973197827487616	TIC 272002251	J08154662-7555199	3.61	ACC7	72 \pm 13	6.6 \pm 0.4	–
5263064233169730176	TIC 272188405	J08283204-7309141	2.71	ACC7/SSB1	54 \pm 5	5.6 \pm 0.3	–

Table B.2. Seismic parameters for potential binary systems in *Gaia* DR3, with non-linear and acceleration solutions. (continued)

Gaia DR3	KIC/TIC	2MASS	ruwe	Type	ν_{\max} [μHz]	$\Delta\nu$ [μHz]	$\Delta\Pi_1$ [s]
5263213113916261632	TIC 272287351	J06565265-5946213	1.0	FSB1	24 \pm 2	2.86 \pm 0.02	–
5213574080932420480	TIC 272319734	J05294124-6253141	1.33	FSB1	46 \pm 3	4 \pm 1	–
5215057081599975808	TIC 272357006	J08331569-7307287	6.44	ACC9	120 \pm 10	9.7 \pm 0.7	–
5213102253005183872	TIC 272359491	J09151348-7605020	3.48	ACC7	8 \pm 1	1.4 \pm 0.3	–
5210011079142768512	TIC 272433558	J09144941-8321461	2.85	ACC9	64 \pm 11	6 \pm 7	–
5214774781989654528	TIC 272470568	J08025796-7407426	1.04	FSB1	20 \pm 3	1.9 \pm 0.3	–
4657844345523214208	TIC 277106385	J05543030-6005429	1.26	SSB1	37 \pm 3	4 \pm 9	–
5207546077152039168	TIC 277982904	J03293558-6335450	2.22	ACC7	24 \pm 3	2.9 \pm 0.2	–
5211551666731265408	TIC 278052130	J07560887-7604013	1.0	FSB1	29 \pm 3	3.5 \pm 0.2	170
5194046891861557248	TIC 278138367	J06353992-8050536	3.3	ACC9	30 \pm 2	3.8 \pm 0.2	–
5211449515229239040	TIC 278180570	J06101040-7912317	1.03	FSB1	21 \pm 2	3.7 \pm 0.2	–
5208024295990636544	TIC 278287412	J07190737-8234586	4.17	ACC7	55 \pm 4	5.5 \pm 0.6	–
5206891283618161664	TIC 278385439	J06565847-5544313	1.22	FSB1	55 \pm 7	6 \pm 1	–
5194608325693228672	TIC 278520557	J07093443-7000214	2.47	ACC7	39 \pm 4	4 \pm 1	–
5496838306658206976	TIC 278865799	J06492488-5734092	3.01	ACC7	61 \pm 7	5.9 \pm 0.1	–
5497231760022509184	TIC 278987334	J08490581-7731526	3.19	ACC9	35 \pm 3	4.1 \pm 0.1	–
5484065005200867840	TIC 279055252	J04561674-5625359	1.53	ACC7	112 \pm 19	9.1 \pm 0.3	–
5483051645196440832	TIC 279089666	J06333104-5722072	1.44	FSB1	50 \pm 5	5.3 \pm 0.4	–
5497425304132285568	TIC 279214919	J08410767-7740578	2.82	ACC7	31.76 \pm 0.04	3.7 \pm 0.3	–
5484038960518997760	TIC 279249643	J06474352-5523263	1.73	ACC7	49 \pm 4	5.2 \pm 0.2	–
5485060509900567808	TIC 279321702	J07215602-5845314	1.12	FSB1	4.0 \pm 0.3	0.68 \pm 0.02	–
5480351645196440832	TIC 279324213	J06062575-6105402	1.02	SSB1	9 \pm 2	1.4 \pm 0.5	–
5497413969715029760	TIC 279358754	J06514930-5334272	1.18	FSB1	30 \pm 3	3.6 \pm 0.6	–
5503425442164209536	TIC 279479933	J07030847-5318366	1.19	FSB1	160 \pm 3	11.0 \pm 0.2	–
549139603338918528	TIC 279515228	J04571347-7239399	1.18	FSB1	44 \pm 5	4.7 \pm 0.1	–
5490258416761559680	TIC 279516900	J07155985-5457418	1.23	SSB1	17 \pm 2	2.0 \pm 0.2	–
5479738701823690496	TIC 279615774	J02422438-7248296	7.32	ACC7	126 \pm 6	11.0 \pm 0.2	–
4722143029570673920	TIC 279673593	J03222204-7111495	1.94	ACC7	125 \pm 3	10.7 \pm 0.1	–
4672387139115873536	TIC 279728461	J04143400-6159051	1.51	SSB1	44 \pm 5	4.7 \pm 0.2	–
4642496537557475456	TIC 280095693	J06392204-7313031	3.3	ACC7	17 \pm 2	2.2 \pm 0.1	–
4639676702548772224	TIC 280096634	J04371315-7350358	3.37	ACC7	48 \pm 3	4.4 \pm 0.2	–
4647271785275998976	TIC 280833472	J02573707-6416233	1.78	ACC7	10 \pm 1	1.6 \pm 0.2	–
5505674738015141632	TIC 281430572	J05423857-6519437	1.02	FSB1	31 \pm 2	3.6 \pm 0.2	–
5292708269245134720	TIC 281496939	J04592613-5818214	2.31	ACC7	23.8 \pm 0.5	3.00 \pm 0.02	–
5209451221566295552	TIC 281978234	J03135294-8446041	2.46	ACC7	12 \pm 1	1.41 \pm 0.03	–
5217308400375689856	TIC 282089836	J09355840-7510463	1.27	SSB1	65 \pm 9	5.3 \pm 0.4	–
5217281427984292480	TIC 282090220	J09004423-7321011	0.99	FSB1	14.8 \pm 0.4	1.80 \pm 0.01	–
5512716319719058944	TIC 285924829	J07550956-6036010	2.27	ACC7	13 \pm 2	1.7 \pm 0.2	–
5487071684169825280	TIC 287275818	J07214911-5643278	1.09	SSB1	11 \pm 1	1.5 \pm 0.3	–
5210620483462625536	TIC 287530023	J08435236-7531126	2.81	ACC9	45 \pm 4	5 \pm 1	–
5219749144392700800	TIC 287591080	J07401780-5806498	1.18	FSB1	72 \pm 3	6.8 \pm 0.2	–
5219677332539908096	TIC 287717229	J08340367-7045429	2.12	ACC7	13 \pm 3	1.78 \pm 0.01	–
5220129300538538112	TIC 287774787	J08504620-6702363	3.97	ACC7/SSB1	57 \pm 6	5.4 \pm 0.5	–
5216707173676159616	TIC 287868987	J09304288-6755390	6.93	ACC9	20 \pm 2	2.54 \pm 0.03	–
520947777346026752	TIC 287955025	J09140589-7540495	2.16	ACC7	10.3 \pm 0.6	1.52 \pm 0.02	–
5216563481249944064	TIC 287978038	J09213350-6704330	1.77	ACC7	8.7 \pm 0.4	1.24 \pm 0.01	–
5215409646876021248	TIC 288060359	J09052296-7636054	0.99	FSB1	36 \pm 3	3.9 \pm 0.2	–
5291154178281296640	TIC 290156160	J06550767-4922287	2.05	ACC7/SSB1	55 \pm 4	5 \pm 4	–
5219051641705537280	TIC 290370177	J09374086-7056182	2.05	ACC7	14 \pm 1	1.7 \pm 0.2	–
4769044725277256960	TIC 290714798	J07414755-5447113	3.26	ACC7	46 \pm 6	4.9 \pm 0.1	–
4795575631617690368	TIC 290716947	J05384415-5951292	3.05	ACC7	43 \pm 5	4.4 \pm 0.4	–
4793241918187803520	TIC 290751023	J05545964-4946406	1.01	FSB1	52 \pm 4	5.2 \pm 0.3	–
5492068178541785728	TIC 291461967	J06093176-4854147	3.52	ACC9	35 \pm 5	3.4 \pm 0.4	–
5493577601848808960	TIC 291556838	J06005045-5820012	1.3	SSB1	61 \pm 3	5.2 \pm 0.1	–
5477417186100566656	TIC 293271532	J06321032-6145505	1.23	SSB1	78 \pm 6	7.0 \pm 0.1	–
5491157125781445376	TIC 294095029	J07185263-5349257	1.27	FSB1	31 \pm 3	3.8 \pm 0.4	–
5486914217785332992	TIC 294160989	J06535020-5426224	2.85	ACC7	16 \pm 2	2.2 \pm 0.1	–
5485794227753528960	TIC 294207523	J07260091-5817420	1.05	SSB1	34 \pm 3	4.1 \pm 0.3	–
5486579622653064704	TIC 294271830	J07143391-5702565	1.09	FSB1	16 \pm 2	2.0 \pm 0.2	–
5490375892707358592	TIC 294324175	J06592536-4835452	1.84	ACC7/SSB1	112 \pm 28	9.7 \pm 0.1	–
5486675761201871872	TIC 294330112	J07584833-5302179	2.9	ACC9	10 \pm 2	1.5 \pm 0.2	–
5490362698567825920	TIC 294393328	J07030454-5406583	0.99	FSB1	34 \pm 3	4.1 \pm 0.2	388
4665732826024724096	TIC 299833107	J04564990-7136586	2.87	ACC7	37 \pm 3	4.0 \pm 0.7	–
5266992856935028352	TIC 299901027	J06115330-7153506	5.77	ACC9	2.9 \pm 0.5	0.5 \pm 0.2	–
5267194136282158336	TIC 300033707	J08334313-6258284	2.29	ACC7	41 \pm 4	4.1 \pm 0.1	–
5267484304272699776	TIC 300034205	J04533050-6640314	2.44	ACC7	80 \pm 6	7.0 \pm 0.4	–
5267122908544543872	TIC 300085356	J07381462-6943004	1.01	FSB1	29 \pm 4	3.4 \pm 0.3	–
5267532094372365312	TIC 300443129	J08223299-7028596	1.49	FSB1	42 \pm 4	4.5 \pm 0.1	289
5269181606629815936	TIC 300447343	J07521166-6636093	2.06	ACC7/SSB1	30 \pm 5	3.1 \pm 0.1	–
5281221018436996864	TIC 300514120	J07462349-6536575	2.25	ACC7	42 \pm 4	4.8 \pm 0.1	–
5267699872974355456	TIC 300657225	J07495039-6927304	1.19	FSB1	5.4 \pm 0.5	0.9 \pm 0.4	–
5274872575736238208	TIC 300703597	J06385939-6508062	1.43	FSB1	16 \pm 3	2.1 \pm 0.1	–
5270676495766568320	TIC 300932817	J06351599-6242385	1.08	FSB1	6 \pm 1	1.0 \pm 0.4	–

Table B.2. Seismic parameters for potential binary systems in *Gaia* DR3, with non-linear and acceleration solutions. (continued)

Gaia DR3	KIC/TIC	2MASS	ruwe	Type	v_{\max} [μHz]	$\Delta\nu$ [μHz]	$\Delta\Pi_1$ [s]
5274200121296704512	TIC 300971433	J04161593-5913255	2.35	ACC7	30 \pm 5	3.85 \pm 0.01	–
5274276056318130816	TIC 300971919	J04530896-6336573	2.32	ACC7/SSB1	86 \pm 6	7 \pm 1	–
5223531597534254336	TIC 302049162	J07271834-6700515	2.41	ACC7	207 \pm 2	12.7 \pm 0.4	–
5223288644122939904	TIC 302138510	J09305298-7146094	2.94	ACC7/SSB1	9 \pm 2	1.36 \pm 0.03	–
5272092529306163200	TIC 302215573	J08574728-6930456	2.16	ACC7/SSB1	72 \pm 2	6.85 \pm 0.04	–
5272198494740303488	TIC 302368978	J08302999-7328313	2.53	ACC7	160 \pm 3	12.3 \pm 0.1	–
5222424183167121280	TIC 302447060	J09130899-7136229	3.62	ACC7	12 \pm 1	1.8 \pm 0.3	–
5223701300282134016	TIC 302449055	J08592837-6642531	1.06	FSB1	33 \pm 1	5.3 \pm 1.5	–
5223235867566342784	TIC 302595966	J08494880-6918287	1.79	ACC9	51 \pm 2	5.65 \pm 0.02	–
4616077197287694464	TIC 302967104	J03484586-8108559	1.48	SSB1	47 \pm 3	4.5 \pm 0.2	–
5223005004483154816	TIC 303156867	J09034278-6757029	0.97	FSB1	36 \pm 4	4.2 \pm 0.4	–
5223013663137299840	TIC 303167279	J09042039-7641484	1.46	ACC7	61 \pm 2	6.2 \pm 0.1	–
5219469215607206144	TIC 303603508	J09321150-7015322	1.1	FSB1	93 \pm 3	7.9 \pm 0.2	–
5271283258245872896	TIC 303862170	J05044499-6432448	4.34	ACC7/SSB1	46 \pm 5	4.7 \pm 0.8	–
5247618259467351552	TIC 304216188	J05363462-6329402	2.15	ACC7	35 \pm 6	4 \pm 1	–
5270772080262139520	TIC 306631417	J04211214-6749147	2.4	ACC9	85 \pm 6	7.15 \pm 0.04	–
5269735142014405632	TIC 306739511	J08361007-6759125	1.51	ACC7	37 \pm 5	4.4 \pm 0.2	271
5271183027030121984	TIC 306772169	J08532418-6537551	1.0	SSB1	50 \pm 6	5.0 \pm 1.2	55
5269442465763274368	TIC 306822746	J08485100-6837431	2.09	ACC7/SSB1	46 \pm 2	4.8 \pm 0.2	–
5221346734788172032	TIC 307157616	J08162050-7116348	0.97	FSB1	7 \pm 1	1.0 \pm –	–
5272944169780763392	TIC 307284748	J05183268-6732320	1.34	SSB1	213 \pm 12	14 \pm 1	–
52712981587535545856	TIC 307285936	J05522178-6818439	1.38	SSB1	83 \pm 4	7.3 \pm 0.6	–
5271159834206954368	TIC 307362903	J08323880-6851520	1.46	SSB1	13 \pm 1	2.2 \pm 0.3	–
5269810080605089792	TIC 307432940	–	1.13	FSB1	31 \pm 5	3.7 \pm 7.7	–
5271536829257054464	TIC 307781031	J08470668-6556183	1.34	SSB1	47 \pm 4	4.7 \pm 10.6	–
5221598144994099072	TIC 307854325	J08562544-7015498	1.67	ACC7/SSB1	39 \pm 4	4 \pm 1	–
5221584950854687488	TIC 307995562	J08381743-7050421	1.02	FSB1	4.8 \pm 0.3	0.7 \pm 0.1	–
5289900082191519488	TIC 308457039	J07115907-5654248	3.32	ACC9	39 \pm 4	3.9 \pm 0.2	–
5290143624016175232	TIC 308924932	J07562383-6022578	1.91	ACC7	105 \pm 3	9.7 \pm 0.1	–
5290060645249714176	TIC 309061659	J08205243-5953477	0.87	FSB1	12.4 \pm 0.4	1.827 \pm 0.004	–
5290127131343313280	TIC 309062385	J07334790-6154336	0.95	FSB1	5 \pm 2	1.0 \pm 0.2	–
5195885137865072256	TIC 309433242	J09061684-7847327	1.0	FSB1	34 \pm 3	4.0 \pm 0.3	257
5194953164321405568	TIC 309484023	J08390684-7958598	1.78	ACC7/SSB1	27 \pm 3	4 \pm 1	–
5277982544378055680	TIC 309551781	J08204447-6201554	1.36	FSB1	124 \pm 3	11.60 \pm 0.05	–
5195177189815490560	TIC 309580362	J09385520-8013118	2.13	ACC7	42 \pm 3	4.2 \pm 0.1	–
5276107773972764544	TIC 309623810	J08065590-7059432	2.11	ACC7	19 \pm 2	2.3 \pm 2.8	–
5277802121392594304	TIC 309781270	J08250785-6232186	1.22	SSB1	62 \pm 8	6.8 \pm 0.2	–
4760316698900404864	TIC 309790820	J08592494-6331200	2.7	ACC9	83 \pm 10	7.0 \pm 0.2	–
5301945781830996992	TIC 310210585	J07513542-5526491	1.85	ACC7/SSB1	75 \pm 5	6.3 \pm 0.3	–
5276801875049305728	TIC 310389158	J05563673-7710335	2.59	ACC7	6.4 \pm 0.4	0.97 \pm 0.03	–
5276782805393069824	TIC 310539352	J07015957-6657036	3.33	ACC9	86 \pm 7	8.1 \pm 0.9	–
4642661666163539072	TIC 314827873	J02100569-7345248	1.02	FSB1	3.6 \pm 0.3	0.7 \pm 0.1	–
5190209527561246592	TIC 317247322	J05061863-6157415	1.07	FSB1	24 \pm 4	3.3 \pm 0.2	–
5189829886809918592	TIC 317247383	J08022263-8219546	2.88	ACC7	43 \pm 6	4.6 \pm 0.2	–
5551597112457896448	TIC 319562970	J06055742-5021081	1.19	FSB1	38 \pm 3	4 \pm 1	–
5551385009793282048	TIC 319563340	J06463128-4808016	1.08	FSB1	14 \pm 2	2 \pm 1	–
5498703864355926400	TIC 319610746	J06581153-4929590	1.89	ACC7	36 \pm 3	4.1 \pm 0.4	–
5208898098497606016	TIC 322902124	J06062050-8025109	3.4	SSB1	57 \pm 4	6.1 \pm 0.2	–
5208639300948105728	TIC 322902777	J07532015-7814046	1.36	SSB1	47 \pm 3	5.0 \pm 0.2	–
5209074123437345920	TIC 323065874	J09191955-8211351	1.62	ACC7/SSB1	34 \pm 3	4.2 \pm 0.2	–
5196482584995376640	TIC 323067265	J08023568-8547552	1.69	ACC7	11 \pm 2	1.6 \pm 0.1	–
5196247358226629504	TIC 323174630	J08124632-6137352	1.32	FSB1	13 \pm 2	1.7 \pm 0.2	–
5193479715660300288	TIC 323240580	J08205769-6729532	1.06	FSB1	23 \pm 4	2.9 \pm 0.4	–
5196947433598223104	TIC 323242564	J08084690-7957496	1.93	ACC7	5 \pm 1	1.3 \pm 4.6	–
5196275155255154176	TIC 323425092	J08551773-7916530	3.41	ACC7/SSB1	45 \pm 3	5 \pm 1	–
4614493934903216000	TIC 323431850	J05513126-8011492	2.93	ACC7	82 \pm 7	6.8 \pm 0.3	–
4614272211511868160	TIC 323443202	J04065298-8211368	1.2	FSB1	34 \pm 4	3.8 \pm 0.7	–
5197085804562213376	TIC 323462634	J07293988-7952545	2.19	ACC7/SSB1	5 \pm 1	0.86 \pm 0.05	–
5197081543954913536	TIC 323624414	J08130573-6106381	1.21	FSB1	27 \pm 2	3.2 \pm 0.3	–
5202919641460671232	TIC 323731036	J07381524-5428515	1.73	SSB1	36 \pm 3	4.1 \pm 0.1	–
5203036185398111872	TIC 323875898	–	1.81	ACC7	145 \pm 4	16.0 \pm 0.1	–
5195585039910381440	TIC 323879093	J08360783-8117458	1.05	SSB1	38 \pm 4	4.3 \pm 0.1	–
5201947089063976576	TIC 323972782	J08290864-8038596	2.16	ACC9	66 \pm 2	5.7 \pm 0.2	–
5201999796905414272	TIC 323976674	J04353573-5332314	2.09	ACC7	10 \pm 2	1 \pm 1	–
5485632698326267264	TIC 339671056	J07124444-5832189	1.03	FSB1	26 \pm 2	2.8 \pm 0.1	–
5487151059462839168	TIC 339672534	J07225480-5630198	1.07	SSB1	39 \pm 3	4.2 \pm 0.3	–
5487172259421092608	TIC 339729616	J04180609-5659496	1.08	FSB1	17 \pm 3	2.2 \pm 0.4	–
5293377700027602176	TIC 339731798	J03225995-5856058	2.8	ACC7	46 \pm 4	4.6 \pm 5.2	–
5486021719284713344	TIC 339860880	J07135073-5753110	1.65	SSB1	35 \pm 3	4.0 \pm 3.8	–
5486182320999628416	TIC 339962211	J04044879-5714077	2.76	ACC7	79 \pm 10	7.2 \pm 0.2	–
5489156499952970496	TIC 340141697	J05063756-5733082	2.5	ACC9	241 \pm 23	15 \pm 999	–
5293888629338203648	TIC 340314088	J07443858-5710060	1.12	FSB1	100 \pm 13	8.3 \pm 0.7	–
5488913915902709376	TIC 340362689	J06203872-5623574	2.08	ACC7/SSB1	8.4 \pm 0.3	1.28 \pm 0.02	–

Table B.2. Seismic parameters for potential binary systems in *Gaia* DR3, with non-linear and acceleration solutions. (continued)

Gaia DR3	KIC/TIC	2MASS	ruwe	Type	ν_{\max} [μHz]	$\Delta\nu$ [μHz]	$\Delta\Pi_1$ [s]
5295457254474182656	TIC 340486978	J09173162-6449081	0.95	FSB1	3.2 \pm 0.3	0.6 \pm 0.9	–
5295135578603834496	TIC 340488243	J07563364-5559404	2.67	ACC7/SSB1	122 \pm 24	9.5 \pm 0.1	–
5295241234799574912	TIC 340635200	J08063064-5456477	2.07	ACC7	44 \pm 5	5.3 \pm 0.2	–
5295808578501403776	TIC 341265200	J07114819-6138180	2.15	ACC7	5.0 \pm 0.3	0.86 \pm 0.02	–
5296151905306402688	TIC 341417158	J08495211-6416015	1.05	SSB1	8 \pm 3	1 \pm 1	–
5294578259350299264	TIC 341489972	J07371367-5140328	2.14	ACC7	27 \pm 1	4.31 \pm 0.02	–
5294650758398245632	TIC 341490164	J09061261-6630118	1.3	SSB1	2.7 \pm 0.2	0.62 \pm 0.01	–
5290878372662419072	TIC 341555989	J07404365-5536597	1.8	ACC7	101 \pm 8	8.9 \pm 0.4	–
5294998964286027520	TIC 341622577	J03544304-5756220	2.25	ACC7/SSB1	8 \pm 1	1.35 \pm 0.02	–
5319984640172245376	TIC 341799755	J08074416-5425183	6.63	ACC9	27 \pm 2	2.70 \pm 0.05	–
5320016392870338560	TIC 341848360	J07155312-6151443	2.53	ACC7	16 \pm 2	2 \pm 1	–
5314589959391304704	TIC 342883448	J08031225-5649154	1.73	ACC7	71 \pm 5	5.7 \pm 0.2	–
5316299253296986624	TIC 342968443	J05540508-4706054	1.18	SSB1	60 \pm 4	6 \pm 1	–
5293963966641355648	TIC 344086993	J06203555-5204114	2.15	ACC7	7.7 \pm 0.5	1 \pm 1	–
5496961486320395520	TIC 348842735	J07061728-4854017	0.99	FSB1	20.8 \pm 0.2	3 \pm 1	–
5287084198549723392	TIC 348844774	J07373672-6441512	1.47	SSB1	104 \pm 8	9 \pm 1	–
5479422626590560512	TIC 348899507	J06065803-6216211	1.39	SSB1	7 \pm 1	1.2 \pm 0.3	–
5282245969431419520	TIC 349058825	J07543526-6303320	3.27	ACC7	5 \pm 1	1 \pm 2	–
5286917485099169792	TIC 349097515	J07224796-5927111	2.86	ACC9	119 \pm 6	10.1 \pm 0.1	–
5293211841273532800	TIC 349153580	J08013823-5803235	1.14	FSB1	31 \pm 4	4 \pm 1	342
5285791172876409088	TIC 349268482	J09425498-7516229	1.56	ACC7	15 \pm 3	2.1 \pm 0.6	–
5293071863996766592	TIC 349410948	J08112048-6057355	2.14	ACC7/SSB1	60 \pm 6	5.8 \pm 0.1	–
5288848502396427008	TIC 349683234	J06231070-6700193	2.46	ACC7	71 \pm 6	6.2 \pm 0.1	–
5288394404095429248	TIC 349761739	J06535882-6437160	2.36	ACC7	33 \pm 4	4.0 \pm 0.2	–
5288790365719480448	TIC 349784605	J07380563-6226019	1.27	FSB1	37 \pm 6	4.5 \pm 0.3	–
5287648076218179584	TIC 349785677	J06201674-6310478	2.23	ACC7	11 \pm 2	1.30 \pm 0.02	–
5287574134060511616	TIC 349787921	J07271419-6416211	1.06	SSB1	39 \pm 5	3.8 \pm 0.3	–
5291921018920173440	TIC 349790377	J08354550-5906589	1.15	SSB1	17 \pm 1	1.9 \pm 0.1	–
5287348115701453440	TIC 349834140	J07464982-6415305	2.97	ACC7	73 \pm 6	6.4 \pm 0.4	–
5287657215908366336	TIC 349965881	J07325036-6258226	1.15	SSB1	9 \pm 2	1 \pm 2	–
5289203404134397184	TIC 349972696	J05083414-7250153	0.98	FSB1	5.2 \pm 0.4	1.0 \pm 0.8	–
5288091900958468736	TIC 350146218	J07301502-6250149	1.44	ACC7/SSB1	38 \pm 3	4.1 \pm 0.2	–
4759817967294712064	TIC 350335258	J05115517-6039179	1.1	FSB1	123 \pm 8	11 \pm 2	–
4766589137855770624	TIC 350336507	J05495250-5623132	1.27	FSB1	4 \pm 1	1 \pm 1	–
4759773608871910144	TIC 350344410	J05313061-4940034	2.31	ACC7	19 \pm 2	2.2 \pm 0.1	–
4759940150524052352	TIC 350344761	J08351987-5907304	2.97	ACC7/SSB1	43 \pm 3	5 \pm 1	–
4759792261914375040	TIC 350432704	J04331531-5707285	3.67	ACC7/SSB1	9 \pm 2	1.3 \pm 0.2	–
4768303345202254464	TIC 350442275	J05563477-5022076	2.04	ACC7	4.4 \pm 0.3	0.78 \pm 0.02	–
4765741581893027712	TIC 350521426	J05410154-5444221	2.92	ACC7/SSB1	66 \pm 4	6.33 \pm 0.05	63
4765256151805606656	TIC 350582497	J05563690-5535001	1.0	FSB1	135 \pm 9	11 \pm 1	–
4767359513253312768	TIC 350619336	J05561659-5410005	2.36	SSB1	34 \pm 3	3.8 \pm 0.5	–
4767488469645984768	TIC 350622703	J05023489-5511163	2.0	ACC7	50 \pm 5	4.7 \pm 0.2	–
4767905321993138304	TIC 350656935	J05370077-5309557	2.13	ACC7	34 \pm 3	3.9 \pm 0.3	–
4767752902193955072	TIC 350716888	J05322973-5430002	0.98	FSB1	28 \pm 3	3.7 \pm 0.4	–
4767825401241889408	TIC 350763118	J06080543-4637577	1.32	FSB1	80 \pm 6	6.8 \pm 0.1	–
4767270010430553088	TIC 350767794	J05531934-5442530	0.98	FSB1	78 \pm 6	6.7 \pm 0.4	–
5495593242882063872	TIC 350860253	J06141137-5645143	1.1	FSB1	34 \pm 3	4.1 \pm 0.1	382
5499262798516663936	TIC 350954078	J06284984-5102461	2.49	ACC7	73 \pm 5	7.0 \pm 12.6	–
4795737362906098560	TIC 354569864	J07105747-6704014	0.98	FSB1	179 \pm 4	17.7 \pm 0.2	–
5276721679420187520	TIC 354998345	J06513181-6707262	1.59	ACC7	13 \pm 2	1.8 \pm 0.2	–
5301238520977393920	TIC 355087487	J06472164-5834572	1.69	ACC7	113 \pm 22	9.45 \pm 0.02	–
5505246100278904704	TIC 355221669	J06031755-5548253	1.68	ACC7	39 \pm 3	4.6 \pm 1.1	–
5504475445706553728	TIC 355278964	J03001697-6820048	1.77	ACC7	163 \pm 3	12.2 \pm 0.1	–
5297763686273730432	TIC 355376024	J07294212-6628058	1.65	ACC7/SSB1	125 \pm 8	10 \pm 1	–
5504223073427974272	TIC 355411527	J04305039-5301023	2.38	ACC7	24 \pm 17	3.32 \pm 0.02	–
5297689950276926720	TIC 355695859	J08162389-7942210	1.0	SSB1	45 \pm 3	4.6 \pm 0.2	–
5297383530129246464	TIC 355697718	J08485087-6416292	1.17	FSB1	5.7 \pm 0.4	0.91 \pm 0.03	–
5272574527711640704	TIC 355700618	J08351286-6314378	3.11	ACC7	73 \pm 4	7.0 \pm 0.1	–
5297439021104335104	TIC 355702219	J06581012-5346149	1.29	SSB1	68 \pm 2	6.03 \pm 0.01	–
5297789249920822016	TIC 355843133	J05402337-5937252	8.45	ACC9	48 \pm 5	5 \pm 1	–
5297393082138510208	TIC 355847385	J06583564-5407433	7.91	SSB1	9.5 \pm 0.5	1.7 \pm 0.1	–
5272499348609285632	TIC 356019770	J08183208-6637436	1.18	SSB1	75 \pm 2	6.57 \pm 0.04	–
5297546017333946880	TIC 356687683	J08541665-6505063	1.57	ACC7	33 \pm 6	3.8 \pm 0.2	–
5298164526987441792	TIC 356782955	J08175593-7854443	1.05	FSB1	12.6 \pm 0.4	1.79 \pm 0.03	–
5248371631089733760	TIC 357490822	J08485707-6519509	1.82	ACC7	36 \pm 1	3.6 \pm 0.3	–
5248735294568738432	TIC 357902723	J08480471-6432417	1.17	SSB1	5.8 \pm 0.4	1.0 \pm 0.2	–
4624577212444372224	TIC 358154073	J04380233-7548284	1.15	FSB1	53 \pm 4	5.5 \pm 0.3	–
4764502333505225088	TIC 358335780	J03460533-5658575	4.24	ACC7	11 \pm 1	2 \pm 6	–
4764411520716806016	TIC 358335984	J05528339-5502035	2.9	ACC7	44 \pm 5	4.6 \pm 0.4	–
4663125918322590208	TIC 358709248	J05372723-6347260	2.17	ACC7	35 \pm 5	4.5 \pm 0.5	–
4758887780457543168	TIC 364324970	J06102562-7630593	1.38	SSB1	6 \pm 2	1.284 \pm 0.005	–
5275326089924148352	TIC 364392239	J06321449-6724352	1.49	ACC7/FSB1	37 \pm 4	3.9 \pm 5.7	–
4628080600087737344	TIC 364424220	J05560603-5117567	1.39	FSB1	19 \pm 4	2.3 \pm 1.5	–

Table B.2. Seismic parameters for potential binary systems in *Gaia* DR3, with non-linear and acceleration solutions. (continued)

Gaia DR3	KIC/TIC	2MASS	ruwe	Type	ν_{\max} [μHz]	$\Delta\nu$ [μHz]	$\Delta\Pi_1$ [s]
4646368845711415936	TIC 370010028	J06553566-6947096	4.13	ACC7	65 \pm 2	6.19 \pm 0.04	–
4655789323906870400	TIC 370115081	J04364524-6657221	0.98	FSB1	35 \pm 2	4.0 \pm 0.1	–
5262366421243256704	TIC 370236614	J07464889-7314255	2.65	ACC7	39 \pm 4	3.8 \pm 0.1	–
4620512386675622784	TIC 370237878	J07034621-7147587	2.84	ACC7	9.0 \pm 0.3	1.35 \pm 0.02	–
5246869251530754688	TIC 370334476	J08555892-6846103	1.1	SSB1	5 \pm 1	1.0 \pm 1.2	–
5246893127247160960	TIC 370371011	J04493959-6516019	2.01	ACC7	38 \pm 4	3.4 \pm 0.2	–
5219576074394110976	TIC 370433620	J07125499-6041165	1.16	SSB1	11 \pm 1	1.66 \pm 0.03	–
5219305280994582400	TIC 370700642	J09242821-7427134	2.48	ACC7	38 \pm 4	4.65 \pm 0.03	–
5243400361063781120	TIC 370701760	J09083981-6824357	2.27	ACC7	6.1 \pm 0.4	1.07 \pm 0.03	–
5218479448982842496	TIC 370752695	J09172641-7057485	1.16	FSB1	140 \pm 3	14.1 \pm 0.1	–
5478306927228809856	TIC 372850505	J05441525-6808053	1.22	SSB1	17 \pm 2	2.4 \pm 0.2	–
4657954193667549184	TIC 373927033	J05372649-7527010	2.87	ACC7/SSB1	21 \pm 2	3 \pm 1	–
5284590746696865536	TIC 375037249	J06535822-6304448	1.11	FSB1	30.6 \pm 0.3	3.39 \pm 0.03	–
5479827453027856384	TIC 375056443	J06561919-6212422	2.63	ACC7	26 \pm 4	3 \pm 1	–
4794300988403882496	TIC 375091650	J05262443-5018506	1.2	SSB1	53 \pm 4	5.0 \pm 0.1	–
479418959771929600	TIC 375149326	J03403364-5610434	3.14	ACC9	104 \pm 7	8.5 \pm 0.1	–
4792616158632718976	TIC 375150124	J05490830-5126574	1.08	FSB1	39 \pm 5	4.2 \pm 0.5	–
5220501794463126528	TIC 375177123	J08522248-7200128	1.21	FSB1	135 \pm 3	9.5 \pm 0.1	–
4798631792907566848	TIC 376984532	–	2.51	ACC7	84 \pm 2	7.6 \pm 0.1	–
4624267974799199360	TIC 376984837	J04070410-7733586	1.4	SSB1	9 \pm 2	1.1 \pm 0.2	–
4621608221812179456	TIC 377016448	J04371534-7927332	5.33	ACC9	31 \pm 4	3.1 \pm 0.4	–
5491614320757636864	TIC 380027093	J04371816-7228366	0.95	FSB1	68 \pm 22	5.6 \pm 0.2	–
4763855648869575808	TIC 381950542	J04052368-5340400	3.45	ACC7	17 \pm 2	2.1 \pm 0.2	–
4763109076178022784	TIC 381979348	J05190132-5701503	1.22	FSB1	7 \pm 1	1.3 \pm 0.3	–
4763426731958850688	TIC 382030284	J06005526-5454490	1.71	ACC7	31 \pm 3	4 \pm 1	294
4763554000429667456	TIC 382069031	J05473867-5825383	1.07	FSB1	74 \pm 7	6.3 \pm 0.1	–
4763335923467190784	TIC 382145042	J05044080-5530045	1.12	FSB1	37 \pm 5	4.1 \pm 0.6	–
4762746202980936064	TIC 382160429	J05213840-5735326	2.26	SSB1	9 \pm 1	1.5 \pm 0.4	–
4769468960670370432	TIC 382201415	J07280597-5110344	1.95	ACC7	34 \pm 5	4.0 \pm 0.2	301
4770057268110576768	TIC 382246176	J07124162-5240521	3.19	ACC7/FSB1	94 \pm 6	8.5 \pm 0.2	–
4768544653645049344	TIC 382267999	J07231937-7235203	1.0	FSB1	31 \pm 3	3.7 \pm 0.1	–
5289082664014092160	TIC 382438298	J05351522-7108155	1.08	SSB1	5.0 \pm 0.3	1 \pm 1	–
5289385201509970048	TIC 382513483	J07490672-5624372	4.89	ACC9	110 \pm 9	8.5 \pm 0.2	–
5289095617636349184	TIC 382515733	J07300520-6417109	2.04	ACC7	34 \pm 3	3.8 \pm 0.1	–
5275489333041399040	TIC 382571748	J06595564-6441561	0.86	FSB1	5.2 \pm 0.4	1.0 \pm 1	–
5288057987896325376	TIC 382629445	J07323201-6413567	1.5	ACC7/SSB1	106 \pm 6	8.0 \pm 0.1	–
4653847517645638656	TIC 388107420	J04195966-6923554	1.77	ACC7/SSB1	35 \pm 4	4 \pm 4	–
4668185595948376960	TIC 388130365	J07530079-6707140	1.99	ACC7/SSB1	80 \pm 9	8 \pm 1	–
4619204929911561600	TIC 388197254	J05012723-6706191	1.08	SSB1	59 \pm 2	6.91 \pm 0.02	–
5202020412748178944	TIC 388238367	J09273418-7753194	1.29	SSB1	3.2 \pm 0.5	0.54 \pm 0.02	–
5193839221602761984	TIC 388241213	J08040367-6836483	1.16	FSB1	9 \pm 1	1.29 \pm 0.03	–
4659284396506303104	TIC 389434570	J05532100-4710142	0.75	FSB1	58 \pm 9	6 \pm 2	–
4794905852941884544	TIC 389858283	J03281729-5752558	1.6	ACC7	3.1 \pm 0.2	0.52 \pm 0.02	–
5263537229328779136	TIC 391901960	J05193476-7146023	3.58	ACC9	72 \pm 2	8 \pm 2	–
5212605548626868736	TIC 391925320	J07050966-7535322	1.74	ACC7/SSB1	88 \pm 7	8.0 \pm 0.1	–
5262547153466831616	TIC 391947348	J07244001-7342376	1.15	FSB1	30 \pm 2	4.0 \pm 0.3	–
4623634243784876800	TIC 392012013	J04415134-7733380	3.43	SSB1	33 \pm 3	3.44 \pm 0.05	–
463262288780311680	TIC 394339943	J06440317-7239417	2.35	ACC7	13 \pm 1	1.6 \pm 0.4	–
4619779424736847360	TIC 394342862	J03194321-6223378	3.21	ACC7/SSB1	44 \pm 7	4.8 \pm 0.1	–
4618947747269568256	TIC 394358831	J05122576-8132305	1.89	ACC7	35 \pm 13	5.1 \pm 0.4	–
5216429130374974848	TIC 397136227	J09295135-6806095	2.57	ACC7	35 \pm 4	3.9 \pm 3.9	–
5217241227089989504	TIC 397187975	J08594248-7343292	0.96	FSB1	20 \pm 3	2 \pm 1	–
4620697620025724544	TIC 400733105	J05555844-7931278	1.53	ACC7	39.7 \pm 0.4	4.6 \pm 0.1	–
4653097307122838016	TIC 407615866	J07375852-6722352	1.28	FSB1	11 \pm 1	1.6 \pm 0.5	–
4652654272654721280	TIC 407616368	J05223620-8300143	6.89	ACC9	50 \pm 4	5.2 \pm 0.1	–
4652547757463936640	TIC 407616488	J02543941-8159071	4.47	ACC9	21 \pm 3	2.6 \pm 0.4	–
4652253152771108224	TIC 407622294	J04142585-7338423	2.36	ACC9	91 \pm 9	8.2 \pm 0.1	–
4614267847825117952	TIC 410389666	J03172327-8407310	1.42	FSB1	96 \pm 3	8.3 \pm 0.2	–
4639991021139156352	TIC 426016293	J02415382-7514171	1.84	ACC7	52 \pm 6	5.1 \pm 0.5	–
4640872661962787968	TIC 426033055	J03302821-7204143	1.19	SSB1	47 \pm 3	4.9 \pm 0.2	–
4642094769136524288	TIC 431479837	J04371212-7330456	2.0	ACC7	64 \pm 2	5.95 \pm 0.02	–
5493720400922804864	TIC 445457581	J06050554-5719183	1.1	FSB1	33 \pm 1	4.59 \pm 0.05	–
4792711816144840576	TIC 452358322	J07143876-5014215	2.15	ACC7	33.8 \pm 0.5	3.3 \pm 0.2	–
5218937017617971840	TIC 452384679	J09183383-7053491	0.92	FSB1	13 \pm 1	1.9 \pm 0.2	–
5216015718301763072	TIC 452409532	J09113223-7553255	1.18	FSB1	50 \pm 5	5.0 \pm 0.3	361
5215816156940715392	TIC 452422606	J08314463-7451179	1.58	ACC7	114 \pm 5	8 \pm 999	–
5216262606059199488	TIC 452439271	J08480822-7457518	6.06	ACC9	31 \pm 5	3.7 \pm 0.2	–
5216268983933366272	TIC 452475855	J09183461-7421455	0.97	SSB1	141 \pm 3	11.6 \pm 0.1	–
5217706457948985472	TIC 452521916	J07391819-7732129	2.08	ACC7	15.4 \pm 0.4	1.80 \pm 0.02	–
5203898550407467776	TIC 452626114	J07574773-7653549	2.49	ACC7	40 \pm 4	4.2 \pm 0.2	–
5217423539862739968	TIC 452630986	J07000099-5048386	1.3	FSB1	57 \pm 5	6.0 \pm 0.7	–
521827397747029632	TIC 452674187	J09403084-7148164	1.09	FSB1	166 \pm 15	11.6 \pm 0.1	–
5205403128991120768	TIC 452682649	J06510810-5115536	1.95	ACC7	79 \pm 2	7.2 \pm 0.1	–

Table B.2. Seismic parameters for potential binary systems in *Gaia* DR3, with non-linear and acceleration solutions. (continued)

Gaia DR3	KIC/TIC	2MASS	ruwe	Type	ν_{\max} [μHz]	$\Delta\nu$ [μHz]	$\Delta\Pi_1$ [s]
5218405541186313984	TIC 453214606	–	1.59	ACC7	8 ± 1	1.2 ± 0.3	–
4655968750454788096	TIC 29780874	J05345305-8534269	2.37	ACC7	–	–	–
4661781731011633920	TIC 30110465	J06165168-7648066	3.28	ACC7	–	–	–
4676752750034268160	TIC 38574156	J03141606-7453110	0.96	FSB1	–	–	–
4677908504257062272	TIC 38814392	J08493960-6310551	3.84	ACC9	–	–	–
4644341586788077440	TIC 50347845	J02511217-7057355	1.25	FSB1	–	–	–
4761178200617028992	TIC 55401680	J05110355-5741591	1.36	SSB1	–	–	–
4664821090369171072	TIC 55602824	J05425215-6127545	2.48	ACC9	–	–	–
5302422591921453184	TIC 118083037	J05072546-7816135	1.2	SSB1	–	–	–
5302783231737426688	TIC 118415674	J04404585-6916432	1.26	FSB1	–	–	–
4651422476046772608	TIC 140973799	J03594530-7212144	1.62	ACC7	–	–	–
4651109596266452608	TIC 141184207	J04024443-7435268	1.83	ACC7/SSB1	–	–	–
5260414822463795584	TIC 142109390	J06253147-7700018	6.67	ACC9	–	–	–
5280320724573054848	TIC 167306447	J07500953-6208487	2.11	ACC7	–	–	–
4658903450103813120	TIC 179240913	J05243272-7618311	0.86	FSB1	–	–	–
4791870277432435712	TIC 219150014	–	2.04	ACC7/SSB1	–	–	–
4773443335904067584	TIC 219418125	J06555265-4908583	2.59	ACC7	–	–	–
4764702169743425664	TIC 220476340	J06431284-5557525	4.35	ACC7	–	–	–
5551493307392086528	TIC 237953677	J06354566-4716550	1.15	SSB1	–	–	–
5498733349308368000	TIC 237977386	J06063882-5606023	1.02	FSB1	–	–	–
5501933374822142976	TIC 238015657	J06345197-5316548	2.46	ACC9	–	–	–
5497700701732025216	TIC 238027284	J06445014-4933180	2.18	ACC7	–	–	–
5497482620472227200	TIC 238069034	J06484456-5224141	0.95	FSB1	–	–	–
5504938404523017088	TIC 238087839	J07230868-5051213	0.98	FSB1	–	–	–
4628997008669603200	TIC 238225417	J03060196-7503181	1.9	ACC7	–	–	–
5500913642212236544	TIC 238952289	J06362306-5056084	1.07	FSB1	–	–	–
4647070540288380416	TIC 259929806	J02570124-6302056	1.91	ACC7/SSB1	–	–	–
5499778641268753280	TIC 260353824	J06211242-5244460	1.42	SSB1	–	–	–
5496192206137947264	TIC 260369469	J05270908-5610041	2.55	ACC7	–	–	–
4623692449181297024	TIC 261237085	J05542343-8403233	3.92	ACC7/SSB1	–	–	–
4640780543503766400	TIC 267114873	J03345318-7207104	1.11	FSB1	–	–	–
4499432786609919232	TIC 268432384	J08013180-5814222	2.33	ACC7	–	–	–
5792747893870047104	TIC 270626764	J05363956-4915428	1.07	FSB1	–	–	–
4768074470688913408	TIC 270677206	J04084767-6017476	2.31	ACC9	–	–	–
5213835833419224064	TIC 272233070	J08235472-7508225	1.77	ACC7/SSB1	–	–	–
4651086162959874304	TIC 277015270	J05340323-5235591	0.99	SSB1	–	–	–
5194716219564918528	TIC 278197936	J06554251-8050166	1.91	ACC7	–	–	–
5208317556357601024	TIC 278293328	J08463603-8107237	2.27	ACC7	–	–	–
5208547491726818688	TIC 278542508	J07101080-8344353	3.25	ACC9	–	–	–
5483224462920921728	TIC 278683066	J06510278-5802412	1.22	SSB1	–	–	–
5483533391328605696	TIC 278823077	–	2.09	ACC7/SSB1	–	–	–
5483398460636302208	TIC 278989213	J07471539-5326589	2.02	ACC7/SSB1	–	–	–
5483977971983639040	TIC 279089558	J06535156-5625493	1.0	SSB1	–	–	–
5484888848647307008	TIC 279216292	J02232209-7655531	1.03	SSB1	–	–	–
4671983034232400000	TIC 279728136	J03285859-6357422	1.04	FSB1	–	–	–
4642392049593036800	TIC 280095907	J05581147-7614120	1.55	ACC7	–	–	–
5209445105532925568	TIC 282052909	J09133614-7944387	2.18	ACC7	–	–	–
5216436796894846592	TIC 282054485	J08505092-7557176	1.22	SSB1	–	–	–
5508559925245505024	TIC 284344740	J05582166-7358421	1.16	SSB1	–	–	–
5220106760550184064	TIC 287837391	J09374327-7009036	6.37	ACC9	–	–	–
5220143864770280320	TIC 287874790	J08535724-6638563	4.69	ACC7/SSB1	–	–	–
5215407482212472192	TIC 288028377	J08355355-7739497	2.13	ACC7	–	–	–
5215409853034473728	TIC 288105905	J09062694-7635116	1.18	FSB1	–	–	–
4794011748125962624	TIC 290716422	J05372771-4712040	1.56	FSB1	–	–	–
5493300215680701312	TIC 291635130	J07254540-5148252	0.98	FSB1	–	–	–
5486952838131834624	TIC 294275677	J07181701-5559229	1.09	FSB1	–	–	–
5490361152379608576	TIC 294393245	J07094358-5457396	1.01	FSB1	–	–	–
5281317294423579520	TIC 300037774	J06103646-6757404	1.06	FSB1	–	–	–
5264427833746553088	TIC 300385358	J04551461-7155566	2.41	ACC7	–	–	–
5264430921825651072	TIC 300385370	J05123299-7226105	2.12	ACC7	–	–	–
5224168249125783040	TIC 302657125	J04413136-8545398	1.23	FSB1	–	–	–
5222161198027363840	TIC 302798090	J09013717-7044525	4.5	SSB1	–	–	–
5223837437865753856	TIC 302954083	J04513165-8539571	1.04	SSB1	–	–	–
5248158394553198208	TIC 303004627	J09133809-6511544	0.99	SSB1	–	–	–
5219475022402163584	TIC 303694038	J08210598-7444270	1.06	FSB1	–	–	–
5246716178895997824	TIC 304025532	J09295859-6759215	1.08	FSB1	–	–	–
5246762049146633728	TIC 304212423	J09072231-6834435	1.12	FSB1	–	–	–
5246866056075026816	TIC 304345412	J09262676-6634223	2.31	ACC7	–	–	–
5271603693307818880	TIC 307923655	J04161325-7107187	2.6	ACC7	–	–	–
5289670696577237632	TIC 308923835	J06552659-5720508	1.67	ACC7	–	–	–
5277557376973778048	TIC 308995524	J07102852-6535324	1.44	ACC7	–	–	–
5290486499846722432	TIC 309064008	J08114694-5501566	1.9	ACC7/SSB1	–	–	–

Table B.2. Seismic parameters for potential binary systems in *Gaia* DR3, with non-linear and acceleration solutions. (continued)

Gaia DR3	KIC/TIC	2MASS	ruwe	Type	ν_{\max} [μHz]	$\Delta\nu$ [μHz]	$\Delta\Pi_1$ [s]
5196790448251335552	TIC 309432609	J05090543-5610336	2.05	ACC7	–	–	–
5290315835027393280	TIC 309554989	J05571935-6543530	1.24	SSB1	–	–	–
5302236808815091840	TIC 309784425	–	2.6	ACC7	–	–	–
5278130531770906368	TIC 309926820	J08263111-6103378	0.94	FSB1	–	–	–
4679466619609262976	TIC 319258490	J05470569-6249018	2.03	ACC7	–	–	–
4614138277251688960	TIC 325562463	J06092804-8358502	2.16	ACC7	–	–	–
5487527092439863168	TIC 339885998	J06174632-4914521	1.64	ACC7/SSB1	–	–	–
5487983424125398016	TIC 340320603	J07435640-5824333	1.9	ACC7	–	–	–
5291536769670383744	TIC 341489024	J07500542-6108050	2.26	ACC7	–	–	–
5291720662990850816	TIC 342006398	J06383663-6127122	3.09	ACC9	–	–	–
5319265632588136192	TIC 342171209	J02282717-7430218	1.73	ACC7	–	–	–
5315850824349914240	TIC 342834576	J07052202-5923283	2.63	ACC7/FSB1	–	–	–
5314582262810172160	TIC 342883798	J06370238-8319297	1.04	FSB1	–	–	–
5292856703315596160	TIC 349269343	J07220761-6037476	1.9	ACC7	–	–	–
5288386535714453888	TIC 349575671	J07484713-6213134	1.32	SSB1	–	–	–
5292742938222042240	TIC 350031646	J08222631-5847545	1.49	ACC7	–	–	–
4765832811294366080	TIC 350653244	J07271140-5518163	2.84	ACC7	–	–	–
5500307643801082624	TIC 350858688	J05502285-5346427	2.79	ACC9	–	–	–
5300816239793218688	TIC 355006005	J09273212-6826113	1.24	SSB1	–	–	–
5272521235762178048	TIC 355539266	–	0.98	FSB1	–	–	–
5301418050612344832	TIC 356092254	–	1.52	ACC7/SSB1	–	–	–
5296547248456763904	TIC 356204615	J08435021-6315034	2.39	ACC7	–	–	–
5296809481981345536	TIC 357725483	J08384994-6322362	3.03	ACC7	–	–	–
4779688444510804864	TIC 358288261	J04323721-5052455	1.19	FSB1	–	–	–
5290933348242363392	TIC 358466399	J08133140-6002001	2.38	ACC7	–	–	–
5248724333810560128	TIC 358868488	J07594233-5504205	1.22	SSB1	–	–	–
4639718415271165824	TIC 370138769	J03012829-7313485	1.04	SSB1	–	–	–
5219162245703744896	TIC 370328820	J09345652-7540108	4.98	ACC9	–	–	–
5218471443165599232	TIC 371235833	J09081107-7210218	1.4	SSB1	–	–	–
4758873074489717248	TIC 374859387	J06180443-7638308	1.08	SSB1	–	–	–
4755845015169829632	TIC 374942083	J08381778-5822203	1.08	FSB1	–	–	–
4764681519540571520	TIC 381925580	J05371899-5636218	1.02	FSB1	–	–	–
4769386054918213376	TIC 382157562	J05243796-5035409	1.01	FSB1	–	–	–
4730064495451694592	TIC 382424067	J07160306-5743006	1.56	ACC7	–	–	–
5290923555717110400	TIC 382631928	J06193340-4940328	1.56	ACC7/SSB1	–	–	–
4618724168452172928	TIC 394343471	J05060113-7040561	1.16	FSB1	–	–	–
5206163956676376320	TIC 404709506	J06003395-7913146	2.43	ACC9	–	–	–
5493610071801733760	TIC 445325068	J05000846-5013171	2.78	ACC7	–	–	–
5493486857779946112	TIC 445516540	J07264806-5122507	1.05	FSB1	–	–	–
5203241008094891392	TIC 452532108	J07405692-5319194	1.76	SSB1	–	–	–
5218050776887463040	TIC 453266469	J09455152-7131149	1.01	FSB1	–	–	–
2106015055861957888	KIC 7948193	J19081539+4343599	1.12	FSB1	112 ±2	9.07 ±0.03	–
2082203924676158336	KIC 9181877	J20020952+4530259	2.06	SSB1/ACC7	–	–	–
2130855188197597184	KIC 10198347	J19102813+4716385	2.37	ACC7	42 ±2	4.4 ±0.4	–
3116645737061826944	TIC 42436617	J06254713-0353203	4.24	ACC9	–	–	–
2164981623949160960	TIC 63445000	J21195800+4838052	3.24	ACC7	–	–	–
5032718162056733824	TIC 63798520	J00554390-2753371	3.67	SSB1	–	–	–
2003282255649179392	TIC 64366713	J22321871+5402126	2.37	ACC7	–	–	–
2999159140060320128	TIC 67262475	J05582039-1052292	1.45	ACC7	–	–	–
4547035804164877824	TIC 165509120	J17183979+1617000	2.65	ACC9	–	–	–
4892933366168367872	TIC 178871420	J04280319-2559322	2.31	SSB1/ACC7	–	–	–
3223184531138993280	TIC 199823594	J05402438-0204200	1.35	FSB1	–	–	–
1125337614021152256	TIC 207339706	J09003272+7525449	9.31	ACC9	–	–	–
3127391779597616000	TIC 237415575	J06492944+0341302	2.07	ACC7	–	–	–
4575184916742587008	TIC 257530105	J17130948+2755561	1.1	SSB1	–	–	–
1205269051344217088	TIC 284428523	J16072217+2149214	4.76	ACC9	–	–	–
3241986626651247360	TIC 284858336	J05080497+0753541	25.52	ACC9	–	–	–
2170445612615808512	TIC 289966090	J21034762+5317094	2.27	ACC7	–	–	–
2124678475467156992	TIC 298554304	J18065346+5049219	10.17	ACC7	–	–	–
3388785550811667072	TIC 311362722	J05124311+1322212	1.88	ACC7	–	–	–
2147817903832181632	TIC 359634548	J18425630+5527047	5.41	ACC7	–	–	–
2162139936140541952	TIC 468581123	J20562444+4354024	1.6	SSB1/ACC7	–	–	–

Table B.3. APOGEE radial velocity measurements for *Gaia* DR3 binaries.

KIC	2MASS	$P_{\text{orb,DR3}}$ [d]	N	ΔT [d]	σ_{RV} [km/s]	mean ΔRV [km/s]	Binary [d]
2991448	J19271797+3806475	3328.4	2	16	0.064	0.013	x
2991448	J19271797+3806475	1201.2	2	16	0.064	0.013	x
3630240	J19060409+3843351	561.8	5	11	0.209	0.024	x
3730801	J19042876+3848423	57.6	3	31	6.804	0.019	x
3942719	J19115818+3902135	339.3	3	31	0.828	0.018	x
3952580	J19240489+3900592	45.7	2	16	19.004	0.014	x
4446300	J19012602+3933549	104.7	3	31	0.751	0.011	x
4914923	J19163489+4002501	99.2	2	74	4.068	0.009	x
6933899	J19065834+4226082	4063.7	2	26	0.005	0.011	
6947945	J19262433+4229049	110.6	2	43	12.901	0.015	x
7206837	J19350373+4244165	4.1	2	43	0.442	0.018	x
7668623	J19050258+4322466	4.8	3	427	39.705	0.014	x
7669332	J19062757+4322023	16.1	2	9	36.882	0.014	x
8016496	J19072417+4348317	711.7	2	427	0.205	0.024	x
8408931	J18440812+4426509	18.6	3	4	9.897	0.017	x
8414062	J18561527+4427183	791.4	5	19	0.212	0.046	x
8677016	J19050879+4448309	347.4	5	19	0.652	0.038	x
8738809	J18591050+4457017	762.5	5	19	0.229	0.016	x
9204313	J18590801+4540561	1072.9	5	19	0.041	0.019	
9328372	J18584987+4550576	95.9	3	19	1.071	0.075	x
9390670	J18594346+4557377	1041.9	5	19	0.164	0.019	x
9693187	J18510009+4625209	103.8	2	1	0.371	0.021	x
9897838	J19383112+4647332	630.0	6	42	0.140	0.026	x
10355856	J19501427+4728252	4.5	3	2	12.849	0.020	x
10775748	J18445125+4806250	6.5	2	1	15.469	0.047	x
11507653	J19280539+4924572	180.9	3	4	5.412	0.018	x
12317678	J19463773+5101135	80.8	2	5	1.992	0.024	x
2016676	J19274515+3727100	842.5	2	1	0.011	0.015	
2167774	J19321701+3731246	137.0	2	16	0.653	0.004	x
2422539	J19041102+3746108	118.3	5	11	3.122	0.008	x
2438368	J19211415+3746578	645.9	2	1	0.002	0.010	
2443035	J19252964+3744385	181.6	2	1	0.249	0.021	x
2449020	J19304378+3745086	310.2	2	1	0.055	0.017	x
2695592	J19064544+3754106	823.6	2	1	0.033	0.023	
2991448	J19271797+3806475	3328.4	2	16	0.064	0.013	x
2991448	J19271797+3806475	1201.2	2	16	0.064	0.013	x
3222519	J19111347+3820199	638.5	5	11	0.129	0.004	x
3439353	J19205281+3830283	522.2	2	16	0.182	0.014	x
3454626	J19363912+3834080	57.6	2	2	3.276	0.017	x
3458643	J19401962+3831015	399.5	3	53	2.190	0.004	x
3532734	J19111567+3838265	49.5	2	31	0.046	0.016	
3553435	J19344010+3840524	113.0	4	12	9.232	0.038	x
3630240	J19060409+3843351	561.8	5	11	0.209	0.024	x
3663047	J19423515+3846510	275.9	3	5	0.588	0.021	x
3833819	J19032549+3856334	327.3	3	31	0.900	0.013	x
3836911	J19083005+3854427	105.2	2	1	1.486	0.012	x
3847697	J19224762+3859230	889.5	3	40	1.016	0.008	x
3857864	J19334713+3854105	1277.4	4	12	0.126	0.008	x
3862485	J19381848+3858427	705.9	3	5	0.300	0.023	x
3869326	J19440792+3856121	732.5	3	53	2.018	0.006	x
3958615	J19303237+3901286	4.3	2	1	0.026	0.018	
3963755	J19354697+3905234	732.2	3	2	0.090	0.030	x
4042863	J19084656+3908428	183.8	5	11	0.564	0.015	x
4055294	J19241086+3907357	773.5	2	16	0.274	0.004	x
4056014	J19245972+3911026	797.8	2	1	0.085	0.008	x
4058998	J19281100+3911320	544.1	2	16	1.134	0.007	x
4064179	J19332703+3909019	611.0	2	2	0.003	0.005	
4065054	J19342059+3911303	1256.1	3	5	0.032	0.016	
4072847	J19414610+3909441	837.9	3	5	0.030	0.007	x
4073771	J19422940+3909088	889.5	4	12	0.194	0.033	x
4135933	J18584130+3917235	151.2	3	31	0.115	0.005	x
4159982	J19284176+3917395	1001.7	5	13	0.193	0.039	x
4242873	J19005046+3921272	56.7	5	11	4.047	0.023	x
4283451	J19452429+3921440	225.9	3	28	1.768	0.096	x
4346953	J19023044+3924283	1128.9	5	11	0.117	0.008	x

Table B.3. APOGEE radial velocity measurements for *Gaia* DR3 binaries (cont.)

KIC	2MASS	$P_{\text{orb,DR3}}$ [d]	N	ΔT [d]	σ_{RV} [km/s]	mean ΔRV [km/s]	Binary [d]
4470280	J19325679+3931207	701.7	2	2	0.037	0.015	
4480938	J19430914+3932335	923.6	4	28	0.343	0.008	x
4543371	J19011769+3938293	3.1	3	31	0.030	0.015	
4568872	J19344311+3936355	79.9	3	5	0.419	0.020	x
4570120	J19355625+3939394	348.4	3	28	0.391	0.008	x
4644949	J19151456+3947520	217.4	2	74	14.214	0.013	x
4669400	J19420788+3947570	1065.3	3	5	0.015	0.010	
4758020	J19392385+3952379	290.4	3	5	0.288	0.025	x
4761037	J19421008+3953561	1.3	2	2	0.072	0.020	x
4761037	J19421008+3953561	874.7	2	2	0.072	0.020	x
4930617	J19345069+4004116	1024.5	2	2	0.182	0.012	x
5005508	J19202288+4009407	1234.7	2	1	0.052	0.007	x
5023931	J19405704+4010068	209.4	3	28	8.863	0.015	x
5025895	J19421683+4008114	538.6	3	5	0.642	0.014	x
5087190	J19115123+4013021	959.4	2	1	0.023	0.018	
5290071	J19431995+4025391	1005.8	2	2	0.003	0.034	
5360757	J19250988+4030412	57.1	2	74	2.048	0.009	x
5369569	J19352717+4033204	260.0	4	12	1.738	0.017	x
5382824	J19475490+4032009	653.3	2	38	0.985	0.006	x
5395743	J19582034+4032579	199.6	3	5	0.132	0.005	x
5439339	J19155185+4040542	98.0	2	74	11.753	0.009	x
5446355	J19244093+4037109	822.4	2	74	1.969	0.014	x
5449290	J19282423+4041569	995.8	2	43	0.491	0.005	x
5534910	J19285814+4046073	852.0	2	43	0.021	0.006	x
5630215	J19391015+4049146	285.7	3	2	0.047	0.015	x
5650920	J19570728+4050462	530.3	3	5	0.054	0.016	x
5706724	J19285078+4054466	462.1	2	43	1.369	0.015	x
5707338	J19293455+4054186	885.2	2	43	0.084	0.006	x
5793427	J19302545+4105344	1097.4	2	43	0.275	0.014	x
5795626	J19330865+4103086	672.9	2	43	0.478	0.005	x
5808444	J19460744+4103253	490.7	3	5	0.100	0.007	x
5976532	J19450026+4116054	690.0	3	5	0.212	0.007	x
6032639	J19141495+4118432	979.8	2	74	0.876	0.011	x
6211965	J19355461+4135577	1182.0	2	43	0.825	0.009	x
6227242	J19504089+4133247	88.3	2	38	1.611	0.018	x
6271732	J19075561+4136535	1136.2	2	26	0.103	0.005	x
6302852	J19465188+4140126	396.1	2	38	2.315	0.011	x
6590195	J19053056+4203223	55.9	2	26	14.478	0.009	x
6851499	J19122254+4223498	434.3	2	26	1.964	0.006	x
6933666	J19063556+4228102	48.3	2	26	6.341	0.010	x
6951289	J19303877+4225194	552.9	4	228	6.674	0.019	x
7018515	J19055785+4230512	498.3	2	9	1.397	0.011	x
7020972	J19101321+4235287	605.9	2	26	1.419	0.008	x
7025377	J19164706+4231499	1196.1	2	26	0.192	0.005	x
7103951	J19082415+4238093	642.6	2	26	1.425	0.003	x
7191496	J19160765+4246319	803.5	2	26	0.091	0.133	
7348978	J19082289+4259192	307.3	2	9	1.875	0.003	x
7366321	J19313409+4255245	749.1	2	43	0.650	0.013	x
7499531	J18414542+4308496	116.4	3	4	0.481	0.018	x
7531332	J19313658+4309553	81.9	2	43	4.337	0.007	x
7595572	J19095280+4316024	684.7	2	9	0.038	0.006	x
7596350	J19111479+4315088	646.5	2	26	0.840	0.012	x
7661609	J18495226+4320427	106.6	3	4	0.537	0.005	x
7668623	J19050258+4322466	4.8	3	427	39.705	0.014	x
7768447	J19464078+4328213	122.3	2	3	2.040	0.010	x
7820868	J19250515+4335467	989.0	2	84	0.363	0.053	x
7880893	J19112795+4336547	130.2	2	9	0.826	0.007	x
7983221	J19544857+4343055	331.8	2	5	0.192	0.009	x
8093934	J19215733+4359243	675.0	4	3	0.038	0.074	
8098590	J19284090+4355434	837.5	2	1	0.033	0.020	
8127707	J20015409+4358014	118.7	2	24	7.228	0.013	x
8181509	J19473900+4404373	1039.3	2	62	0.231	0.009	x
8192056	J19580204+4401225	883.3	3	2	0.036	0.003	x
8217125	J18574847+4410284	862.6	3	10	0.137	0.018	x
8225926	J19163464+4409268	1085.4	2	84	0.741	0.026	x
8230578	J19231486+4406148	557.6	2	1	0.070	0.012	x

Table B.3. APOGEE radial velocity measurements for *Gaia* DR3 binaries (cont.)

KIC	2MASS	$P_{\text{orb,DR3}}$ [d]	N	ΔT [d]	σ_{RV} [km/s]	mean ΔRV [km/s]	Binary [d]
8260453	J19592289+4408304	1313.2	2	5	0.039	0.007	x
8328348	J20012933+4417205	579.2	2	24	1.819	0.010	x
8358665	J19170268+4422390	148.0	2	1	0.023	0.011	
8363272	J19235349+4418479	937.5	2	1	0.029	0.008	x
8365782	J19273691+4423124	702.8	2	1	0.041	0.005	x
8410006	J18470819+4426322	437.1	3	4	0.045	0.010	x
8458459	J20003730+4426278	890.5	2	24	0.323	0.012	x
8494839	J19263774+4434325	233.6	2	84	12.029	0.042	x
8561238	J19291104+4441085	965.6	2	1	0.008	0.011	
8587948	J20011735+4439452	214.7	2	24	2.271	0.005	x
8619322	J19190884+4446426	984.3	2	1	0.007	0.004	
8625289	J19275253+4445017	388.1	2	84	6.111	0.024	x
8629689	J19345236+4446380	929.2	2	1	0.030	0.006	x
8683589	J19184517+4449131	1337.8	2	1	0.001	0.012	
8738809	J18591050+4457017	762.5	5	19	0.229	0.016	x
8752893	J19261819+4459436	370.0	2	1	0.170	0.007	x
8818802	J19270676+4503429	1214.1	2	1	0.015	0.005	x
8914923	J20031610+4509192	1305.1	2	24	0.300	0.006	x
8936339	J18575109+4516185	796.0	5	19	0.137	0.014	x
8984355	J20032129+4513187	51.5	2	5	0.157	0.011	x
9002884	J18540578+4520474	585.0	5	19	0.072	0.007	x
9031549	J19403884+4521015	141.4	2	1	0.234	0.023	x
9152245	J19232912+4533427	504.4	2	1	0.099	0.015	x
9206941	J19050068+4539045	1008.4	3	10	0.242	0.035	x
9240941	J19571060+4537363	254.1	2	5	0.496	0.008	x
9326421	J18543641+4550541	775.3	5	19	0.518	0.020	x
9430039	J20015898+4554344	0.8	3	2	0.003	0.011	
9509251	J18504770+4609166	219.9	3	20	1.423	0.009	x
9540226	J19480815+4611544	175.5	3	2	0.262	0.014	x
9591529	J19330295+4613427	89.9	6	42	0.687	0.012	x
9696716	J18591290+4626283	249.9	3	10	1.520	0.049	x
9753178	J18491645+4632307	935.7	3	20	0.002	0.013	
9757624	J18594776+4635013	32.6	3	10	5.191	0.026	x
9813102	J18482411+4637472	996.4	3	20	0.336	0.018	x
9835853	J19352912+4638019	107.7	2	1	0.367	0.008	x
9902962	J19454831+4645271	333.7	3	2	0.099	0.022	x
9995162	J18534324+4657405	636.6	2	1	0.194	0.006	x
10001167	J19074937+4656118	120.4	16	112	19.650	0.005	x
10011329	J19263640+4658023	533.8	4	3	0.223	0.016	x
10028634	J19512811+4659150	1070.3	3	2	0.016	0.014	
10059338	J18574084+4701539	1056.9	2	1	0.132	0.009	x
10094550	J19535070+4702380	1199.3	3	2	0.133	0.009	x
10148118	J19375110+4709246	388.2	2	1	0.014	0.010	
10153182	J19443431+4710071	1096.0	2	654	5.840	0.014	x
10160940	J19531756+4708591	272.2	2	654	5.521	0.021	x
10206457	J19251020+4713306	1042.1	2	4	55.000	0.014	x
10215903	J19394466+4717334	784.8	2	1	0.029	0.006	x
10286616	J19460016+4720165	891.9	3	2	0.018	0.014	
10297952	J19584352+4723131	17.7	2	654	0.969	0.035	x
10318734	J18442402+4728147	906.3	2	1	0.162	0.019	x
10352615	J19462274+4726595	821.3	3	2	0.105	0.007	x
10361019	J19555417+4726384	267.6	3	2	0.163	0.007	x
10426854	J19564169+4733296	959.1	3	2	0.023	0.008	
10454887	J18580811+4739078	1157.0	3	20	0.169	0.006	x
10614382	J19480780+4750357	851.0	2	654	0.009	0.004	
10666510	J19285043+4756444	15.7	2	4	3.646	0.011	x
10668443	J19320112+4755406	38.7	2	4	0.771	0.020	x
10684837	J19535439+4756543	443.1	3	2	0.075	0.012	x
10685892	J19550617+4754033	1052.8	2	654	2.294	0.003	x
10777098	J18475055+4808509	64.6	2	20	0.254	0.053	x
10794816	J19232646+4806195	943.6	4	3	0.026	0.047	
10796857	J19264357+4807193	149.1	2	4	0.579	0.025	x
10922167	J19311901+4822074	586.3	2	4	0.011	0.008	
10935853	J19523172+4818406	882.6	3	2	0.035	0.015	
10936814	J19535355+4823527	664.7	3	2	0.119	0.009	x
11138542	J19292894+4844341	970.1	2	4	0.253	0.008	x

Table B.3. APOGEE radial velocity measurements for *Gaia* DR3 binaries (cont.)

KIC	2MASS	$P_{\text{orb,DR3}}$ [d]	N	ΔT [d]	σ_{RV} [km/s]	mean ΔRV [km/s]	Binary [d]
11146152	J19425889+4846276	1250.6	2	5	0.002	0.007	
11305250	J19424145+4900432	627.7	2	5	0.039	0.011	x
11413158	J19460458+4916004	204.2	2	5	0.554	0.009	x
11515377	J19422614+4927364	514.2	2	5	0.101	0.012	x
11567572	J19432356+4934101	1030.1	2	5	0.086	0.009	x
11657306	J19170208+4942536	982.3	2	2	0.056	0.019	
11718785	J19391236+4948558	437.0	2	1	0.063	0.004	x
11808139	J19141503+5004136	935.8	2	2	0.001	0.023	
11823838	J19455292+5002304	894.5	2	5	0.274	0.014	x
11869694	J19384144+5009175	706.1	2	1	0.066	0.020	x
12314910	J19414879+5102085	69.5	2	5	2.815	0.010	x